Characterisation Of Environmentally Friendly Fibres for Composites

A thesis in fullfilment of the requirements for the degree of Doctor of Philosophy

By

Fiona Lamont Gentles

Department of Mechanical and Aerospace Engineering

University of Strathclyde

Glasgow

Scotland

UK

2015

Declaration of Authenticity and Author's Rights

This thesis is the result of the author's original research. It has been composed by the author and has not been previously submitted for examination which has led to the award of a degree.

Signed:

Date:

Acknowledgements

Firstly, I would like to thank my supervisor, Professor James Thomason for his supervision, encouragement and patience throughout my PhD. I would also like to express my sincere gratitude to Professor David Nash and Anne-Marie Hughes for their assistance and encouragement throughout my studies at the University of Strathclyde since 2004.

I wish to thank the University of Strathclyde for their financial support throughout my studies. I would also like to thank my colleagues and friends in the Advanced Composite Group, Dr Liu Yang, Dr Chih-Chuan Kao, Susan Reilly, Peter Jenkins, Eduardo Saez Rodriguez, Jose Luis Rudeiros Fernandez and Kerrie Downes for their support and the enjoyable times that we spent together in and out of the office. As well as the Advanced Composite Group, I would like to recognize the University of Strathclyde Department of Mechanical Engineering Technicians, James Kelly, Andy Crockett, James Gillespie, Jim Docherty and Chris Cameron for their assistance throughout.

Finally but no means last, I wish to show my deepest thanks to my family, James Gentles (Dad), Alison Gentles (Mum), Christine Gentles (Sister), Colston Crawford (Grandpa) and Patrick Cullinane (Husband) for their continuous support and encouragement throughout out my studies.

Abstract

Throughout the past decade, Polypropylene (PP) has been used as a favoured matrix material with different fibres being used as reinforcement in automotive composites. One of the most popular fibres for reinforcing PP matrix is Glass fibre (GF) due to its strength and impact resistance. More recently there has been interest expressed in further reducing the weight of the vehicle and the environmental impact of the vehicle's lifecycle. One plausible way to reduce the 'environmental impact' of the vehicle is by replacing GF with lighter and more 'environmentally friendly fibres'. In order to develop environmentally friendly composites to be used in the automotive industry, it is vital to have an extensive understanding of the fibre reinforcement properties and how it contributes to the overall composite performance.

In this thesis, full characterisation of three environmentally friendly fibres, Polyethylene Terephthalate (PET), Flax and Sisal, were carried out and an insight into the interaction between the fibre under investigation and the PP matrix is given. Further to this, an investigation into the accuracy of using the fibre's diameter to calculate Natural fibre (NF) properties was carried out. due to NF being non – circular in cross section.

Characterisation of the fibre properties was carried out using various techniques. Single fibre tensile tests were used to investigate strength and modulus of each fibre. It was found that using the actual cross-sectional area (CSA) of the Natural fibres gave more accurate results than assuming circularity of NF. The thermoelastic properties of the investigated fibres were determined through a combination of experimental measurements and micromechanical modelling. Dynamic mechanical

thermal analysis and thermal mechanical analysis techniques were employed to characterise unidirectional fibre-polyester composites over a range of off-axis loading angles. The results were input into a number of micromechanical and semi-empirical models. It was found that the investigated fibres were highly anisotropic with the fibres longitudinal modulus being greater than the fibres transverse modulus over a range of temperatures.

Single fibre pull out was used to investigate the interfacial shear strength (IFSS) between the fibre under consideration and PP matrix containing various percentages of maleic anhydride Polypropylene (MAPP). It was discovered that the IFSS increased when the MAPP content increased. The IFSS was found to be low even with 10% MAPP and this was revealed to be caused by the anisotropic nature of the fibre. Furthermore, it was found that assuming circularity of NF in determining IFSS gave less accuracy than using the actual perimeter of the NF. Therefore it is highly recommended that when possible the actual perimeter and area should be used to calculate NF properties.

In order to use the fibres under consideration in composites, a method to obtain the composite fibre weight fraction has to be investigated. The traditional method cannot be used as the matrix is burnt off leaving the reinforcement fibres behind however the matrix and fibres being considered have similar thermal characteristics. The DSC was found to give reasonably accurate results for obtaining the weight fraction of composite.

Along with the investigation into fibre weight fraction, the fibre morphology between the PP matrix and reinforcement fibres was examined. It was found that no transcrystallisation occurred in PP at a melt flow index (MFI) of 47.

Contents

Nomenclature

F_{max}	Maximum Force
P	Fibre Perimeter
le	Embedded Length
A	Fibre Area
D	Fibre Diameter
E	Young's Modulus
L	Gauge Length
E*	Complex Modulus
E''	Storage Modulus
E'	Loss Modulus
E_m	Matrix Modulus
E_f	Fibre Modulus
E_1	Longitudinal Modulus
E_2	Transverse Modulus
Eθ	Off axis Modulus
E_{1f}	Fibre Longitudinal Modulus
E_{2f}	Fibre Transverse Modulus
V_f	Fibre Volume Fraction
V_m	Matrix Volume Fraction
W_f	Fibre Weight Fraction
v_{12}	Longitudinal Poisson Ratio
v_{1f}	Fibre Longitudinal Poisson Ratio
G_{12}	Shear Modulus
G_{12f}	Fibre Shear Modulus
G_m	Matrix Shear Modulus

τ_{IFSS}	Interfacial Shear Strength
σ	Fibre Strength
σ_R	Residual Radial Compressive Stress
ρ	Density
ρ_{linear}	Linear Density
$\mathrm{Tan}(\delta)$	Damping Factor
α_{1f}	Fibre Longitudinal Thermal Expansion
α_m	Matrix Thermal Expansion
α_{12}	Longitudinal Thermal Expansion
α_{2f}	Fibre Transverse Thermal Expansion
T_s	Matrix Stress Free Temperature
T_t	Test Temperature
F	Fibre Packing Factor
η	Fitting Parameter
ΔH_m	Melt Enthalpy
ΔH_c	Crystallisation Enthalpy
ΔH_m^*	100% Crystalline Enthalpy
DSC	Differential Scanning Calorimetry
MAPP	Maleic Anhydride Polypropylene
PET	Polyethylene Terephthalate
PP	Polypropylene
IFSS	Interfacial Shear Stress
TGA	Thermal Gravimetric Analysis
TMA	Thermal Mechanical Analysis
DMA	Dynamic Mechanical Analysis
CSA	Cross Sectional Area

CTE	Coefficient of Thermal Expansion
MFI	Melt Flow Index
NF	Natural Fibre
E-GMA	Ethylene Glycidyl Methacrylate

List of Figures

List of Tables

Chapter 1

Introduction

1.1 Background

Composite materials have been around for many centuries and have been used in a wide variety of applications. One of the first composites manufactured was from mud and straw, which was used as bricks for building applications [1]. In 1935 Owens Corning manufactured a glass fibre reinforced thermoset plastic composite (GFRP) that was said to be the beginning of industrial composites. Five years after the discovery of GFRP, World War II (WWII) began which proved to be a significant event in the history of composites. WWII proved to be a major driving force in the development of composite materials as composites were used on a large scale for military applications [1]. Just after the war in 1946, composite materials began to be used commercially with applications initially in the marine industry. By 1953 the automotive industry started to use composites, with the General Motors Corvette being the first car to be manufactured with composites in it.

Today, the uses of composite materials have increased and they are being used over a variety of industries, such as medical, leisure and energy. Table 1.1 below gives examples of the various industries that use composites and their applications.

Table 1.1:Example of composite material application in industry [1]

Industry	Application
Aerospace	Fuselage, wings, helicopter blades, interior panels, nose cones, tail planes, seats
Automotive	Instrument panels, body panels, drive shaft, gears, bumpers
Energy	Wind turbine blades, Cross arms, electrical insulators, panels, switchgear
Marine	Hull, decks, interior panels
Medical	Heart Valves, Hip replacement, Medical equipment,
Leisure	Caravans, Golf clubs, Skis, Canoes, Racquets, Helmets, Shoes, Bikes

One industry that has been using composites materials more frequently is the Aerospace industry. Currently, Aerospace industry is manufacturing aircraft containing up to 50% by weight of composites, Bell Boeing V22 Osprey, Boeing 787 Dreamliner and Airbus A350. Figure 1.1 shows the breakdown of materials used to manufacture the Boeing 787 Dreamliner and it can be observed that composites contribute mainly to the fuselage and the wings of the plane.

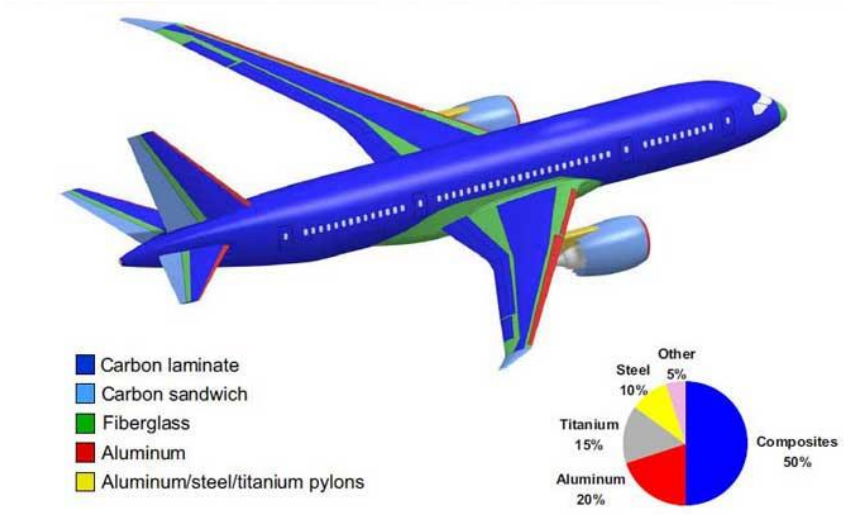

Figure 1.1: Boeing 787 Dreamliner material breakdown [2]

Another industry that has been using composite regularly is the automotive industry. The automotive industry has been increasing the use of composites due to growing concerns about price and depletion of oil and the European regulations for a cleaner and safer environment. A solution to this problem is to reduce the weight of vehicles to improve fuel efficiency which will reduce the vehicles' environmental impact. Reducing the weight of a vehicle by 10% could improve the vehicle fuel efficiency by 7% [3]. One way of reducing vehicle weight is by using a lighter material with similar characteristics as the replaced material. This is where composites can be used, as they are lighter than common metals but have similar strength and rigidity. Composites are lighter than metals due to their low density but are similar when comparing specific properties. Specific properties are related to the Young's Modulus and Strength per unit mass (E/ρ & σ/ρ) and therefore higher specific modulus and specific strength means that the weight of components can be reduced.

At present, a variety of materials are being used in the manufacturing of automobiles such as, Steel, Aluminium, Magnesium and Composites (mainly GFRP) [3]. Steel Alloy is the main material in the automobile and is used in the body of the vehicle. Steel alloy is used as the leading material as it is familiar to the industry, it has a low cost and it has a great ability to absorb energy which can be created in a crash. The other two metals, Aluminium alloy and Magnesium alloy are used as they are lightweight thus reducing the energy consumption of the vehicle. Aluminium and Magnesium alloys are mainly found in the engine components of the vehicle such as the pistons and cylinder head. The automotive industries are also using composites because they are lightweight, corrosion resistant and have good mechanical

properties. The most popular composite used in the vehicles is glass fibre reinforced plastic with the favoured matrix material being Polypropylene. Polypropylene is preferred because of its mechanical properties, processability and low density. GFRP is used in the interior and exterior of the automobile and has good mechanical and structural properties. Along with the advantages of GFRP, there are disadvantages as well such as, high fibre content, cost and poor recyclability. Recyclability of automobiles has become increasingly important, with the automotive industry looking at reducing the environmental impact of vehicles' complete lifecycle as well as reducing the vehicle's weight. A solution to complete lifecycle and weight reduction of the vehicles is to replace glass fibre with lighter and 'environmentally friendly' fibres such as regenerated cellulosic (Rayon), natural (Hemp and Flax) and polymer fibres (Polyethylene Terephthalate).

The work contained in this thesis examines the potential of a range of fibre systems which could be used to meet the above objective. The fibres that are considered include polymer fibre, Polyethylene Terephthalate (PET) and two natural fibres, Flax and Sisal. These fibres were selected on the basis of their low cost, good recyclability and low density. The selected fibres have a lower density than Glass fibre but have good specific properties that could rival and/or replace Glass fibre. The density, strength, modulus and specific properties of the investigated fibres and Glass fibre is presented in Table 1.2.

Table 1.2: Longitudinal properties and specific properties of fibres

Fibre	Density	Strength (MPa)	Modulus (GPa)	Specific Strength	Specific Modulus	Ref
Sisal	1.5	511 – 764	9.4 – 22	340 – 509	6 - 15	[1 - 3]
Flax	1.5	345 – 1100	27.6 – 100	230 – 733	18.4 - 67	[2 - 5]
PET	1.4	302 - 1140	6.5 – 36	215 – 814	4.6 – 25.7	[6 - 8]
E - Glass	2.5	2000 – 3500	70	800 - 1400	28	[7]

In order to develop environmentally friendly composites it is essential to have an in-depth understanding of the reinforcement of fibre's properties as it affects the overall composite performance. The fibres that are being researched bring up challenges. For example the fibres have a different behaviour to that of Glass fibre. Glass fibre is an isotropic material meaning that the material's properties are constant in all directions (longitudinal modulus = transverse modulus) whereas PET, Sisal and Flax are anisotropic materials. An anisotropic material means that the material's properties are not constant but are dependent on the direction (longitudinal modulus ≠ transverse modulus) [1]. Therefore the relationship that can characterise Glass fibre will be insufficient for the investigated fibres. Another challenge is determining properties of the natural fibres, Sisal and Flax, as fibre properties are established using conventional testing procedures. Glass fibres and PET fibres normally have a circular cross sectional area and therefore can produce consistent properties which are repeatable. Natural fibres, however, are non-circular and therefore the normal technique of using the fibre's diameter to calculate fibre properties could provide inaccurate results. The research that is presented in this thesis will address these issues as well as providing an insight into the interaction between the selected fibres and the Polypropylene matrix that is currently used in the automotive industry.

1.2 Project Objectives

The principle objective of this programme of research is to create a deeper understanding of the reinforcement fibre's characteristics and what effects these characteristics will have on the Polypropylene (PP) matrix. The detailed objectives are noted below:

1.2.1 Accurately determine the mechanical properties of the reinforcement fibres that are under consideration.

The objective was to study the mechanical properties such as modulus and strength of the PET and natural fibres. This objective is extremely important for natural fibres. As previously mentioned, the cross sectional area (CSA) of these fibres are irregular whereas PET is circular. Due to the irregular CSA of natural fibres, the determination of the modulus and strength using standard techniques that assumes fibres have a circular CSA could cause inaccurate property results. At present, work carried on natural fibres mainly use the standard method (assume circularity) [8, 12] therefore this research will look at using the 'actual' CSA of natural fibres to determine the properties and will also investigate if assuming circularity of natural fibre can provide accurate determination of the fibre's properties.

1.2.2 Investigate the effect of the reinforcement fibre's anisotropic nature has on the composite properties.

Objective two investigated how the nature of the reinforcement fibres under investigation affects the properties of the composite. The fibres, PET, Sisal

and Flax are anisotropic in nature [12, 13] which will have an influence on the composite properties. Experiments were carried out on unidirectional composites at various fibre orientations to facilitate observation on how the fibre's nature influences the composite properties.

1.2.3 Determine the thermoelastic properties of the investigated reinforcement fibre.

The above objective investigated the thermoelastic properties of the fibre being considered over a range of temperatures. Due to the anisotropic nature of PET and the natural fibres that are under consideration, simple relationships to determine properties for isotropic materials are inadequate therefore further characterisation of fibre transverse properties is required. Determining the longitudinal and transverse thermoelastic properties of the reinforcement fibres will assist in effectively predicting the properties of the composite.

1.2.4 Determine the interfacial shear strength between the fibres that are under consideration and the Polypropylene matrix.

The fourth objective investigates the interfacial shear strength between the fibre and the matrix as it influences the composite properties. Fibre reinforced composite performance is strongly influenced by the stress transfer capability of the fibre matrix interface. A crucial requirement for a successful reinforcement is an effective interfacial bond which will guarantee load transfer from the matrix to the fibre reinforcement. Similar to objective one, this objective will investigate the method in determining the interfacial shear

strength for natural fibres. The typical method uses the circumference of the fibre in calculating the interfacial shear strength (assuming circularity) whereas previously mentioned natural fibre are not circular. The objective will investigate using the natural fibres' perimeter to determine the interfacial shear strength and provide an understanding of the interfacial bond between PET fibre and PP, which has not been researched before**.**

1.2.5 Investigate the effect the fibre weight fraction of a composite system has on the Polypropylene matrix and investigate if the fibre weight fraction can be calculated by experimental techniques.

The last objective investigated the effect the weight fraction of the fibres had on the composite and whether the new method in determining composite fibre weight fraction for these composites can be found. An alternative method for calculating fibre weight fraction needs to be determined for these composites as the traditional technique of burning off the matrix leaving the reinforcement, cannot be used due to the matrix and reinforcement having similar thermal properties. It has been reported in the literature that the fibres under consideration can act as a nucleation agent which can cause transcrystallsation therefore can alter the composite mechanical properties by changing the interfacial characteristics [15]–[18].

This objective looks into calculating the composite fibre weight fraction through experimental technique, as currently calculating the weight of fibre in a composite can be time consuming and tedious. As part of this study on

weight fraction it is necessary to further investigate whether the presence of fibre affects the crystalline morphology of the PP matrix.

Once these objectives are reached, suggestions will be given on the best approach to determine properties of reinforcement fibres and whether the fibres being considered are suitable as reinforcement in composites for the automotive industry.

1.3 Thesis Outline

The thesis is divided into seven distinct chapters and their outlines are shown below.

Chapter 1 is a background into the research programme, key objectives and the layout of the thesis.

Chapter 2 presents a literature review of previous research work undertaken by others relating to the fibre systems that are being considered and includes any additional information that will aid in a better understanding of the experiments that have been carried out.

Chapter 3 describes the research undertaken in characterising the considered reinforcement fibres. This chapter provides full details of the experiments such as design, procedures and testing approach that were used to characterise the fibres along with the results.

Chapter 4 determines the thermoelastic properties of the selected reinforcement fibres. This chapter provides complete information on the experimental setup, testing procedure and results.

Chapter 5 presents the findings of the study that was undertaken in looking at the interfacial shear strength between the considered fibres and the Polypropylene matrix. This chapter also gives details of the experimental arrangement and procedure that was used to carry out the investigation.

Chapter 6 describes the research undertaken in investigating if the fibre weight fraction in composites could be calculated using experimental techniques and the effect of fibre weight fraction on the Polypropylene matrix. This chapter gives details of the sample preparation, experimental procedure and results.

Chapter 7 presents an overall review of the thesis and summarises key conclusions along with some suggestions for future work.

1.4 References

[1] F. L. Matthews and R. D. Rawlings, *Composite Materials: Engineering and Science.* Woodhead Publishing Limited, 1999.

[2] R. M, "Carbon fibre a new era for aircraft design," *Science in new blogspot*, 2012. [Online]. Available: http://science-in-news.blogspot.co.uk/2012/09/carbon-fibrea-new-era-in-aircraft-design.html.

[3] E. Ghassemieh, "Materials in Automotive Application , State of the Art and Prospects," in *New Trends and Developments in Automotive Industry*, 2011, pp. 365–394.

[4] P. S. Mukherjee and K. G. Satyanarayana, "Structure and properties of some vegetable fibres, Part 1 Sisal Fibre," *J. Mater. Sci.* vol. 19, pp. 3925 – 3934, 1984.

[5] A. K. Bledzki and J. Gassan, "Composites reinforced with cellulose based fibres," *Prog. Polym. Sci*., vol. 24, pp. 221–274, 1999.

[6] B. Lamy and C. Baley, "Stiffness prediction of Flax fibers-epoxy composite materials," *J. Mater. Sci. Lett*., vol. 19, pp. 979–980, 2000.

[7] A. K. Bledzki, S. Reihmane, and J. Gassan, “Properties and modification methods for vegetable fibers for natural fiber composites,” *J. Appl. Polym. Sci.*, vol. 59, no. 8, pp. 1329–1336, Feb. 1996.

[8] C. Baley, “Analysis of the Flax fibres tensile behaviour and analysis of the tensile stiffness increase,” Compos. Part A Appl. Sci. Manuf., vol. 33, pp. 939–948, 2002.

[9] T. Kunugi, A. Suzuki, and M. Hashimoto, “Mechanical properties and superstructure of high-modulus and high-strength PET fiber prepared by zone annealing,” *J. Appl. Polym. Sci.*, vol. 26, no. 6, pp. 1951–1960, Jun. 1981.

[10] S. Kawabata, “Micromeasurement of the mechanical properties of single fibers,” in *Modern Textile Characteristics Method*, 1996, pp. 311 – 329.

[11] T. Kunugi and A. Suzuki, “Preparation of high-modulus Poly (ethylene terephthalate) fibers by vibrating hot drawing,” *J. Appl. Polym. Sci.*, vol. 62, pp. 713–719, 1996.

[12] M. C. Symington, W. M. Banks, O. D. West, and R. a. Pethrick, “Tensile testing of cellulose based Natural Fibers for structural composite applications,” *J. Compos. Mater.*, vol. 43, no. 9, pp. 1083–1108, Jan. 2009.

[13] C. Baley, Y. Perrot, F. Busnel, H. Guezenoc, and P. Davies, “Transverse tensile behaviour of unidirectional plies reinforced with Flax Fibres,” *Mater. Lett.*, vol. 60, no. 24, pp. 2984–2987, Oct. 2006.

[14] F. R. Cichocki Jr and J. L. Thomason, “Thermoelastic anisotropy of a natural fiber,” *Compos. Sci. Technol.*, vol. 62, pp. 669–678, 2002.

[15] C. Saujanya and S. Radhakrishnan, “Structure development and properties of PET fibre filled PP composites,” *Polymer (Guild).*, vol. 42, pp. 4537–4548, 2001.

[16] N. Zafeiropoulos, C. Baillie, and F. Matthews, “A study of transcrystallinity and its effect on the interface in Flax fibre reinforced composite materials,” *Compos. Part A Appl. Sci. Manuf.*, vol. 32, no. 3–4, pp. 525–543, Mar. 2001.

[17] Y. X. Pang, D . Jia, H. J. Hu, D. J. Hourston, and M. Song, “Effects of compatiblizing agent on the morphology, interface and mechanical behaviour of Polypropylene/ polyethylene terephthalate blends,” *Polymer (Guild).*, pp. 357 – 365, 2000.

[18] M. A. López Manchado, M. Arroyo, J. Biagiotti, and J. M. Kenny, “Enhancement of mechanical properties and interfacial adhesion of PP/EPDM/Flax fiber composites using maleic anhydride as a compatibilizer,” *J. Appl. Polym. Sci.*, vol. 90, no. 8, pp. 2170–2178, Nov. 2003.

Chapter 2

Literature Review

2.1 Introductory Remarks

A literature review on are Polyethylene Terephthalate (PET) and natural fibre is presented in this chapter. The chapter provides background information on the manufacturing processes of the fibres, reviews the literature on the fibres' properties and the use of the fibres under consideration in composites. A review into fibre anisotropy, interfacial shear strength and transcrystallinity is also presented.

2.2 Polyethylene Terephthalate

2.2.1 Background

Polymers are used everyday and exist in either a natural (cellulose, lignin, protein) or synthetic (nylon, PVC, man-made rubber) form. The chemical make-up of a polymer consists of repeated units with each unit referred to as a monomer. The repeated units are held together by chemical bonds. These bonds work by atoms from a monomer sharing electrons with another monomer developing a repeated unit, which produces the polymer's chemical structure.

One of the most popular synthetic, aromatic and semi crystalline thermoplastic polymers used to date is Polyethylene Terephthalate, PET [1], [2]. Its popularity is due to the desirable properties that the material can bring such as low cost, good

insulation properties, thermal stability, strength, resistance to the environment and recyclability [3], [4]. The main current application for Polyethylene Terephthalate is consumer bottle manufacturing as it can be recycled leading to a low environmental impact but it is also used in a wide variety of products such as food packaging, rope, clothing and shopping bags [4], [5]

Polyethylene Terephthalate also known as PET was first patented in 1941 by two employees of Calico Printer's Association of Manchester, John Whinfield and James Dickson. They developed a concept from Wallace Carothers, who was responsible for creating Nylon. Whinfield and Dickson also created the first polyester fibre in 1941 which was called '*Terylene*' and it was closely followed by DuPont polyester fibre called '*Dacron'* in 1951 [6]. PET manufacturing has been on an increase since it was developed and various companies produce the polymer and retail it under different names. The different trade names for PET can be seen in Table 2.1 [7].

Table 2.1: Trade names of PET and Manufacturer [7]

Trade Name	**Manufacturer**
Arnite	DSM Engineering
Diolen	ENKA- Glazstoff
Mylar	E. I. Du Pont de Nemours & Co. Inc
Rynite	Du Pont de Nemours & Co. Inc
Melinex	Imperial Chemical Industries Ltd

2.2.2 Chemical Structure

The chemical make up of Polyethylene Terephthalate consists of hydrogen, carbon and oxygen with the chemical formulae of $[C_{10}H_8O_4]_n$ and shown below in Figure 2.1.

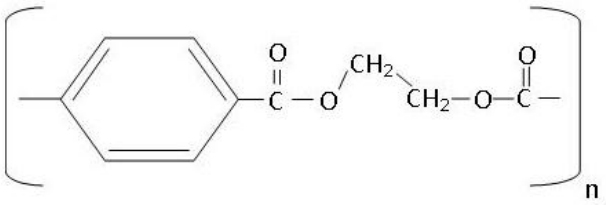

Figure 2.1: PET Structure

PET has a high melting temperature of approximately 250^{o}C with a glass transition temperature in the range of 65^{o}C – 90^{o}C which depends on the molecular weight as it can be polymerised with a mw between 20,000 – 50,000 [3].

2.2.3 Formulation

PET is manufactured from chemicals that can be found in petroleum and can be produced from two processes. The difference between these processes is the start-up reactions.

The first starting reaction to produce PET is a transesterfication reaction and is favoured due to easier purification[7]. The process uses Dimethyl Terephthalate ($C_{10}H_{10}O_4$) and Ethylene glycol ($C_2H_6O_2$) which is a diglycol ester. The process consists of two stages. In the first stage, a polycondensate is formed by combining

the diglycol ester with oligomers. After the precondensate is formed transesterfication takes place using a small amount of metal salt as the catalyst at a processing temperature around 200^{o}C. During the tranesterfication bis-(2-hydroxyethyl) terephthalate ($C_{12}H_{14}O_6$) and methanol (CH_3OH) is produced, Figure 2.2. The methanol from the tranesterfication is continually being removed as it prevents chain growth, due to forming a stable end group [4].

The second starting reaction to manufacture polyethylene terephthalate is an esterfication reaction. PET is produced by reacting terephthalic acid and ethylene glycol in company of an antimony catalyst. The byproduct of this process is bis-(2-hydroxyethyl) terephthalate and water [8] – [10].

The second stage in this manufacturing process is the polycondensation reaction of the bis-(2-hydroxyethyl) terephthalate, a byproduct from both starting reactions mentioned above. The polycondensation is performed in a vacuum at a temperature of 280^{o}C with a heavy metal salt being used as a catalyst for the process [4]. The polycondensation process polymerises bis-(2- hydroxyethyl) terephthalate. The polymersation bis-(2- hydroxyethyl) terephthalate produces by products of ethylene glycol and Polyethylene Terephthalate, Figure 2.3. The by product, ethylene glycol is continually removed from the process like the methanol in the first starting reaction but can be recycled and used in the first starting reaction as it is one of the starting products [10].

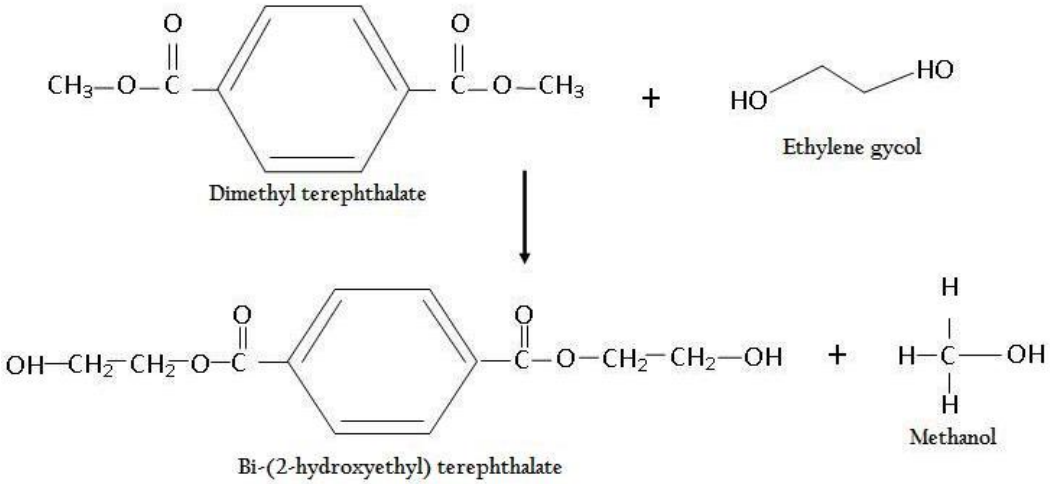

Figure 2.2: Process 1, stage 1 - transesterfication

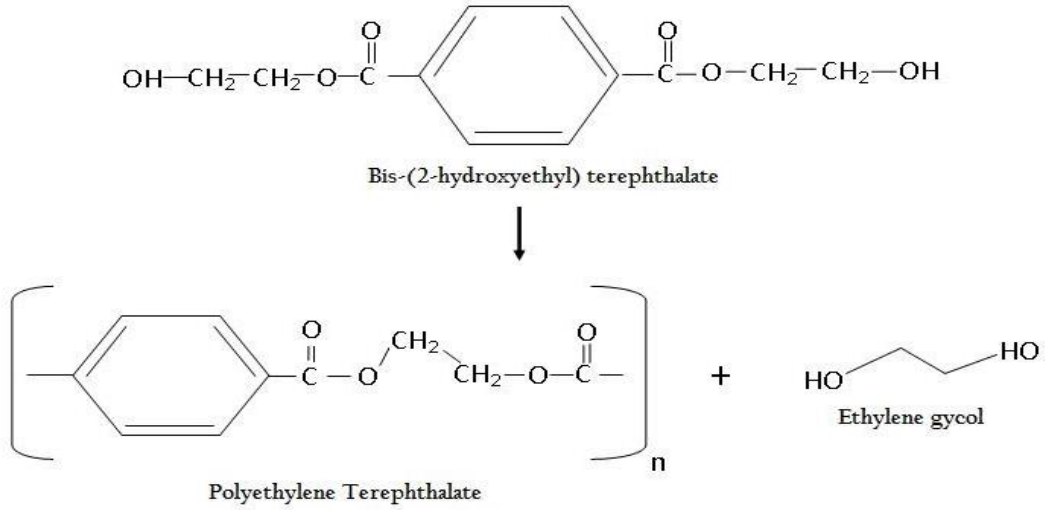

Figure 2.3: Process 1, stage 2 - polycondensation

2.2.4 Structure

The structure of Polyethylene Terephthalate fibre is influenced by different parameters which affects the polymer's properties. The main parameter that can affect the structure of PET is the manufacturing process. The temperature of the process controls the crystallinity and orientation of the molecules in the fibre. Crystallinity is related to the structural order of a polymer and exists as three-dimensional order, which can be found by using X-ray diffraction. Crystallinity of PET is extremely important as it influences the tensile strength, stiffness, melting point and the modulus.

PET is a semi crystalline polymer and it can become completely amorphous at room temperature when quenched from the melt. PET crystallisation rate is influenced by temperature history and molecular orientation. The determination of the molecular orientation of a material is extremely crucial as it is used to understand the properties and structure of a polymer [11], [12]. The root of crystallisation is influenced by the nucleation rate and the rate of crystal growth on the nuclei [11]. The structure of the Polyethylene Terephthalate is split into crystalline and amorphous regions. Polyethylene Terephthalate has two forms of ethylene glycol linkage; these forms are trans (extended form of ethylene glycol) and gauche (relaxed form of ethylene glycol) [13]. Figure 2.4 and 2.5 show the structure of the gauche and trans conformer. At the start of PET crystallisation the gauche linkage is dominant over the trans ethylene glycol linkage but when the Polyethylene Terephthalate is fully crystallised, the trans linkage is the only ethylene glycol linkage that is present [13]. Ajji et al. [12] proposed that Polyethylene Terephthalate fibre structure consists of

three phases; the crystalline phase, mesophase and amorphous phase. The crystalline phase is when the fibre is completely crystallised and consists exclusively of trans conformers and the crystal perfection can be increased with the drawing ratio and rate. The mesophase comprises of trans conformers that have not crystallised but have a high orientation and can act as a link from the amorphous phase to the crystalline phase. The final phase is the amorphous phase which only consists of gauche conformers and has a random orientation [12].

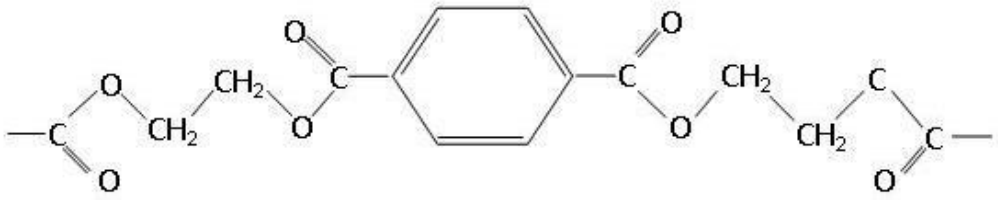

Figure 2.4: Gauche conformer structure

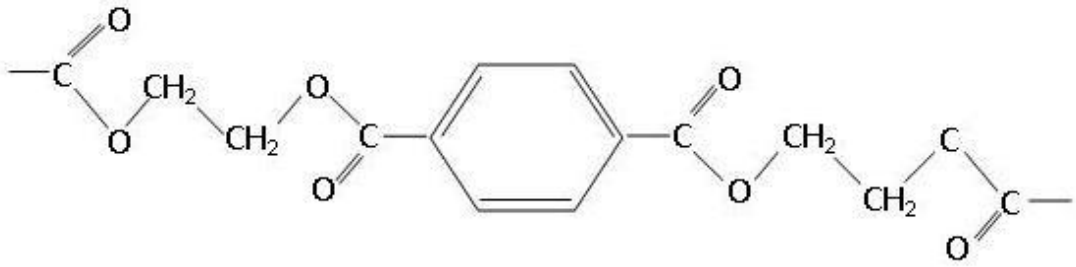

Figure 2.5: Trans conformer structure

Crystallisation of a polymer occurs above the glass transition temperature. Polyethylene Terephthalate crystallinity is affected by heat treatment. The crystal size of PET increases initially at the start of heat treating then starts to decrease as

heat treating continues. Gupta and Kumar investigated the effect of heat treatment on the PET structure [14]. They observed that the crystallinity increased as the annealing temperature increased. It was also detected that heat treating at low temperatures the PET fibre shrinkage is small. The main effect for small shrinkage is due to the removal of stresses and strains that have been built in during fibre manufacture process which causes the fibre to become stable as the molecules start to relax. As the molecules relax, longitudinal pulling of the crystallites occurs along the fibre direction [14]. As the heat treating temperature increases, the mobility of the molecules increase which causes the shrinkage of the fibre to increase.

Orientation plays an important role in the Polyethylene Terephthalate properties especially on the dynamic mechanical properties [15]. PET has two dynamic mechanical transitions which are γ transition and β transition which is most commonly know as the glass transition. The γ transition happens at approximately -40^{o}C and the β transition happens around 80^{o}C. At the β transition the Polyethylene Terephthalate modulus changes significantly due to it softening from a rigid glass-like to a rubber-like solid [16].

2.2.5 Fibre Manufacturing

2.2.5.1 Melt Spinning

Polyethylene Terephthalate filament is manufactured by melt spinning which produces an amorphous structure. Melt spinning is the initial step in the manufacturing process of Polyethylene Terepthalate fibre and it changes the bulk material in to a continuous filament. The process of melt spinning starts when the polymer is melted and pushed through a spinneret then the melted polymer solidifies

into a fibre and is wound round a bobbin. The melt spinning process can be seen in Figure 2.6.

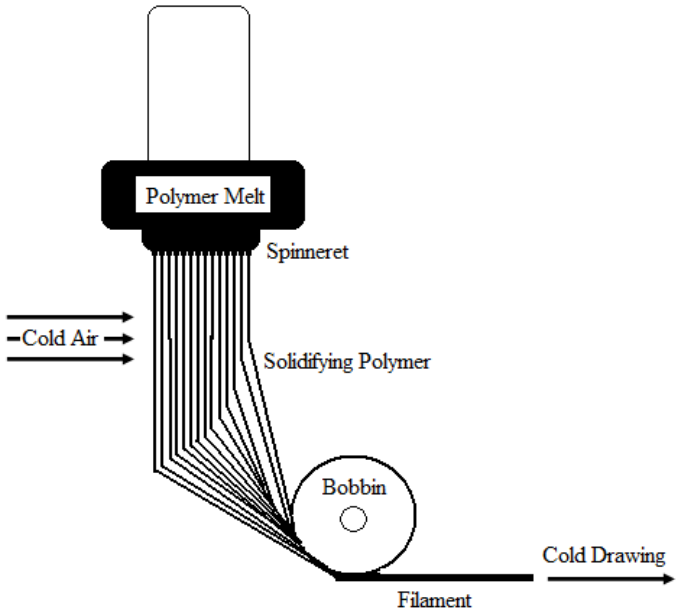

Figure 2.6: Melt Spinning Process

The main parameter that is influenced by melt spinning is the orientation of the molecular chain. Melt spinning produces a filament, which has a crystallisation less than 1%. Dumbleton [17] looked into the effect of melt spinning on the orientation of Polyethylene Terephthalate and noticed that the orientation was induced in the spinneret but relaxes out immediately after the spinneret stage. Dumbleton also discovered a mechanism called stream orientation, which occurs in the free jet stream of the melt spinning process. The development of the stream orientation happens when the molten polymer is a short distance below the spinneret. When the PET is below the spinneret, the free jet stream necks the polymer leading to the molecules being stretched in the direction of motion, this causes the PET to be orientated. Stream orientation occurs above the melting point of PET therefore enough thermal

mobility could be produced to correct the orientation back to random if sufficient time is available [17]. Crystallisation rate during melt spinning is slow, therefore the structure of the fibre is considered to be a deformed network of entangled molecules in which the deformation that has occurred is "frozen in". The number of entanglements increases with increasing the molecular weight of PET and the distance between the entanglements is also dependent on the molecular weight of PET [17]. The orientation that is formed during melt spinning can be measured by fibre shrinkage. Shrinkage of the fibre occurs when the temperature is raised above the glass transition as the molecules achieve enough mobility to relax the strain that has been introduced in spinning process. The shrinkage force is influenced by the thermal expansion of Polyethylene Terephthalate. The coefficient of linear thermal expansion of PET is approximately $10^{-4}/^{o}C$. Polyethylene Terephthalate is ductile at room temperature due to partial freeing of molecules at the γ transition ($-40^{o}C$) [17].

The spin orientation of the PET fibres varies by altering the speed of the bobbin. Increasing the speed of the bobbin and molecular weight will increase the birefringence, shrinkage and shrinkage force. The stretch on the spun fibre is increased when the speed of the bobbin is increased leading to the decrease in time for the relaxation of the molecular orientation. Dumbleton concluded that the filament right after melt spinning may not be amorphous as many processing conditions affects the fibre's crystallinity [17].

2.2.5.2 Cold Drawing

After the melt spinning process the Polyethylene Terephthalate fibres is put through a process called cold drawing.

Cold Drawing was initially used in the manufacture of plastic fibres. Julian Hill discovered the process in 1930 which is similar to the drawing process for metals. The drawing process is achieved after the polymer is spun in to filaments by melt spinning. The filament is then stretched out by a draw machine which reduces the diameter but increases the filament's length. The draw machine stretches the PET filament by using two sets of rollers with the second set of rollers fixed to rotate faster than the first leading to stretching of the PET fibre and is shown in Figure 2.7. The filament's initial structure is amorphous but after drawing the fibre aligns, and the crystallinity of the structure increases which changes the tensile strength and stiffness.

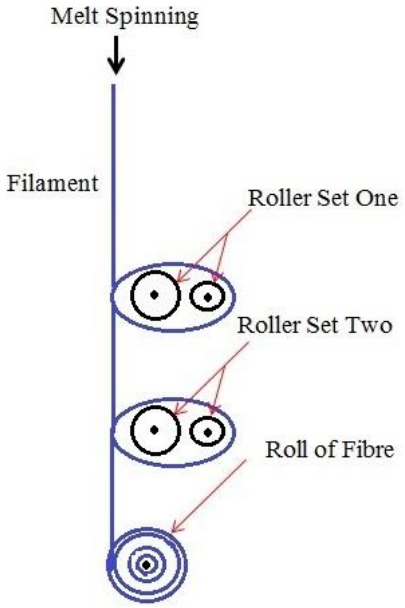

Figure 2.7: Cold Drawing Process

The draw ratio is the ratio of the cross sectional area of undrawn material to the drawn material. The natural draw ratio is the amount of strain in the neck of the material which can be determined by the material hardening characteristics.

Various works have been published on the effect and influence of Cold drawing on Polyethylene Terephthalate. Ward and Allison [20] investigated the cold drawing behaviour of PET over various test conditions. It was found that cold drawing can occur at about -50^{o}C which is approximately 100^{o}C below the glass transition temperature and that rate of drawing can affect the temperature of the drawing process. At low drawing rate, heat that is produced during the process will dissipate away from the neck of the polymer quickly leading to no temperature rise. However as the rate of drawing increases, the process starts to become adiabatic leading to an increase in drawing temperature. Ward and Allison concluded that the natural draw ratio of PET was dependent on the temperature of the drawing [18].

Foot and Ward [19] investigated the cold drawing of amorphous Polyethylene Terephthalate and discovered that the PET natural draw ratio decreased as the temperature decreased due to the polymer being strain hardened at a lower temperature. They determined that the natural draw ratio is the ultimate stretching of a polymer network and that thermal motion at high temperatures may reduce the number of effective entanglements. Foot and Ward concluded that the natural draw ratio can be reduced if the molecular weight is increased and the temperature is decreased [19].

The effect of drawing of Polyethylene Terephthalate structure at 36^{o}C was investigated by Bhat and Naik [20]. Bhat and Naik found that as the draw ratio

increased, the crystallinity index also increased. Therefore at 36^{o}C the density and degree of crystallinity of the fibre increased with nearly all of the crystalline nuclei aligned along the fibre axis direction. Bhat and Naik also investigated the effect of drawing at 200^{o}C. It was found that a thermomechanical process induced crystallisation at 200^{o}C as the chain segments of the fibre in the crystalline region rotated and aligned along the direction of the fibre axis. This resulted in the fibre's structure being highly oriented and crystallised.

Blundell et al. investigated the orientation of the Polyethylene Terephthalate before crystallisation occurred in the drawing process [21]. It was observed that the crystallisation of PET depended on the rate of drawing and the behaviour changed as the rate of drawing increased. The onset of crystallisation at a fast draw rate was detected at the end of the deformation stage of the drawing process. Increasing the temperature, decreased the level of orientation at any given draw ratio. Blundell et al. discovered that decreasing the draw rate and increasing the temperature caused a relaxation effect to occur on the entangled molecular chain system. The relaxation effect competed with the deformation that was being applied to the PET filament.

2.2.6 Mechanical Properties

As previously mentioned, the mechanical properties such as modulus, strength and shrinkage of the PET fibre are influenced mainly by the manufacturing process. The manufacturing condition that influences the structure of the fibre is the draw ratio, temperature and the spinning speed.

The effect of spinning speed and drawing temperature on PET fibre mechanical properties was investigated by Huisman and Heuvel [22]. They discovered that the

modulus and shrinkage is influenced by the crystallinity of the fibre. Increasing the crystallinity of the fibre increases the modulus and decreases the shrinkage of the fibre. The crystallinity of the fibre is affected by the spinning speed of the bobbin which has been mentioned briefly in the PET structure section. Huisman and Heuvel researched the effect of spinning speed on the mechanical properties of PET yarn at two different drawing temperatures; moderate & high (close to PET melting point). The spinning speed ranged from 1000 to 5000m/min at 300^{o}C with the yarns having the same diameter. Huisman and Heuvel initially researched the yarn shrinkage and found that at increased spinning speed, the shrinkage of the fibre decreased. The reason for the decrease in shrinkage is related to the amount of amorphous region in the yarn. Increasing the spinning speed decreases the volume of amorphous region due to the crystallinity volume increasing in the PET yarn [22]. Huisman and Heuvel then researched the affect the spinning speed has on the fibre's modulus. They found that increasing the spinning speed, increased the modulus of the fibre caused by the fibre exhibiting high crystallinity [22]. The final mechanical property that Huisman and Heuvel investigated was the fibre tenacity and it was reported that the tenacity was affected by two important attributes; 1. Molecules folding at the boundary of the crystal boundary this is called chain folding and cannot contribute to the modulus or tenacity 2. The tie-chain distribution length. Figure 2.8 shows the structure of the fibre at low and high spinning speed. It can be observed that at high spinning speeds the tie chains are long and have a board distribution compared to the low spinning speed tie chains.

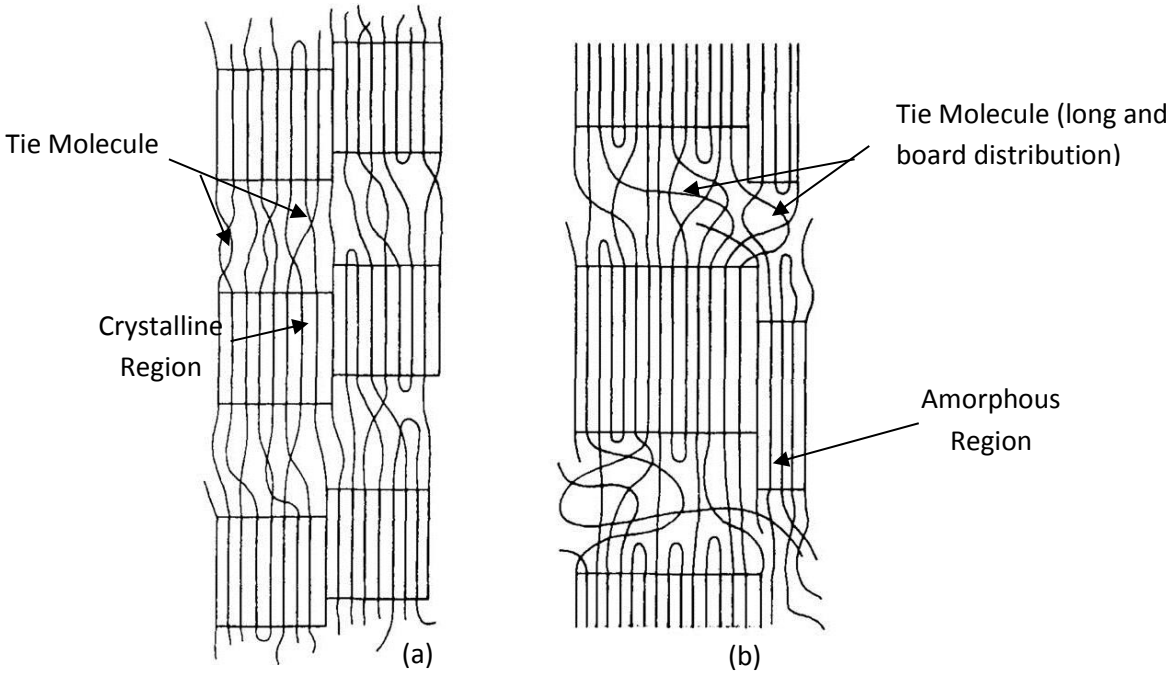

Figure 2.8: PET structure a) low spinning speed and b) high spinning speed [22]

Huisman and Heuvel discovered that the tenacity decreased at high spinning speed due to the long length of the tie chains which increased the amount of chain folding at the crystal boundary as well as tie chains have distributions being board [22]. The tie molecules join one crystal to another and are essential in bearing the load when a fibre is placed in tension [1], [15], [23], [24]. If the tie molecules length distribution is large, the molecules will not help in bearing the load placed on the fibre. The draw ratio also affects the mechanical properties of the PET fibre and has been reported by several researchers such Okumura, Foot, Rudolf and Bhat [19], [20], [25], [26]. The general consensus from the studies is that increasing the draw ratio, increases the fibre strength and modulus due to the fibre being highly orientated and crystallised.

Various methods based on spinning, drawing and annealing to improve the mechanical properties of PET fibre have been developed over the years [27] – [29].

Zone annealing was one of the first methods to produce high modulus and strength PET fibre. This method was developed by Kungui at al. [27] and created a PET fibre with a modulus of 19.4 GPa and strength of 1.14 GPa. Kungui went on to develop a method using a vibrating hot drawing technique to produce high modulus PET with Suzuki [29]. They managed to produce a fibre with a storage modulus of 36 GPa by hot drawing PET fibre under vibrations.

Heat treatment of PET fibre also affects the mechanical properties of the fibre. A series of investigations on how heat treatment affects the mechanical properties of PET fibre was carried out by Gupta and Kumar [14], [15], [23], [30]. They investigated the effect of heat treating fibres at constant length (taut annealed) and free to shrink (free annealed) at various temperatures. They noticed after carrying out tensile tests on the fibre, that for the free annealed fibre the elongation increased as the annealing temperature increased whereas for taut annealed the elongation slightly decreased as the annealing temperature increased. As well as elongation changing the tensile modulus and strength also changed. The tensile modulus and strength decreased as the heat setting temperature increased for the free annealed fibre. The tensile modulus for taut annealed fibre did not change significantly and was close to the modulus of the fibre that had not been annealed. Therefore they determined that the orientation of the fibre plays the significant part in determining the modulus than the fibre's crystallinity [30]. Gupta and Kumar also noticed a 'kink' at low stress in the stress – strain graph for free annealed fibre. This kink was also observed by Cho

[24]. The cause for the ‘kink’ was due to the amorphous and crystalline regions of the fibre being arranged in series rather than in parallel which reduce the number of tie molecules that will help in taking the force when the fibre is placed in tension. Due to the reduction in the number of tie molecules, the stress on the molecules is significant therefore causing them to break at low load which leads to the fibre yielding. Therefore the ‘kink’ which appears in the stress – strain graph is the fibre yielding [23], [24] and the ‘kink’ is shown in Figure 2.9.

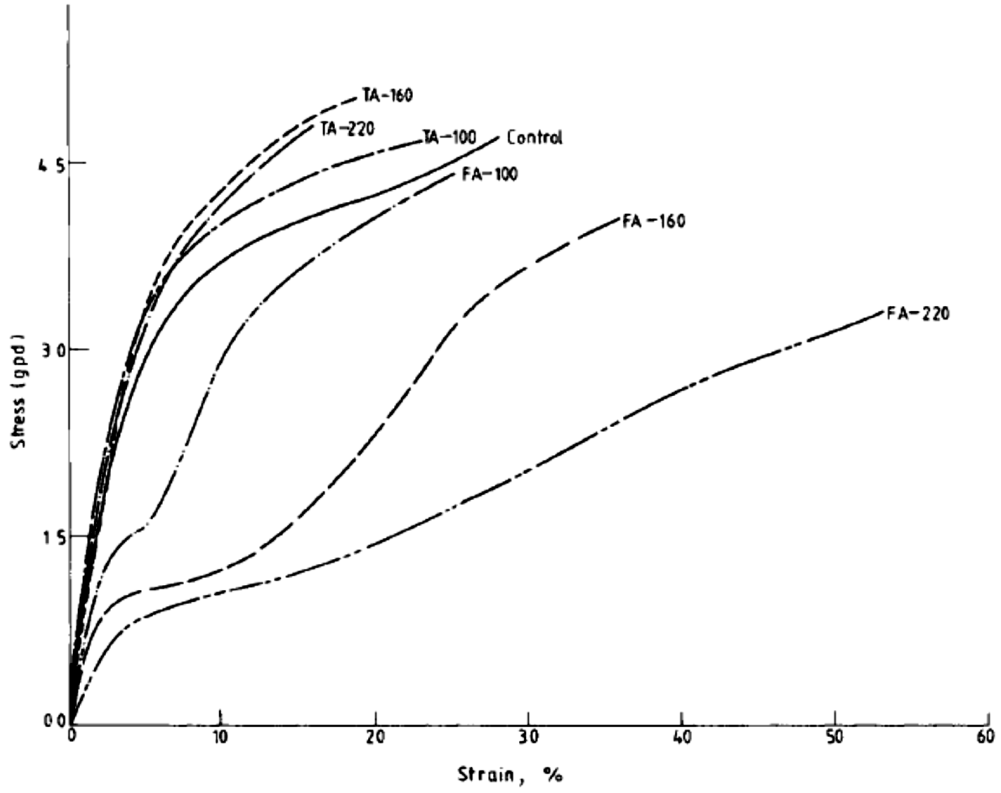

Figure 2.9: Stress – strain graph of PET fibre free annealed and taut annealed [23]

2.2.7 Polymer Composites

Research into polymer-polymer composites has been on an increase in the past ten years because these composites can be easily recycled. Polymer blending is an

important technique for manufacturing new materials with desirable characteristics. There are also many advantages of polymer blending such as time saving; low manufacturing costs and potential to achieve specific material properties [31].

The manufacturing of all-polymer composites has three crucial preparation steps before composites can be produced and these are listed below [32] –[34]:

1. Blending of the polymer components
2. Drawing
3. Annealing

Injection moulding is the manufacturing technique frequently used to produce polymer-polymer composites. Injection moulding is therefore used to produce PP-PET composite and is usually done above the melting temperature of PP but below the PET melting temperature. This is due to the PP melting but the PET fibres morphology is protected. The PET fibres produced in this process should be in the order of a few microns to keep the fibres' orientation. The PET fibres are distributed randomly in the PP matrix after injection moulding. The size of the fibres are in the order of a few microns to stop the PET fibre relaxing, so that the molecular orientation of the fibre is kept therefore producing a microfibrillar composite [32], [35], [36]. PET has higher strength and the modulus than PP therefore the PET fibres will take the main load when experiencing a tensile strain [37].

The existence of PET fibres affects mechanical properties of PP matrix. Addition of PET fibres into PP composite increases certain mechanical properties such as stiffness, tensile strength and Young's modulus. [39], [43].

Friedrich et al. [33] investigated the effect of ethylene glycidyl methacrylate (E - GMA) compatiblizer on the mechanical properties of recycled PET fibre and PP. They observed no improvement in the modulus or strength of the composite as the percentage of compatibilizer increased and a slight increase in impact strength with increase in compatibilizer content.

Cheung and Chan [38] also investigated the mechanical properties of PET and PP blend with compatibilizer of EPOLENE E-43. It was found that with no compatibilizer, increasing the PET content between 10% and 50% had no significant affect on the strength or modulus. Whereas adding 70% PET content the strength and modulus increased. The cause for the increase is due to the PET strength being the dominant material and PET has a higher tensile strength than PP. Adding EPOLENE E – 43 compatibilizer to the PET/ PP composite blend improved the strength and modulus of the composite as there was better interaction between the PET and PP.

In general, the mechanical properties of PP improved with the addition of PET but the improvements were not significant which can be related to the interaction between the two materials being poor. This is proven by the impact properties of the PP/PET being lower than neat PP and only increases with the addition of compatibilizer s [33], [37], [39]. Further examination of the interfacial strength between PET and PP needs to be carried out and will be investigated in this thesis.

2.3 Natural Fibre

2.3.1 Background

The first natural fibre composite was manufactured by the Egyptians 3000 years ago. The Egyptians constructed the composite out of straw and clay and was used to build walls. The oldest natural fibre reported is Hemp which was used in China 2800BC to manufacture cloth. Natural fibres can be manufactured from animals and plants and appear in everyday items such as sports equipment and clothing. This section of the literature review will highlight natural fibres that are manufactured from plants.

2.3.2 Chemistry

Plant natural fibres are made up of bundles of elementary fibres located either in the stem or leaf of the plant. An elementary plant fibre is one cell from the plant's leaf or stem with a diameter ranging from 10 -50 µm and a length of 1 – 50 mm [40]. The amount of elementary fibres that are needed to create a natural fibre varies between plants. Natural fibres are made up of many components. Four main components that make up the elementary fibre are cellulose, hemicellulose, pectin, lignin and wax. Different plants have various compositions of these components, which determine the fibre's properties. A brief description of the components that compose an elementary natural fibre is given below.

2.3.2.1 Cellulose

Cellulose is the main component that makes up plant natural fibres and appears in the cell wall as microfibrils [41]. It is responsible for the fibre's structure which establishes the chemical and physical properties of the fibre. Cellulose is a linear

condensation polymer made up of thousands of glucose units called D-anhydrogluscose which are connected together by β – 1, 4 – glycosidic linkage and arranged in a crystalline form [42]. The crystal structure of natural cellulose is known as cellulose I and man-made cellulose is known as cellulose II. The type of cellulose in the natural fibre relates to the fibre's mechanical properties. The mechanical properties are determined by the cellulose's geometrical condition and cell geometry which varies between fibres [40], [42]. The cellulose structure, shown in Figure 2.10, provides hydroxyl groups which are able to interact with water by hydrogen bonds. The level of moisture up take of the cellulose depends on the environmental humidity at which the fibre reaches equilibrium. Cellulose is known to degrade at temperatures of around 350^{o}C [43] – [45].

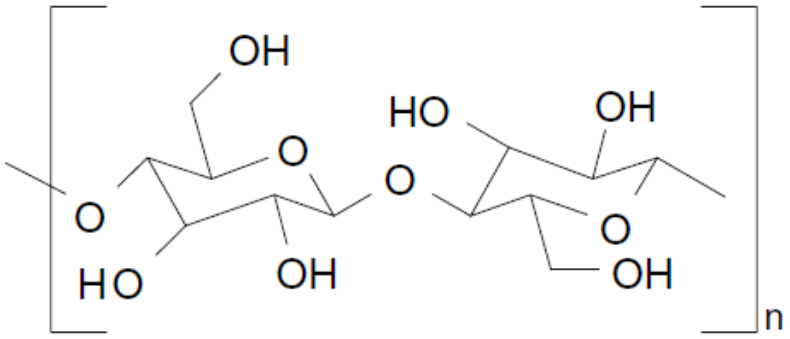

Figure 2.10: Repeated cellulose unit [46]

2.3.2.2 Hemicellulose

Hemicellulose is made up of a collection of polysaccharides [40], [42], [47]. Polysaccharides are repeated carbohydrate molecules which are bound together by glycosidic bonds. The hemicellulose is joined to the pectins covalently and to the cellulose and pectins by hydrogen bonding. The hydrogen bond performs as a crosslink between the cellulose microfibrils and the cellulose – hemicellulose

network and is believed to be the fibre cell's structural component [48]. Hemicellulose forms a matrix with lignin which embeds the microfibrils of the cellulose.

2.3.2.3 Lignin

Lignin is a complex hydrocarbon polymer with aromatic and aliphatic elements. The hydrocarbon can be made up of three different monomer units: coumaryl, coniferyl or sinapyl and are shown in Figure 2.11 [41]. As mentioned above, the lignin is covalently bonded to the hemicellulose. The main application of the lignin is to provide rigidity and strength to the cell wall. A cell wall without any lignin will not be able to tolerate extreme forces. Lignin has a glass transition temperature around 90^{o}C where it begins to soften and a melting temperature of around 170^{o}C therefore it is considered to be a thermoplastic [40].

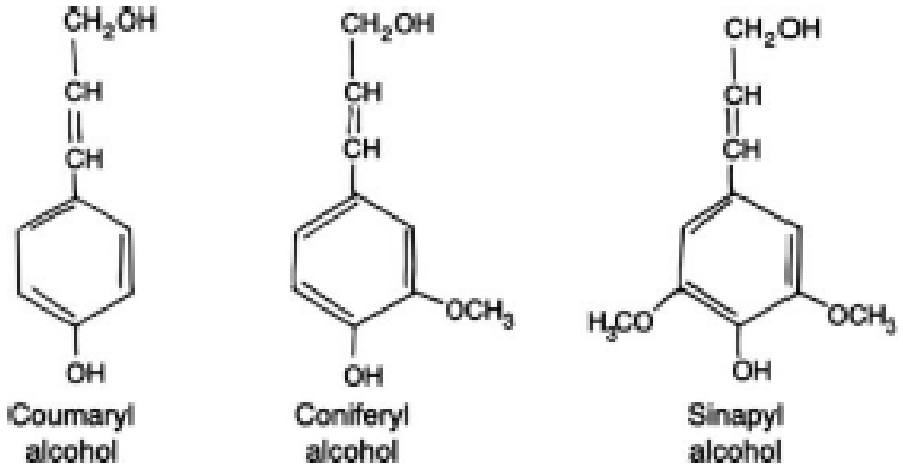

Figure 2.11: Various types of lignin monomers [41]

2.3.2.4 Pectins and Waxes

Pectins is a combined name for heteropolysaccharides and consists mainly of polygalacturonic acid and are hydrophilic [40]–[42]. Pectins and hemicellulose combined are called the polysaccharide matrix and provide the plant with elasticity. Waxes formulate a minor quantity of the plant structure and comprise of various types of alcohol. The waxes are insoluble in water and provide a barrier against water loss and bacterial attacks [41], [47].

2.3.3 Structure

Elementary natural fibre structure consists of two cell walls which are split up into a primary and secondary wall with a void in the middle known as the lumen. A cell wall consists of semi crystalline cellulose microfibrils embedded in a hemicellulose – lignin matrix of varying composition. The lumen of the cell controls the water uptake of the plant and is shown in Figure 2.12 [49].

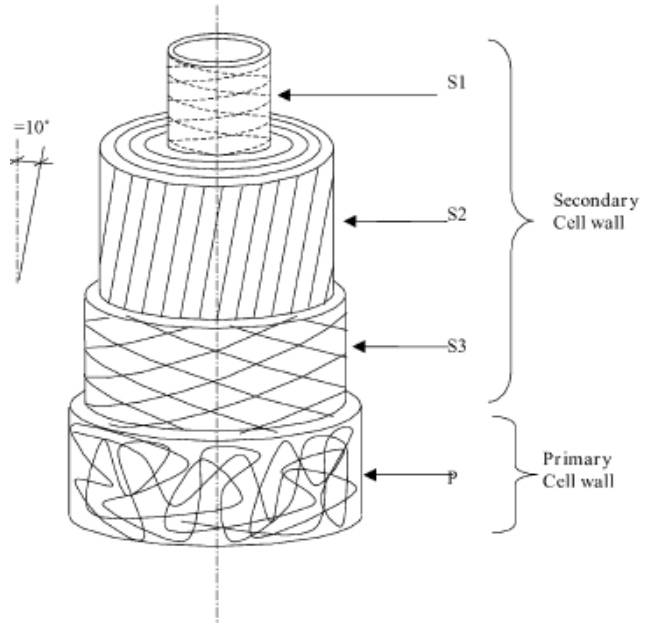

Figure 2.12: Flax fibre structure [49]

The primary cell wall consists of randomly orientated cellulose microfibrils that are packed closely together. The secondary cell wall can be split into three layers which are the inner S1, middle S2 and outer S3. The difference between the secondary cell wall layers is the orientation of the cellulose fibrils which is illustrated in Figure 2.12. The S2 middle layer is the thickest and considered to be the most important as it defines the mechanical properties of the fibre [41]. The mechanical performance of the fibre is associated with the cellulose microfibril angle (MFA) which is related to the angle at which the microfibrils are wound around the middle secondary layer (S2) against the vertical cell axis. If the MFA angle is small this indicates the cellulose microfibrils are close to being orientated vertically leading to the Young's modulus of the fibre being high. However, if the MFA angle is large the Young's modulus of the fibre is low. Different natural fibres have different MFA; for example, Flax and Sisal fibres have an MFA of 10^{o} and 20^{o} respectively.

2.3.4 Extraction

Extracting natural fibres from plants can be done in two ways depending on what part of the plant the fibre is taken from. The two methods used to obtain fibres from plants are 'decorticating' and 'retting'. Decorticating is mainly used to manufacture fibres from the leaf part of the plant whereas retting is used to obtain fibres from the plant's stem. The fibres that are manufactured from the stem of the plant are usually called bast fibres.

2.3.4.1 Decorticating

Decorticating is a process that takes place after the leaves of the plant have been separated from the stem. The leaves are placed into a machine called the decorticator. The decorticator has unsharpened knives that rotate on a wheel which crush and beat the leaves until only the fibres remain. Once the decorticating process has been completed the fibres are then placed into a vat of water for twelve hours. This allows the removal of chorophyll sap mucilage and pectic substances. The fibres are then removed from the water and dried [41].

2.3.4.2 Retting

Retting is a microbial process that removes the chemical bonds that hold the stem together and allows the bast fibres to separate from the non-fibre section of the stem. There are two types of retting; water and dew also known as field. The difference between the two process is the location of where retting takes place. Water retting is when the plant is placed in to a tank of water and left for the microbial process to take place. The fibres are then removed from the water and dried. Dew retting happens in a field immediately after harvesting the plant and is believed to be the oldest and favoured method. The stem of the plant are distributed evenly along the field and left for the retting process to occur. The temperature and moisture of the environment encourages the microbial process which starts to degrade the stem of the plant to produce the fibres. The plant is frequently rotated to allow retting to occur evenly throughout the plant [41].

2.3.5 Mechanical Properties

The mechanical properties of natural fibres are not only influenced by the structure of the plant but also by the age of the plant, harvesting, chemical composition, fibre diameter, global location and climate [40], [42], [48], [50], [51].

Two key parameters that influence the properties of natural fibres are the microfibril angle and chemical composition as briefly mentioned in the chemical structure section above. This is also illustrated in Table 2.2 which shows various natural fibres with the microfibril angle and modulus. It can be seen from the table that Ramie fibre has the smallest MFA and the largest Young's modulus whereas Coir fibre has the largest MFA and the smallest Young's modulus. The chemical composition of the natural fibre is influenced by the climate and location of the plant and therefore the composition can vary between the same plant species. An example of the chemical composition for different plant species is shown in Table 2.2. It is believed that the lignin part of the chemical composition impacts on the structure, properties and morphology of the fibre [52]. It can be seen from Table 2.2 that fibres with high lignin content such as jute and a low MFA angle have Young's moduli similar to a fibre like Sisal with a larger MFA but a lower lignin percentage. Therefore the research shows that the mechanical properties of the fibre are not influenced by only one single parameter but by many [53].

Table 2.2: Chemical composition, MFA and Mechanical properties of Various Natural fibres [52]

Fibre	Cellulose (wt%)	Hemicellulose (wt%)	Pectins (wt%)	Lignin (wt%)	Microfibril angle (^{o})	Modulus (GPa)	Strength (MPa)
Ramie	68.6	13.1	1.9	0.6	7.5	128	870
Jute	61	20.4	0.2	13	8	13	550
Flax	71	18.6	2.3	2.2	10	100	1100
Sisal	78	10	-	8	20	15	640
Coir	43	0.3	4	45	45	5	140

Along with MFA and fibre's chemical composition which affects fibre properties, global location and climate also have an influence. Work done by Stamboulis, Ballie and Peijs [48] on Flax fibre showed that increasing the relative humidity of the fibre environment, increased the moisture content in the fibre. It was also shown by their research that the average ultimate tensile strength (UTS) increased for uncoated Flax fibre as the relative humidity increased. Davis and Bruce [54] also conducted research into the effects of relative humidity on Flax fibre and found that dynamic and static modulus of the fibre decreased as the relative humidity increased.

It has been reported by Baley [49], [55] that the diameter of the fibre is another parameter that influences the fibre's mechanical properties. For Flax fibre, Baley found that, as the fibre's diameter increased, the Young's modulus decreased. A reason for this decrease in Young's modulus could be related to the lumen of the fibre (a large hole in the centre of the fibre) which increases with the diameter of the fibre, whereas Mukherjee and Satyanarayana [56] did not see a variation of the modulus associated with the fibre diameter when investigating Sisal. Several researchers have reported such as Park and Thomason [57], [58] that natural fibres

are not circular therefore using the diameter of the fibre to calculate the various mechanical properties would be a likely cause of inaccuracy of results. Thomason researched into the effects on the mechanical properties assuming circularity of the Flax and Sisal. It was reported that using the diameter to obtain the area of the fibre overestimated the actual area of Flax and Sisal by nearly double which would have an overall effect on the fibre's properties.

The final parameter that has been said to influence the fibre mechanical properties are the processing and handling of natural fibres. Processing of natural fibres is not the most delicate of processes therefore there is a strong possibility of fibre damage before being used. The damage on the fibre shows up in a form of a 'kink band' when looked at closely which reduces the fibre's strength in both tension and compression [59]. Bos et al. [59] and Bruce et al. [54] researched the effects that these flaws have on the fibre's mechanical properties. Bos et al. found that increasing the fibre length during tensile testing decreased the strength of the fibre - the smaller the length of the fibre reduces the amount of flaws present. Bruce et al looked at the effect that fibre damage could cause to the modulus of Flax and Nettle fibres. They observed that as the volume of damage to the fibres increased, so the fibres' modulus decreased.

The findings reported in the section above gave possible reasons why mechanical properties of natural fibres can vary between the same and different species of plants. Natural fibres are influenced by many different parameters which is reason why there is such a variation in mechanical properties.

2.3.6 Natural Fibre Reinforced Composites

Natural fibres as reinforcement for composites are desirable as they have attractive properties such as being environmentally friendly, low density, low cost and recyclable. Natural fibres are also less abrasive than many conventional fibres, for instance Glass and Carbon, providing advantages in material processing therefore prolonging tooling life [42], [47].The problem with natural fibre composites is the fibre itself, with the major concern being the hydrophilic nature of the fibres. The hydrophilic properties of natural fibres make them incompatible with the matrix material which is commonly hydrophobic in nature. This commonly leads to adhesion between the fibre and matrix being poor. A vital requirement for successful fibre reinforcement is an excellent bond that will ensure the load is transferred between the fibre reinforcement and the matrix. Various methods have been tried to improve the bond strength between the fibre and the matrix. One such method is fibre surface treatment which modifies the surface of the fibre such that it makes more compatible for the matrix thereby creating a stronger bond. Another method is adding a coupling agent, also known as a compatibilizer, to the matrix material which allows it to react with the hydroxyl group present on the fibre's surface resulting in an improved compatibility between fibre and matrix.

The interfacial strength of jute and hemp fibre with a Polypropylene matrix was investigated by Park [58]. Park looked at the surface treatment and the addition of a coupling agent to the Polypropylene (PP) matrix in order to improve the interfacial strength. The coupling agent Maleic Anhydride Polypropylene (MAPP) combined with Polypropylene increased the interfacial strength between the fibre and matrix.

This result has also been observed by Peijs et al. [60]. The interfacial strength increased as the content of MAPP added to the PP increased. A reason for this increase in interfacial strength is that MAPP introduces polar groups to PP which allows the hydroxyl (OH) group in the fibre to react producing a covalent bond between the fibre and matrix [58]. A diagram of the reaction between MAPP and natural fibre OH group is shown in Figure 2.13 below.

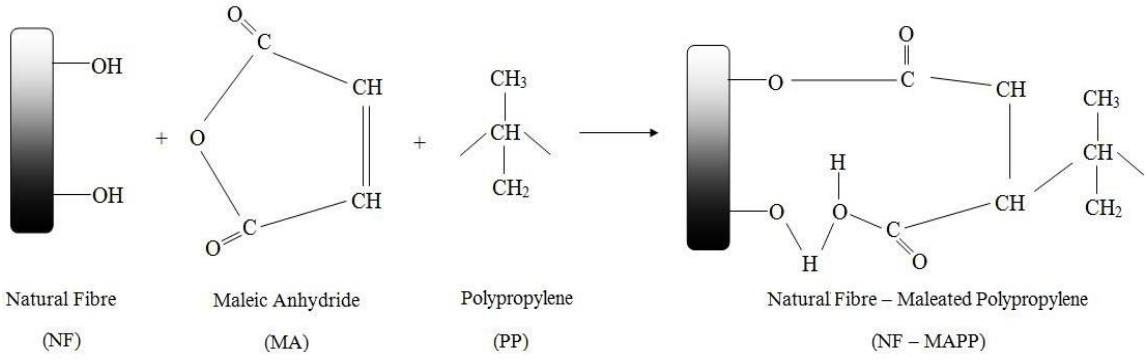

Figure 2.13: Chemical reaction between natural fibre's OH group and MAPP – PP [58]

Together with a coupling agent, Park also looked at the fibre surface treatment to improve the bond strength between the fibre and matrix. Surface treatment to natural fibres has also been investigated by several other researchers such as Valadez – Gonzalez [23] and Sydenstricker [62]. The general consensus from the research is that surface treatment of the fibre improves the properties of the composite due to improving the interaction between fibre and matrix. [58], [61]-[63]. There are many different types of surface treatment such as silane and acetylation but the most common one used is alkaline treatment in particular sodium hydroxide (NaOH). Sodium hydroxide removes parts of the hemicellulose, lignin and wax from the fibre surface creating a larger contact area which the matrix material can interact with.

Along with increasing the contact area, the surface roughness of the fibre increases, thus allowing for a better interaction between the fibre and the matrix [61], [63].

Mechanical properties of natural fibre composites such as impact, strength, modulus, fibre content and the effect of fibre length have also been studied by many researchers [60], [64]-[66]. Garkhail [60] reported upon Flax – PP composite and looked at the effect of fibre length and volume fraction on the mechanical properties of the composite. It was found that increasing the fibre length that was used in the matrix only slightly increases the modulus and strength of the composite but levels off after an optimum length, whereas the impact properties of composite are greatly influenced by the fibre length. Garkhail observed by a 'Notched Charpy Impact' test that increasing the fibre length increased the impact properties to an optimum length. Once past the optimum length, the impact properties either level off or decrease. This observation has also been made by Thomason on glass – fibre reinforced Polypropylene [67]. Baiardo [64] and Wambua [65] also investigated the effect of fibre volume fraction in natural fibre composites. All the researchers noted similar results to one another in that increasing the fibre volume fraction increased the modulus of the composite.

2.4 Fibre Anisotropy

It is essential to fully understand the relevant properties of the constituent materials, to effectively predict the properties of a composite. In certain cases for anisotropic fibre reinforced composites the simple relationship that is used to characterise isotropic materials is not sufficient. Therefore further investigation is needed to

successfully measure the thermal and mechanical behaviour of these fibres. In the case of natural and PET fibre, the majority of the research has focused on the longitudinal properties and not the degree of anisotropy of these fibres.

Few researchers have reported on the thermo - mechanical behaviour and degree of anisotropy in composites to help establish the fibres' true potential [68] – [71]. Ntenga et al. [68] used an inverse method which was developed by Levenberg – Marquardt to approximate the elastic anisotropy of Sisal and found that Sisal fibre was highly anisotropic. Baley et al. [69] used micromechanical models to estimate the transverse Young's modulus of Flax fibre. It was discovered that the transverse modulus was only 8 GPa compared to the fibre's longitudinal modulus of 59 GPa. Kawatabata [70] directly measured the transverse modulus of PET fibre by compression and found transverse modulus to be 1.09 GPa which is significantly lower than the longitudinal modulus of 15.6 GPa. Cickocki and Thomason [71] explored the five thermo – elastic constants (longitudinal, transverse and shear modulus, longitudinal and transverse coefficient of thermo expansion) over a temperature range using a specified volume fraction of unidirectional composites and micro – mechanical models. They noticed that the longitudinal Young's modulus of Jute exceeded the transverse modulus by a factor of five. The results above obtained by various researchers highlight the anisotropic nature of PET and natural fibre.

Pejis et al investigated the role of fibre anisotropy in the performance of Polyethylene fibre reinforced composites [72]. It was found that transverse and shear strength of the composite are influenced mainly by the highly anisotropic

characteristics of the Polyethylene fibre and not the bond between the matrix and the fibre.

2.5 Interface

The composite interface is where the load that is applied to the matrix is transferred to the fibre reinforcement. The bond between the fibre reinforcement and matrix strongly determines the mechanical properties of the composite [73]. Therefore the fibre reinforcement must have an excellent bond to improve the matrix strength and stiffness [74]. A critical requirement for successful reinforcement is an excellent interfacial bond which will guarantee load transfer from the matrix to the fibre reinforcement. To achieve a high-quality bond, good wetting of the fibres by liquid matrix is needed as the reinforcement and the matrix are brought into close contact. Once the reinforcement is wetted by the matrix bonding will occur. They are four main types of bonding mechanisms; mechanical bonding, electrostatic bonding, interdiffusion bonding and chemical bonding. Figure 2.14 below shows the various types of bonding mechanisms.

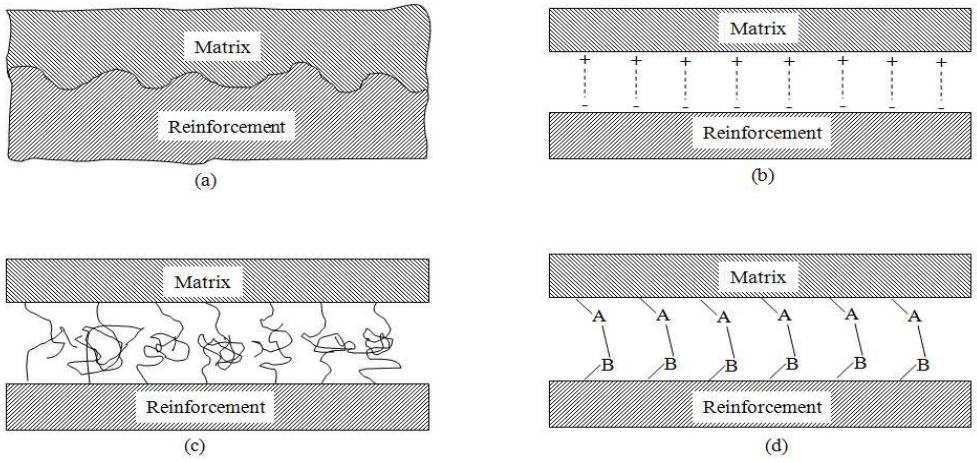

Figure 2.14: Four main bonding mechanisms

Mechanical mechanism, Figure 2.14a, also known as interlocking depends on the surface roughness of the reinforcement. The mechanical bonding is more effective the greater the reinforcement's surface roughness. The electrostatic mechanism, Figure 2.14b, occurs when the surface of the either the matrix or the reinforcement is positively charged and the other is negatively charged which produces an electrostatic attraction. Interdiffusion mechanism, Figure 2.14c, take place when the atoms or the molecules of the matrix and reinforcement interpenetrate. The chemical mechanism, Figure 2.14d, happens when a chemical bond is produced between the chemical groups on the reinforcement and matrix surface. The bond strength depends on the type of chemical bond and bonds produced per unit area.

The interfacial properties of the fibre/ matrix interface can be studied by micromechanical testing. There are four main micromechanical tests which are fragmentation , pull out, microindentation and microbond [73], [75], [76], and are shown below in Figure 2.15.

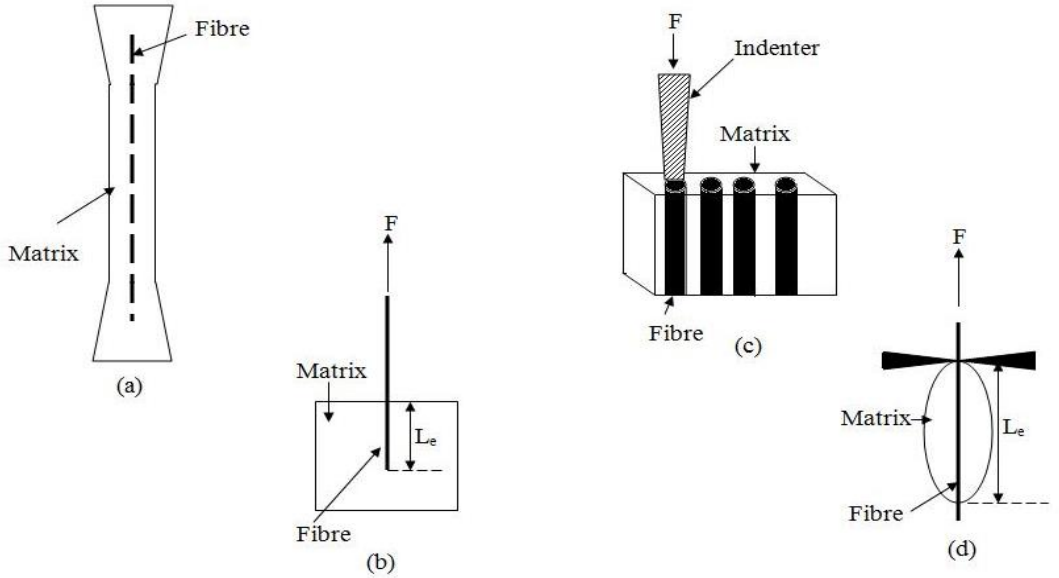

Figure 2.15: Micromechanical tests: a) fragmentation, b) pull out, c) microindentation and d) microbond

2.5.1 Single Fibre Pull Out Test

Single fibre pull out is the most commonly used test to measure interfacial shear strength due to its straightforward sample manufacturing and measurements [76]. The single fibre pull out test consists of one end of a single fibre embedded into the matrix at a desired length, Figure 2.15b. The matrix is constrained and a load is applied directly on to the fibre making the fibre be in tension. The force applied to the fibre increases until a maximum force, F_{max}, is achieved at which point the fibre completely debonds from the matrix. Just after complete debond a drop in the force is usually observed in the load – displacement curve. The fibre then starts to pull out of the matrix against internal frictional forces. F_{fr}. The force applied to the fibre will gradually decrease until the fibre is completely pulled out of the matrix. It has been reported that the fibre can initially debond from the matrix before F_{max} is achieved [77], [78]. Initial debond is caused by an initiation of a crack which propagates through the interface between the matrix and the fibre. The force keeps increasing till F_{max} due to the frictional force in the debonded region being included into the adhesive force from the intact region of the interface. Therefore once the F_{max} is achieved the crack propagation becomes unstable and the complete embedded length debonds from the matrix and the force drops to F_{fr}. This process can be seen clearly in force – displacement graph, Figure 2.16.

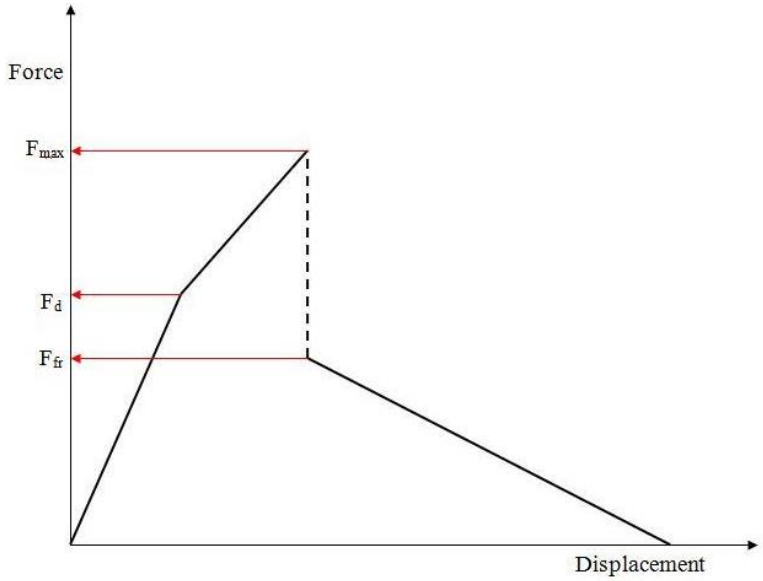

Figure 2.16: Force - Displacement Curve with initial debonding from matrix

After the pull out test, the apparent interfacial shear strength (IFSS), $\tau_{app,}$ can be approximated from the maximum force and the fibre's embedded area. The equation to estimate the apparent interfacial shear strength is shown below [50], [78] – [80].

$$\tau_{IFSS} = \frac{F_{max}}{\pi P l_e} \tag{2.1}$$

where P is the fibre's perimeter and l_e is the embedded length of the fibre in the matrix.

Equation 2.1 assumes that the shear stress is uniformly distributed along the fibre – matrix interface which is not the case. Therefore the IFSS established by using equation 2.1 can be used to compare the bond strength between different fibre and matrices.

Various models have been developed to describe the stress distribution along the interface and interfacial failure between the fibre and the matrix [75], [78], [81] –

[83]. These models are usually categorized under two types; Ultimate shear stress controlled approach and Energy controlled approach. The ultimate shear stress controlled approach is used to calculate the local shear stress at start point of where the fibre initially debonds from the matrix and remains constant regardless of crack length. The second approach, the energy controlled, is based on fracture mechanics and is used to calculate the energy released from the interface as the fibre debonds from the matrix. For more information about various types of Ultimate shear stress controlled approach and Energy controlled approach can be found in references [75], [78], [81], [82], [84].

2.6 Transcrystallisation

Transcrystallisation occurs in a fibre – polymer composite and occurs when the nucleation density of the fibre is higher than the nucleation density of the molten polymer. A transcrystalline layer is formed at the fibre / matrix interface which is highly orientated. The fibre's nucleation density disrupts the growth of the crystals by hindering the growth in the lateral direction, consequently forcing the crystals to grow in the only direction possible – perpendicular to the fibre. An example of a transcrystalline layer is shown below in Figure 2.17.

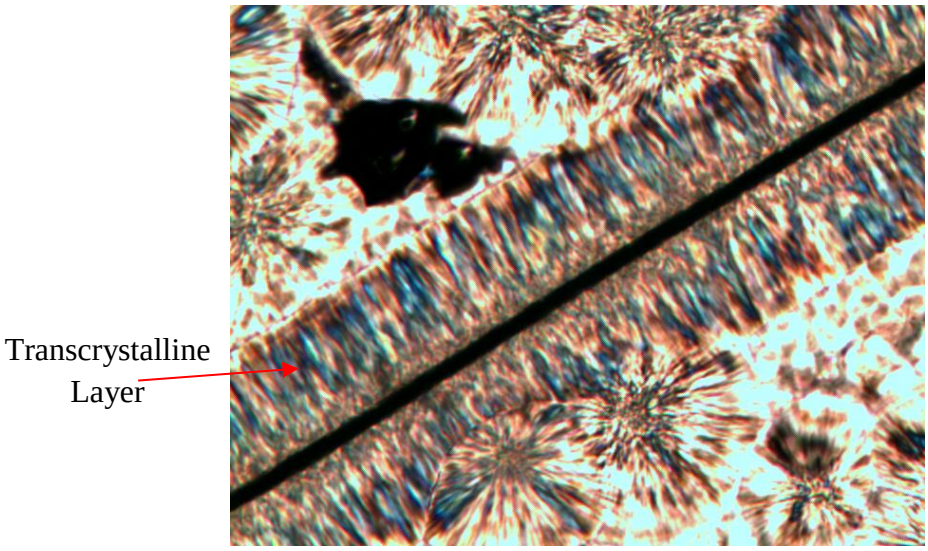

Figure 2.17: Transcrystalline layer on pitch carbon in a Polypropylene matrix

Transcrystallisation can be observed by various methods such as microscopy (Figure 2.17) and Differential Scanning Calorimetry (DSC). The crystallisation temperature and molecular weight of the polymer can control the transcrystallisation. The crystallisation temperature of the polymer affects the crystal growth, the crystal growth decreases as the crystallisation temperature of the polymer increases [85]. Folkes and Harwick [86] observed that at low molecular weight the greater the nucleation occurs along the fibre therefore as the molecular weight of the polymer increases the nucleation along the fibre decreases. This association can be related the melt flow index (MFI) of the polymer as the MFI has an inverse relationship to molecular weight. Therefore at high MFI, low molecular weight, the nucleation along the fibre is greatest.

PET and natural fibre has been reported to influence the crystallisation of PP due to the interaction between the crystals of PET and PP. The crystallisation temperature increases of PP in the presence of natural and PET fibre and can be seen by the DSC

[87] – [89]. Transcrystallisation is induced in the PP matrix as the fibres acts as a strong nucleation agent. The transcrystallinity depends on the concentration of fibre that is added to the PP matrix. At high concentration the fibres are close together inhibiting the development and expansion of the transcrystalline region, whereas at low concentration the transcrystalline region is well developed as the distance between fibres is large [32], [37]. PP-PET/natural fibre interface can be changed with the addition of compatilisers. The formation of transcrystallisation of PP spherulites on the fibres surface is prohibited by the presence of Maleic Anhydride (MA) compatibiliser. The modulus for PP-PET is higher than the PP-g-MAPP at the same volume fraction of fibre as the MA provokes the development of the transcrystalline morphology [39], [90]. It has also been noted that the addition of compatibiliser in the PP-PET blend obstructs the PET nucleating effect of the PP matrix during the melt cooling [39].

2.7 Summary

The literature review presented in this chapter shows that there is a lack of understanding of the anisotropic nature of the fibre that are being considered in this thesis. As mentioned in the review the nature of the fibre influences the properties of the composite. Due to the fibre anisotropic nature, the transverse properties of the fibre needs to be investigated. Very little research has investigated the transverse properties of PET, Sisal and Flax especially over a temperature range and the influence of these properties has on the whole composite. Along with the fibre anisotropic nature influencing composite behaviour, the interfacial shear strength also has an impact on the composite properties. The literature review shows that

there is a small volume of research investigating the interfacial shear strength between the natural fibres that are being considered (Sisal and Flax) in a Polypropylene matrix but no research at all for PET fibre in a Polypropylene matrix. The investigation into the interfacial shear strength is vital as it give an indication if the fibre can help improve the properties of the composite matrix. Another gap in the literature is lack of research using the natural fibre actual area/ perimeter to calculate the fibre properties and interfacial shear strength. The research presented in this thesis will address the gaps in the literature that is mentioned above and contribute to the knowledge base in the world of composites.

2.8 Reference

[1] G. Urbanczky, A. Jeziorny, "Peculiarities of the fine structure of PET fiber and the relationship to their basic properties and relationship to their basic physical properties," in *Polymer Handbook*, 1997, pp. 839 – 857.

[2] R. Guzatto, M. Becker da Roza, E. L. Gasparotto Denardin, and D. Samios, "Dynamical, morphological and mechanical properties of poly(ethylene terephthalate) deformed by plane strain compression," *Polym. Test.*, vol. 28, no. 1, pp. 24–29, Feb. 2009.

[3] R. De, P. Daubeny, C. W. Bunn, and C. J. Brown, "The crystal structure of Polyethylene Terephthalate," *Proc. R. Soc. A Math. Phys. Eng. Sci.*, vol. 226, pp. 531 – 542, 1954.

[4] L. H. Buxbaum, "The degradation of Polyethylene Terephthalate," *Angewandle Chem.*, vol. 7, no. 3, pp. 182 – 190, 1986.

[5] I. A. Abu - Isa, C. B. Jaynes, and J. F. O'Gara, "High-impact-strength Poly(ethylene terephthalate) (PET) from virgin and recycled resins," *Journal Appl. Polym. Sci.*, vol. 59, pp. 1957–1971, 1996.

[6] J. Gordon Cook, '*Handbook of textile fibres vol II man-made fibr*es', Woodhead Publishing Limited, 1984

[7] F. Awaja and D. Pavel, "Recycling of PET," *Eur. Polym. J.*, vol. 41, no. 7, pp. 1453–1477, Jul. 2005.

[8] R. Saint-Loup, T. Jeanmaire, J.-J. Robin, and B. Boutevin, “Synthesis of (Polyethylene Terephthalate/poly-caprolactone) Copolyesters,” *Polymer (Guild).*, vol. 44, no. 12, pp. 3437–3449, Jun. 2003.

[9] D. Paszun and T. Spychaj, “Chemical recycling of Poly(ethylene terephthalate),” *Ind. Eng. Chem. Res.*, vol. 36, no. 4, pp. 1373–1383, Apr. 1997.

[10] V. B. Gupta, A. K. Mukherjee, and S. . Cameotra, “Polyethylene Terephthalate fibres,” in *Manufacutred Fibre Technology*, 1997, pp. 271 – 318.

[11] F. S. Smith and R. D. Steward, “The crystallization of oriented Poly(ethylene terephthalate),” *Polymer (Guild).*, vol. 15, no. 5, pp. 283 – 286, 1974.

[12] A. Ajji, J. Gu, K. C. Cole, and M. M. D, “Orientation and structure of drawn Poly (ethylene terephthalate),” Polymer (Guild)., vol. 37, no. 16, pp. 3707–3714, 1996.

[13] P. G. Schmidt, “Polyethylene Terephthalate structural studies,” *J. Polym. Sci. Part A Gen. Pap.*, vol. 1, no. 4, pp. 1271 – 1292, 1963.

[14] V. B. Gupta and S. Kumar, “The effect of heat setting on the structure and mechanical properties of Poly(ethylene Terephthalate) fiber . I . structural Changes,” *Polymer (Guild*)., vol. 26, pp. 1865–1876, 1981.

[15] V. B. Gupta and S. Kumar, “The effect of heat setting on the structure and mechanical properties of Poly (ethylene Terephthalate) fiber . 111 . anelastic properties and their dependence on structure,” *Polymer (Guild).*, vol. 26, pp. 1885–1895, 1981.

[16] I. M. Ward, “The molecular structure and mechanical properties of Polyethylene Terephthalate fibers,” *Text. Res. J.*, vol. 31, no. 7, pp. 650–664, Jul. 1961.

[17] J. H. Dumbleton, “Spin orientation measurement in Polyethylene Terephthalate,” *Text. Res. J.*, vol. 40, no. 11, pp. 1035–1041, Nov. 1970.

[18] S. W. Allison and I. Ward, “The cold drawing of Polyethylene Terephthalate,” *Br. J. Appl. Phys.*, vol. 18, pp. 1151 – 1164, 1967.

[19] I. M. Ward and J. S. Foot, “The cold drawing of amorphous Polyethylene Terephthalate,” *J. Mater. Sci.*, pp. 955 – 960, 1975.

[20] N. V. Bhat and S. G. Naik, “Effect of drawing of Poly(ethylene Terephthalate) fiber on molecular orientation,” *Text. Res. J.*, vol. 54, no. 12, pp. 868–874, Dec. 1984.

[21] D. J. Blundell, A. Mahendrasingam, C. Martin, W. Fuller, D. H. Mackerron, and J. L. Harvie, “Orientation prior to crystallisation during drawing of Poly (ethylene Terephthalate),” *Polymer (Guild).*, vol. 41, no. 2000, pp. 7793–7802, 2002.

[22] R. Huisman and H. . Heuvel, “The effect of spinning speed and drawing temperature on structure and properties,” *J. Appl. Polym. Sci.*, vol. 37, pp. 595–616, 1989.

[23] V. B. Gupta and S. Kumar, “The effect of heat setting on the structure and mechanical properties of Poly (ethylene Terephthalate) fiber . IV. tensile properties other than modulus and their dependence on structure,” *Polymer (Guild).*, vol. 26, pp. 1897–1905, 1981.

[24] D. Hwan Cho, W.-R. Yu, J. H. Youk, and J. H. Yoo, “POLYMER Formation of micro-crystals in Poly (ethylene Terephthalate) fiber by a short heat treatment and their influence on the mechanical properties,” *Eur. Polym. J.*, vol. 43, pp. 3562–3572, 2007.

[25] W. Okumura, Y. Ohkoshi, Y. Gotoh, M. Nagura, H. Urakawa, and K. Kajiwara, “Effects of the drawing form and draw ratio on the fiber structure and mechanical properties of CO 2 -laser-heated- drawn Poly (ethylene Terephthalate) fibers,” *J. Polym. Sci. Part B Polym. Phys.*, vol. 42, no. 1, pp. 79–90, 2004.

[26] A. Rudolf, J. Gersak, and M. S. Smole, “The effect of heat treatment conditions using the drawing process on the properties of PET filament sewing thread,” *Text. Res. J.*, vol. 82, no. 2, pp. 161–171, Oct. 2011.

[27] T. Kunugi, A. Suzuki, and M. Hashimoto, “Mechanical properties and superstructure of high-modulus and high-strength PET fiber prepared by zone annealing,” *J. Appl. Polym. Sci.*, vol. 26, no. 6, pp. 1951–1960, Jun. 1981.

[28] A. Suzuki and N. Mochiduki, “Mechanical properties and superstructure of poly(ethylene terephthalate) fibers zone-drawn and zone-annealed by CO2 laser heating,” *J. Appl. Polym. Sci.*, vol. 82, no. 11, pp. 2775–2783, Dec. 2001.

[29] T. Kunugi and A. Suzuki, “Preparation of high-modulus Poly(ethylene Terephthalate) fibers by vibrating hot drawing,” *J. Appl. Polym. Sci.*, vol. 62, pp. 713–719, 1996.

[30] V. B. Gupta and S. Kumar, “The effect of heat setting on the structure and mechanical properties of Poly (ethylene Terephthalate) fiber . 11 . the elastic modulus and its dependence on structure,” *Polymer (Guild).*, vol. 26, pp. 1877–1884, 1981.

[31] M. M. Abolhasani, A. A. Azar, and S. Shokoohi, “PET / EVA / PP ternary blends : an Investigation of extended morphological properties,” *J. Appl. Polym. Sci.*, vol. 3, no. November 2008, 2009.

[32] X. Si, L. Guo, Y. Wang, and K. Lau, “Preparation and study of Polypropylene/Polyethylene Terephthalate composite fibres,” *Compos. Sci. Technol.*, vol. 68, no. 14, pp. 2943–2947, Nov. 2008.

[33] K. Friedrich, M. Evstatiev, S. Fakirov, O. Evstatiev, M. Ishii, and M. Harrass, “Microfibrillar reinforced composites from PET/PP blends: processing, morphology and mechanical properties,” *Compos. Sci. Technol.*, vol. 65, no. 1, pp. 107–116, Jan. 2005.

[34] P. Taepaiboon, J. Junkasem, R. Dangtungee, T. Amornsakchai, and P. Supaphol, “In situ microfibrillar-reinforced composites of isotactic Polypropylene/recycled Poly(ethylene Terephthalate) system and effect of compatibilizer,” *J. Appl. Polym. Sci.*, vol. 102, no. 2, pp. 1173–1181, Oct. 2006.

[35] X. D. Lin and W. L. Cheung, “Study on PET / PP microfibrillar composites . I . morphological development in melt extrusion,” *Polymer (Guild).*, no. January 2001, 2002.

[36] K. Jayanarayanan, S. S. Bhagawan, S. Thomas, and K. Joseph, “Morphology development and non isothermal crystallization behaviour of drawn blends and microfibrillar composites from PP and PET,” *Polym. Bull.*, vol. 60, no. 4, pp. 525–532, Dec. 2007.

[37] C. Saujanya and S. Radhakrishnan, “Structure development and properties of PET fibre filled PP composites,” *Polymer (Guild).*, vol. 42, pp. 4537–4548, 2001.

[38] M. K. Cheung and D. Chan, “Mechanical and rheological properties of Poly(ethylene terephthalate)/ Polypropylene blends,” *Polym. Int.*, vol. 43, no. 3, pp. 281–287, Jul. 1997.

[39] Y. X. Pang, D. qJia, H. J. Hu, D. J. Hourston, and M. Song, “Effects of compatiblizing agent on the morphology, interface and mechanical behaviour of Polypropylene/ Polyethylene Terephthalate blends,” *Polymer (Guild).*, pp. 357 – 365, 2000.

[40] S. Kalia, B. S. Kaith, I. Kaur, S. Thomas, S. A. Paul, L. A. Pothan, and B. Deepa, Cellulose Fibers: Bio - and Nano - Polymer Composites. *Berlin, Heidelberg: Springer Berlin Heidelberg,* 2011, pp. 1 – 758.

[41] J. Mussig, *Industrial Applications of Natural Fibres*. Chichester, UK: John Wiley & Sons, Ltd, 2010, pp. 1 – 564.

[42] A. K. Bledzki and J. Gassan, "Composites reinforced with cellulose based fibres," *Prog. Polym. Sci*., vol. 24, pp. 221–274, 1999.

[43] B. Wielage, T. Lampke, G. Marx, K. Nestler, and D. Starke, "Thermogravimetric and differential scanning calorimetric analysis of Natural fibres and Polypropylene," *Thermochim. Acta*, vol. 337, pp. 169–177, 1999.

[44] M. Tajvidi and A. Takemura, "Thermal degradation of Natural fiber-reinforced Polypropylene composites," *J. Thermoplast. Compos. Mater*., vol. 23, no. 3, pp. 281–298, Sep. 2009.

[45] T. Nguyen, E. Zavarin, and E. M. Barrall II, "Thermal analysis of lignocellulosic part 1. unmodified materials," *J. macromolecular Sci. Part C Polym. Rev.*, vol. 20, no. 1, 1981.

[46] S. J. Eichhorn, A. Dufresne, M. Aranguren, N. E. Marcovich, J. R. Capadona, S. J. Rowan, C. Weder, W. Thielemans, M. Roman, S. Renneckar, W. Gindl, S. Veigel, J. Keckes, H. Yano, K. Abe, M. Nogi, a. N. Nakagaito, A. Mangalam, J. Simonsen, a. S. Benight, A. Bismarck, L. a. Berglund, and T. Peijs, "Review: current international research into cellulose nanofibres and nanocomposites," *J. Mater. Sci.*, vol. 45, no. 1, pp. 1–33, Sep. 2009.

[47] L. Y. Mwaikambo, M. P. Ansell, A. Dufresne, M. Hughes, C. Hill, and P. M. Wild, "Current international research into cellulosic fibres and composites," *J. Mater. Sci*., vol. 36, pp. 2107–2131, 2001.

[48] A. Stamboulis, C. A. Baillie, and T. Peijs, "Effects of environmental conditions on mechanical and physical properties of Flax fibers," Compos. *Part A Appl. Sci. Manuf*., vol. 32, pp. 1105 – 1115, 2001.

[49] C. Baley, "Analysis of the Flax fibres tensile behaviour and analysis of the tensile stiffness increase," *Compos. Part A Appl. Sci. Manuf*., vol. 33, pp. 939–948, 2002.

[50] V. A. Alvarez, R. A. Ruscekait, and A. Vazquez, "Mechanical properties and water absorption behaviour of composites made from a biodegradable matrix and alkaline - treated Sisal fibers," *J. Compos. Mater*., vol. 37, no. 17, pp. 1575 – 1590, 2003.

[51] G. Schoolenberg and J. L. Thomason, “An investigation of Glass fibre/Polypropylene interface strength and its effect on compsite properties,” Composites, vol. 25, no. 3, pp. 197–203, 1994.

[52] A. K. Bledzki, S. Reihmane, and J. Gassan, “Properties and modification methods for Vegetable fibers for Natural fiber composites,” *J. Appl. Polym. Sci.*, vol. 59, no. 8, pp. 1329–1336, Feb. 1996.

[53] A. G. Kulkarni, K. G. Satyanarayana, K. Sukumaran, and P. K. Rohatgi, “Mechanical behaviour of Coir fibres under tensile load,” *J. Mater. Sci*., vol. 16, no. 4, pp. 905–914, Apr. 1981.

[54] G. C. Davies and D. M. Bruce, “Effect of environmental relative humidity and damage on the tensile properties of Flax and Nettle fibers,” *Text. Res. J.*, vol. 68, no. 9, pp. 623–629, Sep. 1998.

[55] B. Lamy and C. Baley, “Stiffness prediction of Flax fibers-epoxy composite materials,” *J. Mater. Sci. Lett*., vol. 19, pp. 979–980, 2000.

[56] P. S. Mukherjee and K. G. Satyanarayana, “Structure and properties of some Vegetable fibres, Part 1 Sisal Fibre,” *J. Mater. Sci.*, vol. 19, pp. 3925 – 3934, 1984.

[57] J. L. Thomason, J. Carruthers, J. Kelly, and G. Johnston, “Fibre cross - section determination and variability in Sisal and Flax and its effects on fibre performance characterisation,” *Compos. Sci. Technol*., vol. 71, pp. 1008 – 1015, 2011.

[58] J.-M. Park, S. T. Quang, B.-S. Hwang, and K. L. DeVries, “Interfacial evaluation of modified jute and hemp fibers/Polypropylene (PP)-maleic anhydride Polypropylene copolymers (PP-MAPP) composites using micromechanical technique and nondestructive acoustic emission,” *Compos. Sci. Technol*., vol. 66, no. 15, pp. 2686–2699, Dec. 2006.

[59] H. L. Bos, K. Molenveld, W. Teunissen, K. C. Wmc, P. O. Box, and A. A. Wieringerwerf, “Compressive behaviour of unidirectional Flax fibre,” *J. Mater. Sci.*, vol. 39, pp. 2159–2168, 2004.

[60] S. K. Garkhail, R. W. H. Heijenrath, and T. Peijs, “Mechanical properties of Natural-fibre-mat- reinforced thermoplastics based on Flax fibres and Polypropylene,” *Appl. Compos. Mater*, vol. 7, pp. 351–372, 2000.

[61] A. Valadez-Gonzalez, J. M. Cervantes-uc, R. Olayo, and P. J. Herrera-franco, “Effect of fiber surface treatment on the fiber – matrix bond strength of

Natural fiber reinforced composites," *Compos. Part B Eng.*, vol. 30, pp. 309–320, 1999.

[62] T. H. . Sydenstricker, S. Mochnaz, and S. C. Amico, "Pull-out and other evaluations in Sisal-reinforced Polyester biocomposites," *Polym. Test.*, vol. 22, no. 4, pp. 375–380, Jun. 2003.

[63] X. Li, L. G. Tabil, and S. Panigrahi, "Chemical treatments of Natural fiber for use in Natural fiber-reinforced composites: A Review," *J. Polym. Environ.*, vol. 15, no. 1, pp. 25–33, Jan. 2007.

[64] M. Baiardo, E. Zini, and M. Scandola, "Flax fibre - Polyester composites," *Compos. Part A Appl. Sci. Manuf.*, vol. 35, no. 6, pp. 703 – 710, 2004.

[65] P. Wambua, J. Ivens, and I. Verpoest, "Natural fibres: can they replace Glass in fibre reinforced plastics?," *Compos. Sci. Technol.*, vol. 63, no. 9, pp. 1259–1264, Jul. 2003.

[66] P. Herrera-Franco and A. Valadez-González, "Mechanical properties of continuous Natural fibre-reinforced polymer composites," *Compos. Part A Appl. Sci. Manuf.*, vol. 35, no. 3, pp. 339–345, Mar. 2004.

[67] J. L. Thomason and M. Vlug, "Influence of fibre length and concentration on properties of Glass fibre reinforced Polypropylene: 1. tensile and flexural modulus," *Compos. Part A Appl. Sci. Manuf.*, vol. 27, no. 6, pp. 477 – 484, 1996.

[68] R. Ntenga, A.Béakou, J. Atangana Atéba, and L. Ayina Ohandja, "Estimation of the elastic anisotropy of Sisal fibres by an inverse method," *J. Mater. Sci.*, vol. 43, no. 18, pp. 6206–6213, Aug. 2008.

[69] C. Baley, Y. Perrot, F. Busnel, H. Guezenoc, and P. Davies, "Transverse tensile behaviour of unidirectional plies reinforced with Flax fibres," *Mater. Lett.*, vol. 60, no. 24, pp. 2984–2987, Oct. 2006.

[70] S. Kawabata, "Micromeasurement of the mechanical properties of single fibers," in *Modern Textile Characteristics Method*, 1996, pp. 311 – 329.

[71] F. R. Cichocki Jr and J. L. Thomason, "Thermoelastic anisotropy of Natural fiber," *Compos. Sci. Technol.*, vol. 62, pp. 669–678, 2002.

[72] T. Peijs, H. a. Rijsdijk, J. M. M. De Kok, and P. J. Lemstra, "The role of interface and fibre anisotropy in controlling the performance of Polyethylene-fibre-reinforced composites," *Compos. Sci. Technol.*, vol. 52, no. 3, pp. 449–466, Jan. 1994.

[73] L. Zong - Fu and D. T. Grubb, “Single-fibre polymer composites,” *J. Mater. Sci., vol.* 29, pp. 189–202, 1994.

[74] F. L. Matthews and R. D. Rawlings, *Composite Materials: Engineering and Science*. Woodhead Publishing Limited, 1999.

[75] M. R. Piggott, “The single-fibre pull out method: its advantages, interpretation and experimental realization,” *Compos. Interface*s, vol. 1, no. 3, pp. 211–223, 1993.

[76] C. Wang, “Fracture mechanics of single-fibre pull-out test,” *J. Mater. Sci*., vol. 32, pp. 483–490, 1997.

[77] E. Pisanova, S. Zhandarov, and E. Mader, “How can adhesion be determined from micromechanical tests ?,” *Compos. Part A Appl. Sci. Manuf.*, vol. 32, pp. 425–434, 2001.

[78] E. Mader and S. Zhandarov, “Characterization of fiber/matrix interface strength: applicability of different tests, approaches and parameters,” *Compos. Sci. Technol*., vol. 65, no. 1, pp. 149–160, Jan. 2005.

[79] L. Yang and J. L. Thomason, “Interface strength in Glass fibre–Polypropylene measured using the fibre pull-out and microbond methods,” *Compos. Part A Appl. Sci. Manuf*., vol. 41, no. 9, pp. 1077–1083, Sep. 2010.

[80] J. P. Craven, R. Cripps, and C. Viney, “Evaluating the silk/epoxy interface by means of the microbond Test,” *Compos. Part A Appl. Sci. Manuf*., vol. 31, no. 7, pp. 653–660, Jul. 2000.

[81] R. J. Scheer and J. A. Nairn, “A comparison of several fracture mechanics methods for measuring interfacial toughness with microbond tests,” *J. Adhes.*, vol. 53, no. 1–2, pp. 45–68, Sep. 1995.

[82] J. A. Nairn, “Analytical fracture mechanics analysis of the pull out test including the effects if friction and thermal stresses,” *Adv. Compos. Lett.*, vol. 9, no. 6, pp. 373–383, 2000.

[83] P. S. Chua and M. R. Piggott, “The Glass fibre-polymer Interface : II work of fracture and shear stresses,” *Compos. Sci. Technol*., vol. 22, pp. 107–119, 1985.

[84] P. S. Chua and M. R. Piggott, “The Glass fibre-polymer interface : I theoretical consideration for single fibre pull-out tests,” *Compos. Sci. Technol.*, vol. 22, pp. 33–42, 1985.

[85] H. Quan, Z.-M. Li, M.-B. Yang, and R. Huang, “On transcrystallinity in semi-crystalline polymer composites,” *Compos. Sci. Technol.*, vol. 65, no. 7–8, pp. 999–1021, Jun. 2005.

[86] M. J. Folkes and S. Hardwick, “The molecular weight dependence of transcrystallinity in fibre reinforced thermoplastic,” *J. Mater. Sci. Lett.*, vol. 3, pp. 1071 – 1073, 1984.

[87] M. Arroyo and M. A. Lo, “Thermal and dynamic mechanical properties of Polypropylene and short organic fiber composites,” *Polymer (Guild).*, vol. 41, pp. 7761–7767, 2000.

[88] M. A. López Manchado, M. Arroyo, J. Biagiotti, and J. M. Kenny, “Enhancement of mechanical properties and interfacial adhesion of PP/EPDM/Flax fiber composites using Maleic Anhydride as a compatibilizer,” *J. Appl. Polym. Sci.*, vol. 90, no. 8, pp. 2170–2178, Nov. 2003.

[89] G. Eder, P. Phinyocheep, N. Suppakarn, and W. Sutapun, “Quiescent crystallization of natural fibers – Polypropylene composites,” *J. Appl. Polym. Sci.*, vol. 106, pp. 2997 – 3006, 2007.

[90] A. Ershad-langroudi, F. Jafarzadeh-dogouri, and M. Razavi-nouri, “Mechanical and thermal properties of Polypropylene / recycled Polyethylene Terephthalate / chopped Rice husk composites,” *Polymer (Guild).*, 2008.

Chapter 3

Initial Characterisation of Fibres

3.1 Introductionary Remarks

The chapter describes the experimental investigation on characterising the candidate materials. A description of the experiments undertaken and results for each material that is being investigated is presented in this chapter.

3.2 Experimental Programme

Various experiments were carried out to characterize PET, Sisal and Flax fibres. The fibres were supplied from various companies. PET fibre was obtained from SABIC. Sisal and Flax were acquired from Wigglesworth and sourced from Brazil and Germany respectively. The experiments consisted of single fibre tensile testing, bundle tensile testing, thermogravimetric analysis (TGA) and differential scanning calorimetry (DSC). In order to gain the best results, care must be taken over sample preparation and the tests were carried out on standardised equipment. The fibre properties that were characterised were the axial modulus, strength and crystallisation and degradation temperatures of the fibres. Single fibre tensile test was also carried out on thermally treated PET due to a phenomenon occurring when undertaking single fibre pull out experiment in Chapter 5. Full details of the sample preparation and experimental procedure are detailed in the following sections.

3.2.1 Single Fibre Tensile Testing

3.2.1.1 Sample Preparation

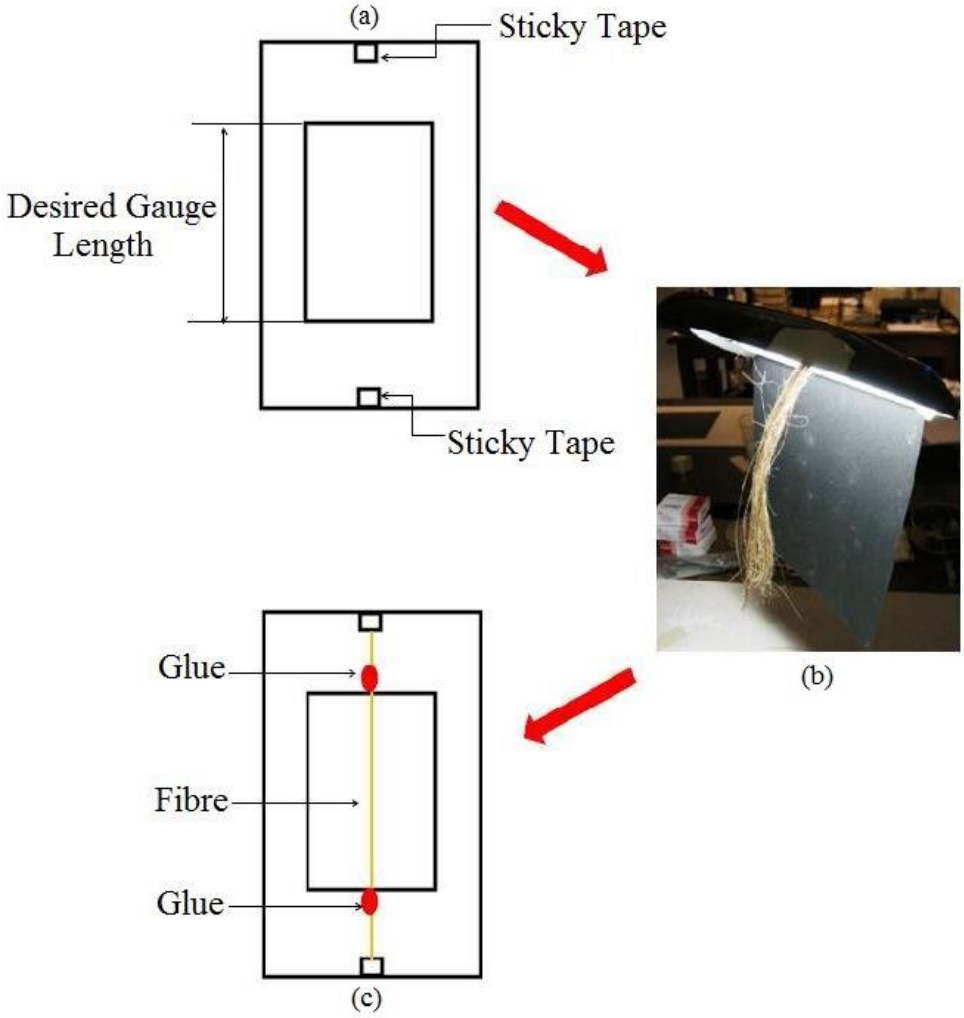

Figure 3.1: Tensile test preparation

The single fibre tensile test is important as it measures the fibre's Young's modulus and strength on an individual fibre basis. The preparation of test samples is shown in Figure 3.1. A window of the desired gauge length was cut out of the hard card (250 gsm) using a scalpel and a ruler. Small tabs of double sided sticky tape were place at each end of the card and this can be seen in Figure 3.1a. A bundle of fibres was cut

from a fibre roving. The bundle was then attached to a lamp so that the extraction of single fibres would be made easier (Figure 3.1b). Single fibres were carefully removed from the bundle using tweezers trying not to touch the part of the fibre that is being used as the gauge length. The single fibre was placed across the card and temporary held in place using the tabs of tape. A small droplet of Loctite gel superglue was placed at edge of the gauge length ends to permanently stick the fibre to the card (Figure 3.1c). Once the super glue had dried the apparent diameter of the fibre was then measured, using a Nikon Epiphot inverted optical microscope and associated image analysis software, Figure 3.2. The fibre's diameter was measured several times along its length and the average of the diameter was used to estimate the fibre cross sectional area.

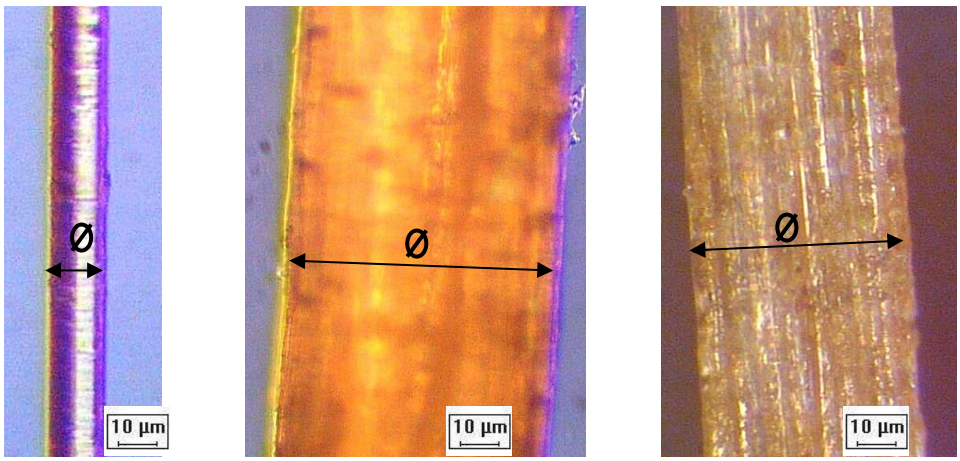

(a) (b) (c)

Figure 3.2: Measurement of diameter a) PET, b) Sisal & c) Flax

3.2.1.2 Tensile Test Study

The tensile test sample was attached to an Instron 3342 Tensile Test machine which can be seen in Figure 3.3. The specimen was attached by a vice clamp at the bottom and by either a bulldog clip or vice clamp at the top of the machine depending on the type of fibre and load cell used. Table 3.1 shows the test parameters for each type of fibre used. The 100N load cell and the vice clamp was used for the natural fibres due to the higher loads required and the increased probability of fibre slippage.

Table 3.1: Fibre test parameters

Fibre Type	Clamp (Vice or Bulldog)	Load Cell (10 or 100N)
PET	Bulldog	10
Sisal	Vice	100
Flax	Vice	100

The card window was cut at both sides in the middle to allow the fibre to hang freely as shown in Figure 3.3.

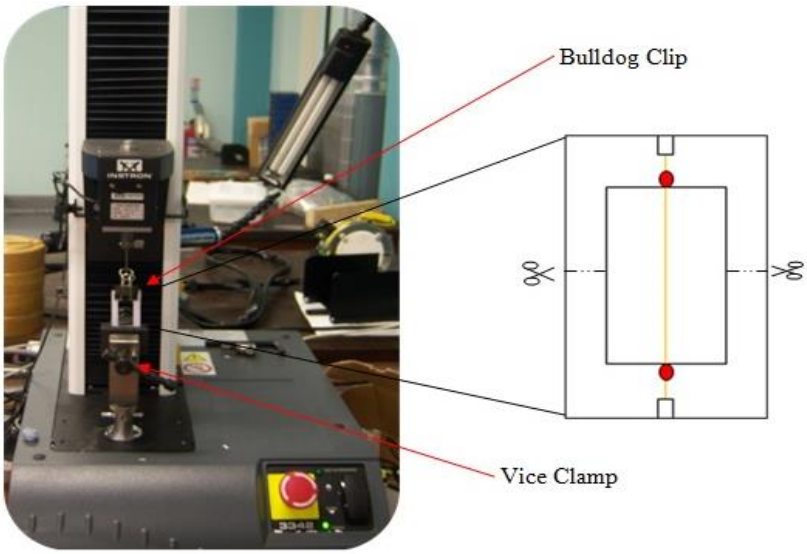

Figure 3.3: Setup of sample on the tensile test machine

The program to control the Instron machine was commercial software called Bluehill revision two. The input values needed for the Bluehill software to calculate the fibre's modulus and strength were the gauge length and fibre's diameter.

The extension rate of the crosshead was set according to the ASTM D3822-01 standards for each type of fibre tested, for example natural fibre's strain rate was set at 5% per minute [1]. At least three different gauge lengths were tested which allowed the true fibre modulus to be calculated and to observe the effect of gauge length on the fibre's strength and modulus. The Bluehill software creates a real time load versus extension graph and an example of one can be seen in Figure 3.4.

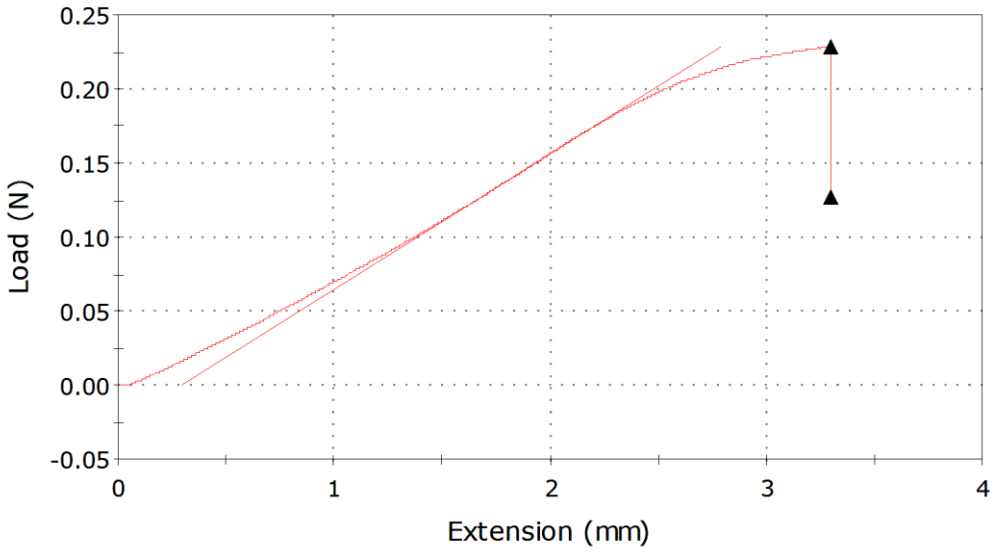

Figure 3.4: Typical tensile test graph for PET

The Bluehill software uses 'load – extension' graph to calculate the strength and modulus of the fibre. Equation 3.1 is the equation used in the software to calculate the strength of the fibre.

$$\sigma = \frac{F_{max}}{A_f} \tag{3.1}$$

where σ is the fibre strength, F_{max} is the maximum force to break the fibre and this is taken from the load – extension graph and A_f is the cross sectional area of the fibre. The modulus of the fibre is calculated differently as it uses the gradient of the slope on the 'load – extension' graph.

$$E = \frac{L}{A_f}\frac{[F_2 - F_1]}{[l_2 - l_1]} = \frac{L}{A_f}\frac{\Delta F}{\Delta l} \tag{3.2}$$

where E is the Young's modulus, L is the gauge length, F and l is taken from the 'load – extension' graph and is the force and extension respectively.

For a more accurate estimation of the Young's modulus, it is advised to take in to account the system compliance. A detailed description of the method can be found in [2, 3]. In the experiment the single fibres are mounted on to card therefore leading to the whole system compliance, C_S, having to be calculated. This is done by assuming that the specimen is entirely straight in the loading direction and that throughout the course of the test there is no slippage before the break. The measured displacement, ΔL when the fibre is fully strained is the total of the fibre's extension, Δl_f and the deformation of the system, Δl_s. The system deformation takes in to account the glue, card and clamp.

$$\Delta L = \Delta l_f + \Delta l_s \tag{3.3}$$

Combining the equations 3.2 and 3.3,

$$\frac{1}{E} = \frac{1}{E_f} + C_s \frac{A_f}{l_f} \quad (3.4)$$

where E is the measured fibre modulus and $C_S = \frac{\Delta l_s}{\Delta F}$ is the system compliance. A graph of (1/E) versus (A_f/l_f) is plotted. The system compliance is the gradient of the trendline and the intercept at which the trendline crosses the y – axis is $1/E_f$. An example is shown in Figure 3.15 on page 81.

3.2.1.3 Cross Sectional Area & Perimeter of Natural Fibres

In order to obtain a better estimate of the properties of natural fibres, an additional action was taken at the end of the natural fibre tensile testing. Throughout the tensile test, the natural fibres were assumed circular, in order to estimate the fibres cross section. However this is not the case, therefore to get a more accurate estimate of strength and modulus the cross sectional area had to be measured. Along with determining the cross sectional area, the perimeter was also analysed. The ends of the fibres, that had not gone through the tensile test, (fibre attached to the card window) were used for further analysis as the tested fibre section would be damaged and therefore removed using a scalpel. Both ends of the fibre were used from each tensile test sample and attached to a card with superglue as shown in Figure 3.5a. The fibres were then embedded in epoxy resin supplied by Sturers vertically and left for 24 hours for the resin to set, Figure 3.5b. Once the resin had set, the block of resin was ground and polished to prepare the sample for observation under the microscope, Figure 3.5c. The preparation stage was split up in to two stages, grind and polish.

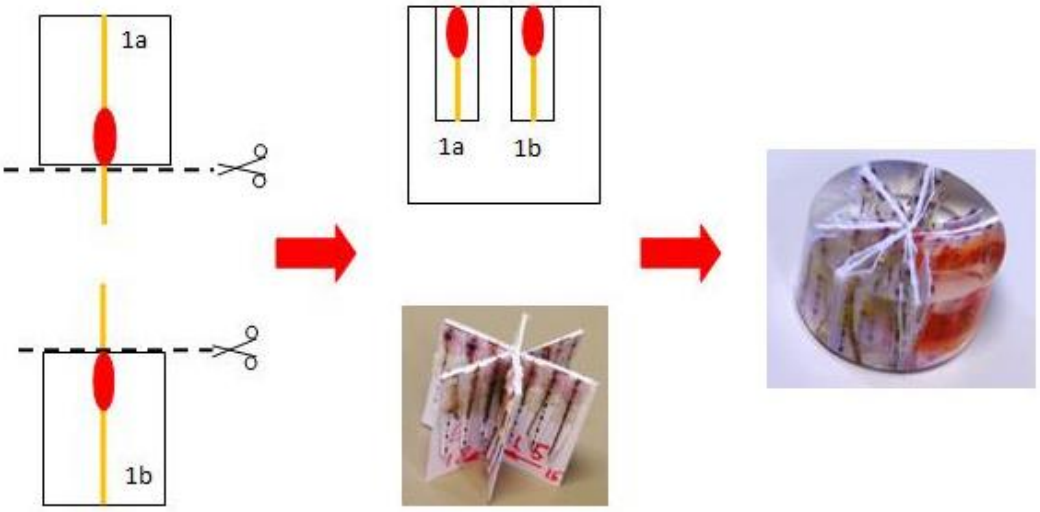

Figure 3.5: Natural fibre cross sectional preparation

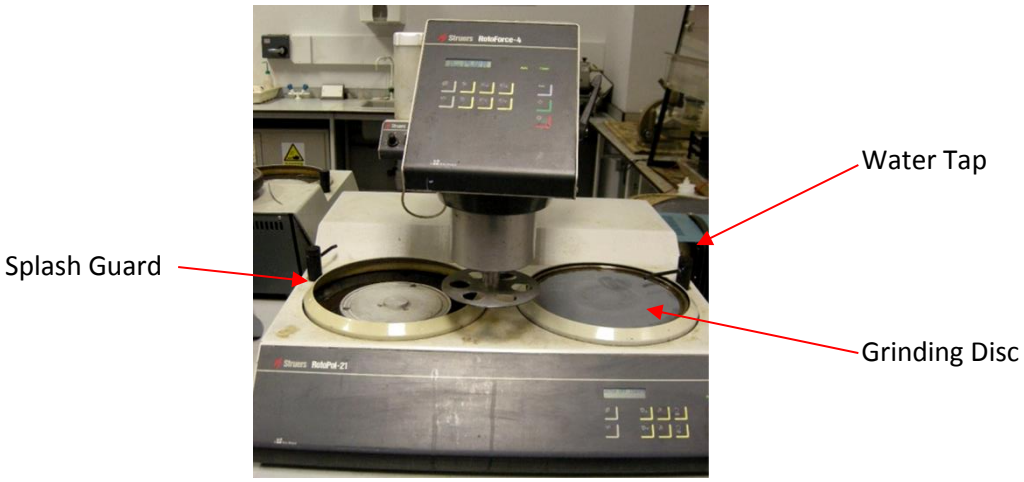

Figure 3.6: Struers rotopol 21 machine (grinding and polishing)

The machine used for the grinding stage was Struers Rotopol 21 and is shown Figure 3.6. Grinding is an essential step in the preparation of cross section analysis as it allows an even surface of the resin to be achieved which makes it easier to see under the microscope. Three different grades of grinding paper were used in this stage, 120,

1200 and 2400 each paper getting finer which reduces the amount of material removed from the resin block. For each grade of paper the following process was carried out.

1. The grinding paper was placed in the holder and a water jet was placed in a position so that the water would spread over the whole grinding paper. The water jet was used as it acted as a lubricant and removed the resin debris away from the sample.
2. The rotation speed used was set to 300 rpm. Once the machine had been set up it was ready to grind the block of resin. The block of resin was turned clockwise slowly throughout the grinding process to ensure that the surface of the resin was even. In addition to rotating the resin, the sample was checked frequently to make sure that amount of resin removed was sufficient and that the surface was even.

The polishing stage started once an acceptable surface finish was achieved in the grinding process. This stage removes scratches from the surface of the resin caused by grinding and creates a shiny mirror like finish which allows the fibres to be seen clearly under the microscope. The polishing stage was carried out on the same machine as the grinding stage but a few parameters were changed. A napless cloth replaced the grinding paper and a diamond solution (diamond suspension three microns and diamond polish blue lubricant) replaced the water. The rotation speed of the machine was lowered to 150 rpm. This was done to get more precision and control when polishing and to limit the amount of diamond solution used as it is very expensive. After the sample is polished the diamond solution needed to be washed off. The diamond solution creates an oily layer making the cross section of the fibres

hard to see. The sample was washed off using liquid soap and warm water. The resin was left to dry under a dryer as the surface can be easily scratched.

Figure 3.7: L.H.S - Grinding paper, R.H.S - Napless cloth

Once the grinding and polishing stage had been completed, the sample observed under the microscope. An Olympus GX51microscope was used to observe the cross section of the fibre. The magnification used ranged between x 200 to x 500 and for each fibre cross section a picture was taken. The pictures were noted with the magnification and tensile test number to help in the analysis of results later in the process.

The pictures were used to determine the cross sectional area and perimeter of the fibre. Before using the image analysis software, the picture of the fibre cross section has to go through four steps before analysis.

1. The picture is imported in to PowerPoint and enlarged to fit the entire slide. This helps in step 2.

2. The cross section of the fibre is traced using the free form tool. The free form tool allows the user to trace around the fibre as accurately as possible and then change points if necessary. (Figure 3.8a)
3. The paint tool was then used to fill in the fibre area. (Figure 3.8b)
4. The filled in area is then imported in to paint and saved as a jpeg file, ready to be analysed using the image analysis software. (Figure 3.8c)

The jpeg image created in paint was imported into the image analysis software and formatted into binary. Changing the image into binary format allowed the pixels of the picture to be used to calculate the area and perimeter of the fibre. The calibration image went through the same process to allow the image analysis software to accurately determine the fibre area and perimeter which could then be used in the calculation of the single fibre properties and the interfacial shear strength (see Chapter 5 Section 5.3.1).

(a) (b) (c)

Figure 3.8: Cross section preparation for image analysis software

3.2.3 Differential Scanning Calorimetry (DSC)

Differential scanning calorimetry (DSC) measures the heat flow and temperature related to the material transitions as a function of temperature or time. Material

transitions that can be observed and measured are melting point, crystallisation, specific heat capacity and glass transition.

Figure 3.9: DSC set up for TA Q20

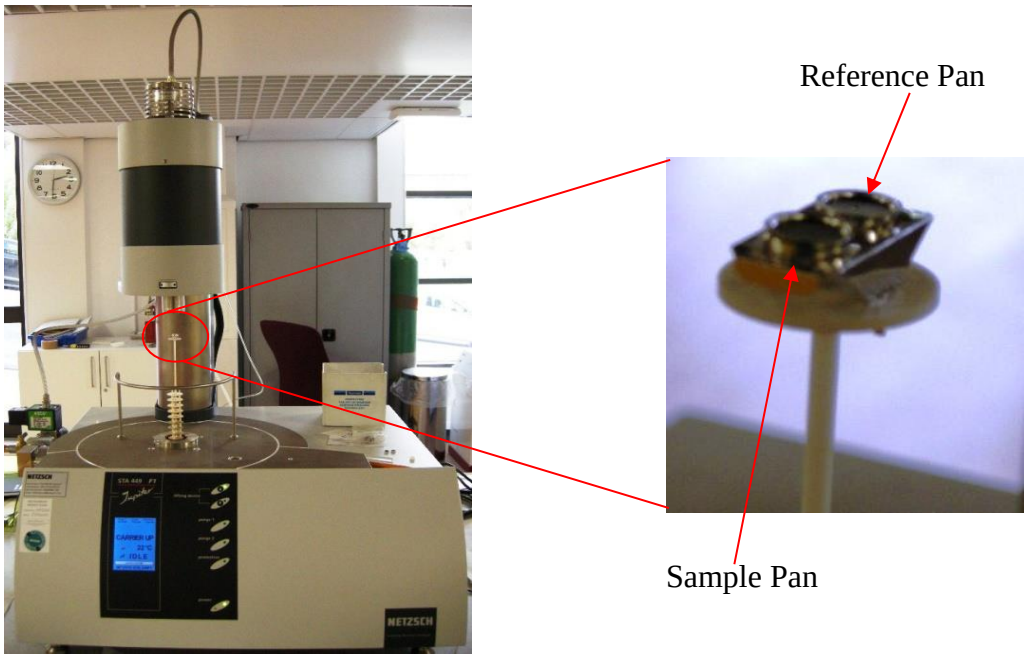

Figure 3.10: DSC / TGA set for NETZCH STA 449 F1 Jupiter

DSC was carried out using PET, Sisal and Flax fibres and the experiment was run in two different DSC machines. TA Q20 and NESZTCH S.T.A 449 F1 Jupiter both run under nitrogen gas and are shown in Figure 3.9 and 3.10 respectively. The reason for using two machines is that different temperature ranges were needed to be used depending on the fibre that was being tested. The NESZTCH could only ramp from

room temperature up whereas TA Q20 could start from -70^{o}C. However the TA Q20 could only ramp up to 500^{o}C but the NESZTCH can go up to 1600^{o}C. The temperature ranges for each machine can be seen in Table 3.2 along with the fibres used.

Table 3.2: Temperature range of the various DSC machines

Machine	Temperature Range	Fibre
TA Q20	**-75^{o}C to 500^{o}C**	**PET**
NESZTCH STA	**Ambient (25^{o}C) to 1600^{o}C**	**Sisal & Flax**

The following process was followed to make up the samples for both DSC machines.

1. A lid and pan were weighed on a Mettler Toledo microbalance. The weight of the pan and lid was then noted.
2. Fibres were then cut to a size that would fit into the pan. The fibres were then placed carefully into the pan and weighed.
3. The empty pan weight taken in step 1 was subtracted away from the weight in step 2. The difference in weight is the mass of the sample and is needed for DSC. The weight of the sample ranged between 5 to 10 mg.

The pan was loaded into the front position of the DSC machine and an empty pan which is known as a reference pan, loaded into the back position, this can be seen in Figure 3.9. A reference pan is used to track any modifications that occurs in the sample pan, to see if the pan or the sample is causing the changes. If the sample causes the changes the results are noted. The procedure used for each type of fibre is detailed below.

Table 3.3: Procedure used for PET and Natural fibres

PET Fibre	Natural Fibre (Sisal & Flax)
Equilibrate at 0°C Isothermal 2 minutes Ramp 20°C/min to 300°C Ramp 5°C/min to 0°C Ramp 20°C/min to 300°C	Ramp 20°C/ min to 800°C from Room Temperature

The typical results that can come out of the DSC machine can be seen in Figure 3.11.

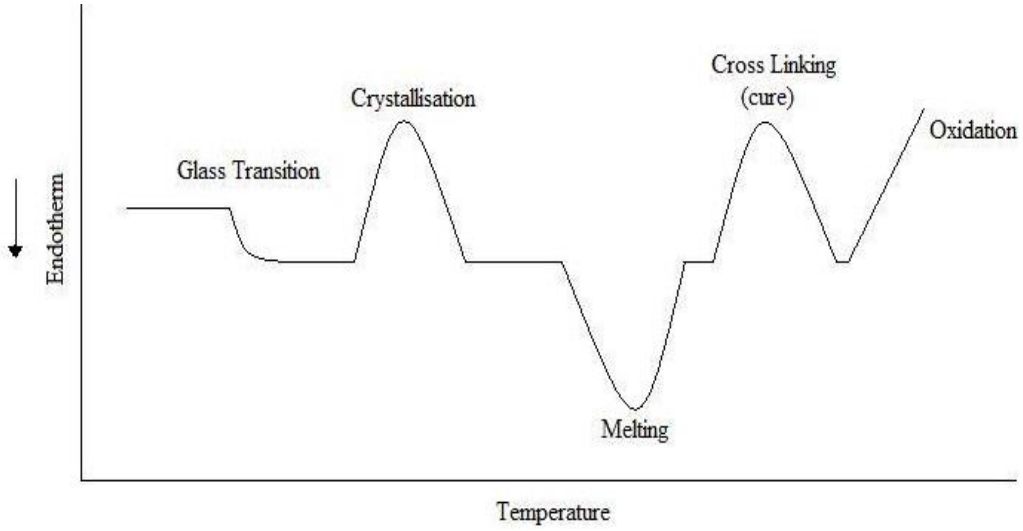

Figure 3.11: Typical DSC thermogram

The DSC results were analysed using TA universal analysis software. The software can calculate the glass transition, melting point and heat flow. The crystallinity of materials can also be calculated by using the following equation 3.6.

$$\% \, Crystallinity = \frac{[\Delta H_m - \Delta H_c]}{\Delta H_m^*} \quad (3.6)$$

where ΔH_m is the melting heat, ΔH_m^* is the heat of 100% crystalline material and ΔH_c is the heat of cold crystallisation which may or may not occur with all the values in term of J/g.

3.2.4 Thermogravimetric Analysis (TGA)

Thermogravimetric analysis (TGA) is used to determine weight change of a material in relation to the temperature. The TGA instrument used was NETSZCH STA which was used as a DSC for natural fibres and is shown in Figure 3.10. The samples were run under nitrogen. The sample preparation and set up of the TGA was the same as the DSC. The sample size used in this experiment was in the range of 5 – 10 mg. The procedure used was to ramp up the temperature of the sample from room temperature at a rate of 20^{o}C per minute to 500^{o}C or 800^{o}C depending on the type of fibre.

3.3 Results and Discussion

3.3.1 Polyethylene Terephthalate

The results of the various experiments described in Section 2 of this chapter for PET fibre is described and discussed below in sections 3.3.1.1 to 3.3.1.4.

3.3.1.1 Single Fibre Tensile Test

Throughout the course of this research programme, the diameter of over 650 individual PET fibres from the same roving have been measured using an optical microscope, Figure 3.2. This allowed a profile to be created of the diameter distribution of the PET fibre and this can be seen in Figure 3.12. It can be seen from

the study that the PET fibre diameter ranged from 16 to 23 microns with the average being 19 microns.

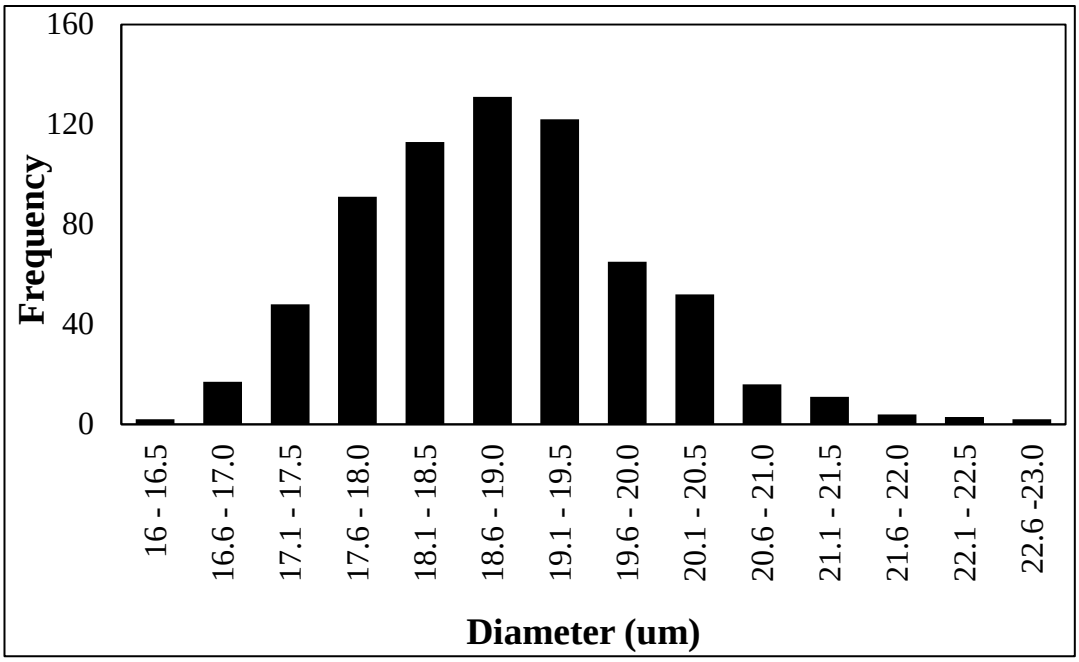

Figure 3.12: PET diameter distribution

A single fibre tensile test was carried out on heat treated and non heat treated PET fibres at various gauge lengths to establish the Young's modulus and strength. For each gauge length at least 60 single fibre specimens were tested. The heat treatment of the PET fibre was as follows: A PET fibre bundle was placed into an oven at 220^{o}C with no constraints applied, which allowed the fibre to shrink. Heat treatment lasted thirty minutes after which the fibre bundle was taken out of the oven to cool at room temperature before the manufacturing of specimens. Typical load – extension graphs of the heat treated and non heat treated PET fibre can be seen in Figure 3.13 and 3.14 respectively.

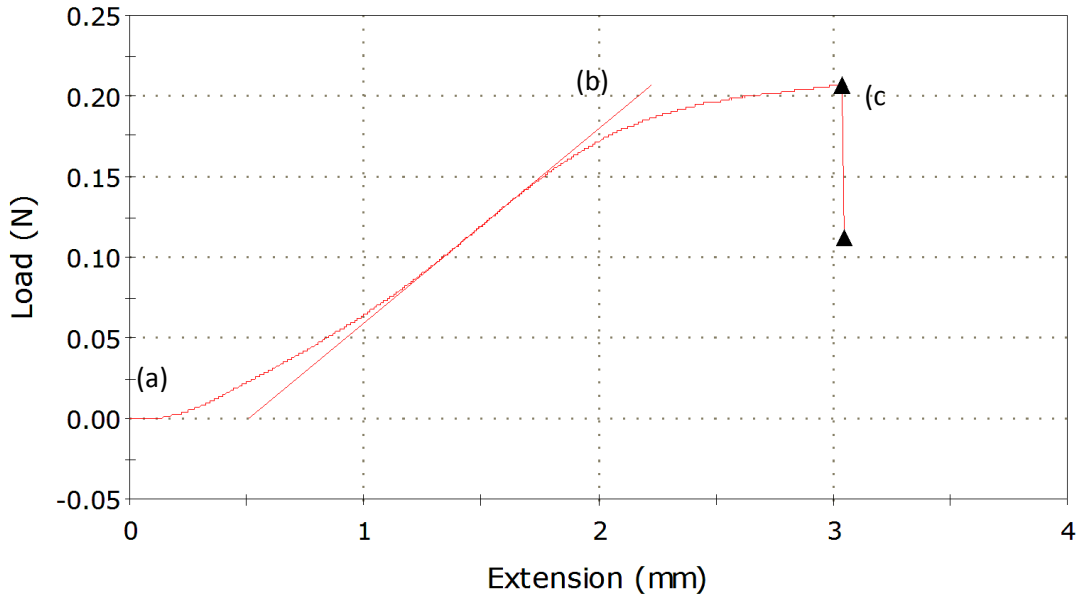

Figure 3.13: Typical PET tensile test 20mm

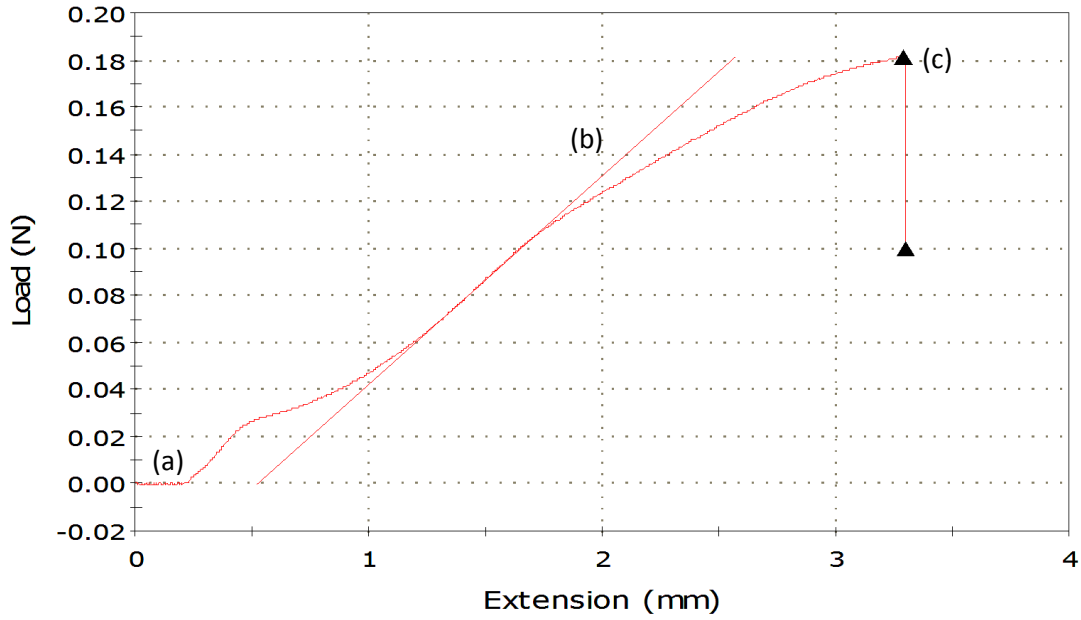

Figure 3.14: Typical PET heat treated tensile test 20mm

The load – extension graph of non heat treated and heat treated PET fibre can be split up in to three sections.

1. a – b: Load is initially being applied to the fibre which stretches the fibre

2. b – c: The load is constantly increasing but at point b the fibre starts to yield causing the slope to change
3. c: At point c, a maximum load is achieved where the fibre breaks.

It is observed that the load – extension graph of the heat treated fibre has an occurrence of an additional change in slope in the initial section a – b. This is due to the heat treatment of the fibre leading to the fibre having an additional yield point. It was observed that the yield point occurred at the same load of approximately 0.03N independent of gauge length. Further explanation of the phenomenon is noted in Chapter 5 Section 5.

Before the Young's modulus of the fibre can be estimated, the system compliance has to be calculated. The graph described in the experimental section to calculate the 'True Young's Modulus' for heat treated and non heated fibre is plotted and can be seen in Figure 3.15. From the graph it is observed that the system compliance differs were it is expected to be the same. The difference could be down to the variation of the card and amount of glue used in the manufacturing of the samples. The type of glue also changed between manufacturing the non-heat and heat treated samples caused by the manufacturer stopped manufacturing the glue that was originally used. Therefore it could be said that to eliminate the error of the card and glue in the experiment a visual extensometer could be used. The 'True Young's Modulus' estimated for non heat treated and heat treated fibre is 10.5 GPa and 5.7 GPa respectively. It is interesting to note that the modulus of heat treated fibres is 44% lower than non-heat treated PET fibre.

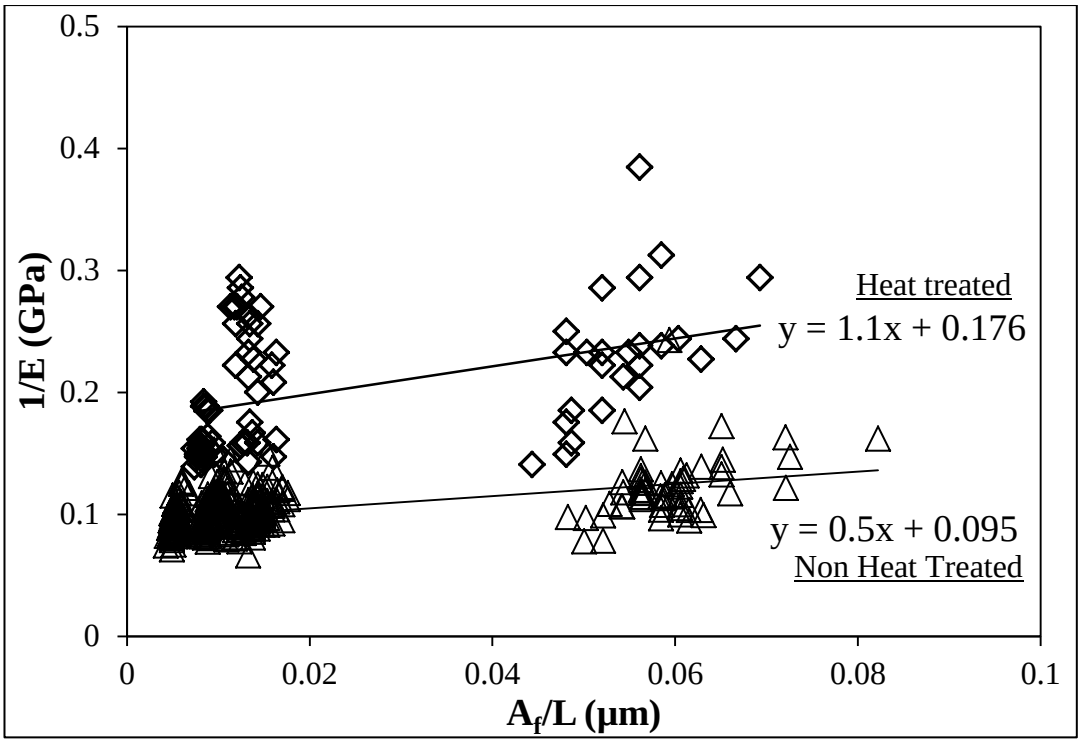

Figure 3.15: Correction of modulus

The experimental and corrected modulus is plotted against gauge length to see if the system compliance makes an effect on the modulus of the fibre, Figure 3.16. It is observed from Figure 3.16 as the gauge length of tensile test specimen increase the less impact it has on the experimental modulus. It can also be seen from Figure 3.16 that the corrected modulus is not affected by the gauge length which confirms with the believed hypothesis that the modulus is not affected by gauge length.

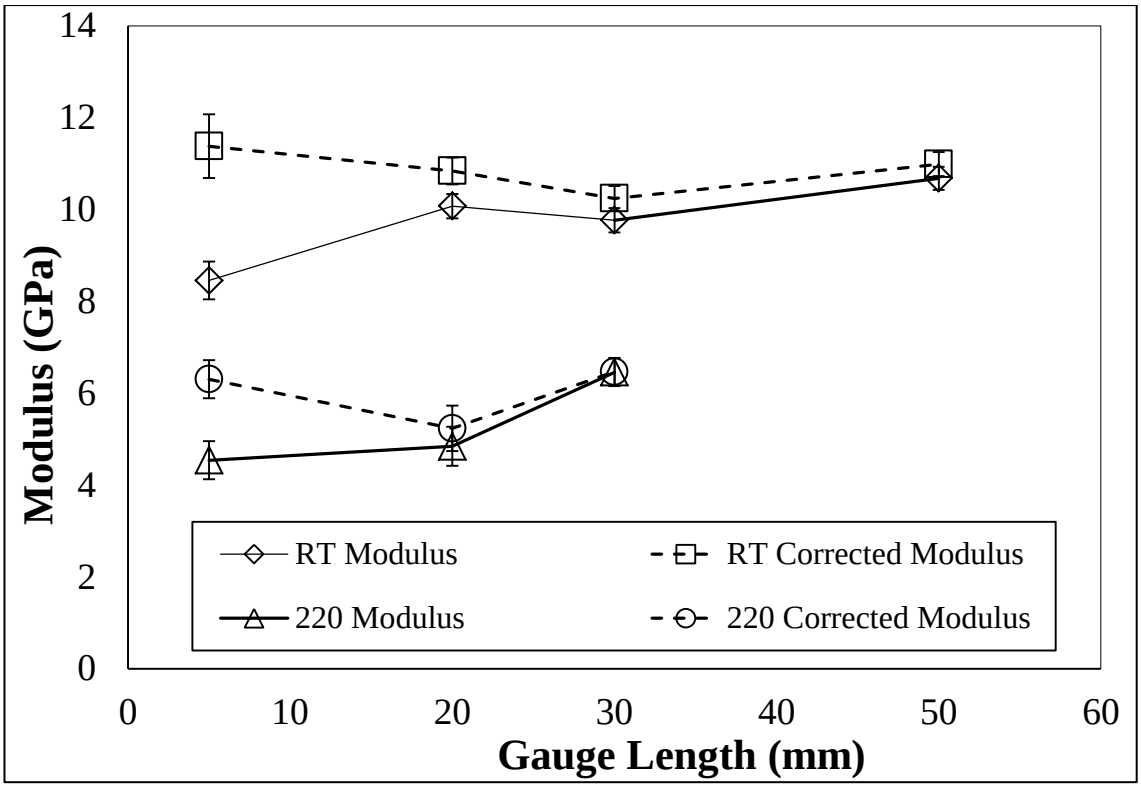

Figure 3.16: Modulus versus Gauge Length

Table 3.4: PET Average Strength and Average Modulus

Gauge Length (mm)	Temperature (^{o}C)	Average Modulus ± St Dev (GPa)	Average Strength ± St Dev (GPa)	Average Strain to Failure ± St Dev (%)	Corrected Average Strain to Failure ± St Dev (%)
5	25	8.5 ± 1.6	0.79 ± 0.08	9.7 ± 1.9	7.4 ± 1.9
20	25	10.1 ± 1.3	0.84 ± 0.09	8.4 ± 0.9	7.8 ± 0.9
30	25	9.8 ± 1.3	0.84 ± 0.09	8.6 ± 0.8	8.2 ± 0.8
50	25	10.7 ± 1.2	0.85 ± 0.08	8.0 ± 0.7	7.8 ± 0.7
5	220	4.5 ± 1.1	0.82 ± 0.09	18.8 ± 4.8	13.8 ± 4.5
20	220	4.6 ± 1.2	0.70 ± 0.06	16.1 ± 3.5	15.0 ± 3.5
30	220	6.5 ± 0.8	0.89 ± 0.07	13.9 ± 1.4	13.1 ± 1.4

The average strength and extension with standard deviation of heat treated and non heat treated PET fibres is summarised in Table 3.4. From the table, it can be observed that the strength is not affected by gauge length and/or heat treatment.

Table 3.4 also shows that the strain does not significantly increase as the gauge length increases but more importantly the heat treatment affects the strain. It can be seen that heat treatment increases strain by approximately 80%. A reason for the fibre strain dramatically increasing and the modulus to decrease could be caused by the heat treatment being above the glass transition temperature which has also been seen several researchers such as Gupta et al and Cho et al [5, 6]. The glass transition temperature for PET fibre is around 80^{o}C and relates to the amorphous region of the material. Gupta et al investigated the effect of heat treatment on the fibre's structure and mechanical properties [5, 7–9]. The amorphous region of the fibre alters due to the fibre relaxing caused by heat treatment. The heat treatment decreases the amorphous orientation factor caused by the fibre being allowed to freely shrink causing the fibre's amorphous region to become disoriented. Therefore when the heat treated fibre is subjected to tensile testing, the disoriented molecules in the amorphous region will stretch and start to become oriented [5, 7]. This process will cause an increase to the fibre's strain but decrease the fibre's modulus compared to the non-heat treated fibre.

3.3.1.3 PET Differential Scanning Calorimetry

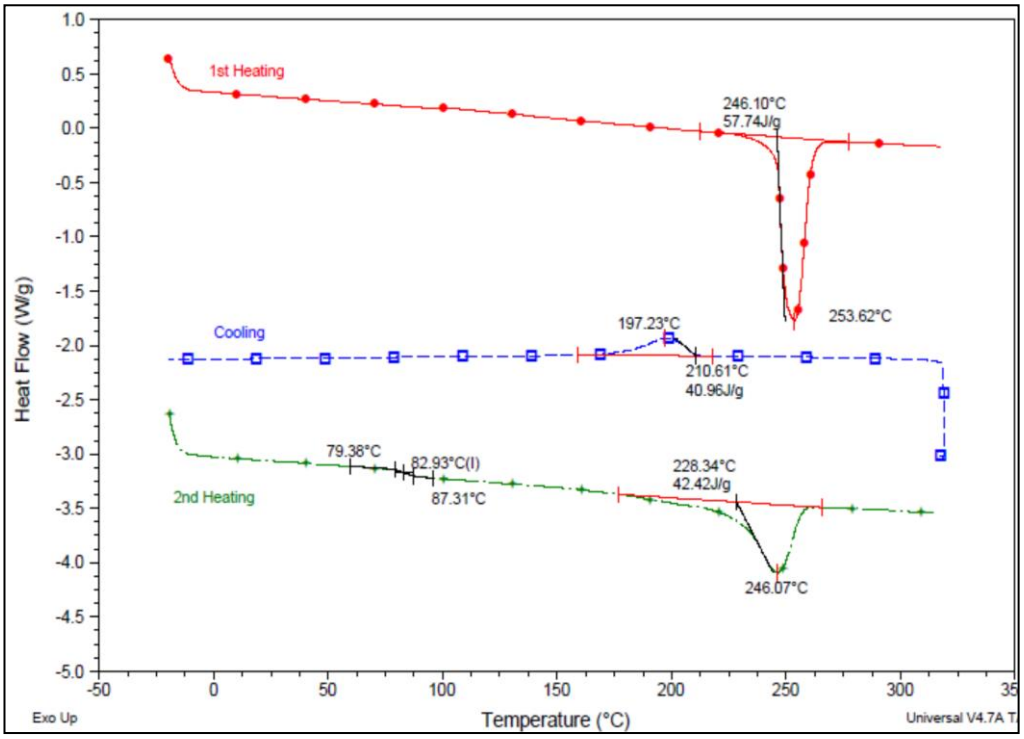

Figure 3.17: PET DSC results

Differential Scanning Calorimetry was carried out on PET fibre as discussed in the experimental section. Figure 3.17 shows some typical results from a DSC heat – cool – heat cycle. The initial heating run shows the onset of melting of the PET fibre at 246.1^{o}C and the melting peak 253.6^{o}C. The crystallinity of the fibre was calculated by taking the ratio of the experimental heat of melting to the heat of melting of 100% crystalline (140.1 J/g [10]) PET. It was found that the fibre was 41% crystallised and therefore 59% amorphous. The cooling run shows the crystallisation of the PET fibre which has now a melt. The crystallisation process has two stages; nucleation and growth. The nucleation temperature is characterised by the onset temperature of crystallisation in the cooling run. The onset or nucleation temperature was found to be 210.6^{o}C and the peak maximum, which is the crystallisation temperature, was

197.2°C. The crystallisation of the PET melt results in a somewhat reduced crystallinity of only 29.2%. The final heating cycle shows the glass transition temperature of PET which was not observed in the first heat cycle. This is likely due to the presence of a greater proportion of amorphous polymer in the melted and recrystallized sample. The glass transition temperature was found to be 82.9°C, which is in the literature value range [11–14]. The crystallinity of the PET for this run was found to be 30.3%, which is to be expected as it is approximately the same crystallinity of that found in the cooling run / crystallisation process.

3.3.1.4 PET Thermogravimetric Analysis (TGA)

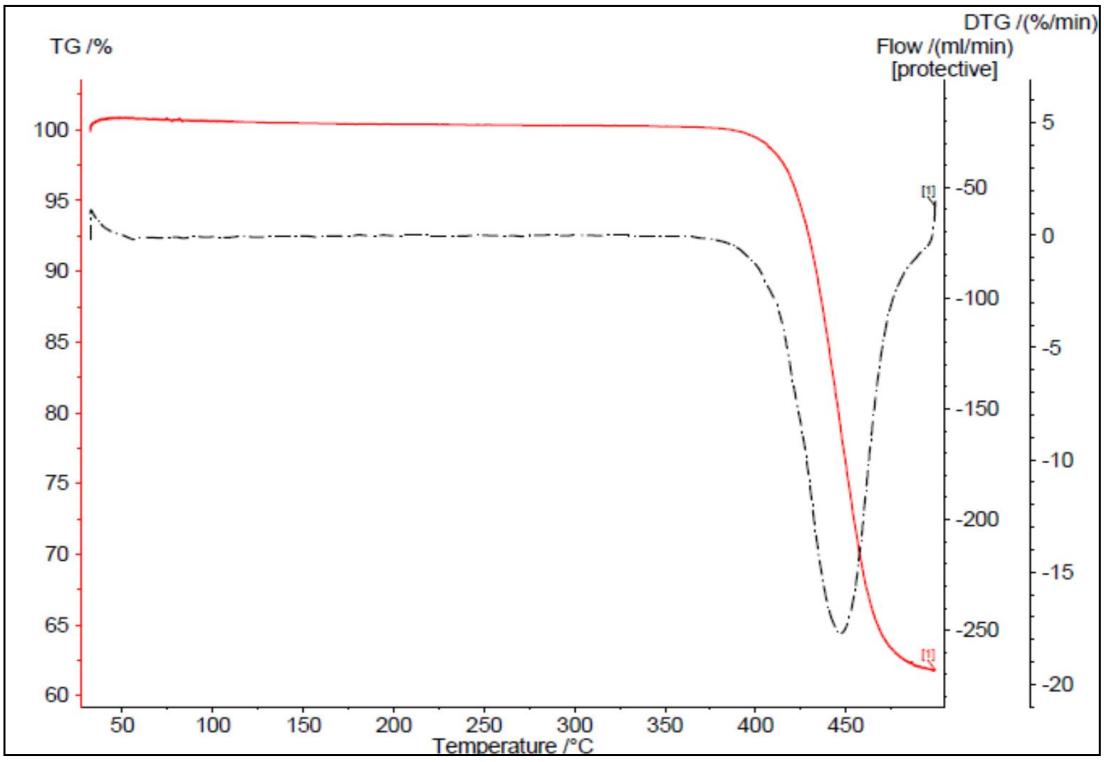

Figure 3.18: PET fibre TGA and DTG

Thermogravimetric analysis (TGA) was carried out on a PET fibre under nitrogen and was ramped from room temperature up to 500°C and the result is shown in

Figure 3.18. The figure shows the percentage weight loss of the fibre and the time derivative weight loss curve (DTG). It can be seen that PET fibre starts to lose weight at 400^{o}C and this weight loss then begins to level off at 500^{o}C. The fibre experiences a weight loss of 35%. Therefore above 400^{o}C the PET fibre starts to degrade. The DTG curve shows that the decomposition peak temperature of the material happens at approximately 450^{o}C.

3.3.2 Natural Fibre

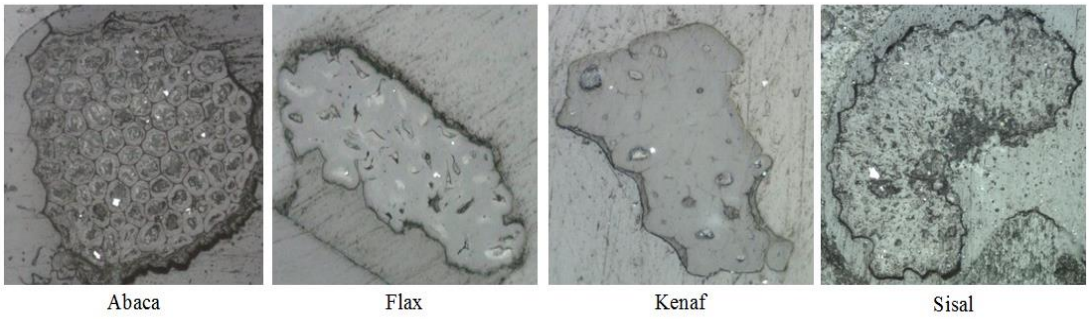

Figure 3.19: CSA of natural fibres

Before any tests were carried out on natural fibres, the fibre cross sectional area (CSA) variability was investigated due to the fibres not being circular, Figure 3.19. This investigation looked at the CSA and perimeter along the fibre's length (intra – fibre) and the difference in CSA and perimeter between fibres (inter – fibre). Sisal and Flax were studied to see if a general pattern occurred. The manufacturing of samples for observation was the same process described in Section 3.1.3 with only two changes.

1. Non tensile tested fibres were used in the embedment in resin

2. The grinding, polishing and photographing were repeated approximately every 2 mm along a fibre length of 14mm. This gave eight CSA results along the length of the fibre.

The results for Sisal and Flax carried out in this study can be seen in Figure 3.20 and 3.21 for CSA and perimeter respectively. It can be observed from Figure 3.20 and 3.21 that variability along the length of the fibre depends on the type of natural fibre. It is also clear that the variability from fibre to fibre is significantly greater than the variability along the fibre for both CSA and perimeter. Therefore using the end of the fibre which is stuck to the card of the tensile test sample would give a good estimate of the strength and modulus of the fibre since the variability along the fibre length does not considerably change compared to the fibre to fibre CSA.

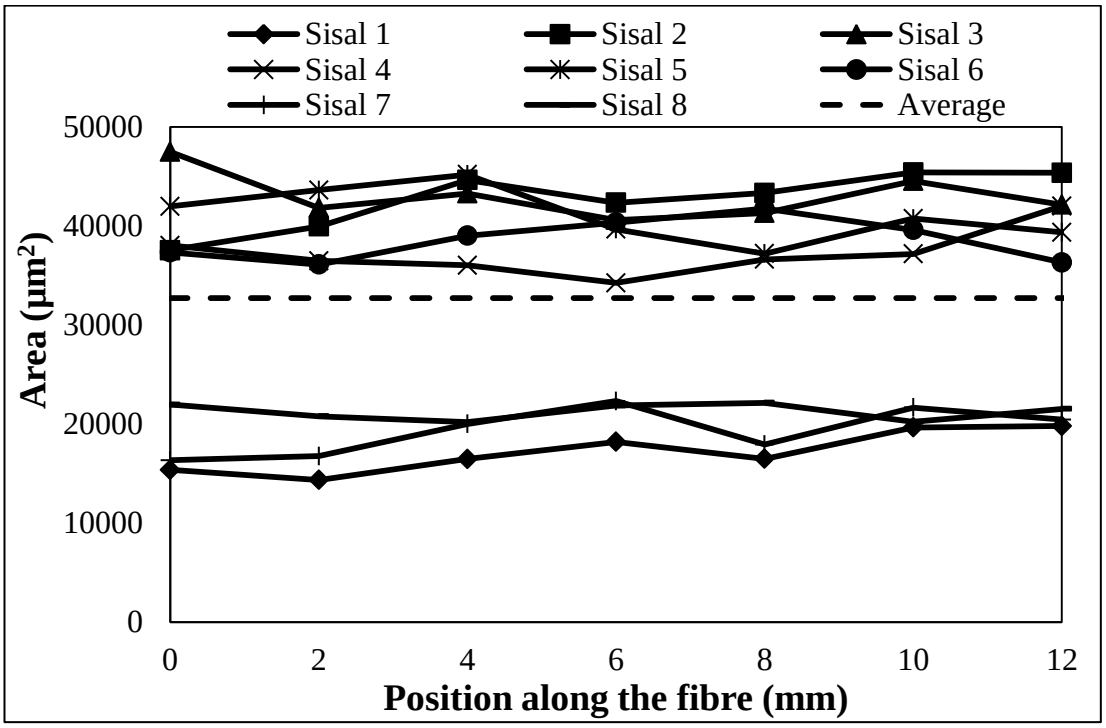

(a)

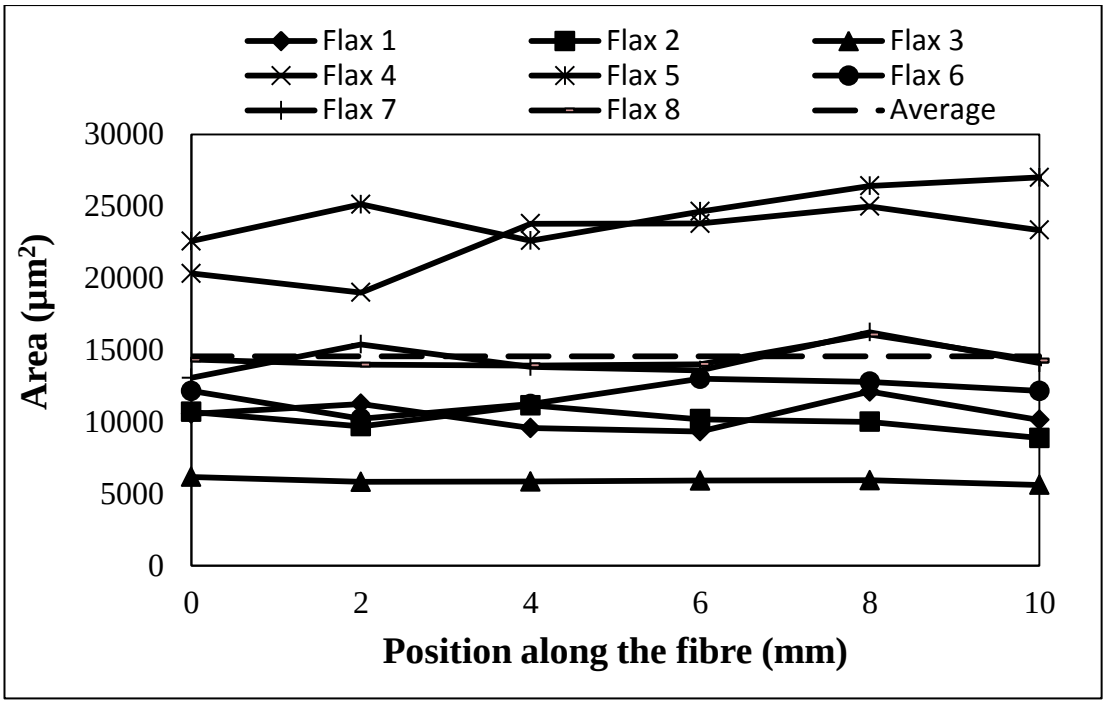

(b)

Figure 3.20: Cross sectional area measurements along the fibre (a) Sisal, (b) Flax

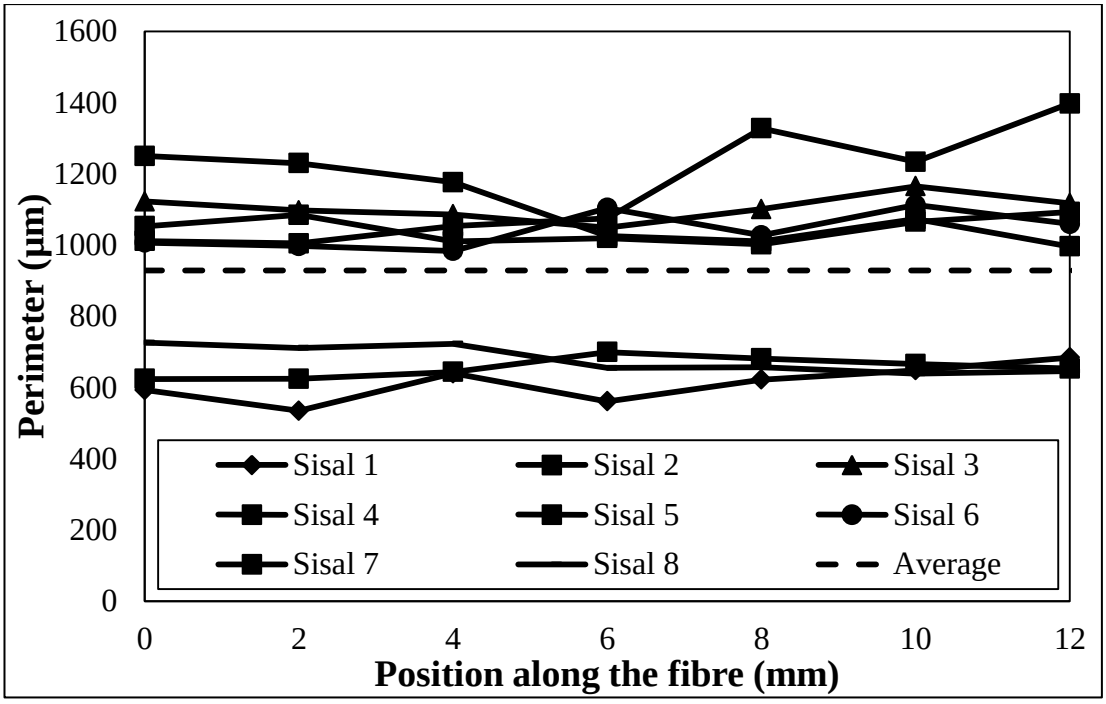

(a)

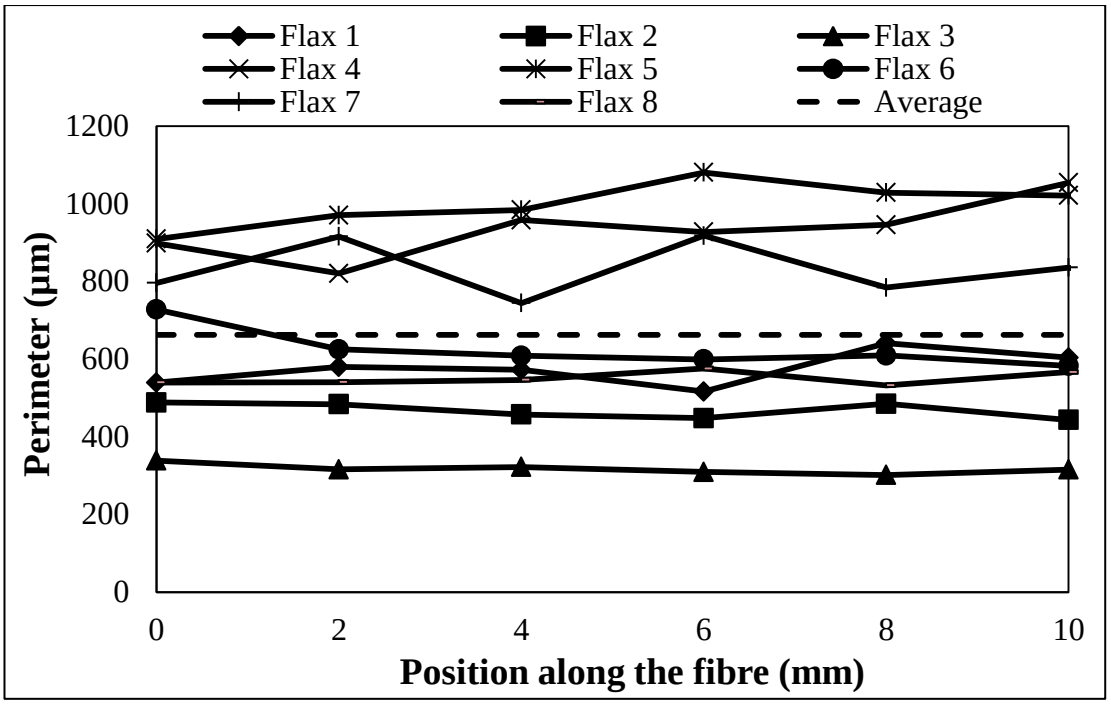

(b)

Figure 3.21: Perimeter measurements along the fibre (a) Sisal, (b) Flax

Analysis of the cross section variation for the fibres is summarised in Table 3.5. Table 3.5 shows the standard deviation of the CSA and perimeter averages calculated as a percentage of the relevant average. The table agrees with the interpretations of Figure 3.20 and 3.21 that the interfibre variability is considerably greater than the intrafibre variability.

Table 3.5: Difference between Intrafibre and Interfibre

Type	Cross Sectional Area			Perimeter		
	Average (mm^2)	Intrafibre StDev (%)	Interfibre StDev (%)	Average (µm)	Intrafibre StDev (%)	Interfibre StDev (%)
Sisal	0.033	2.6	34.2	914.2	4.2	26.8
Flax	0.015	6.2	44.6	662.7	3.5	35.8

2.3.2.1 Sisal Tensile Test

Thirty tensile tests were carried out on Sisal fibre at gauge lengths ranging from 5 to 20mm. Profiles of the Sisal CSA using the diameter method and measuring method is shown in Figure 3.22 and 3.23. Figure 3.22 and 3.23 shows the variability of Sisal CSA as the area ranges from 4500 to 45000 microns. Figure 3.22 show that most of the 'measured' CSA being is in the range 10000 to 20000 microns whereas Figure 3.23 shows that most of the 'diameter' CSA is in the range greater than 45000 microns.

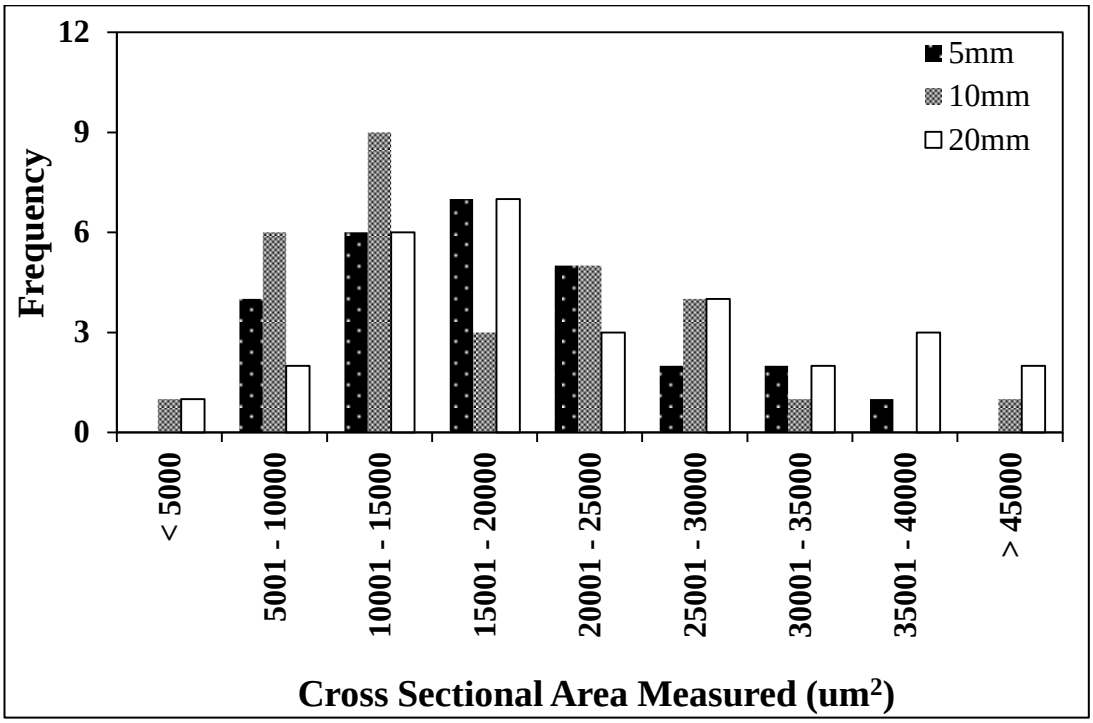

Figure 3.22: Sisal 'measured' CSA distribution

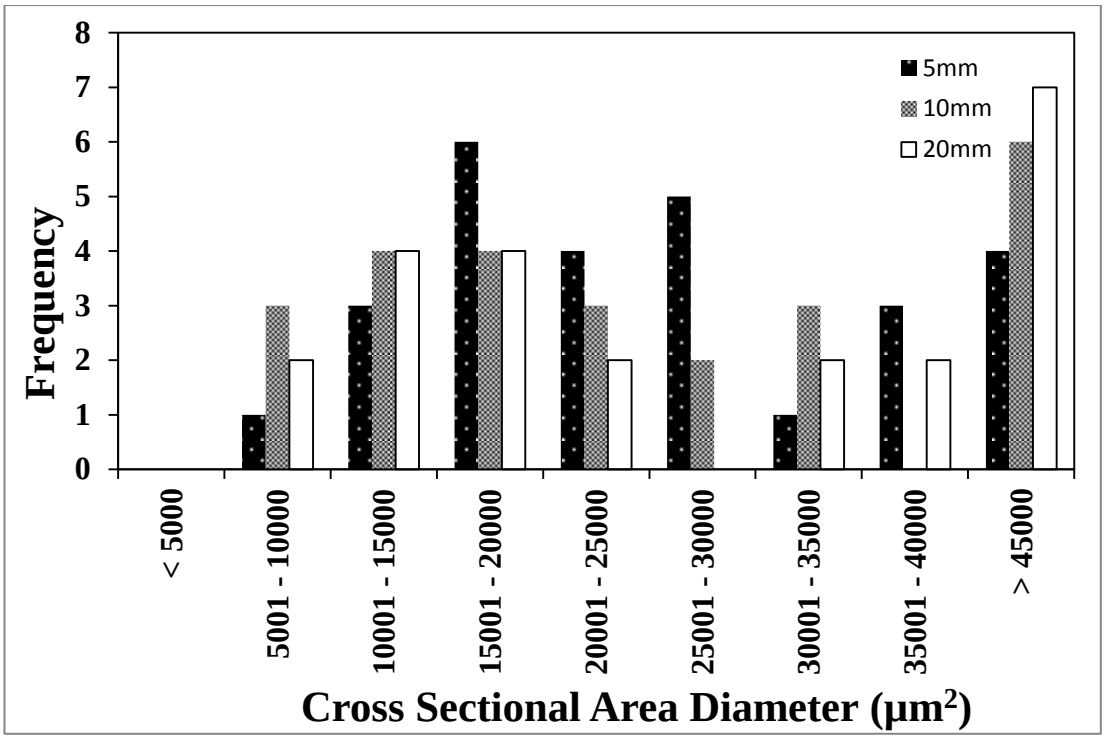

Figure 3.23: Sisal 'diameter' CSA distribution

A typical load – extension graph of Sisal which is created during the tensile testing of the fibre is shown in Figure 3.24.

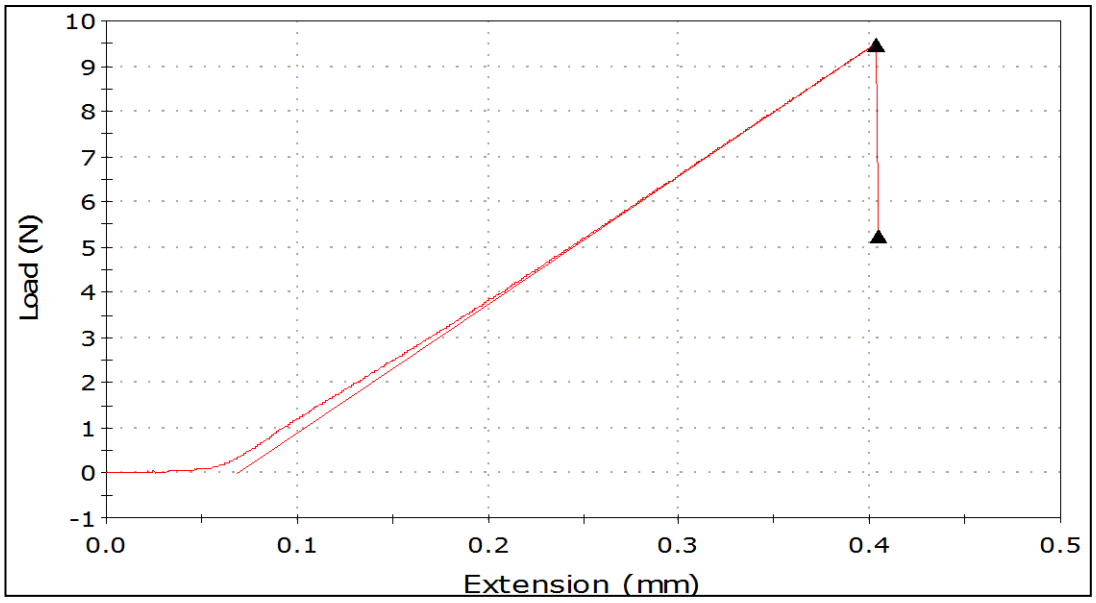

Figure 3.24: Typical Sisal Load versus Extension

The load – extension graph can be split into two parts. In the first part, the load is applied and the fibre stretches. In the second part, a maximum load is achieved causing the fibre to fracture. Just like the PET fibre, the modulus and strength can be calculated from the load – extension graph. The modulus and strength was calculated using two methods. The first method which has been used by many researchers [15–18] uses the assumption that the fibre is circular, therefore the apparent diameter was used to calculate the area. The second method used the actual measurement of the cross sectional area of the fibre. The modulus obtained using the two methods is plotted against gauge length in Figure 3.25. Figure 3.25 shows that using the actual CSA of the fibre gave a significantly higher value for the fibre modulus than that by assuming circularity. It is also observed that modulus at 5mm gauge length is higher than at 10 and 20mm gauge length. One reason for such a difference could be caused by CSA diversity as it is assumed that the larger the area the smaller the modulus [18]. Looking at the CSA distribution in Figure 3.22 it can be seen that the 5mm gauge length CSA distribution is smaller. Another explanation for the discrepancy of the modulus is in the volume of damaged caused to the fibre during the extraction process and the unpredictability in the Sisal's microstructure [19]. The microstructure of Sisal varies between fibres such as microfibrillar angle, defects and cell structure these variations affect the fibre's properties [20]. The average compliance corrected modulus calculated for Sisal using the fibre's diameter and CSA was found to be 16.6 GPa and 20.7 GPa respectively.

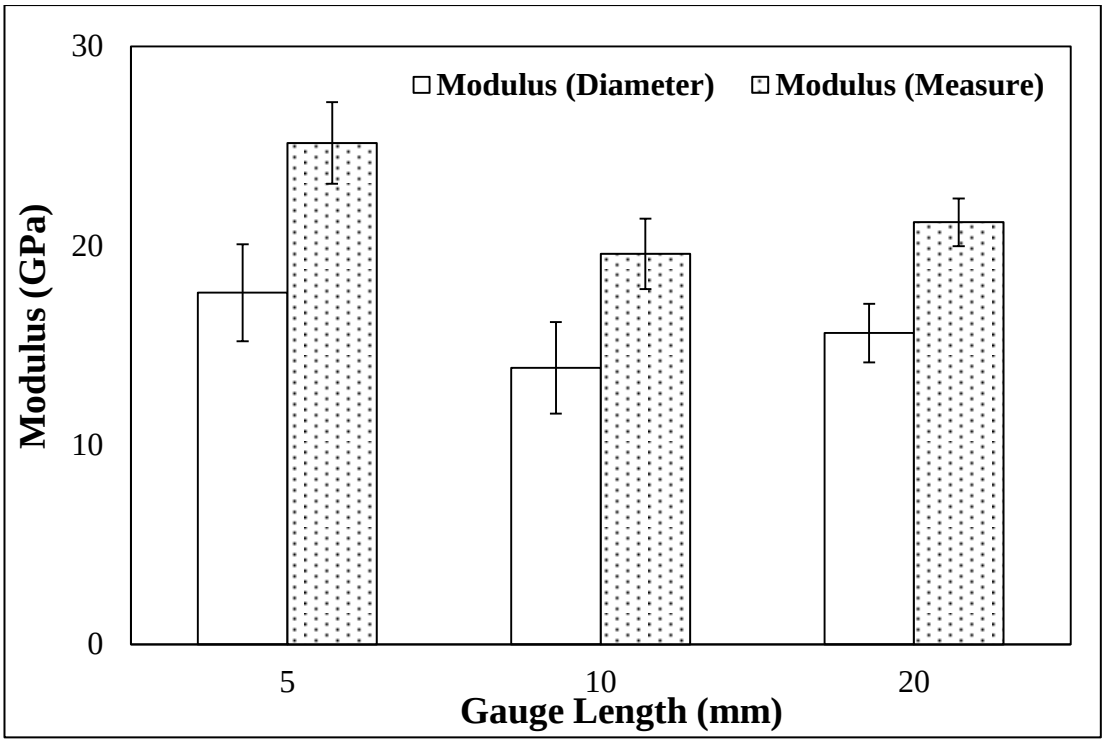

Figure 3.25: Average modulus versus gauge length for the two CSA methods for Sisal

Figure 3.26 shows the average Sisal strength with 95% confidence limits plotted against gauge length. The graph shows that statistically there is no difference between gauge length strengths but there is between the different measurements to calculate the fibre's area. This is different behaviour compared to typical manmade reinforcement fibres such as carbon or glass which show a strong dependence of single fibre strength on gauge length. The strength versus gauge length results for typical manmade fibre characteristically shows that as the gauge length increases the fibre strength decreases. The decrease in strength is attributed to the increased number of surface flaws on the fibre as the gauge length increased therefore weakening the fibre resulting in lowering of the fibre strength [14, 15]. Using the measured CSA gives a higher strength than assuming the circularity of the fibre which leads to a 26% reduction in strength.

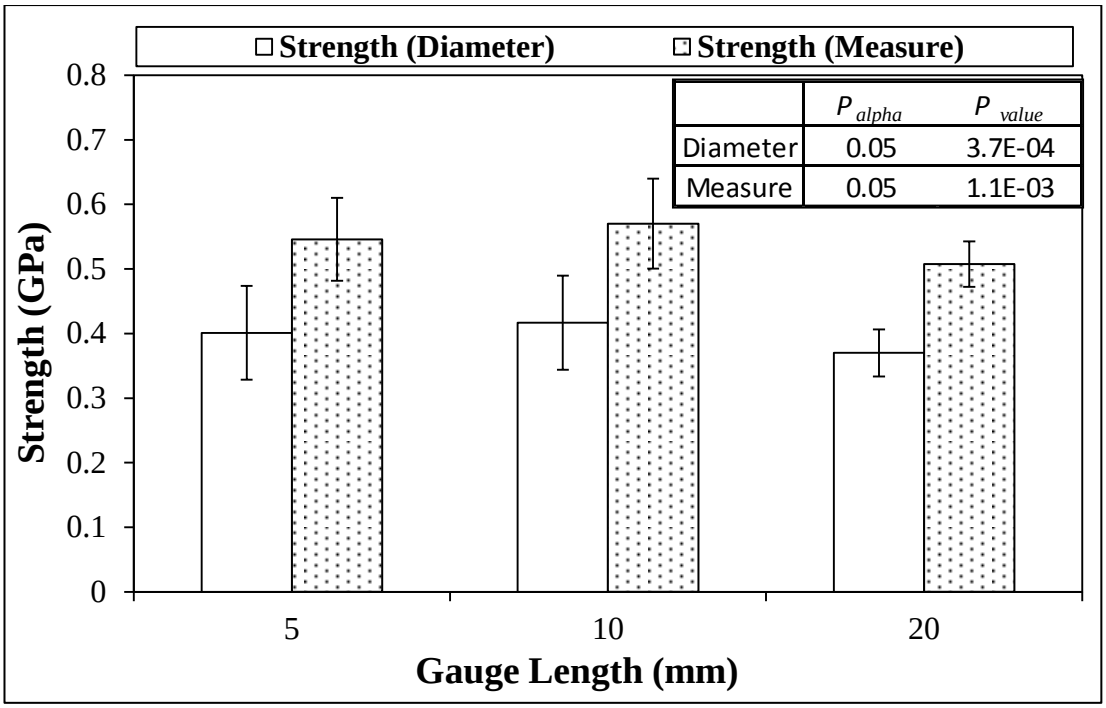

Figure 3.26: Average Sisal strength versus gauge length for the two CSA methods

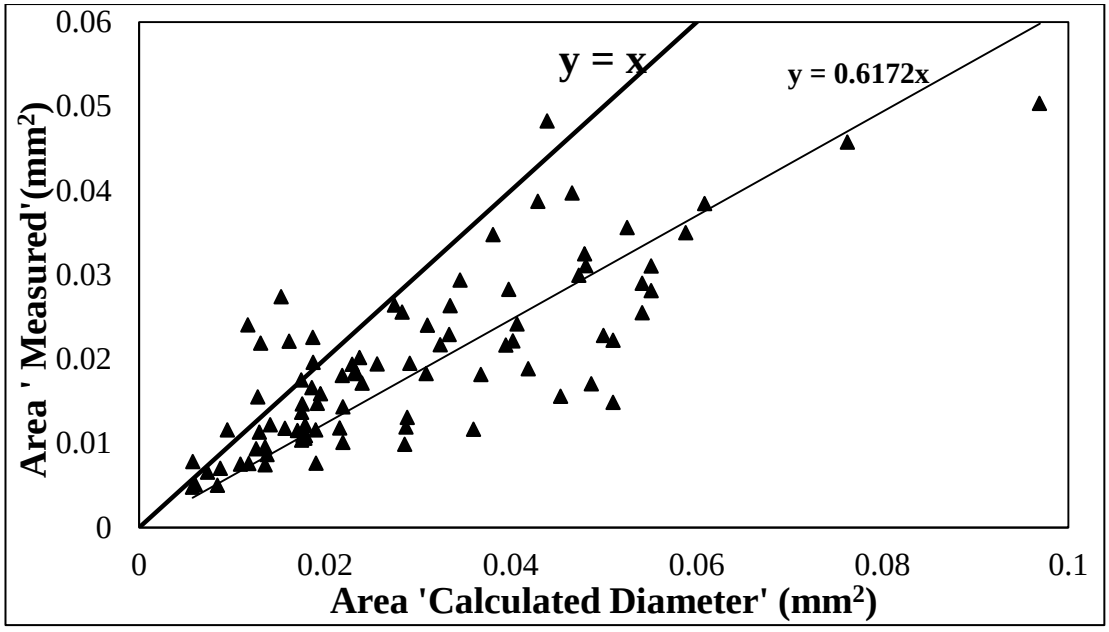

Figure 3.27: Sisal CSA measured against Sisal CSA calculate

Figure 3.27 was plotted comparing the CSA measured against the area calculated assuming the fibre being circular. The figure shows that by assuming Sisal fibre is

circular overestimates the area, therefore leads to underestimation of the fibre's mechanical properties by approximately 40%, as is observed in Figure 3.25 and 3.25.

2.3.2.2 Flax Tensile Test

A tensile test was carried out on thirty Flax fibre specimens for each gauge length. The gauge lengths that were used was the exact same as Sisal, 5, 10 and 20 mm. The variation from fibre to fibre can be seen in the CSA profiling in Figure 3.28 and 3.29. the figures shows that the area of Flax fibre ranges from 1500 to 16000 microns. Figure 3.28 shows the measured CSA with most of the fibres tested in the range of 2000 to 10000 microns. Figure 3.29 shows the calculated CSA of the diameter method with most of the fibres tested in the range of 4000 to 5000 microns.

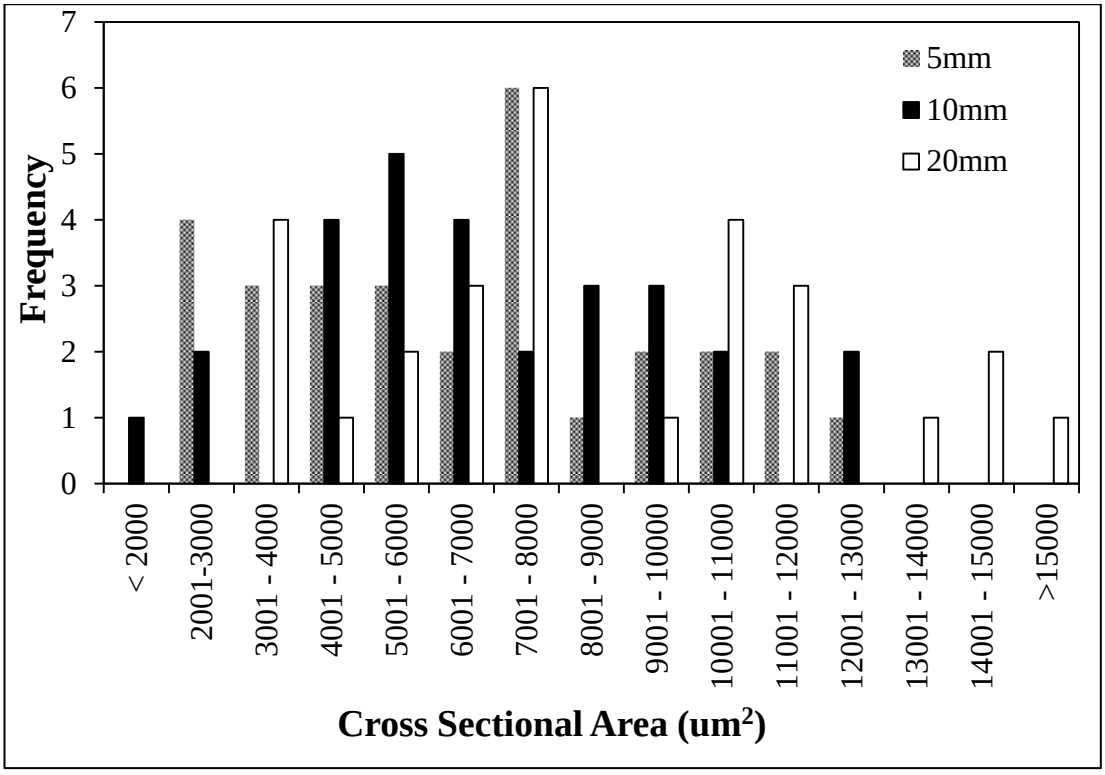

Figure 3.28: Flax 'measured' CSA distribution

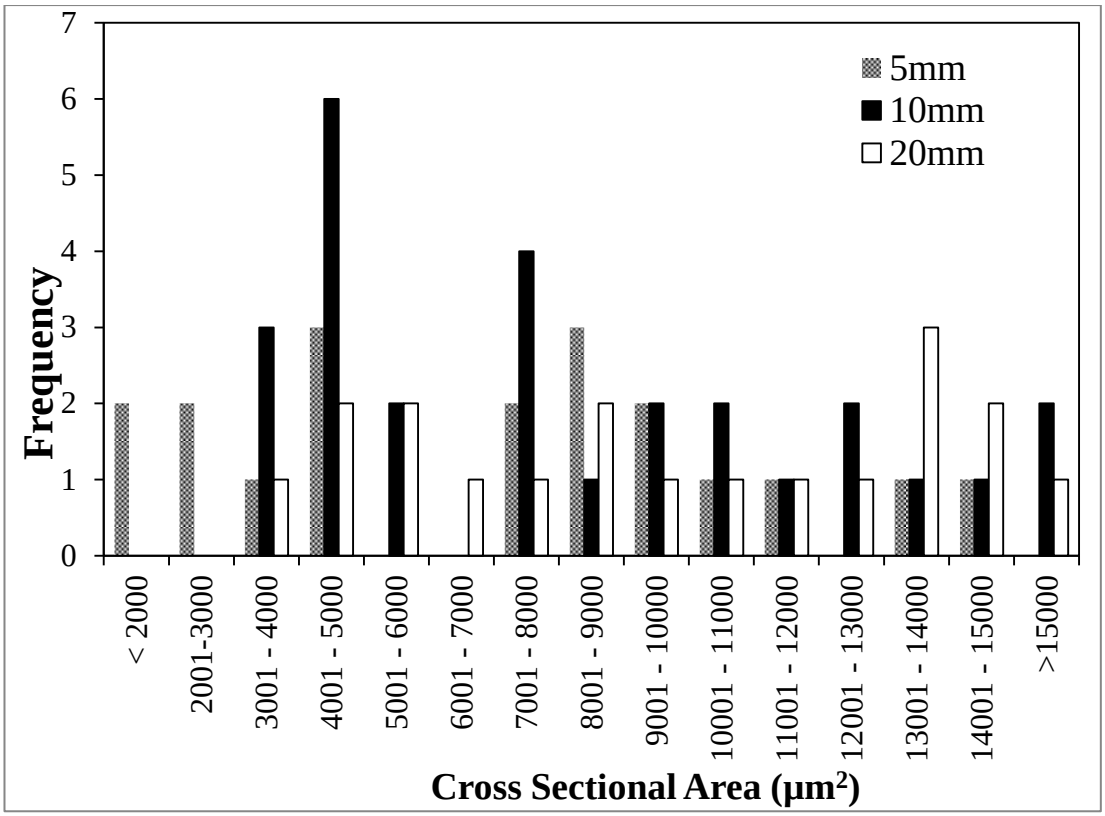

Figure 3.29: Flax 'diameter' CSA distribution

A typical Flax tensile test graph can be seen in Figure 3.30. Just like Sisal the load increases causing the fibre to stretch until a maximum load is achieved. At the maximum load the fibre fractures causing the load to drop.

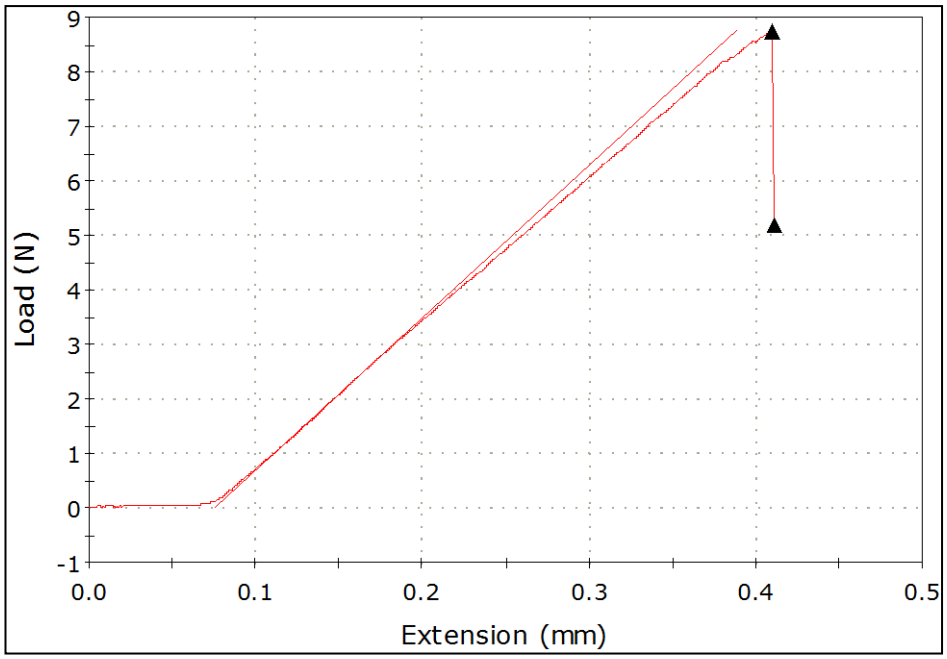

Figure 3.30: Typical Flax tensile test graph at a gauge length of 20mm

Once again the modulus and strength of the fibre is calculated twice, assuming circularity of the fibre and then using the measured CSA. Figures 3.31 and 3.32 shows the modulus and strength with 95% confidence limits versus gauge length. Figure 3.31 shows that the modulus increases as the gauge length increases as would normally be expected from equation 3.4. Statistically the moduli calculated from the two methods are not different but the average modulus is different. Similarly to the results for Sisal fibres, assuming the Flax fibre is circular results in a lower average modulus than using the measured CSA of the fibre. Comparing the confidence limits of the diameter and CSA method it can be seen that the CSA confidence limits are smaller. The compliance corrected modulus for Flax fibre calculated assuming circularity and using the CSA were found to be 36.2 GPa and 50 GPa respectively. The results obtained for the modulus is equivalent to that reported by Charlet et al, 56 GPa [23]. However, Charlet et al does not report how the Flax samples are

manufactured for testing and does not mention if the modulus was compliance corrected. Figure 3.32 shows that statistically both methods result in a similar strength value at any individual gauge length and that the gauge length has no significant effect on the measured fibre strength. Nevertheless, the overall average fibre strength obtained by the CSA method is higher than the by diameter method. CSA method increases the average strength value by approximately 15% from the diameter method.

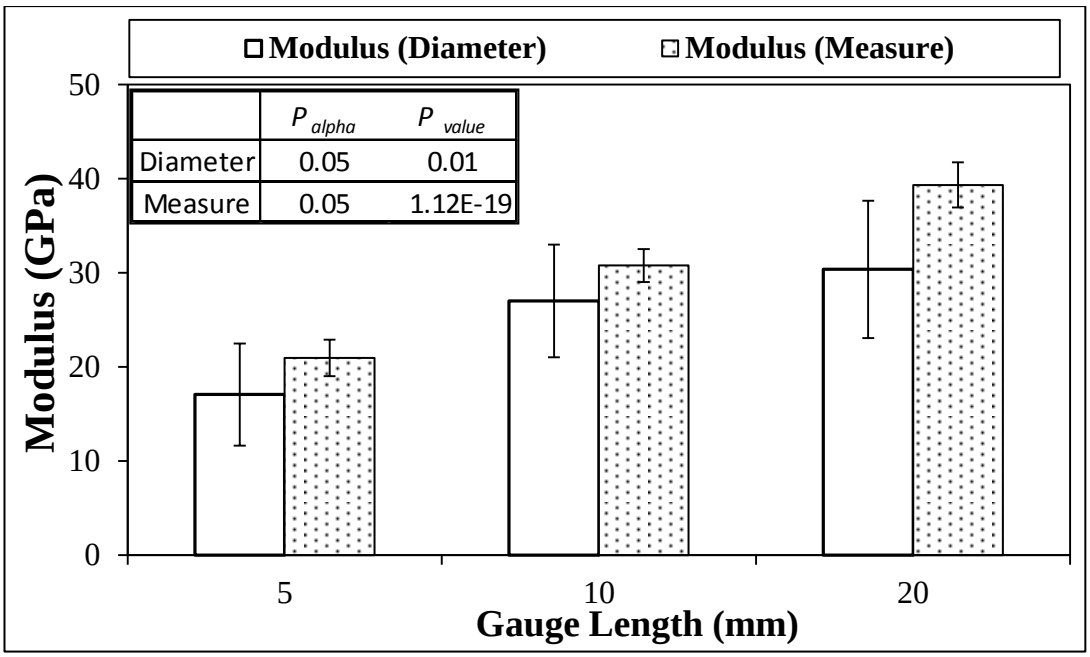

Figure 3.31: Average corrected Flax modulus against gauge length using both CSA methods

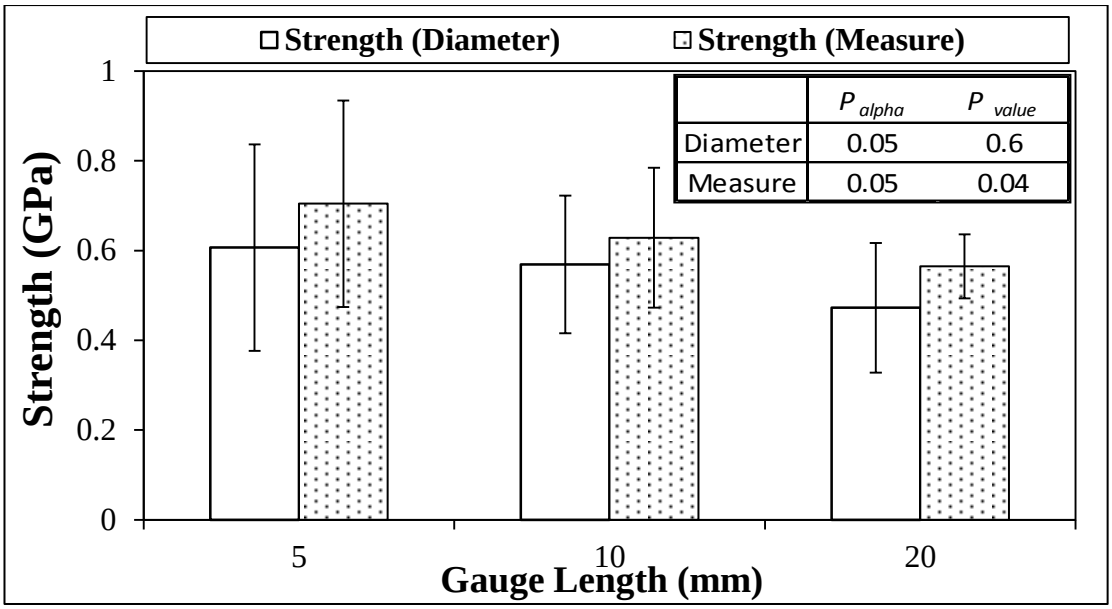

Figure 3.32: Average Flax strength against gauge length using both CSA methods

To compare the difference in the two methods used to calculate the modulus and strength of the fibre, a graph of CSA measured versus the area determined from the diameter. Figure 3.33 shows that the diameter overestimates the CSA of the fibre which leads to inaccurate estimation of the fibre's modulus and strength.

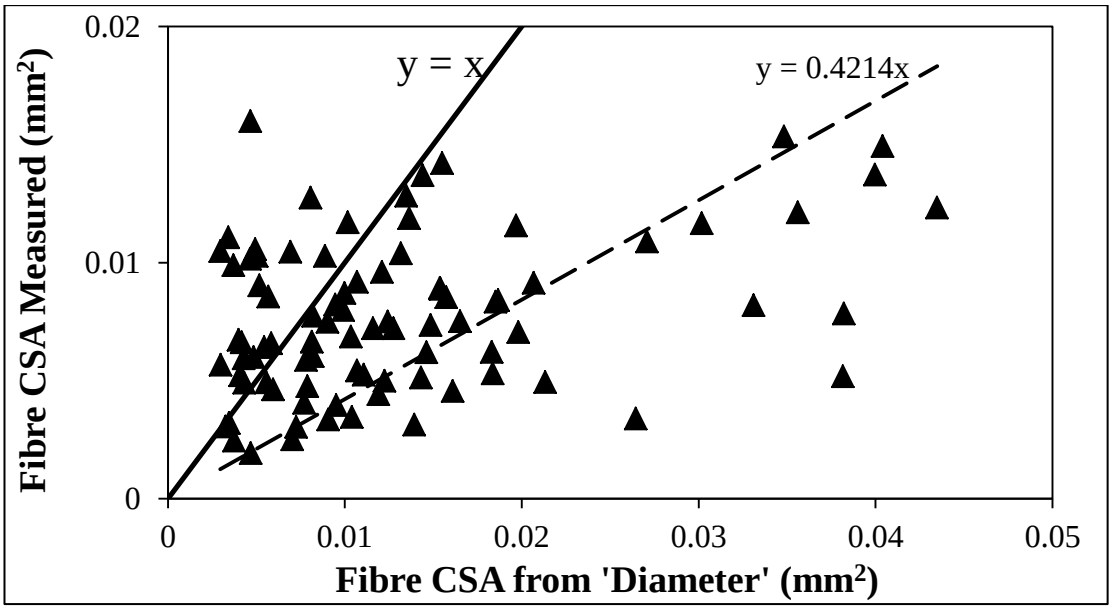

Figure 3.33: Flax CSA measured against CSA calculated

3.3.3 Natural Fibre Thermogravimetric Analysis (TGA)

Thermogravimetric analysis (TGA) was carried out on Sisal and Flax and the results are shown in Figure 3.34 and 3.35 respectively. The figures show the weight percentage decrease of each sample and the time derivative weight loss curve (DTG). Sisal and Flax experienced a total weight loss of 70.83% and 86.7% respectively. Comparing the two DTG curves, it can be seen that both fibres have similar characteristics with two distinct peaks. The first small peak, which is approximately 80^{o}C, is related to the fibre becoming dehydrated through losing water. The second peak, which is more prominent, is caused by the thermal degradation of the cellulose which can be seen at 350^{o}C for both fibres [24]. The Sisal graph also shows a shoulder to the left of the second peak at 285^{o}C. This shoulder seems likely to be related to the degradation of the hemicellulose (a constituent part of natural fibre) which has been reported to occur in the range of 250 – 300^{o}C [24 – 26].

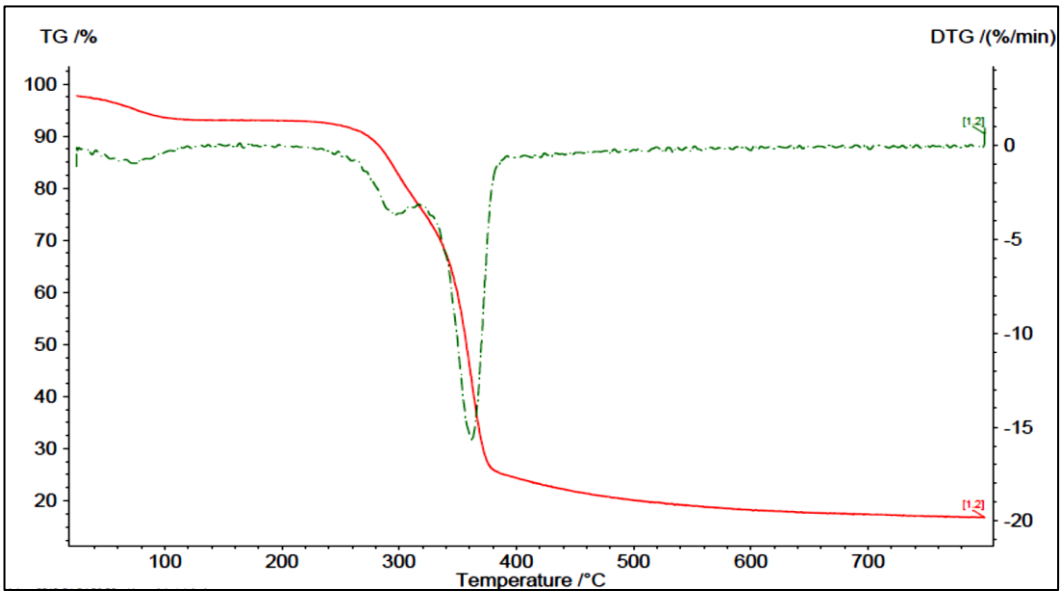

Figure 3.34: Sisal TGA and DTA Graph

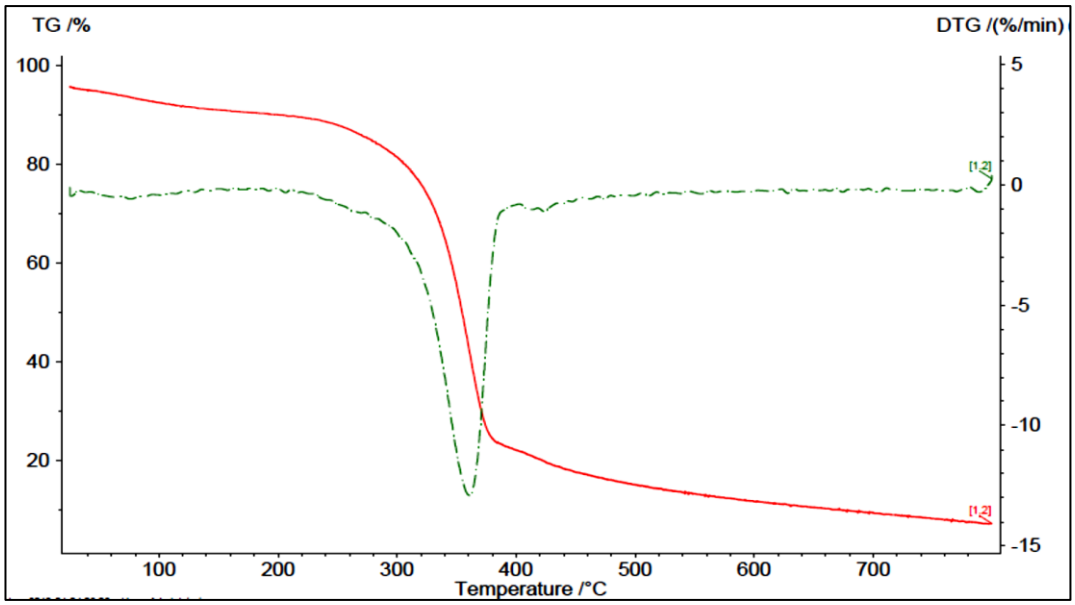

Figure 3.35: Flax TGA and DTG results

3.3.4 Natural Fibre Differential Scanning Calorimetry (DSC)

The results from the DSC for Sisal and Flax are shown in Figure 3.36 and 3.37 respectively. Just like the TGA results, two distinct endothermic peaks can be observed for both fibres. The first peak occurs around 70^{o}C and the second peak appears in the region of 365^{o}C. Comparing these two peaks with the TGA peak temperatures it can be seen the peaks are similar. Therefore it seems likely that the first peak in the DSC results for both fibres relate to water loss and the second peak to the decomposition of the cellulose/ hemicellulose.

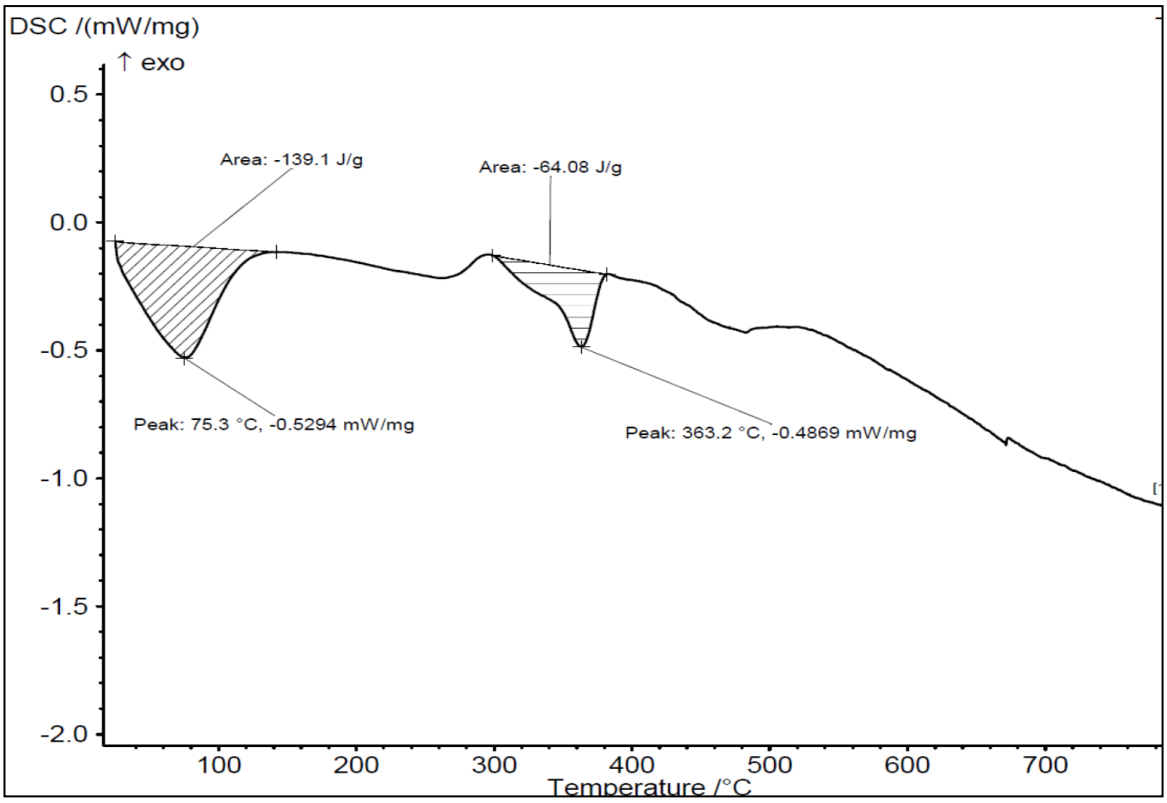

Figure 3.36: Sisal DSC results

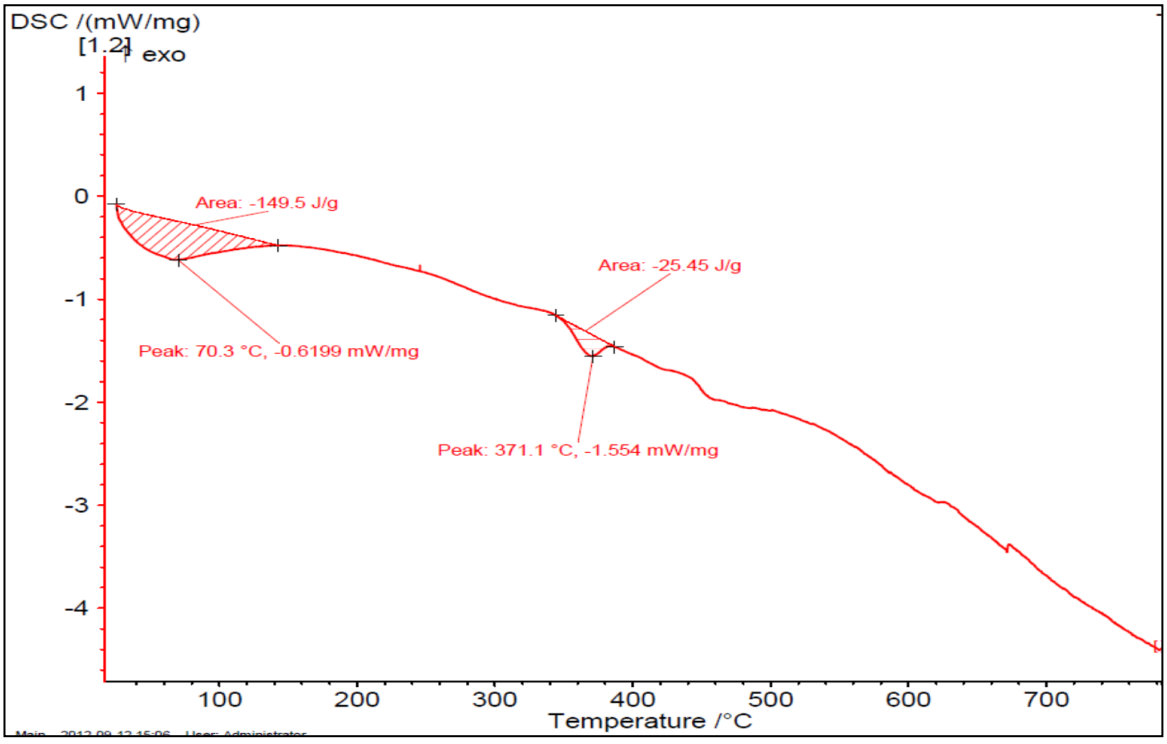

Figure 3.37: Flax DSC results

3.4 Summary

Characterisation of the candidate fibres has been investigated in this chapter. The modulus and strength of the fibres were measured using tensile testing at room temperature. The thermal behaviour of the fibres was investigated using DSC and TGA thermal analysis equipment.

It was found that the PET fibre was 41% crystalline with a melting temperature of 253.6^{o}C, a crystallisation temperature of 197.2^{o}C and a degradation temperature around 400^{o}C. The modulus and strength of the fibre was obtained for heat treated and non – heat treated fibre. It was discovered that the modulus of the fibre decreased after heat treatment whereas the strength was not affected. Similar results were also seen on PET bundle tensile test. The modulus for non – heat treated and heat treated PET fibre was establish to be 10.5 GPa and 5.7 GPa.

Natural fibre, Sisal and Flax was put through similar testing as PET fibre but with the main focus on obtaining the correct cross sectional area instead of the fibre diameter to achieve accurate fibre properties. It was found that the CSA of individual technical fibres of both Sisal and Flax exhibited a range of CSA varying over a full order of magnitude. It was shown that assuming circularity of natural fibres underestimates the modulus and strength for both fibres. The modulus obtained using the CSA method for Flax and Sisal was found to be 50 GPa and 20.7 GPa respectively. The thermal analysis testing showed similar results for both natural fibres. The TGA and DSC showed two peaks, one around 70 – 100^{o}C and the other around 360^{o}C. The initial peak relates to the fibre's hydrophilic nature as it represents the evaporation of

water from the fibres. The second peak shown on both thermal analysis results corresponds to the degrading of the fibre's cellulose/ hemicellulose.

3.5 References

[1] "Standard test method for tensile properties of single textile fibers," *ASTM*, pp. 1–10, 2007.

[2] "Standard test method for tensile strength and young's modulus of fibers," *ASTM*, vol. 03, pp. 1–10, 2008.

[3] C.-T. Li and N. R. Langley, "Improvement in fiber testing of high-modulus single-filament materials," *Journal of the American Ceramic Society*, vol. 68, no. 8, pp. 202–204, Aug. 1985.

[4] "Standard test method for tensile properties of yarns by the single-strand method," *ASTM*, vol. 07, pp. 1–14, 2002.

[5] V. B. Gupta and S. Kumar, "The Effect of Heat Setting on the Structure and Mechanical Properties of Poly (ethy1ene Terephthalate) Fiber . IV . Tensile Properties Other Than Modulus and Their Dependence on Structure," *Polymer, vol.* 26, pp. 1897–1905, 1981.

[6] D. Hwan Cho, W.-R. Yu, J. H. Youk, and J. H. Yoo, "Polymer formation of micro-crystals in poly (ethylene terephthalate) fiber by a short heat treatment and their influence on the mechanical properties," European *Polymer Journal*, vol. 43, pp. 3562–3572, 2007.

[7] V. B. Gupta and S. Kumar, "The effect of heat Setting on the structure and mechanical properties of Poly (ethy1ene Terephthalate) fiber . I. Structural changes," *Polymer*, vol. 26, pp. 1865–1876, 1981.

[8] V. B. Gupta and S. Kumar, "The effect of heat setting on the structure and mechanical properties of Poly (ethy1ene Terephthalate) fiber . 111 . Anelastic properties and their dependence on structure," *Polymer*, vol. 26, pp. 1885–1895, 1981.

[9] V. B. Gupta and S. Kumar, "The effect of heat setting on the structure and mechanical properties of Poly (ethy1ene Terephthalate) fiber . 11 . The elastic modulus and its dependence on structure," *Polymer*, vol. 26, pp. 1877–1884, 1981.

[10] W. J. Sichina, "DSC as problem solving tool: Measurement of percent crystallinity of thermoplastics," *Perkin Elmer Instruments*, 2000. .

[11] N. Benrekaa, A. Gourari, M. Bendaoud, and K. Ait-hamouda, “Analysis of thermally stimulated current and effect of rubbery annealing around glass-rubber transition temperature in polyethylene terephthalate,” *Thermochimica Acta*, vol. 413, no. 1–2, pp. 39–46, Apr. 2004.

[12] Â. Ribelles, N. M. Alves, J. F. Mano, E. Balaguer, and J. M. M. Duen, “Glass transition and structural relaxation in semi-crystalline poly (ethylene terephthalate): a DSC study,” *Polymer*, vol. 43, pp. 4111–4122, 2002.

[13] Y. U. Shi and S. A. Jabarin, “Glass-Transition and Melting Behavior of Poly (ethylene terephthalate)/ Poly (ethylene 2 , 6-naphthalate) Blends,” *Journal of Applied Polymer Science*, no. June 2000, pp. 11–22, 2001.

[14] J. Menczel and R. Bruce Prime, *Thermal Analysis of Polymers: Fundamental and Applications*. 2009.

[15] Z. P. Xia, J. Y. Yu, L. D. Cheng, L. F. Liu, and W. M. Wang, “Study on the breaking strength of jute fibres using modified Weibull distribution,” *Composites Part A: Applied Science and Manufacturing*, vol. 40, no. 1, pp. 54–59, Jan. 2009.

[16] M. C. Symington, W. M. Banks, O. D. West, and R. A. Pethrick, “Tensile testing of cellulose based natural fibers for structural composite applications,” *Journal of Composite Materials*, vol. 43, no. 9, pp. 1083–1108, Jan. 2009.

[17] Y. Li, K. L. Pickering, and R. L. Farrell, “Determination of interfacial shear strength of white rot fungi treated hemp fibre reinforced Polypropylene,” *Composites Science and Technology*, vol. 69, no. 7–8, pp. 1165–1171, Jun. 2009.

[18] C. Baley, “Analysis of the Flax fibres tensile behaviour and analysis of the tensile stiffness increase,” *Composites Part A: Applied Science and Manufacturing*, vol. 33, pp. 939–948, 2002.

[19] F. D. A. Silva, N. Chawla, and R. D. D. T. Filho, “Tensile behavior of high performance natural (Sisal) fibers,” *Composites Science and Technology*, vol. 68, no. 15–16, pp. 3438–3443, Dec. 2008.

[20] Y. Li, Y. Mai, and L. Ye, “Sisal fibre and its composites : a review of recent developments,” *Composite Science and Technology*, vol. 60, no. 2000, pp. 2037–2055, 2006.

[21] L. Yang and J. L. Thomason, “Effect of silane coupling agent on mechanical performance of glass fibre,” *Journal of Materials Science*, vol. 48, no. 5, pp. 1947–1954, Nov. 2012.

[22] R. Moreton, “The Effect of Gauge Length on the Tensile Strength of R.A.E Carbon Fibres,” Fibre Science and Technology, pp. 273 – 284, 1968.

[23] K. Charlet, S. Eve, J. P. Jernot, M. Gomina and J. Breard, “Tensile deformation of a Flax fiber,” *Procedia Engineering*, Vol 1, pp 233 – 236, 2009

[24] T. Nguyen, E. Zavarin, and E. M. Barrall II, “Thermal analysis of lignocellulosic Part 1. Unmodified materials,” *Journal of macrocolecular Science, Part C: Polymer Reviews*, vol. 20, no. 1, 1981.

[25] B. Wielage, T. Lampke, G. Marx, K. Nestler, and D. Starke, “Thermogravimetric and differential scanning calorimetric analysis of natural Fibres and Polypropylene,” *Thermochimica acta*, vol. 337, pp. 169–177, 1999.

[26] M. Tajvidi and A. Takemura, “Thermal degradation of natural fiber-reinforced Polypropylene composites,” *Journal of Thermoplastic Composite Materials*, vol. 23, no. 3, pp. 281–298, Sep. 2009.

Chapter 4

Characterisation of the Thermoelastic Properties of the Fibres

4.1 Introductory Remarks

This chapter describes the experimental investigation undertaken to find the transverse thermoelastic properties of natural and polyethylene terephthalate fibre. The properties were determined through a combination of experimental measurements and micromechanical modelling. Dynamic mechanical analysis (DMA) and thermomechanical analysis (TMA) techniques were employed to characterise unidirectional natural and polyethylene terephthalate fibre – polyester composites over a of range off–axis loading angles. Polyester was used as the matrix instead of Polypropylene in the experiments carried out in this chapter as polyester is a thermoset so will not soften at the high temperatures used in the experimental investigation. The results were input into a number of micromechanical and semi–empirical models to determine values for the transverse and longitudinal thermoelastic properties of the fibre. A description of the sample manufacturing, tests and results is given for each material that was investigated.

4.2 Experimental Programme

4.2.1 Materials

The fibres that were used in the investigation of the transverse thermoelastic properties are detailed in the Table 4.1

Table 4.1: Material information

Material	Type	Source
Sisal	Natural Fibre	Wigglesworth (Brasil)
Flax	Natural Fibre	Wigglesworth (Germany)
Polyethylene Terephthalate	Polymer Fibre (TEX 220)	SABIC

The matrix material used to embed the fibres was Scott Bader CRYSTIC 2 – 8500PA which is an orthophthalic polyester resin with a room temperature curing agent called methyl ethyl ketone peroxide. The polyester resin and curing agent used in the manufacturing of the unidirectional composites was supplied by Allscot Distributor Ltd.

4.2.2 Sample Manufacturing

The process for manufacturing unidirectional composites was vacuum infusion. The rig to carry out the vacuum infusion process was previously developed and reported by Symington [1]. A schematic of the vacuum infusion rig is illustrated in Figure 4.1. The aluminium base and perspex top gives good compaction of the fibres without significant damage to the natural fibres.

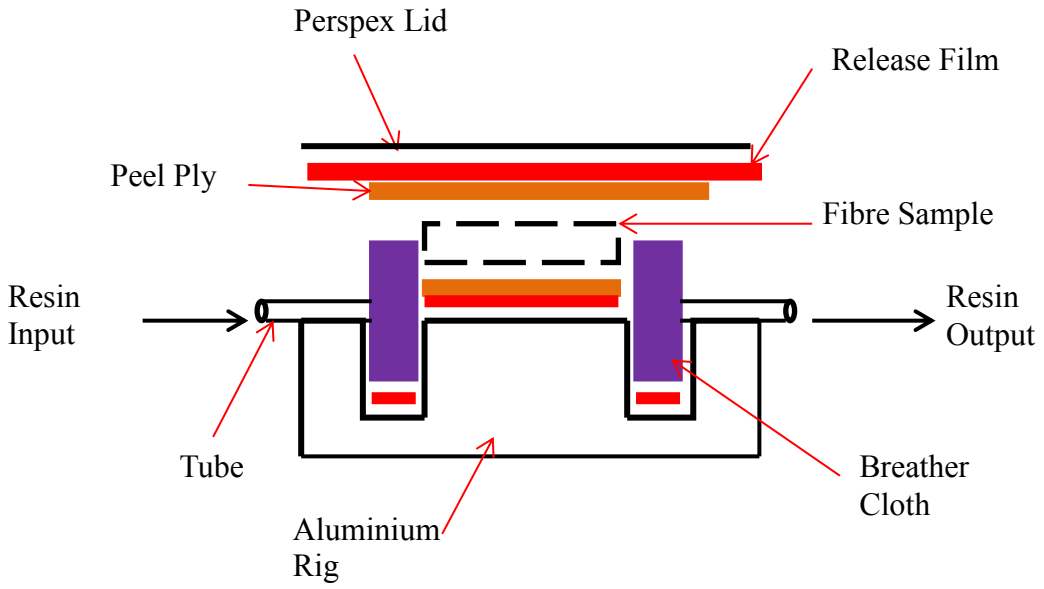

Figure 4.1: Vacuum infusion rig schematic

Before the fibres were put through the vacuum infusion process, the fibres were laid up by hand to a panel of a size 120 by 180 mm. To help manufacture unidirectional composites, several steps were taken to lay up the fibres. Masking tape was placed over the sketched out dimensions of the rig on a clean and uncontaminated surface. The masking tape was placed with the sticky side up along the width of the sketched rig. On each end of the tape another piece of masking tape was used to hold the sticky side up tape in place. The fibres were laid perpendicular to the sticky masking tape so that the tape would hold the fibres in place, as shown in Figure 4.2a. The lengths of the fibres used were slightly longer than the desired length required. The masking tape also aided in keeping the fibre as unidirectional as possible. Once the fibres had covered the required width, another piece of masking tape was placed on top of the fibres and the bottom tape, as shown in Figure 4.2b. Just like the bottom tape, the top tape was used to keep the fibres unidirectional. The fibre lay up was

then cut to the desired length for the vacuum infusion rig, as shown in Figure 4.2c. The fibres were now ready to proceed to the vacuum infusion process to manufacture a unidirectional composite.

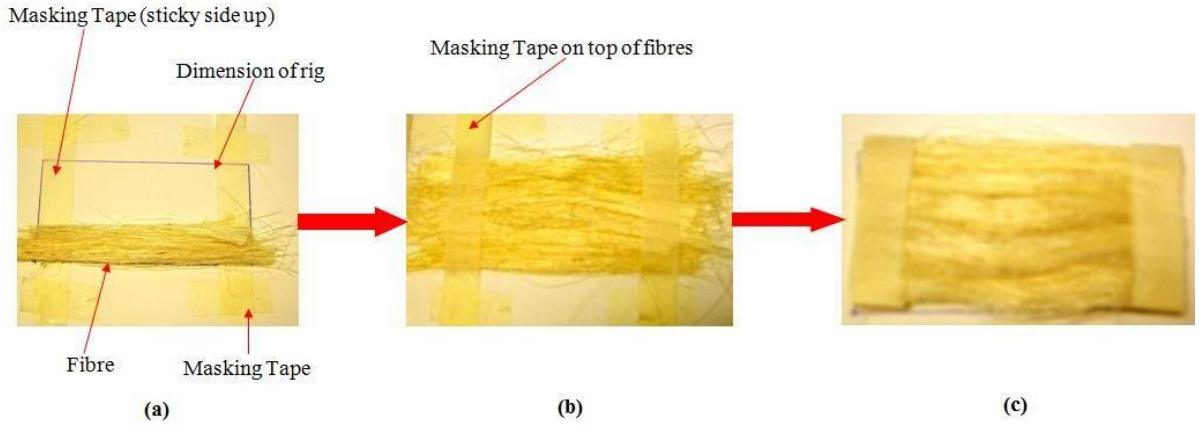

Figure 4.2: Fibre lay-up process

As briefly mentioned earlier, the vacuum infusion rig is manufactured out of aluminium and perspex. These materials were chosen so that the rig could be reused to manufacture numerous specimens whereas the vacuum bagging process can waste a lot of material and the whole rig generally requires to be thrown away after one use. The perspex top was used to aid in the monitoring of the resin flow through the packed fibre. The aluminium base was used as it gives a hard surface which will not deform when a vacuum is applied enabling the composites to be manufactured with an even surface. Before vacuum infusion could take place the rig had to be prepared by adding different types of materials to aid in the infusion process, help in the removal of the composite specimen, and improved the surface finish of the final composite. Firstly, release film was cut to the appropriate size for the top and bottom of the rig and the placement of the film can be seen in Figure 4.1(red). The release

film was used to help in the removal of the materials after the vacuum infusion had been completed. Secondly, breather cloth was used to help the resin flow equally throughout the mould and was placed at the beginning and end of the mould, Figure 4.1(purple). The breather cloth sandwiches the resin inlet and outlet pipes which helps in the resin distribution being even. Lastly, peel ply was used to give a smooth surface to the composite as the release film can occasionally crease when a vacuum is applied. The peel ply was placed on the top and bottom of the rig sandwiching the fibre layup in the middle, Figure 4.1 (brown). Following these steps, the rig was now ready to be sealed for the infusion process. Tacky tape was used to seal the rig. The tape was placed around the resin's inlet and outlet pipes and the top inner edge of the aluminium base, Figure 4.3. The perspex top was then placed on top and G clamps were applied to create a tight seal, Figure 4.3.

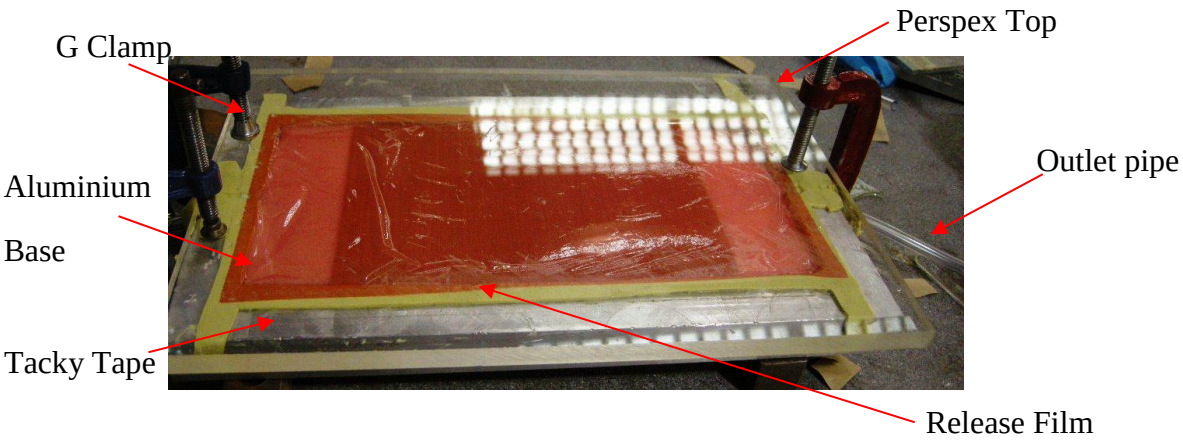

Figure 4.3: Vacuum infusion rig

The seal between the lid and the base was tested before any resin was allowed to flow through the rig. This was done by putting the rig under vacuum and listening for any air entering. This would create voids in the composite during manufacturing. If

any air was entering it was located and sealed with tacky tape. Once a satisfactory seal was formed, the matrix for the composite was then mixed. As previously mentioned, the matrix is a polyester resin but requires the addition of a catalyst to start the curing reaction. The catalyst used was methyl ethyl ketone peroxide and was added to the resin at a ratio 1:100. The resin and the catalyst were mixed together in a pot for about a minute before being degassed. The resin was degassed to remove any bubbles that may have formed while mixing the catalyst into the resin. Degassing the resin reduces the volume of voids created in the composite. The resin was now ready to be used in the vacuum infusion process. The final set up of the full vacuum infusion process is shown in Figure 4.4.

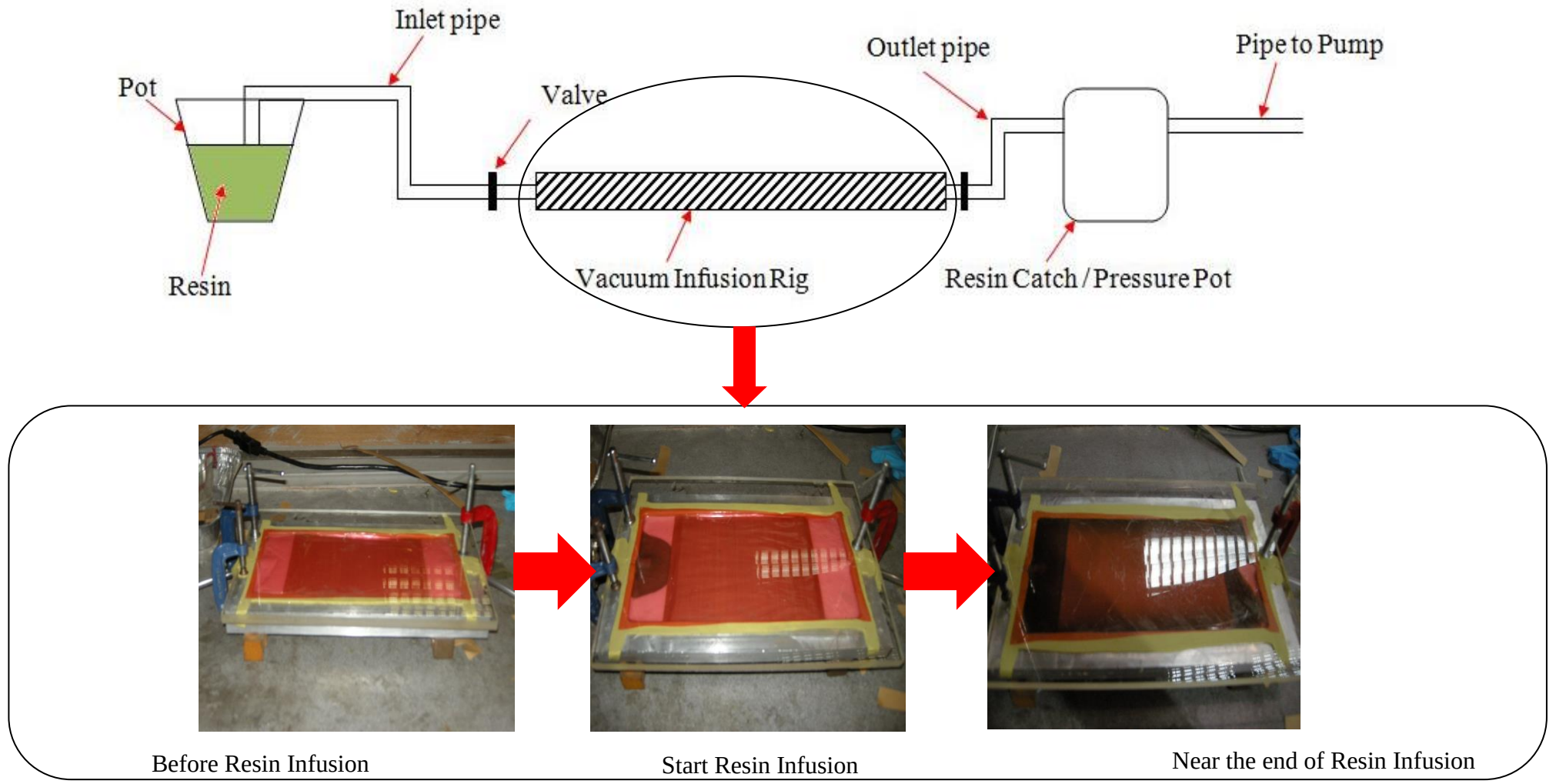

Figure 4.4: Vacuum infusion setup

The vacuum infusion unit consists of seven vital pieces of equipment which are listed and detailed as follows.

1. *Resin Pot* - provides the resin that will form the matrix for the unidirectional composite.
2. *Inlet Pipe -* transports the resin from the resin pot to the vacuum infusion rig
3. *Vacuum Infusion Rig* - is where the resin wets the fibres to form a composite. Figure 4.4 shows illustrations of the resin infusion progression through the rig at various stages.
4. *Outlet Pipe* - sucks the resin through the vacuum infusion rig, thus making sure that the fibres are wetted completely with resin.
5. *Resin Catch/ Pressure Pot* - collects any resin that flows through the outlet pipe. This pot is necessary to protect the vacuum pump.
6. *Vacuum Pump* - provides a vacuum to the rig and allows the smooth adjustable filling of the resin.
7. *Valves* – control the rate of the resin on the inlet and outlet pipe. A high infusion rate increases the number of voids in the composite, Figure 4.5a. The outlet valve also prevents back flow of resin in to the rig when the pump is switched off. This can also cause voids, Figure 4.5b

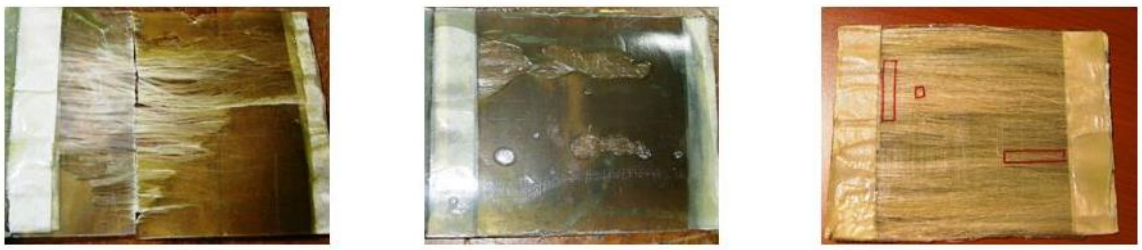

Figure 4.5: Fibre composites after infusion, a) high resin flow rate, b) backflow from outlet pipe, c) composite after final set up

After vacuum infusion, the composite was left to cure at room temperature in the mould for 12 hours. The composite was then removed from the rig and post cured in the oven at 80^{o}C for three hours and a further two hours at 120^{o}C. Once the unidirectional composite had been through the curing process it was cut in to the correct size for thermal analysis experiments. The composite was accurately machined using a Struers Accutom 5 high speed precision cutting wheel with a diamond blade. The DMA and TMA composites were cut at various fibre orientations (0^{o}, 30^{o}, 45^{o}, 60^{o}, 90^{o}) with the dimensions of 30x5x2mm and 4x4x1mm respectively, Figure 4.6. The DMA samples were cut with the guidance that the thickness of the composite should be between 1/10 to 1/32 of the span length and the thickness should only vary by 0.02 mm or less along the length. This is vital as the DMA uses the cube of the sample thickness in the modulus calculation. Along with the thickness the length of the samples has to be at least 5mm longer than the span of the chosen clamp. A resin only specimen was also made in the same way as the fibre composites. The composite and resin samples were dried after being cut to the desired shape in an oven at 120^{o}C for two hours. The samples were then stored in a dry atmosphere in a desiccator with silica crystals until they were required for

testing. This was done as natural fibres are hydrophilic and can absorb water from the atmosphere which could affect the final results.

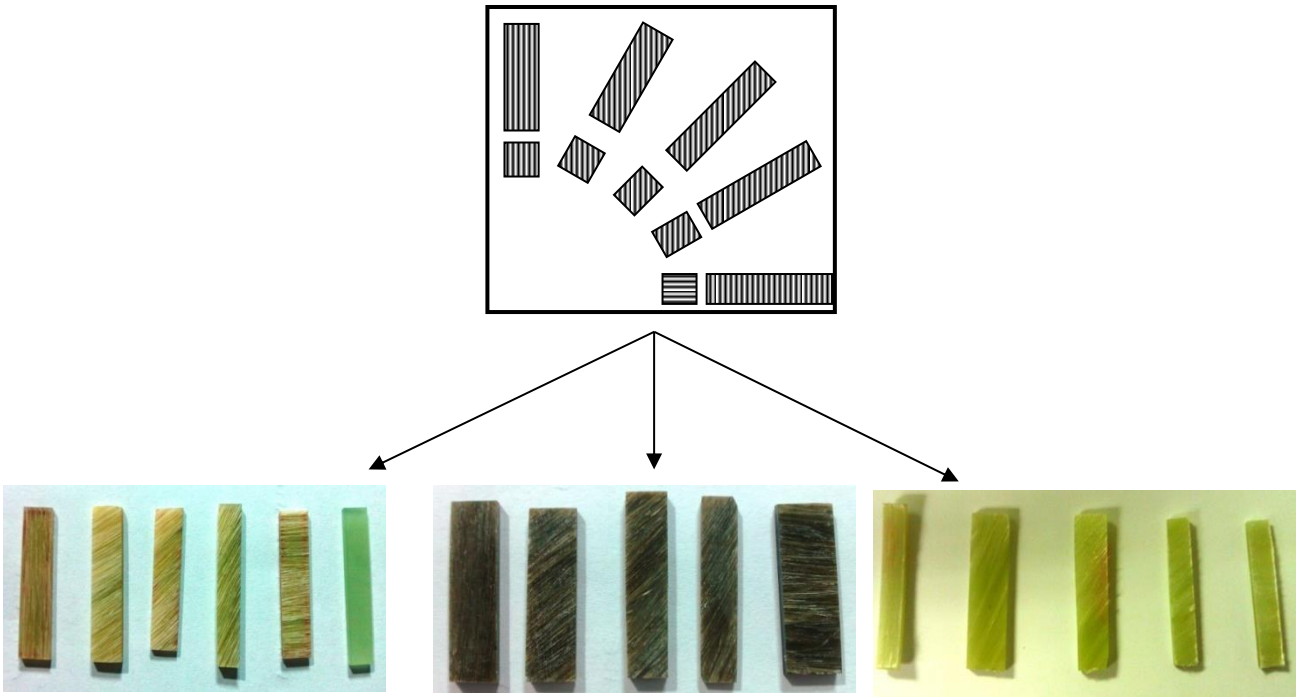

Figure 4.6: Composite specimens at different fibre orientation for the DMA

4.2.3 Dynamic Mechanical Analysis (DMA)

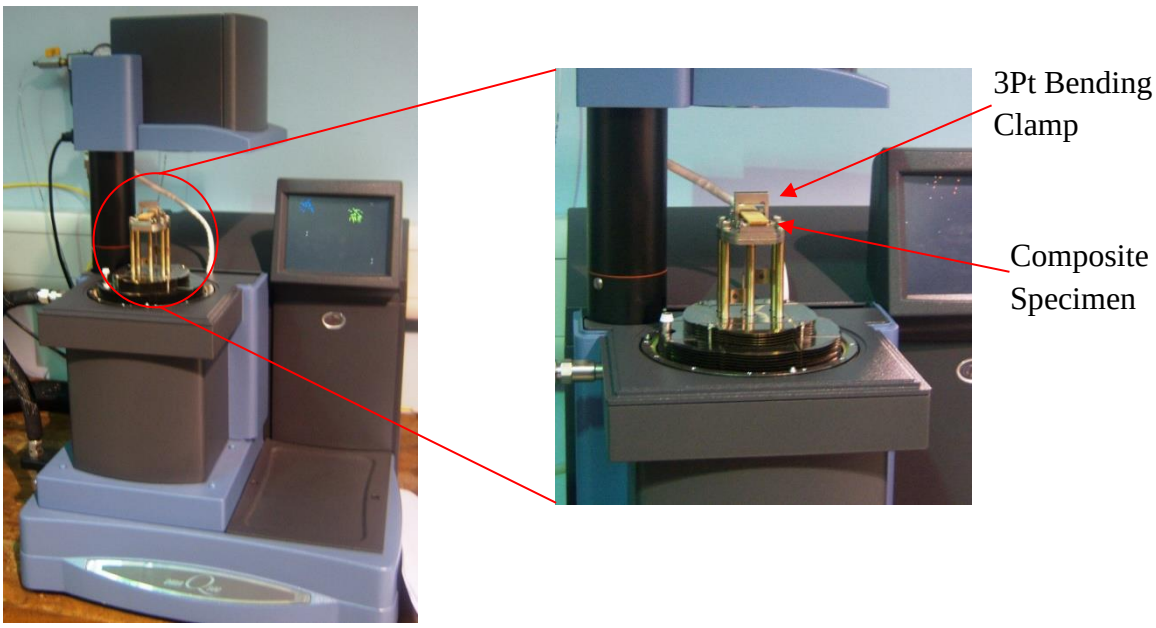

Figure 4.7: DMA Setup

Dynamical Mechanical Analysis (DMA) was used to determine the modulus of the composite over a temperature range. The machine that was used to carry out the dynamic mechanical tests was a Q800 supplied by TA instruments, pictured in Figure 4.7. The DMA comes with a variety of different clamps that can be used for testing, such as fibre/ film, cantilever, etc. The clamp that was used in this investigation was the 3 point bending clamp in the deformation mode. The 3 point bending clamp that was used has two different spans, 50 or 20 mm. As the lengths of the composites are 30 mm long the clamp span that was selected was the 20 mm. The parameters that were required before running the DMA are the width and thickness of the specimen but not the length as the span of the sample is fixed by the clamp. The sample was cooled down using liquid nitrogen supplied by the DMA gas cooling accessory (GCA) to a start temperature of -50^{o}C. The sample was then held at this temperature for five minutes to allow the specimen to reach equilibrium. The temperature then increased at a rate of 3^{o}C/minute until the temperature of 150^{o}C was reached with a preload of 0.1 N and a frequency of 1Hz. All experiments carried out in the DMA were under air.

Typical results that are obtained from the DMA were the complex (E*) modulus which is also known as the dynamic modulus and tan (δ). The complex modulus and tan (δ) are calculated from the strain that is applied to the material during mechanical testing and from the measured stress. Tan (δ) is called the damping factor of the material and measures the material's damping ability. The complex modulus is the measurement of the material's resistance to deformation under load. As a result, the complex modulus takes into account the elastic and viscous properties. For elastic materials, the Hooke's law is followed which means that the stress and strain curves

are in phase ($\delta = 0$), Figure 4.8a. However for viscous materials the stress and strain curves are out of phase by 90^o, Figure 4.8b. Therefore for a viscoelastic material, such as the composites that are being tested, shows a combination of elastic and viscous behaviour leading to the stress and strain curves being out of phase but by no greater than 90^o, Figure 4.8c. This means that two moduli are calculated, an in phase (elastic) and an out of phase (viscous). They are called storage and loss moduli respectively. The connection between tan (δ), the loss modulus, storage modulus and complex modulus is shown in Figure 4.9 along with the equation to calculate each component.

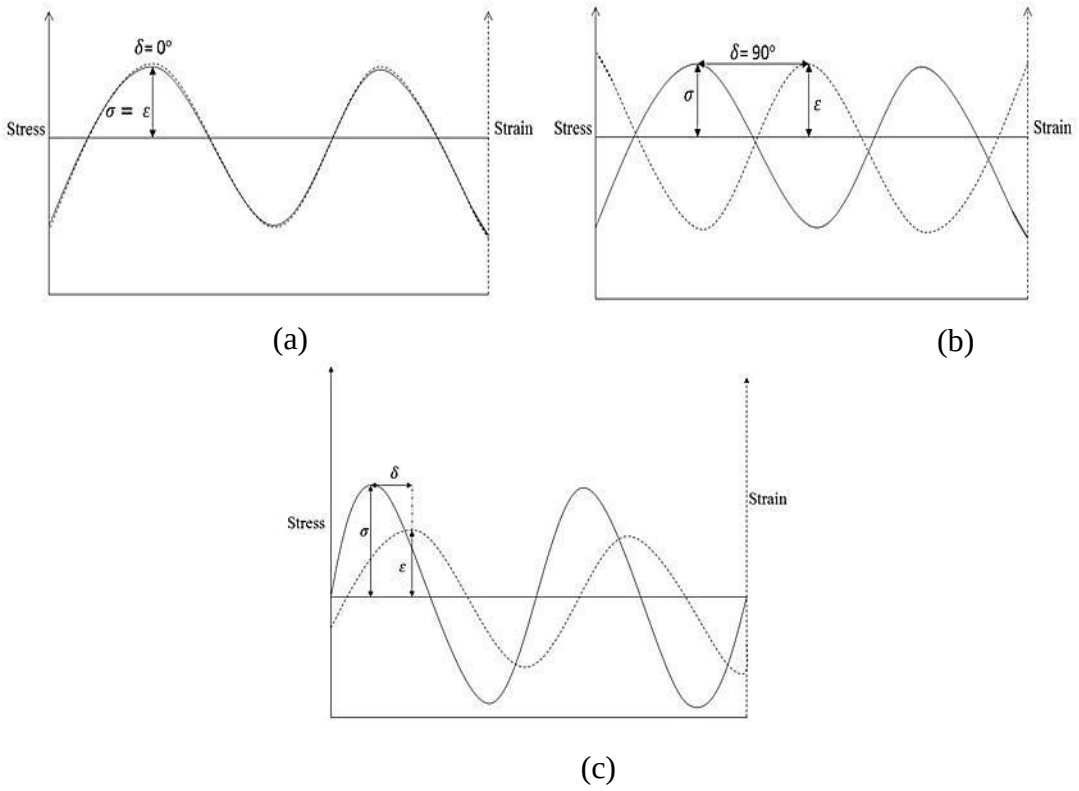

Figure 4.8: DMA calculation for (a) elastic properties, (b) viscous properties and (c) viscoelastic properties

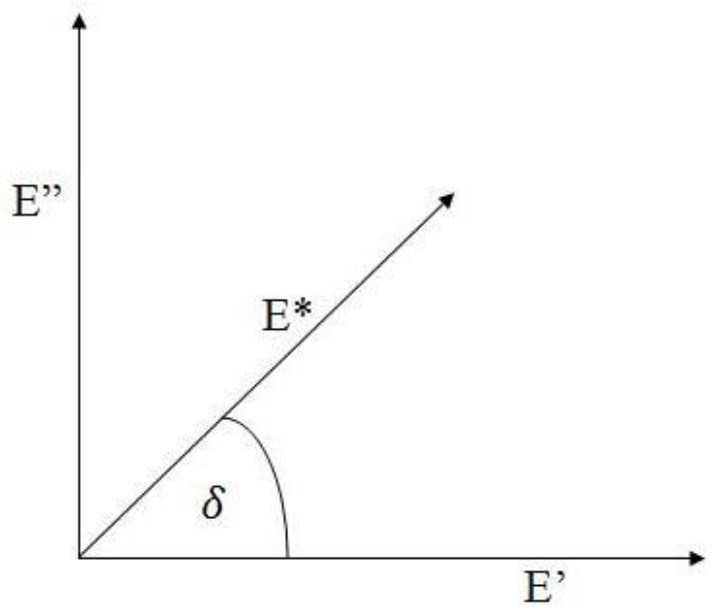

Figure 4.9: Relationship between tan (δ), the loss, storage and complex modulus

Tan (δ):

$$\tan(\delta) = E''/E' \tag{4.1}$$

Storage:

$$E' = E^*\cos(\delta) \tag{4.2}$$

$$E' = \sigma'/\varepsilon \tag{4.3}$$

Loss:

$$E'' = E^*\sin(\delta) \tag{4.4}$$

$$E' = \sigma'/\varepsilon \tag{4.5}$$

Complex:

$$E^* = E' + iE'' \tag{4.6}$$

Therefore

$$E^* = \sqrt{(E')^2 + (E'')^2} \tag{4.7}$$

4.2.4 Thermal Mechanical Analysis (TMA)

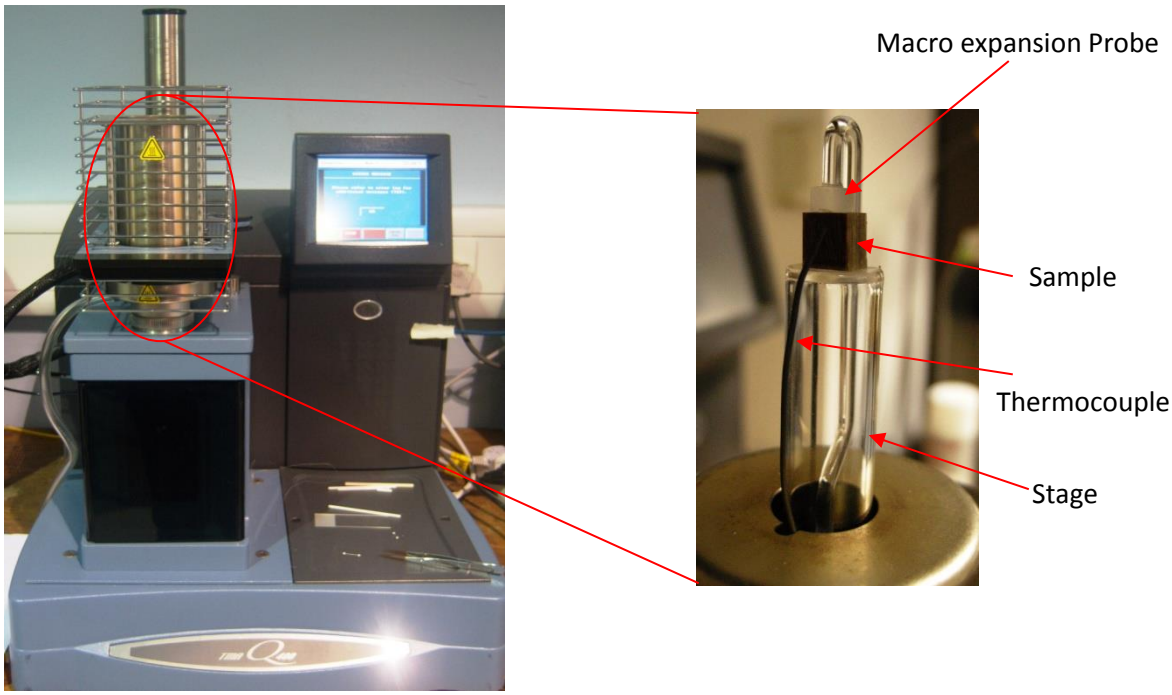

Figure 4.10: TMA setup

Thermal mechanical analysis (TMA) was used to determine length changes in the materials with temperature. The type of TMA machine that was used in this investigation was TA instruments Q400, shown in Figure 4.10. Just like the DMA, the TMA has various probes that can be used, for example, penetration and expansion. The probe that was used was the macro expansion probe which measures thermal expansion of the material by observing dimensional change of the material over a range of temperatures. This probe was selected as it allows for a large contact area of the sample to be tested; therefore readings are more accurate as the fibre composite's surface is uneven. The sample was placed on to the stage and the probe was carefully lowered on top. The parameter that was needed before the experiment can be run was the height of the sample. The sample's height was measured by the

probe as it can measure the distance that the bottom of the probe is away from the top of the stage. The procedure used was to ramp the temperature of the sample from -50°C to 150°C at a rate of 3°C/min with a load of 0.2 N applied to the sample under nitrogen. This allowed for physical properties of the composite such as the coefficient of thermal expansion to be determined.

4.2.5 Fibre Volume Fraction

The fibre volume fraction is required to effectively predict the properties of a composite. Therefore an accurate measurement of volume fraction is extremely important. Fibre volume fraction was calculated in a similar way to measuring natural fibre's cross sectional area (Chapter 3 section 2.2). The process in measuring the volume fraction has three stages.

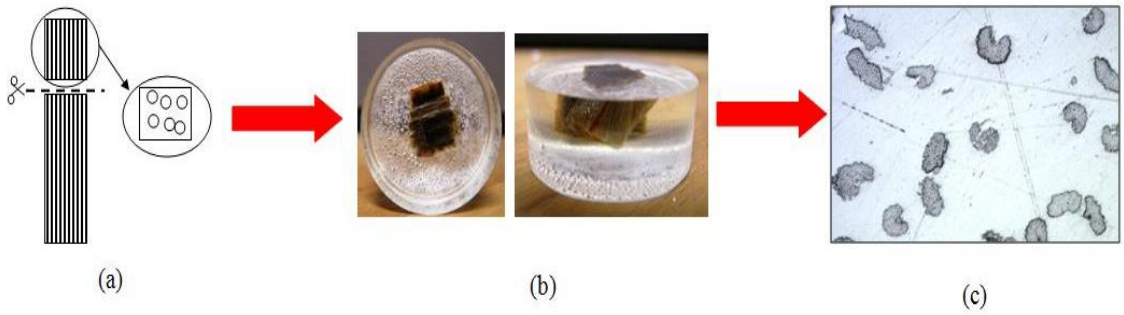

Figure 4.11: Fibre volume fraction measurement process

1. All the composites that were tested were used to calculate the volume fraction. The composites were cut perpendicular to the fibre's orientation to reveal the fibre's cross sectional area. The composite was cut using a Struers Discotom abrasive cutter

2. The cut section was then embedded in EPOFIX resin provided by Sturers and left for 24 hours for the resin to harden. Once the resin had cured the sample had to be ground and polished to get a clear image under the microscope. The process for grinding and polishing the resin block was the exact same method for measuring cross sectional area of natural fibres. More information of the process is in Chapter 3 Section 2.2.
3. After the grinding and polishing stage the composite was observed under the microscope. The microscope used was the Olympus G51 and the magnification was x50. This magnification made it easy to see the fibre but also covered a large area of the composite. Pictures of each composite cross section were taken along its width, as this would give an accurate estimation of the fibre volume fraction. Pictures were then imported in to the image analysis software and formatted to binary. The binary image allowed the software to count the number of pixels in the picture to calculate the area taken up by the fibre. Once the volume fraction had been determined for each picture of the composite the average was then calculated. This was to allow a good estimate of the volume fraction for each type of fibre composite.

4.3 Micromechanical and Semi Empirical Models

Whereas the longitudinal mechanical properties of a composite and their constitutive material can be determined directly by experimental means, micromechanical and semi empirical models are used to determine the transverse properties of fibres reinforcement in a composite. Using these complex mathematical models can reduce costly and time consuming testing, however the analysis is based on the assumption

that they are used for ideal composites and therefore the values that are calculated must be treated as estimations. In order to predict the properties of the composite, values for fundamental quantities such as the elastic modulus, Poisson's ratio and volume fractions of the constituent materials are required.

This is accomplished by using the general relationship between off axis Young's modulus, E_Θ, and the principle properties of a unidirectional reinforced composite ply as shown below in equation 4.8, [2, 3]:

$$E_\theta = \frac{1}{\frac{1}{E_1}cos^4\theta + \frac{1}{E_2}sin^4\theta + \left[\frac{1}{G_{12}} - \frac{2\nu_{12}}{E_1}\right]cos^2\theta sin^2\theta} \tag{4.8}$$

Composite samples must be tested at a minimum of three different fibre orientations, Θ, to determine the values of E_1, E_2 and ($1/G_{12}$ - $2\nu_{12}$ / E_1). where E_Θ, E_1 and E_2 are the off axis, longitudinal composite and transverse composite modulus respectively. G_{12} is the composite shear modulus and ν_{12} is the longitudinal composite Poisson's ratio. This data must then be supplemented with a value for either Poisson's ratio or the shear modulus to determine all the relevant independenct elastic properties of the composite ply. Once the elastic properties of a single unidirectional ply have been established, further micromechanical models can be used to extract values for the elastic properties of the fibre reinforcement.

The rule of mixtures is one of the simplest and most popular models used to predict the longitudinal elastic properties of a unidirectional composite material. It can be used as shown in equation 4.9 below to obtain a value for E_{1f} the axial modulus of the fibre , [3]:

$$E_{1f} = \frac{E_1 - E_m V_m}{V_f} \tag{4.9}$$

E_{1f}, E_m, V_f, V_m are the elastic modulus and volume fraction of the fibre and the matrix respectively. A similar expression for the fibre Poisson's ratio can also be derived, where the values of moduli are substituted for equivalent Poisson's ratio gives:

$$v_{1f} = \frac{v_{12} - v_m V_m}{V_f} \tag{4.10}$$

This expression is most effective with unidirectional continuous fibres, where a basic assumption of equal strain in the two materials constituents holds true [2].

A straightforward equation to obtain the transverse modulus of the fibre, E_{2f} is the inverse rule of mixtures. The equation can be arranged, as shown below in equation 4.11, to obtain a value for the fibre transverse modulus.

$$\frac{1}{E_{2f}} = \frac{1}{V_f}\left(\frac{1}{E_2} - \frac{V_m}{E_m}\right) \tag{4.11}$$

Alternatively the semi–empirical model developed by Halpin and Tsai [2, 3] can also be used to predict the elastic properties, in particular the transverse and shear moduli of fibre reinforced composites. The model is a modification of the inverse rules of mixtures. Therefore the Halpin–Tsai model can also be used to solve for the fibre's transverse modulus, E_{2f} and is shown below in equation 4.12:

$$E_{2f} = \frac{E_m(\eta\beta + 1)}{(1 - \beta)} \tag{4.12}$$

$$\beta = \frac{\left(\frac{E_2}{E_m} - 1\right)}{\left(\eta V_f + \frac{E_2}{E_m} V_f\right)} \tag{4.13}$$

The distribution of the reinforcing fibre is taken into account in the above equation by the fitting parameter, η. Several researchers have adopted a value of η = 2 and η = 1 for calculating the fibre's transverse and shear modulus when applying the Halpin–Tsai relationship. With insufficient experimental information to accurately ascertain this curve fitting parameter for the natural fibre and PET composite, a value of η=2 has been adopted in this research [2, 5–7]

Tsai – Hahn [2, 7] developed another semi empirical model that can be used in determining the transverse and shear modulus of the fibre. This model assumes that the transverse stress in the fibre is more than the stress carried in the matrix, therefore a stress partitioning factor, η, was developed to derive this method. The Tsai – Hahn equation is shown in equation 4.14 below:

$$E_{2f} = \frac{V_f}{\frac{V_f + \eta V_m}{E_2} - \eta \frac{V_m}{E_m}} \tag{4.14}$$

The symbols have their usual meaning. Several researchers have adopted a value of η = 0.5 [2] for the stress partitioning factor for fibres. Therefore this value has been adopted for this research in natural and PET fibre. Many properties used in the micromechanical and semi empirical models can be interchanged. An example is that the fibre longitudinal shear modulus can be calculated by substituting E_{2f}, E_2 and E_m for G_{12f}, G_{12} and G_m in equation 4.14.

The off axis coefficient of thermal expansion (CTE) of the composite can be determined experimentally or calculated by laminate theory. The equation used to calculate the off axis CTE by laminate theory is shown below [8]:

$$\begin{Bmatrix} \alpha_x \\ \alpha_y \\ \alpha_{xy}/2 \end{Bmatrix} = \begin{bmatrix} cos^2\theta & sin^2\theta & -2cos\theta sin\theta \\ sin^2\theta & cos^2\theta & 2cos\theta sin\theta \\ cos\theta sin\theta & -cos\theta sin\theta & cos^2\theta - sin^2\theta \end{bmatrix} \begin{Bmatrix} \alpha_1 \\ \alpha_2 \\ 0 \end{Bmatrix} \quad (4.15)$$

The coefficient of thermal expansion of a fibre can be determined from the coefficient of thermal expansion of the composite obtained by the TMA by using micromechanical and semi empirical models.

The Schapery [2, 7, 9] equation can be used to obtain the longitudinal coefficient of thermal expansion of the fibre (α_{1f}) and equation is shown below:

$$\alpha_{1f} = \frac{[\alpha_1(E_{1f}V_f + E_mV_m) - \alpha_m E_m V_m]}{E_{1f}V_f} \quad (4.16)$$

where α_1 and α_m are the longitudinal coefficient of thermal expansion of the composite and matrix.

Micromechanical models developed by Chamberlain and Chamis [10] can be used to estimate the fibre's transverse thermal expansion, α_{2f}, and are shown below in equations 4.17 and 4.18 respectively:

$$\alpha_{2f} = \alpha_m + \frac{(\alpha_2 - \alpha_m)\left[v_m(F - 1 + V_m) + (F + V_f) + \frac{E_m}{E_{1f}}(1 - v_{12f})\right]}{2V_f} \quad (4.17)$$

$$\alpha_{2f} = \frac{\alpha_2 - (1 - \sqrt{V_f})\left(1 + V_f v_m \frac{E_{1f}}{E_1}\right)\alpha_m}{\sqrt{V_f}} \quad (4.18)$$

where α_2 if the transverse coefficient of thermal expansion of the composite and F is the packing factor. The packing factor refers to how the fibres pack in the composite. The Chamberlain equation takes in to account two types of fibre packing, hexagonal packing (F = 0.9069) and square packing (F = 0.7854) [10].

4.4 Results and Discussion

4.4.1 Fibre volume Fraction

The fibre volume fraction for the PET, Sisal and Flax composites were found for each fibre orientation by using microscopy as previously explained in the experimental section. Pictures of the cross section of the tested composites are shown in Figure 4.12.

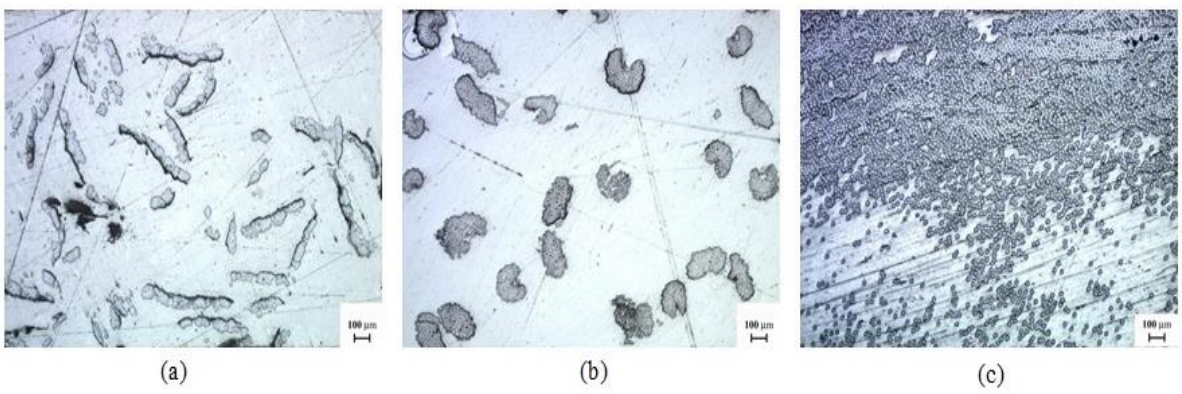

Figure 4.12: Cross section of the different fibre composites, a) Flax, b) Sisal & c) Polyethylene Terephthalate

It can be seen from Figure 4.12 that the natural fibres, Sisal and Flax, are dispersed evenly throughout the composite whereas the PET fibre is not. The PET fibre pictured, Figure 4.12c, shows that the fibres have not evenly dispersed and has congregated on half of the composite with a minimum fibre scatter on the other half.

Fibre volume fraction was measured for each composite at different fibre angles and the results can be seen in Table 4.2. It can be seen in the table that the PET composite has a greater fibre volume fraction than the natural fibre composites; this can also be seen from the composite cross section picture in Figure 4.12. The PET fibre volume fraction ranged from 40 – 60% whereas the natural fibres, Sisal and Flax, their fibre volume fraction ranged from 13 – 20% and 10 – 15% respectively. Average volume fractions were taken from the results and are presented in Table 4.2. The fibre volume fraction is needed for the micromechanical models to calculate the fibre's properties. The fibre volume fraction was found to be 51%, 13% and 14% for PET, Flax and Sisal respectively.

Table 4.2: Fibre volume fraction in the tested composites (off-axis cross section cut right angle to the fibre)

Orientation (^{o})	Polyethylene Terephthalate (%)	Flax (%)	Sisal (%)
0	43.5	15.9	12.6
30	38.8	10	13.2
45	47.8	12	20
60	64.2	13.9	16
90	59.1	14.3	19.2
Average	50.7	13.2	13.6
95% Confidence	±2.4	±2.0	±9.4

4.4.2 Dynamic Mechanical Analysis (DMA)

The DMA measured the modulus of the composites over a range of different fibre orientations. The result that was obtained from the DMA was the complex modulus of the composites and the polyester resin. The DMA results for PET, Flax and Sisal composites at different fibre orientations are shown in Figure 4.13 - 4.15 respectively.

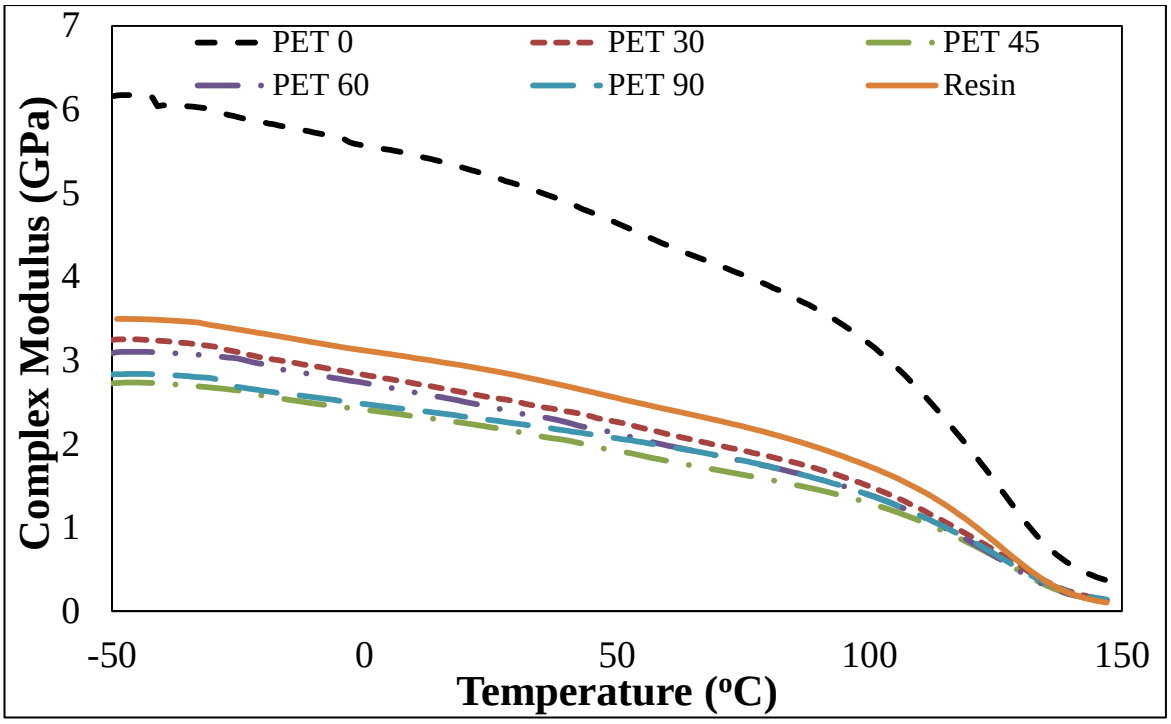

Figure 4.13: PET results obtained from the DMA

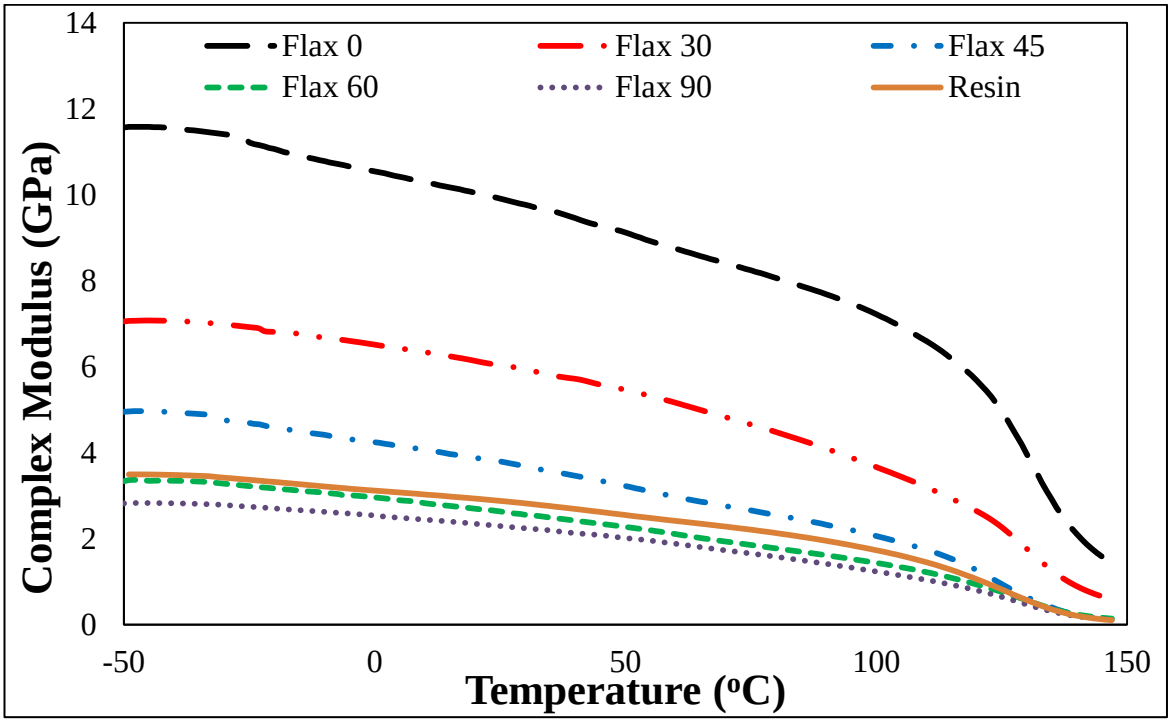

Figure 4.14: Flax results obtained from the DMA

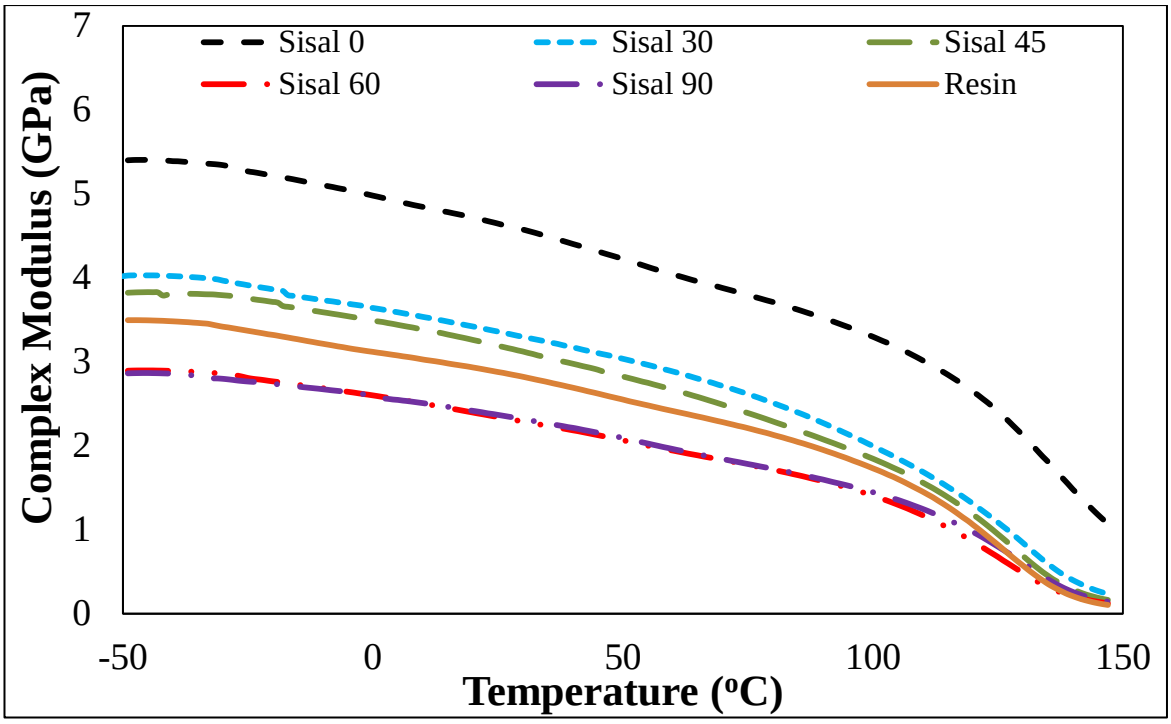

Figure 4.15: Sisal results obtained from the DMA

It can be clearly seen that for all the different fibre composites tested, the modulus decreases as the temperature increases. In addition to the temperature affecting the composite's modulus, the off axis angle also effects the modulus. Increasing the off axis angle decreases the modulus of the composite which is visible in all of the composite results. In the PET and Sisal DMA results, Figure 4.13 and 4.15, it is observed that the modulus for the PET 45^{o} and Sisal 60^{o} fibre orientation is lower than their 90^{o} composite. This may be explained by the volume fraction of the fibre being lower which can be observed in Table 4.2. It can also be seen in the graphs that a typical reduction in stiffness at around 125^{o}C is due to the glass transition temperature (T_g) of the resin which is between 110 – 130^{o}C. It is interesting to note that the transverse stiffness of all the fibre composites is lower than the polyester resin. This is an indication that there will be a likely probability of a low transverse stiffness of PET, Flax and Sisal fibres.

The off axis modulus, E_Θ, (equation 4.8) is related to the composites' mechanical properties such as the longitudinal modulus, E_1, transverse modulus, E_2, the longitudinal Poisson's ratio,v_{12} and the shear modulus, G_{12}. E_1 and E_2 can be approximated using the modulus of the composite for E_0 and E_{90} from the DMA results. The Poisson's ratio values were taken from the literature for the fibres and the polyester resin. The Poisson ratio used for the natural fibres (Sisal and Flax assumed ratio is the same), PET fibre and Polyester resin were 0.33, 0.3 and 0.35 respectively [11–13]. Using equation 4.10 the longitudinal Poisson's ratio of the composite can be calculated to be 0.36 and 0.33 for natural fibre and PET composite correspondingly and are used to solve for G_{12}. The longitudinal shear modulus, G_{12} of the composite was obtained by curve fitting equation 4.8 to the experimental results taken from Figure 4.13, 4.14 and 4.15 at the various temperatures. The experimental and calculated data for the off axis modulus is plotted as a function of temperature and is shown in Figure 4.16, 4.17 and 4.18 for PET, Flax and Sisal. It can be seen from the graphs that the relationship between the calculated and the experimental values are respectable with the coefficient of determination value, R^2, being 0.99, 0.95 and 0.97 for Flax, Sisal and PET respectively. Therefore the micromechanical models can be employed to determine the elastic properties of the fibre.

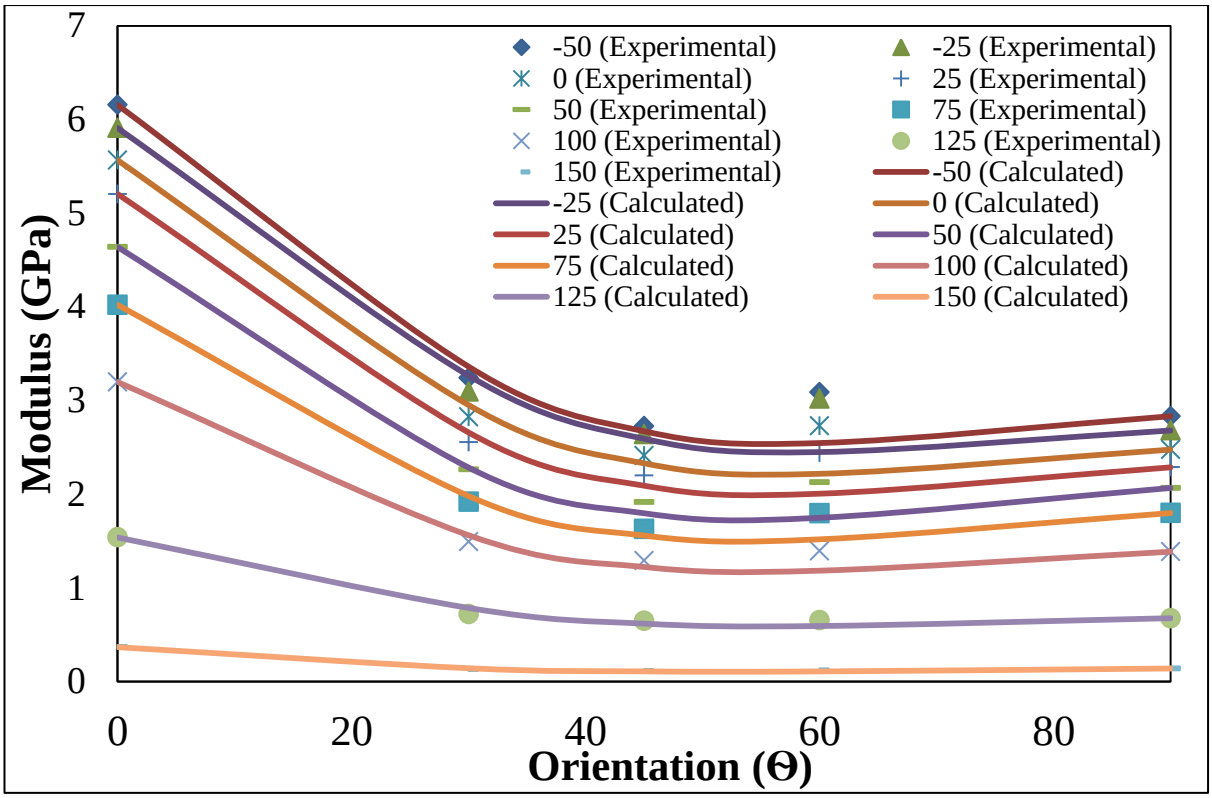

Figure 4.16: PET angle orientation versus modulus plotted as a function of temperature

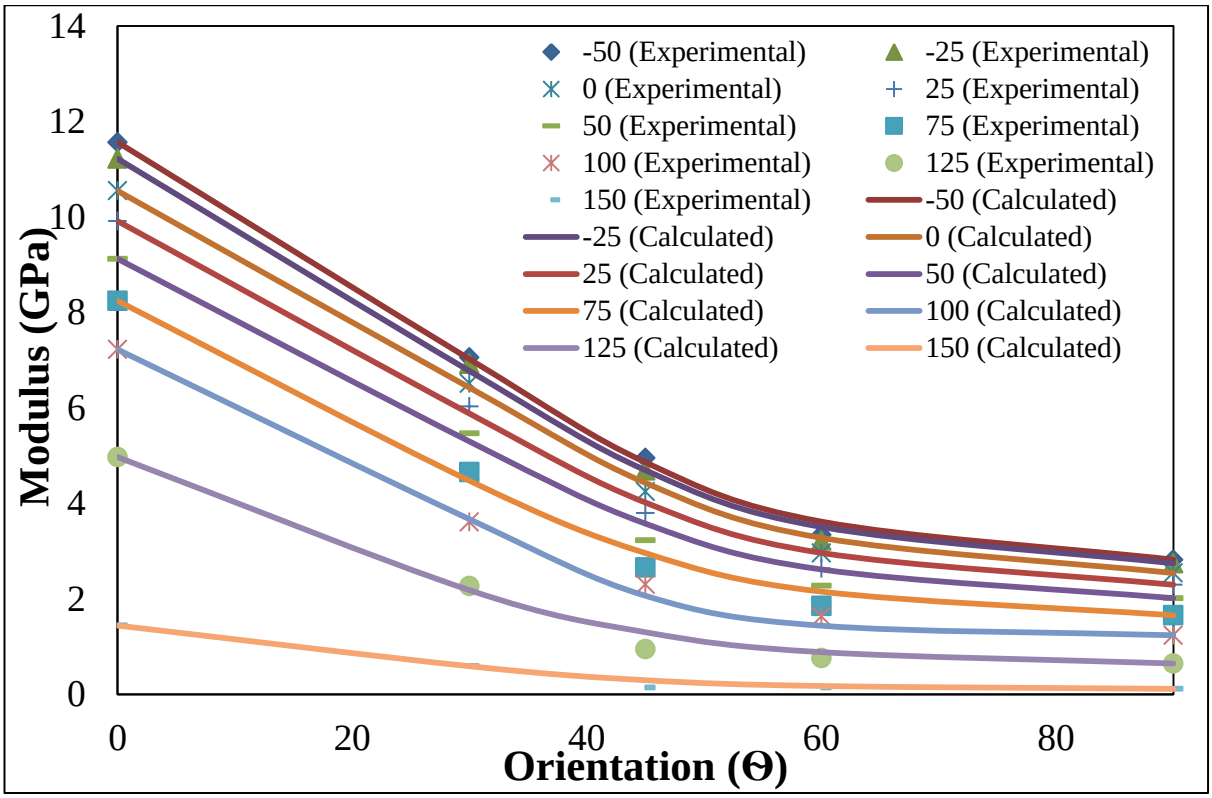

Figure 4.17: Flax angle orientation versus modulus plotted as a function of temperature

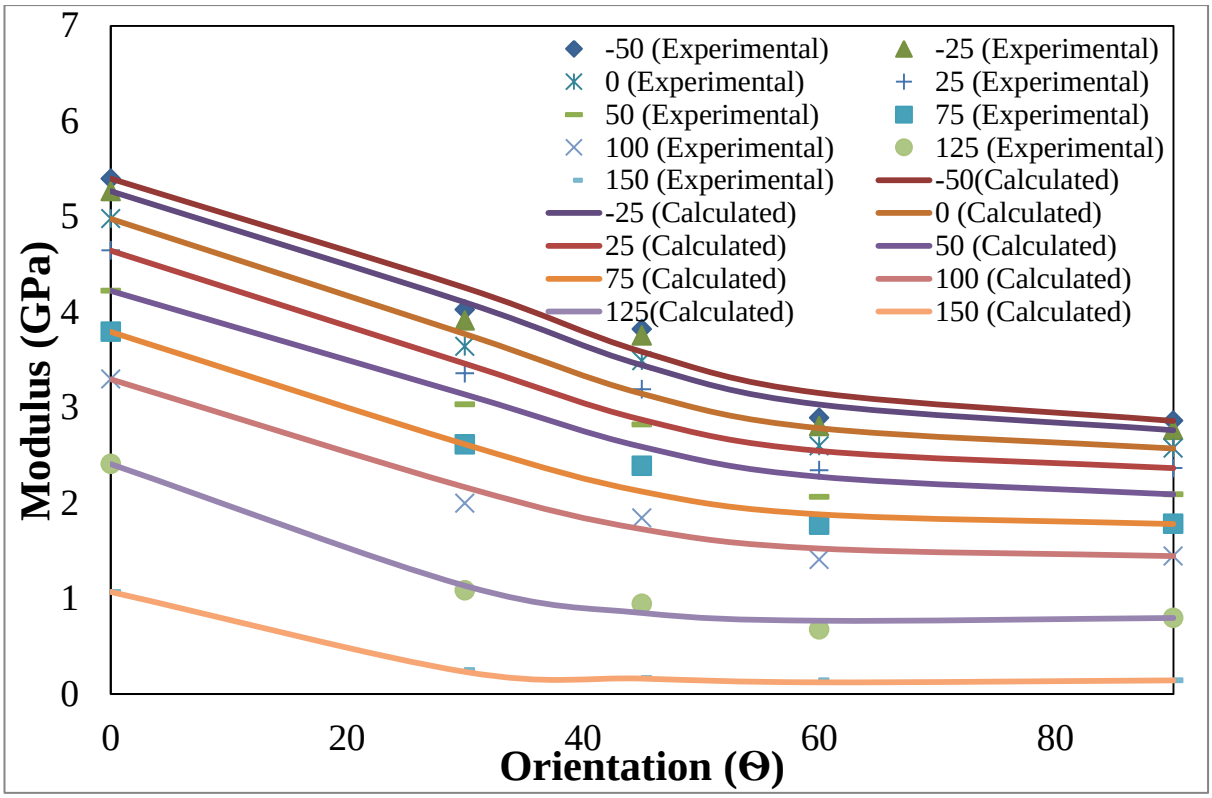

Figure 4.18: Sisal angle orientation versus modulus plotted as a function of temperature

The results of the DMA for resin, 0^o and 90^o composites along with the composite shear modulus obtained by curve fitting equation 4.8 were substituted into equation 4.9 – 4.14 to obtain the fibre values for longitudinal, transverse and shear across a temperature range -50^oC to 125^oC (below the T_g of the resin). The results of the longitudinal modulus are shown in Table 4.3 for PET, Flax and Sisal respectively.

Table 4.3: Longitudinal modulus of the fibres, E_{1f}

Temp (^oC)	***-50***	***-25***	***0***	***25***	***50***	***75***	***100***	***125***
PET (GPa)	8.8	8.5	8.0	7.5	6.7	5.8	4.7	2.3
Flax (GPa)	65.6	63.7	60.3	57	53.1	48.6	44	32.7
Sisal (GPa)	17.1	16.9	16.4	15.5	14.5	13.5	12.9	12.2

Table 4.3 shows that as the temperature increases, the modulus of the fibre decreases this is also see in graph shown in Figure 4.19. The fibre's longitudinal modulus results at room temperature, 25^{o}C, were compared to the tensile test results obtained in Chapter 2. The modulus found by tensile test for PET, Flax and Sisal was found to be 5.7 GPa, 50 GPa and 20.7 GPa respectively. The PET tensile test result used was the heat treated modulus due to the composite having to be post cured at 120^{o}C before testing. Comparing the two results it can be said that they are similar and that the micromechanical model is in good agreement with the tensile test result.

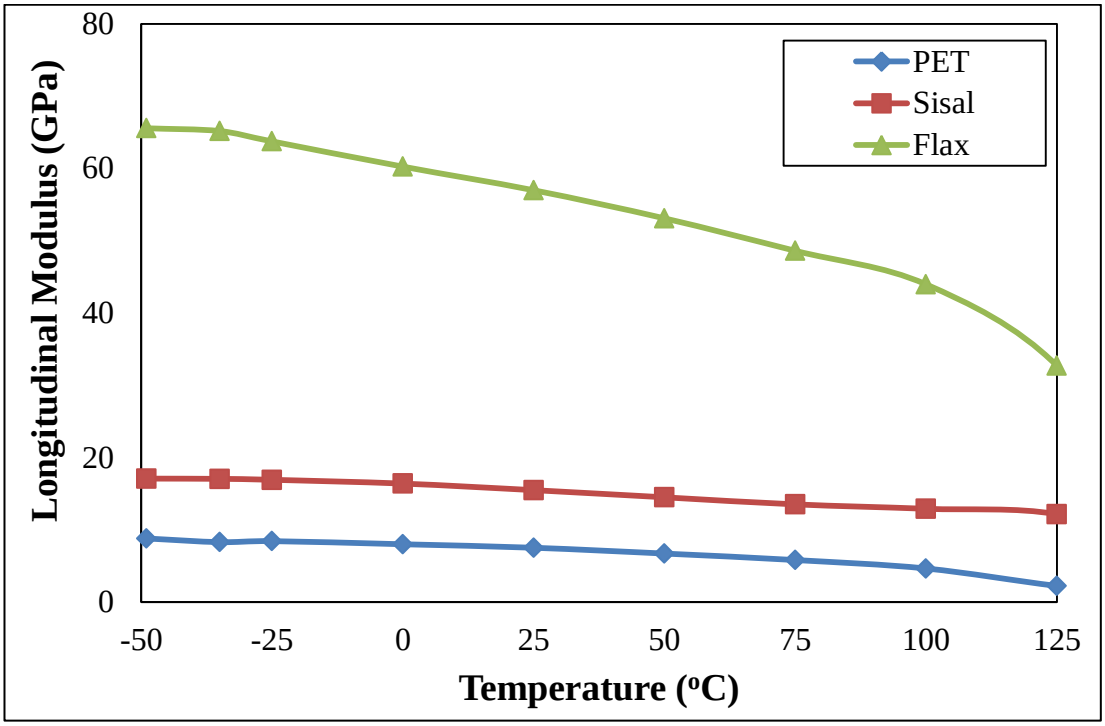

Figure 4.19: Fibre longitudinal modulus against temperature

A comparison of the results obtained from the micromechanical and semi-empirical models (equations 4.10 – 4.14) which were used to calculate the transverse modulus of the fibre, E_{2f}, are shown for PET, Flax and Sisal in Figures 4.20-4.22. The figures show the transverse modulus results at various temperatures with a line connecting the data points together.

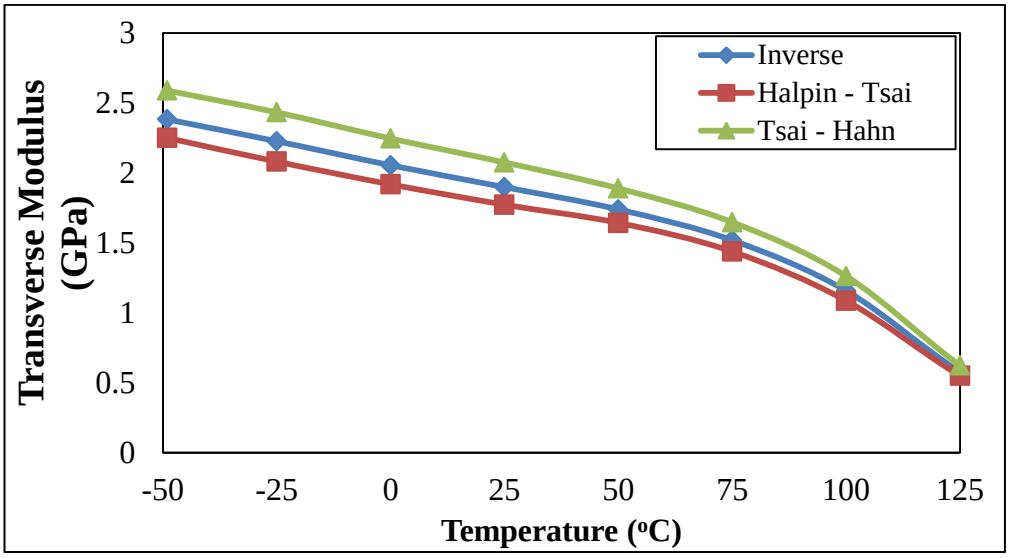

Figure 4.20: PET transverse modulus calculated using micromechanical equations

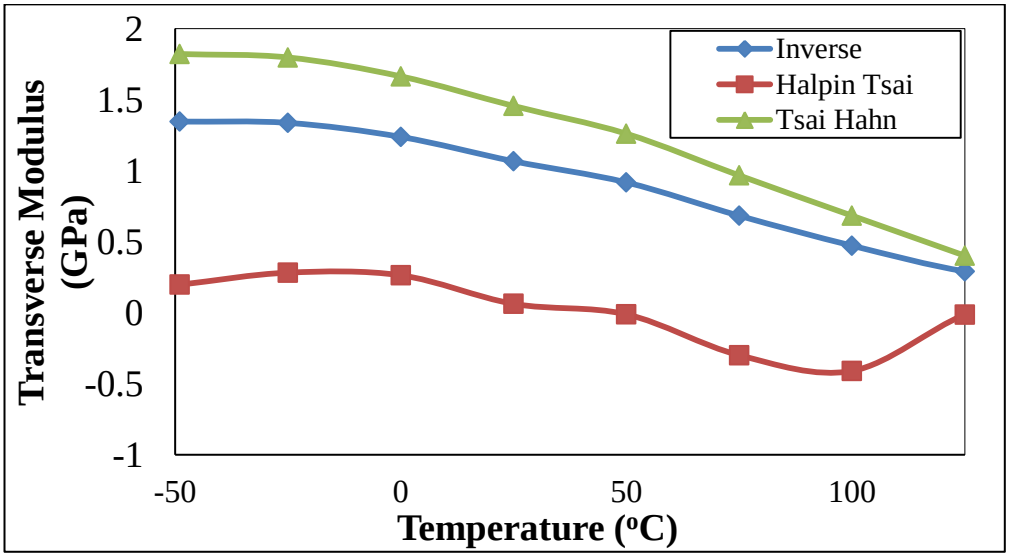

Figure 4.21: Flax transverse modulus calculated using micromechanical equations

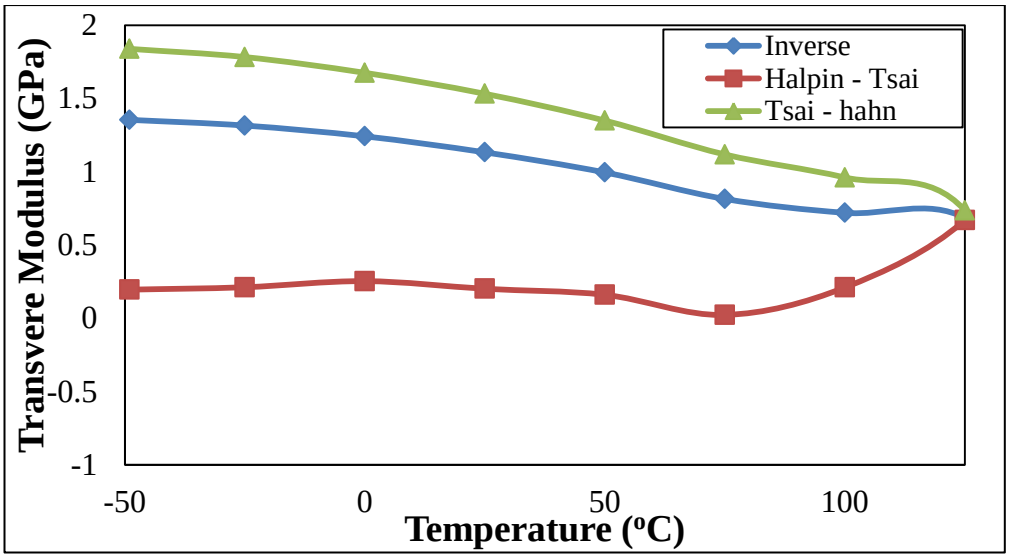

Figure 4.22: Sisal transverse modulus calculated using micromechanical equations

From the graphs it can be seen that results obtained from applying Halpin –Tsai for Flax and Sisal is significantly different than the results attained by Tsai – Hahn and the Inverse rules of mixtures. There are two conditions when Halpin – Tsai cannot be used and this was noted by Jones [5]. The first condition is that the curve fitting parameter $\eta=0$ the equation reduces to the inverse rule of mixtures, which is likely to be the reason for the natural fibre results. The second condition is η = infinity, the Halpin – Tsai equation reduces to the rule of mixtures. It was also observed by Thomason [14] that the Halpin – Tsai equation was unable to be used when investigating glass – reinforced polyamides under certain conditions, as they could not achieve an agreement for β for the five experiments carried out. Consequently, the average transverse modulus was calculated only using the inverse rule of mixtures and Tsai – Hahn for Flax and Sisal. The results of the transverse modulus of each fibre are shown in Table 4.4. Figure 4.20 shows that the PET transverse modulus decreases dramatically after the temperature rises above 75^{o}C. A reason for

this dramatic decrease in the transverse modulus is that it is around the glass transition temperature for PET (70 – 80^{o}C). Similar to the longitudinal modulus results, Table 4.4 shows that the transverse modulus decreases as the temperature increases.

Table 4.4: Transverse modulus of the fibres, E_{2f}

Temp (^{o}C)	***-50***	***-25***	***0***	***25***	***50***	***75***	***100***	***125***
PET (GPa)	2.4	2.2	2.1	1.9	1.8	1.5	1.2	0.6
Flax (GPa)	1.6	1.6	1.5	1.3	1.1	0.82	0.58	0.35
Sisal (GPa)	1.6	1.5	1.5	1.3	1.2	0.97	0.84	0.71

The ratio of the fibre's longitudinal modulus against the fibre's transverse modulus presented as a function of temperature is shown in Figure 4.23. The graph highlights the degree of mechanical anisotropy evident in natural and PET fibres. It can be seen that E_{1f} exceeds the transverse modulus by a factor of 3 for PET, 10 for Sisal and 40 for Flax across the temperature range.

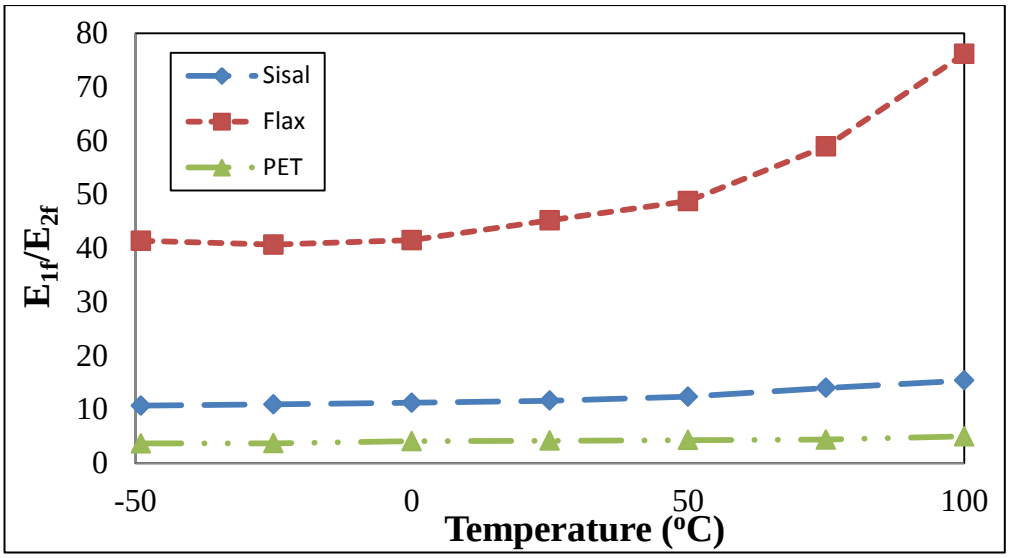

Figure 4.23: Ratio of E_{1f} versus E_{2f} for PET, Flax and Sisal across temperature range

The shear modulus of the reinforcement fibres in the composite were calculated in the same way as the fibre's transverse modulus, by substituting the E_m and E_2 values with G_m and G_{12} to calculate G_{12f}. The results from calculating the shear modulus of the fibres by the micro mechanical and semi empirical models is shown in Figure 4.24, 4.25 and 4.26.

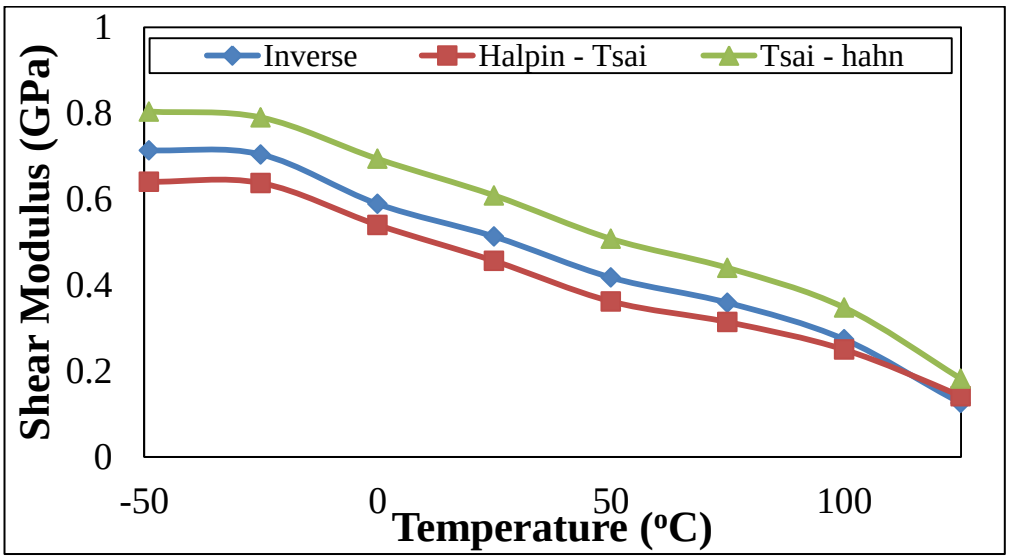

Figure 4.24: Shear modulus of PET fibre, G_{12f}

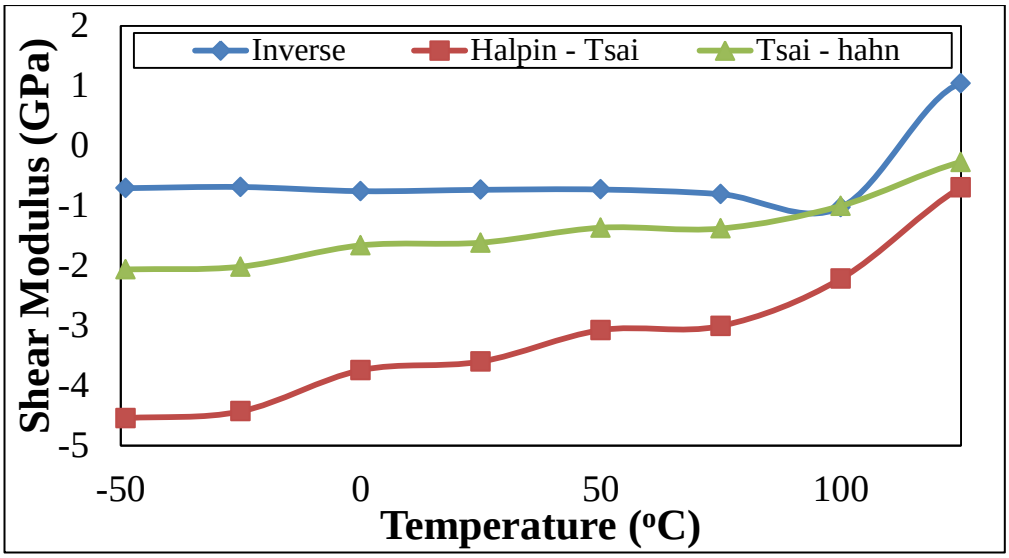

Figure 4.25: Shear modulus of Flax fibre, G_{12f}

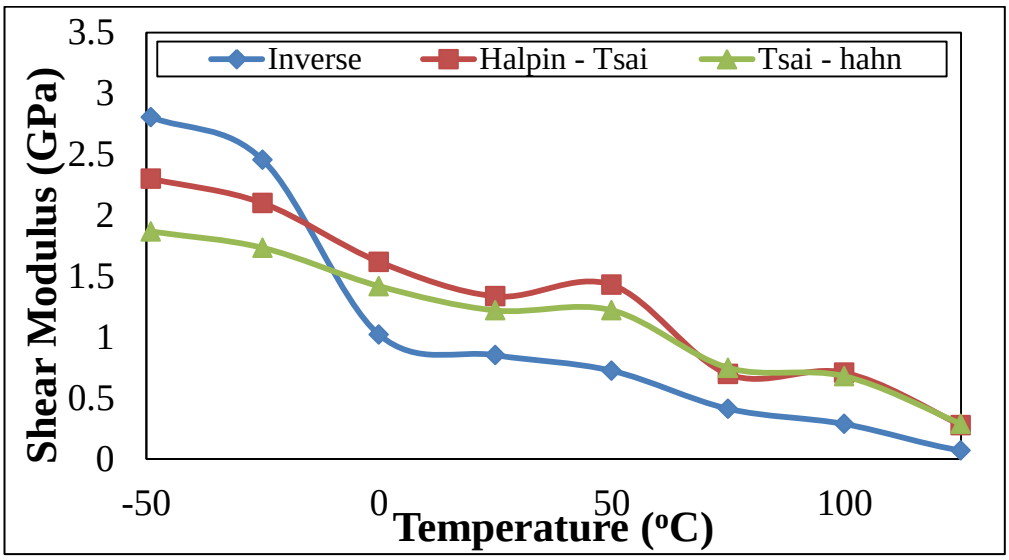

Figure 4.26: Shear modulus of Sisal Fibre, G_{12f}

It is observed that the shear modulus for Flax fibre in Figure 4.25 is negative. An explanation for this is that the micromechanical models used are assuming that the fibres are circular [14, 15]. It can be seen from Figure 4.12a that Flax fibre shape is more elliptical than circular whereas Sisal is reasonably circular therefore the model gives respectable results. Another explanation could be due to the nature of Flax fibre, it is observed in Figure 4.23 that Flax fibre is highly anisotropic compared to

Sisal and PET fibre therefore the Flax geometry could affect the model. However theoretical analysis using micromechanical models into the properties of fibres in the transverse direction has not been developed to date and will not be looked at in this thesis.

Figure 4.24 and 4.26 shows that the shear modulus of the fibre decreases as the temperature increases. The graphs (Figures 4.24 and 4.26) also show that the micromechanical models seem to be in good agreement with one another when predicting the shear modulus of the reinforcement fibre. The average fibre shear moduli were calculated from the micromechanical models for PET and Sisal and are shown in Table 4.5. The PET estimation at room temperature (25^{o}C) is similar to the value of 0.63 GPa achieved by Kawabata [17].

Table 4.5: Calculated Fibre Shear Modulus, G_{12f}

Temp (^{o}C)	***-50***	***-25***	***0***	***25***	***50***	***75***	***100***	***125***
PET (GPa)	0.72	0.71	0.61	0.53	0.43	0.37	0.29	0.15
Sisal (GPa)	2.3	2.1	1.4	1.1	1.1	0.62	0.56	0.21

4.4.3 Thermomechanical Analysis (TMA)

The TMA measured the thermal strain of the polyester resin and the composites at various fibre orientations. The results of the TMA for PET, Flax and Sisal composites are shown in Figure 4.27, 4.28 and 4.29. It can be observed from the TMA results that as the temperature increases from -50 to 150^{o}C, the strain increases. The graphs also show that the thermal strain increases as the fibre orientation increases from 0 to 90^{o}. An interesting thing to note from Figure 4.27 – 4.29 is that

the thermal strain of the composite loaded at 90^{o} is approximately or slightly above the thermal strain of the resin.

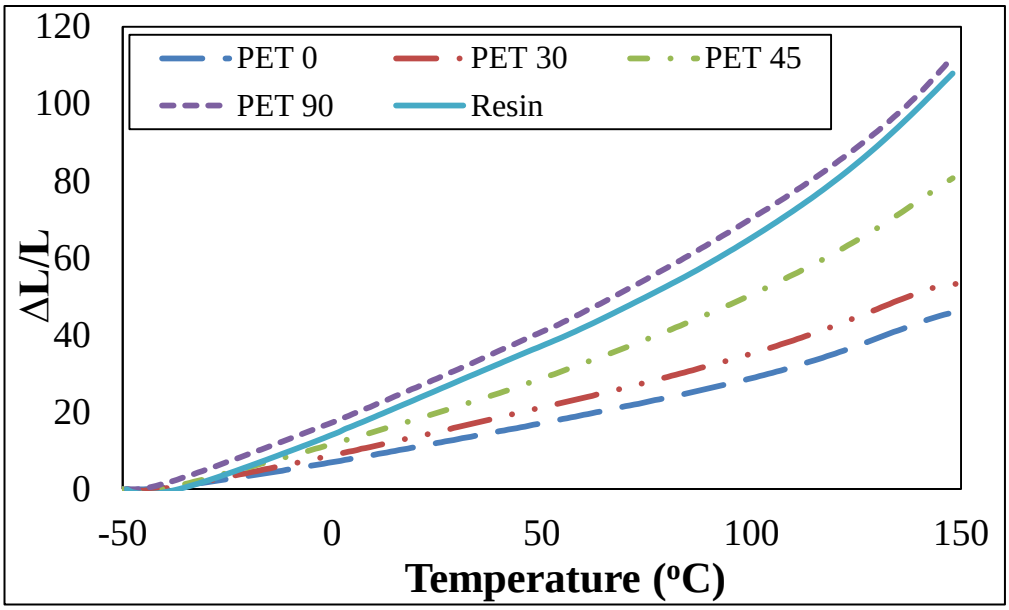

Figure 4.27: Thermal strain of PET composite specimen with varying fibre orientation

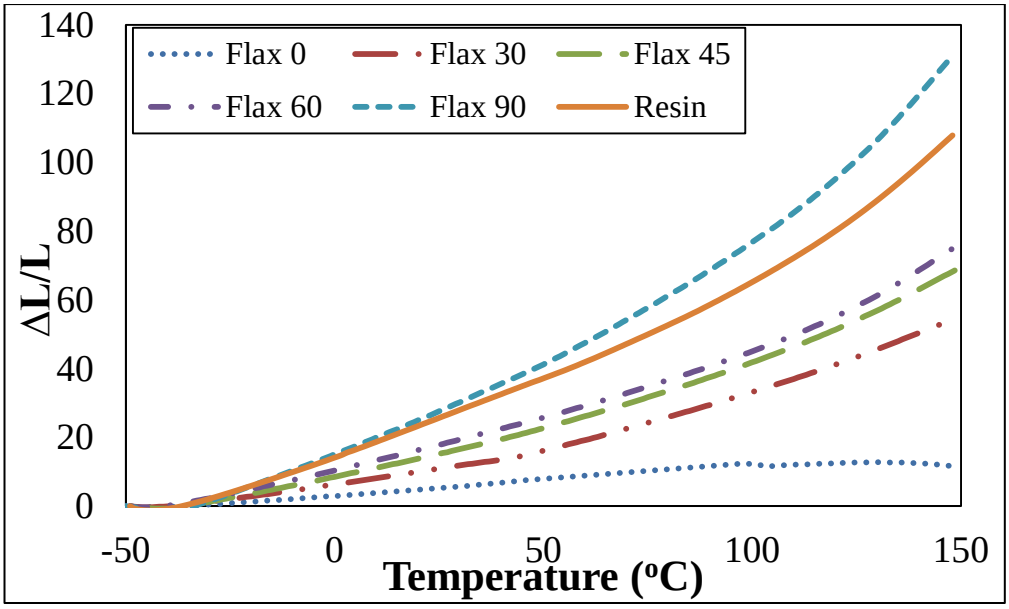

Figure 4.28: Thermal strain of Flax composite specimen with varying fibre orientation

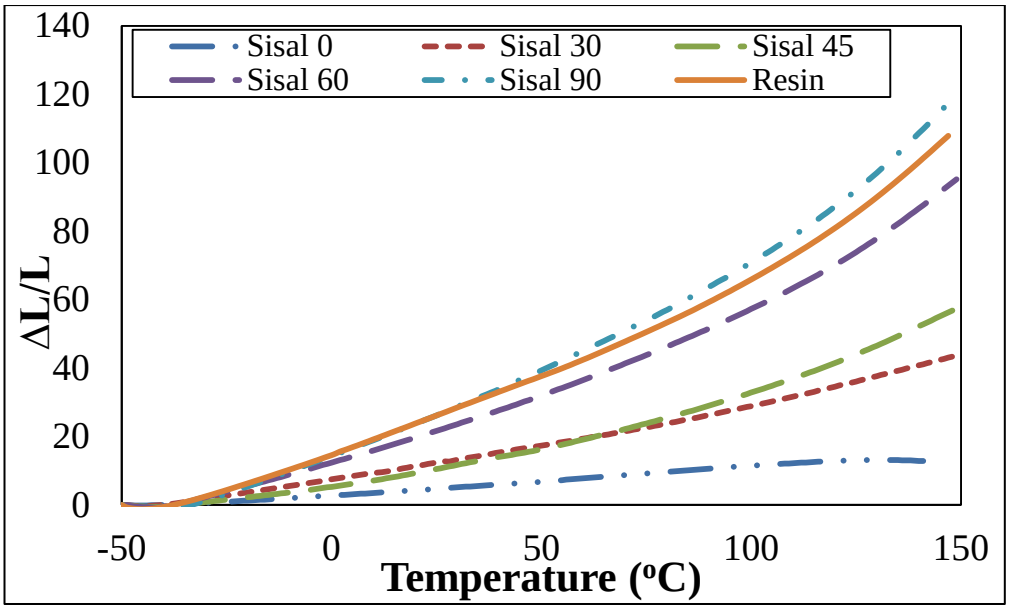

Figure 4.29: Thermal strain of Sisal composite specimen with varying fibre orientation

Similar to calculating the off axis modulus of the composite, laminate theory was used to calculate the off axis coefficient of thermal expansion (CTE) of the composite. Equation 4.15 is used with α_1 and α_2 is substituted with the values obtained for 0^o and 90^o CTE of the composite. The calculated results for the off axis linear coefficient of thermal expansion (LCTE) is plotted as a function of temperature along with the experimental results and is shown in Figure 4.30, 4.31 and 4.32 for PET, Flax and Sisal. It can be observed from the graphs that the off axis CTE calculated by laminate theory is in good agreement with the experimental results obtained by the TMA and the coefficient of determination value, R^2, being approximately 0.9 for all the fibre reinforcements. Interesting to note the CTE result at 125^oC at 0^o orientation for both Sisal and Flax are lower than any other temperature. Since the calculated and experimental CTE is in agreement with one another it can be said that micromechanical models can be used to calculate the longitudinal and transverse CTE of the fibres.

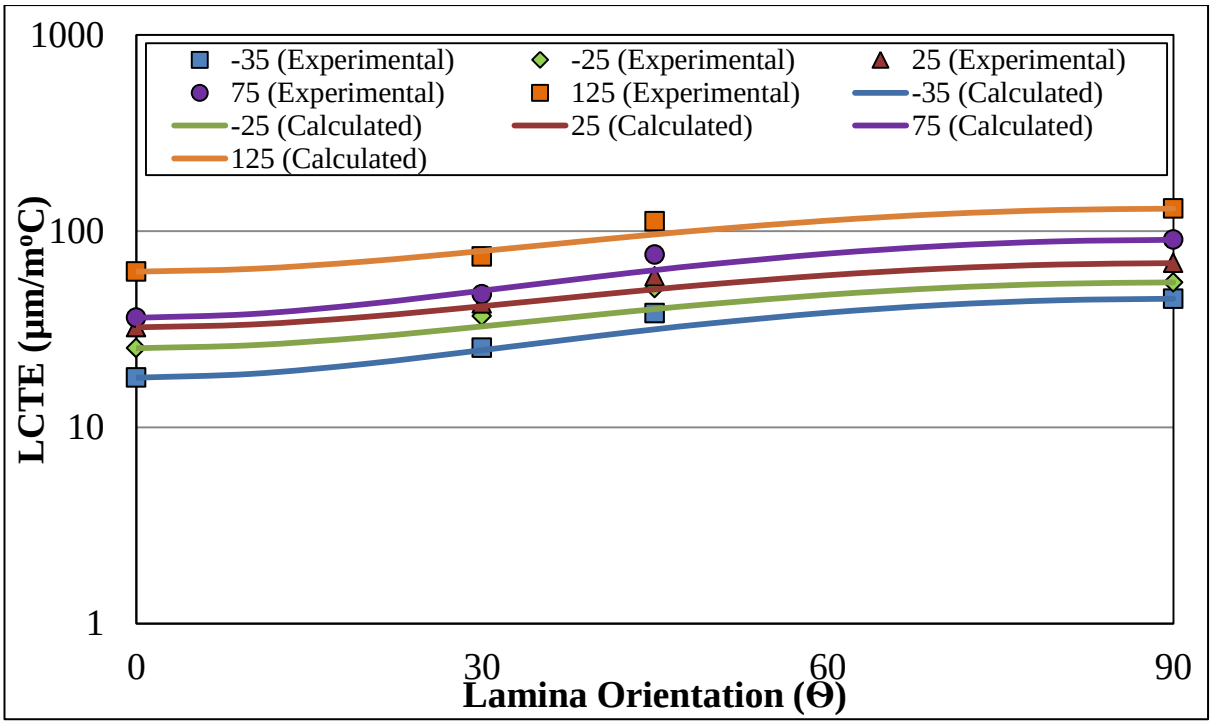

Figure 4.30: PET angle orientation versus LCTE as a function of Temperature

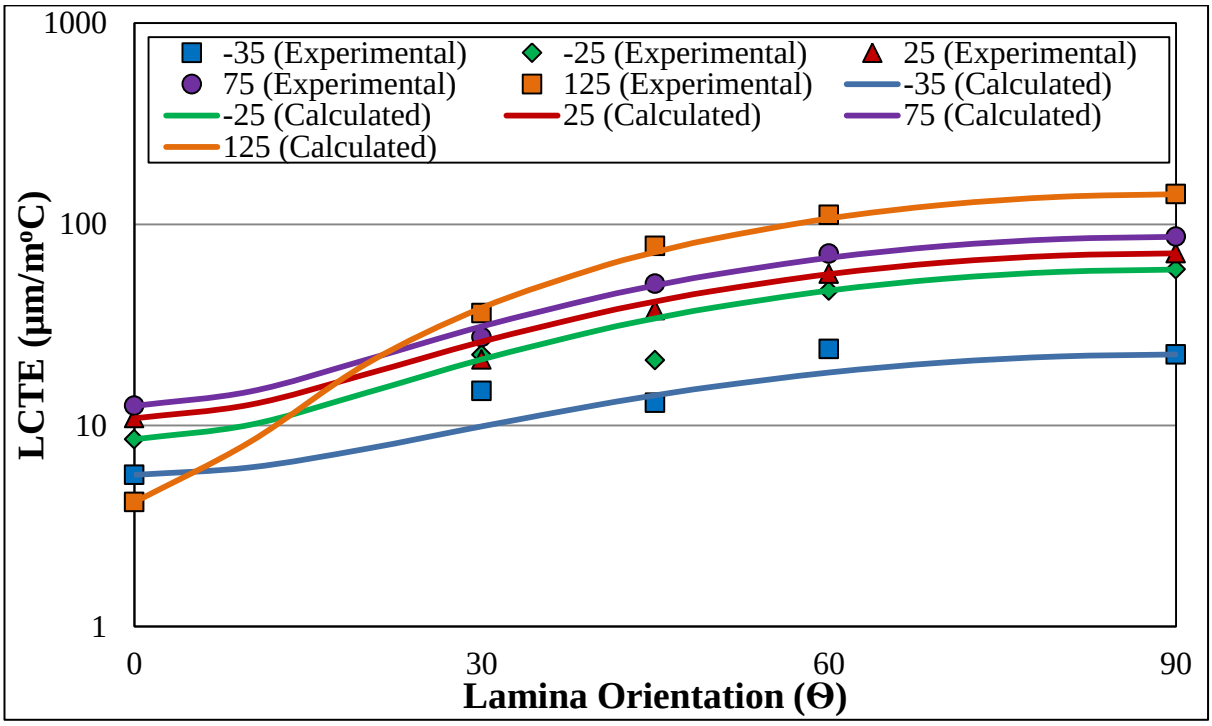

Figure 4.31: Flax angle orientation versus LCTE as a function of Temperature

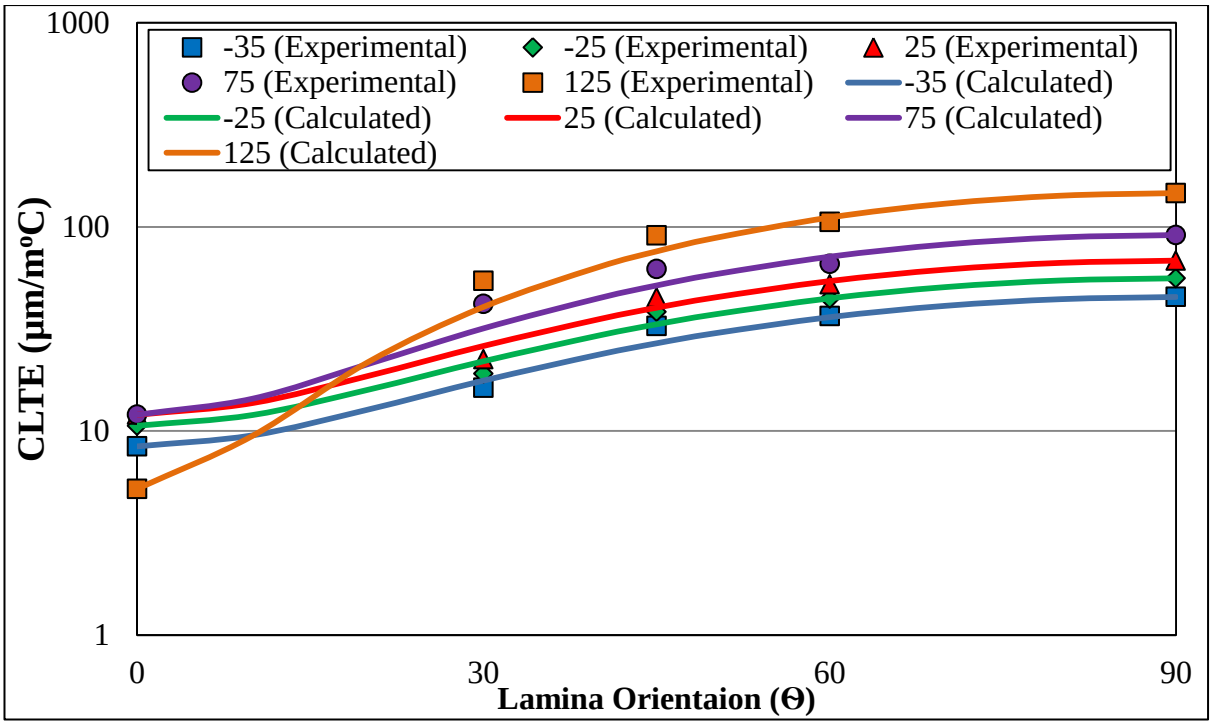

Figure 4.32: Sisal angle orientation versus LCTE as a function of temperature

The results from the TMA for 0^o and 90^o composites and the resin were substituted in to equation 4.16, 4.17 and 4.18. This was done to obtain the longitudinal and transverse coefficient of thermal expansion of each fibre across a temperature range of -35^oC to 125^oC (before T_g of the resin). The reason for obtaining the longitudinal and transverse CTE was to help in the investigation of the interfacial shear strength between the fibres and PP in Chapter 5. The CTE for PET, Flax and Sisal using the different equations for the longitudinal and transverse direction is shown in Figure 4.33, 4.34 and 4.35 respectively.

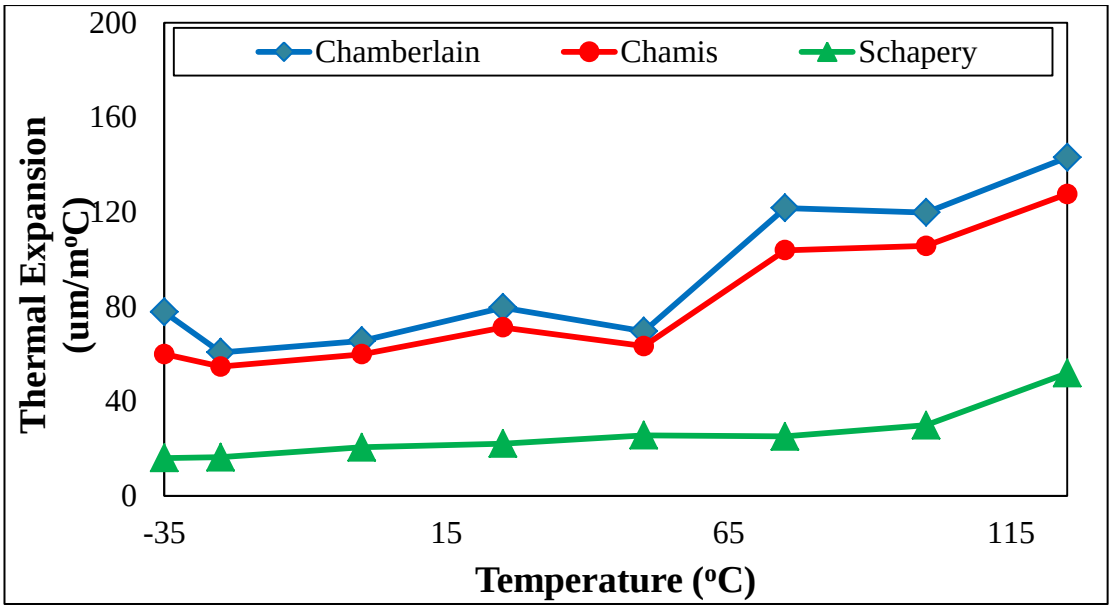

Figure 4.33: PET fibre coefficient of thermal expansion (CTE)

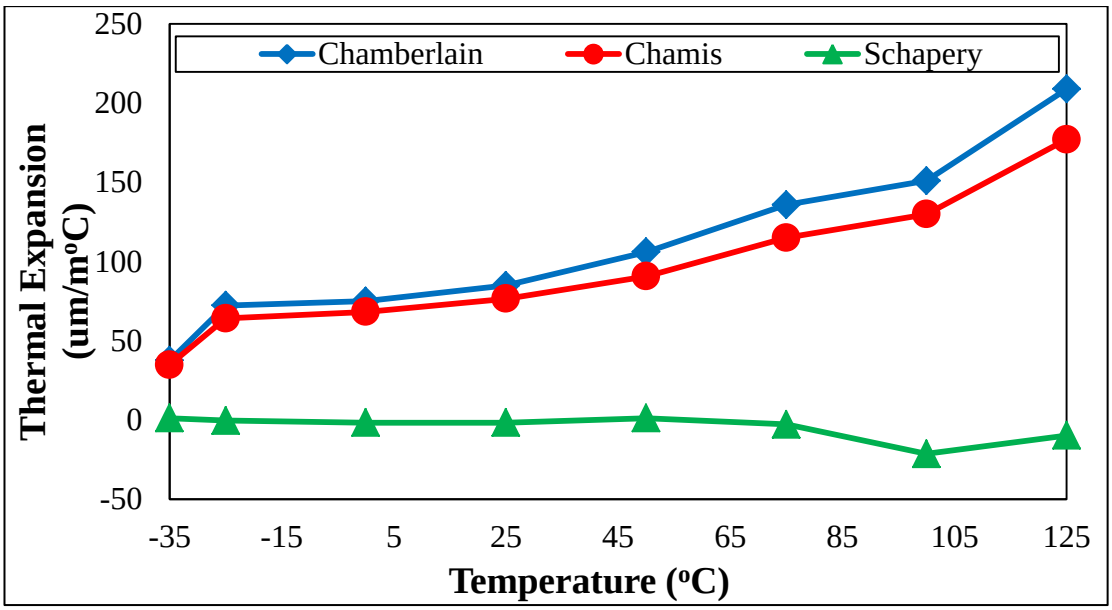

Figure 4.34: Flax fibre coefficient of thermal expansion (CTE)

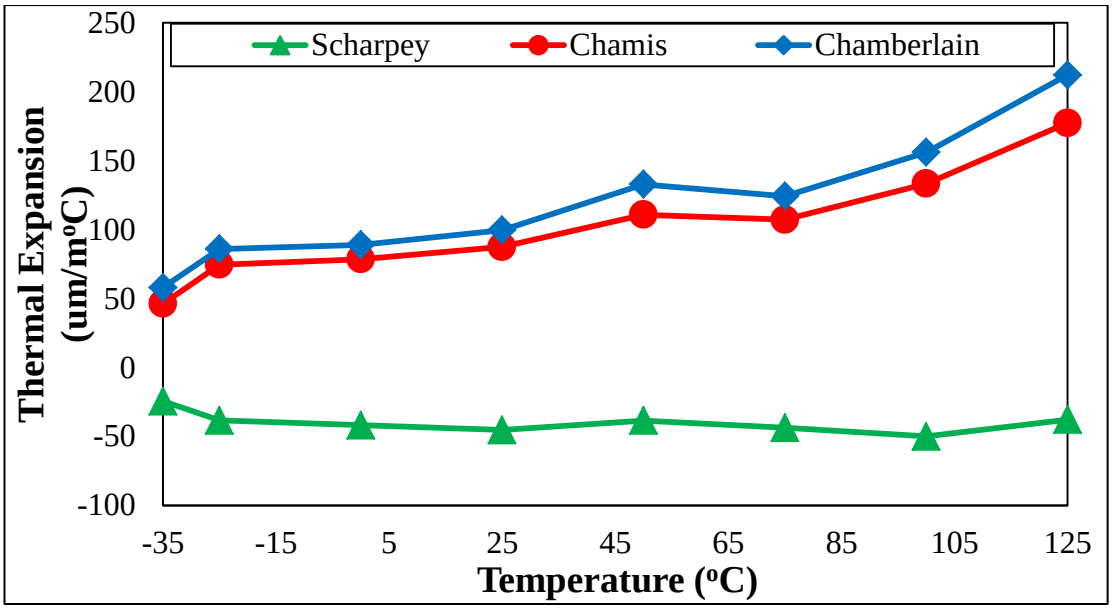

Figure 4.35: Sisal fibre coefficient of thermal expansion (CTE)

It can be seen for all the fibres tested, that the longitudinal CTE is lower than the transverse CTE and that the micromechanical and semi-empirical models for α_{2f} are in good agreement with each other, equations 4.17 and 4.18.

The PET thermal expansion is a rough guide to the difference between the longitudinal and the transverse direction, as the PET fibre has been heat treated in the composite before testing. The heat treatment needed to be done to post cure the polyester resin. Heat treatment removes stresses in the PET fibre that are created in the fibre manufacturing process therefore erasing thermal shrinkage [18]. It would be expected that the PET fibre should have a negative longitudinal CTE due to the fibre's length decreasing as the temperature increases. This is not seen in Figure 4.33 due to the PET fibre being heat treated in the composite before testing. Figure 4.33 shows that the PET longitudinal and transverse CTE is approximately 22.1 µm/m^{o}C and 70.3 µm/m^{o}C respectively at room temperature. The transverse CTE value is

close to the bulk thermal expansion of PET which varies from 60 to 120 μm/m^{o}C [18, 19]

The Flax and Sisal (Figure 4.34 and 35) longitudinal CTE is approximately -1.6 μm/m^{o}C and -45.3 μm/m^{o}C respectively at room temperature (25^{o}C). This behaviour is similar to that reported for jute fibre which also has a negative value at room temperature [2]. This result is in contrast to that of the transverse CTE of the Flax and Sisal fibre, 72.5 μm/m^{o}C and 76.3 μm/m^{o}C. The transverse CTE is completely different in magnitude and directionality to the longitudinal CTE of the natural fibres.

Table 4.6: Thermoelastic properties of PET fibre

	-50^{o}C	-25^{o}C	0^{o}C	25^{o}C	50^{o}C	75^{o}C	100^{o}C	125^{o}C
E_{1f} (GPa)	8.8	8.4	8.0	7.5	6.7	5.8	4.6	2.3
E_{2f} (GPa)	2.4	2.2	2.1	1.9	1.8	1.5	1.2	0.6
G_{12f} (GPa)	0.72	0.71	0.61	0.52	0.43	0.37	0.29	0.15
α_{1f} (μm/m^{o}C)		16.4	20.5	22.1	25.6	25.2	29.9	51.9
α_{2f} (μm/m^{o}C)		54.1	59.9	70.3	63.3	99.7	104.2	128.2

Table.4.7: Thermoelastic properties of Flax fibre

	-50^{o}C	-25^{o}C	0^{o}C	25^{o}C	50^{o}C	75^{o}C	100^{o}C	125^{o}C
E_{1f} (GPa)	65.6	63.7	60.2	57	53.1	48.6	44	32.7
E_{2f} (GPa)	1.6	1.6	1.5	1.3	1.1	0.82	0.58	0.5
α_{1f} (μm/m^{o}C)		-0.3	-1.6	-1.6	1.2	-2.7	-21.3	-9.7
α_{2f} (μm/m^{o}C)		60	65.1	72.5	82.6	104	119.3	162.3

Table 4.8: Thermoelastic properties of Sisal fibre

	-50°C	-25°C	0°C	25°C	50°C	75°C	100°C	125°C
E_{1f} (GPa)	17.1	16.9	16.4	15.5	14.5	13.5	12.9	12.2
E_{2f} (GPa)	1.6	1.5	1.5	1.3	1.2	0.97	0.84	0.71
G_{12f} (GPa)	2.3	2.1	1.4	1.1	1.1	0.62	0.56	0.21
α_{1f} (μm/m°C)		-38.3	-41.9	-45.3	38.5	-43.7	-49.9	-37.7
α_{2f} (μm/m°C)		63.2	68.9	76.3	89.6	92.6	115.8	156.9

4.5 Summary

Thermoelastic behaviour of PET, Flax and Sisal composites has been investigated and quantified in this chapter. The off–axis properties of the unidirectional PET and natural fibre composites were established through a series of mechanical and thermo mechanical experiments. The results were then incorporated into a number of micromechanical and semi – empirical models to estimate the thermoelastic fibre properties of PET, Flax and Sisal. The longitudinal and transverse properties of the fibres were found to be significantly different, highlighting the highly anisotropic structure of the natural fibres and PET fibre. A summary of the findings in this study are shown in Table 4.6, 4.7 and 4.8. The tables highlights that the Flax, Sisal and PET have highly anisotropic properties. Therefore the likely use of only longitudinal fibre properties in composite property modelling will lead to an inaccurate prediction of the composite performance. It has also been observed in this chapter that using micromechanical models to predict properties of non-circular fibres can provide inaccurate results. This is shown in the results obtained for Flax shear modulus

where the micromechanical models gives a negative modulus and this is due to the Flax cross section being more oval shaped than circular.

4.6 References

[1] M. C. Symington, "Vacuum infusion of Natural Fibre composites for structural applications," *in ECCM 13*, 2008.

[2] F. R. Cichocki Jr and J. L. Thomason, "Thermoelastic anisotropy of a natural fiber," *Composites Science and Technology*, vol. 62, pp. 669–678, 2002.

[3] F. L. Matthews and R. D. Rawlings, *Composite Materials: Engineering and Science*. Woodhead Publishing Limited, 1999.

[4] W. Patterson and A. Force, "The Halpin-Tsai Equations: A Review," *Polymer Engineering and Science*, vol. 16, no. 5, 1976.

[5] R. Jones, *Mechanics of Composite Material*, 2nd Edition. Taylor and Francis, 1999.

[6] C. L. T. Iii and E. Liang, "Stiffness predictions for unidirectional short-fiber composites : Review and Evaluation," *Composite Science and Technology*, vol. 59, pp. 655 – 671, 1999.

[7] P. K. Mallick, *Composite Engineering Handbook*. 1997, pp. 1 – 1238.

[8] R. F. Gibson, "Analysis of Lamina Hygrothermal Behaviour," *in Principle of Composite Material Mechanics*, 3rd ed., Taylor and Francis, 2010, pp. 181 – 217.

[9] R. A. Schapery, "Thermal expansion coefficients of composite materials based on energy principles," *Journal of Composite Materials*, vol. 2, no. 3, pp. 380–404, Jul. 1968.

[10] Z. Haktan Karadeniz and D. Kumlutas, "A numerical study on the coefficents of thermal expansion of fibre reinforced composite materials," *Composite Structures*, vol. 78, pp. 1 – 10, 2007.

[11] P. Herrera-Franco and A. Valadez-González, "Mechanical properties of continuous natural fibre-reinforced polymer composites," *Composites Part A: Applied Science and Manufacturing*, vol. 35, no. 3, pp. 339–345, Mar. 2004.

[12] T. Peijs, H. A. Rijsdijk, J. M. M. de Kok, and P. J. Lemstra, "The role of interface and fibre anisotropy in controlling the performance of Polyethylene-

fibre-reinforced composites," *Composites Science and Technology*, vol. 52, no. 3, pp. 449–466, Jan. 1994.

[13] M. Baiardo, E. Zini, and M. Scandola, "Flax fibre–polyester composites," *Composites Part A: Applied Science and Manufacturing*, vol. 35, no. 6, pp. 703–710, Jun. 2004.

[14] J. L. Thomason, "Structure – property relationships in Glass-Reinforced Polyamide, Part 1 : The effects of fiber content," *Polymer Composites*, vol. 27, no. 5, pp. 552 – 565, 2006.

[15] R. F. Gibson, "Effective moduli of a continous fiber reinforced lamina," in *Principle of Composite Material Mechanics*, Taylor and Francis, 2012, pp. 89 – 131.

[16] H. Miyagawa, T. Mase, C. Sato, E. Drown, L. T. Drzal, and K. Ikegami, "Comparison of experimental and theoretical transverse elastic modulus of Carbon fibers," *Carbon*, vol. 44, no. 10, pp. 2002–2008, Aug. 2006.

[17] S. Kawabata, "Micromeasurement of the mechanical properties of single fibers," in *Modern Textile Characteristics Method*, 1996, pp. 311 – 329.

[18] H. G. Wiedemann and T. McKarns, "Thermal characteristics of polymer fibers," *Thermochimica Acta*, vol. 169, pp. 1–13, 1990.

[19] W. D. Callister Jr, "Properties of selected engineering materials," in *Materials Science and Engineering An Introduction*, John Wiley & Sons, Ltd, 2003, p. 753.

[20] J.P Herman and C.L Beatty, "Thermal Stresses and Physical Aging," in *Characterisation and Failure Analysis of Plastics*, 2003, p. 296.

Chapter 5

Interfacial Shear Strength

5.1 Introductory Remarks

This chapter describes the experimental investigation of the interfacial shear strength (IFSS) for a range of candidate materials. A description of the test and the results for each type of material that is being investigated is given.

5.2 Experimental Programme

5.2.1 Materials

The three candidate materials that were used in the pull-out investigation were supplied by various companies and are listed below in Table 5.1.

Table 5.1: Fibre material for pull-out

Material	Type	Source
Sisal	Natural Fibre	Wigglesworth (Brazil)
Flax	Natural Fibre	Wigglesworth (Germany)
Polyethylene Terephthalate Fibre	Polymer Fibre, TEX 220	SABIC

The matrix material used in the pull-out test was supplied by SABIC. The matrix was Polypropylene (PP) with a melt flow index of 47g/ 10min @ 230^{o}C and extrusion

blended mixtures of various concentration of PP + Maleic Anhydride Modified Polypropylene (Polybond 3200) (MAPP). Maleic Anhydride (MA) is an adhesion additive and is meant to aid the interfacial interaction between the fibre and the matrix (For further details refer to Chapter 2 page 41).

5.2.2 Test Description

The test procedure is to initially prepare a sample which is made by embedding fibres in a polymer film which are then attached to a card ready for the pull-out test. It is worthwhile in describing the manufacturing process in detail, but the same procedure was followed for all fibres. In addition, a detailed description of the test rig and experimental procedure is also given.

5.2.3 Sample Preparation

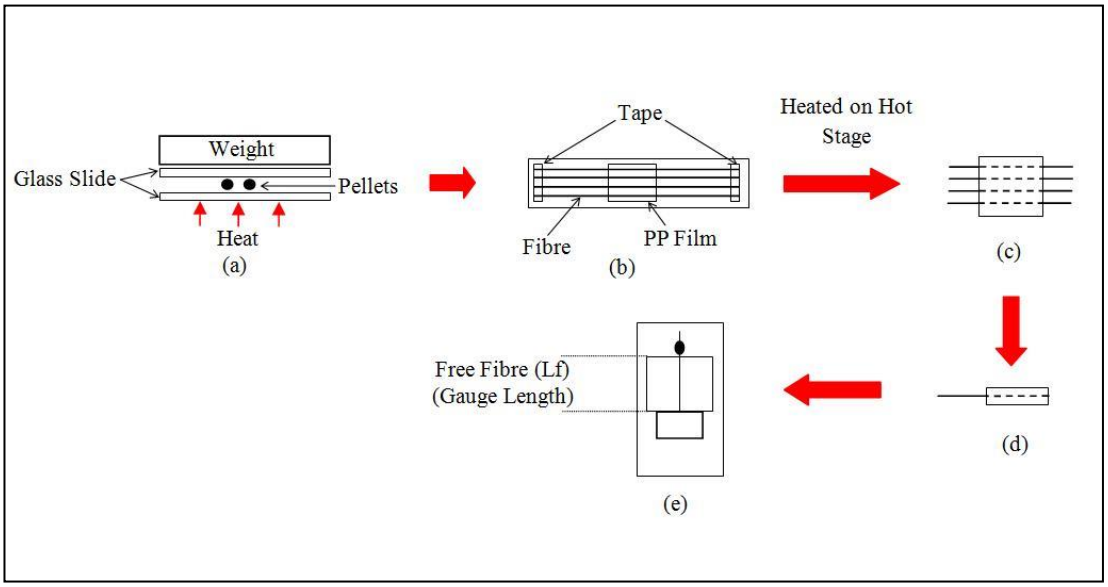

Figure 5.1: Pull-out sample preparation

The method that was employed in the manufacturing of pull-out samples was taken from Thomason and Schoolenberg [1]. This method was chosen, as many samples could be made at the same time through one production process, which is expected to

help in the repeatability of the test which is a common problem referenced by researchers [2, 3]. The pull-out sample preparation was maintained identical and consistent for each fibre as it was crucial to ensure repeatability of the test; therefore a step by step manufacturing process was developed. The procedure for creating samples is shown in Figure 5.1 and is described in three stages.

The initial stage of the pull-out sample production was the creation of the PP film. To manufacture PP film, a glass slide was placed on a hot stage with two or three PP pellets depending on the thickness of film required. The pellets were heated at 220^{o}C for thirty seconds and then another glass slide was placed on top, sandwiching the PP pellets between the slides. The pellets were sandwiched between the slides for ten seconds before a weight was placed on top of slides for a further thirty seconds creating a holding pressure and this can be seen in Figure 5.1a. The mass of the weight was varied depending on the desired thickness of the film. The slides were then removed from the hot stage and left to cool for several minutes at room temperature. The films produced had a thickness range between 0.15 – 0.40 mm depending on what fibre was being used and the thickness was evenly distributed throughout. The need for films of different thickness is due to the different fibres diameters used to generate the samples. The final part of this stage was to cut the film in to a 13x13mm square.

The second stage in the manufacturing process was to embed the fibre into the film. To embed the fibre, PP film was placed in the middle of a glass slide. PET fibres were then extracted from a bundle and laid in parallel across the film. Care was taken not to contaminate the surface of the test length of the fibre. The fibres were held in

place by double sided tape which was positioned at each end of the glass slide as can be seen in Figure 5.1b. A second PP film was then carefully placed on top of the fibres and film, making sure the edges of both films matched up. A glass cover slip was placed on top of the PP film to reduce oxidation during the heating in air in the next step. The final part of this stage was to place the fibre and film assembly into the Mettler FP 82 hot stage for four minutes to allow enough time for the fibre to be embedded into the PP film [4]. The manufacturing temperature of the pull-out samples was determined by the type of fibre as the elevated processing temperature could degrade or change the properties of the various fibres. The temperature used for each fibre is shown in Table 5.2. The glass slide was removed from the hot stage and left to cool.

Table 5.2: Pull-out sample preparation conditions

Material	Hot Plate (^{o}C)	Weight (Kg)	Diameter (µm)	Single Film Thickness (mm)	Hot Stage (^{o}C)
Polyethylene Terephthalate Fibre	220	1	19	0.15 – 0.2	220
Sisal Fibre	220	0.5	150 - 300	0.3 – 0.4	190
Flax Fibre	220	0.5	150 - 300	0.3 – 0.4	190

The final section of the sample preparation procedure was to prepare the single fibre specimens for the pull-out test. Care was taken when removing the specimen from the glass slide so that the fibres would not get damaged or break, Figure 5.1c.The specimens got harder to remove from the slide as the MAPP content increased in the PP matrix. This could be caused by the MAPP interacting with the glass slide causing a bond. The sample was then cautiously cut in half creating double the number of available samples which had gone through the same manufacturing process. A single fibre with film attached was then separated making sure the length of the embedded fibre was a suitable for pull-out test. This is important because if the embedded length was too long the fibre would break instead of pulling out of the matrix (Figure 5.1d). Finally, the single pull-out sample was then mounted to card by super gluing the free fibre to the card. The free fibre length (l_f) was set to 5mm (Figure 5.1e). The fibres' diameter for each sample was measured using a Nikon Epiphot inverted optical microscope and associated image analysis software.

The manufacturing conditions of the pull-out specimens varied based on the type of fibre that was being investigated. The PET fibres had an approximate diameter of 19 µm (<10% variation) therefore the thickness of a single PP film was between 0.15 – 0.2 mm. The natural fibres' diameters were significantly greater than PET fibre; consequently the thickness of the film was studied by increasing the thickness to investigate whether the IFSS increases and the outcomes are detailed in the results section. The hot stage processing temperature was another variable that required investigation. The natural fibres sample manufacturing temperature had to be lowered as the fibres start to degrade at temperatures above 200^{o}C [5]. For this reason the temperature was lowered to 190^{o}C. This temperature was high enough for

PP to become adequately fluid to embed the fibres. The manufacturing temperature of PET pull-out specimens was also investigated due to the PET fibre melting temperature being only 40^{o}C higher than 220^{o}C which is the manufacturing temperature for GF pull-out samples for which the original pull process was developed for [6]. The outcomes of this investigation are discussed further in the results section. Table 5.2 shows the final conditions that were selected for each type of fibre.

5.2.4 Test Rig

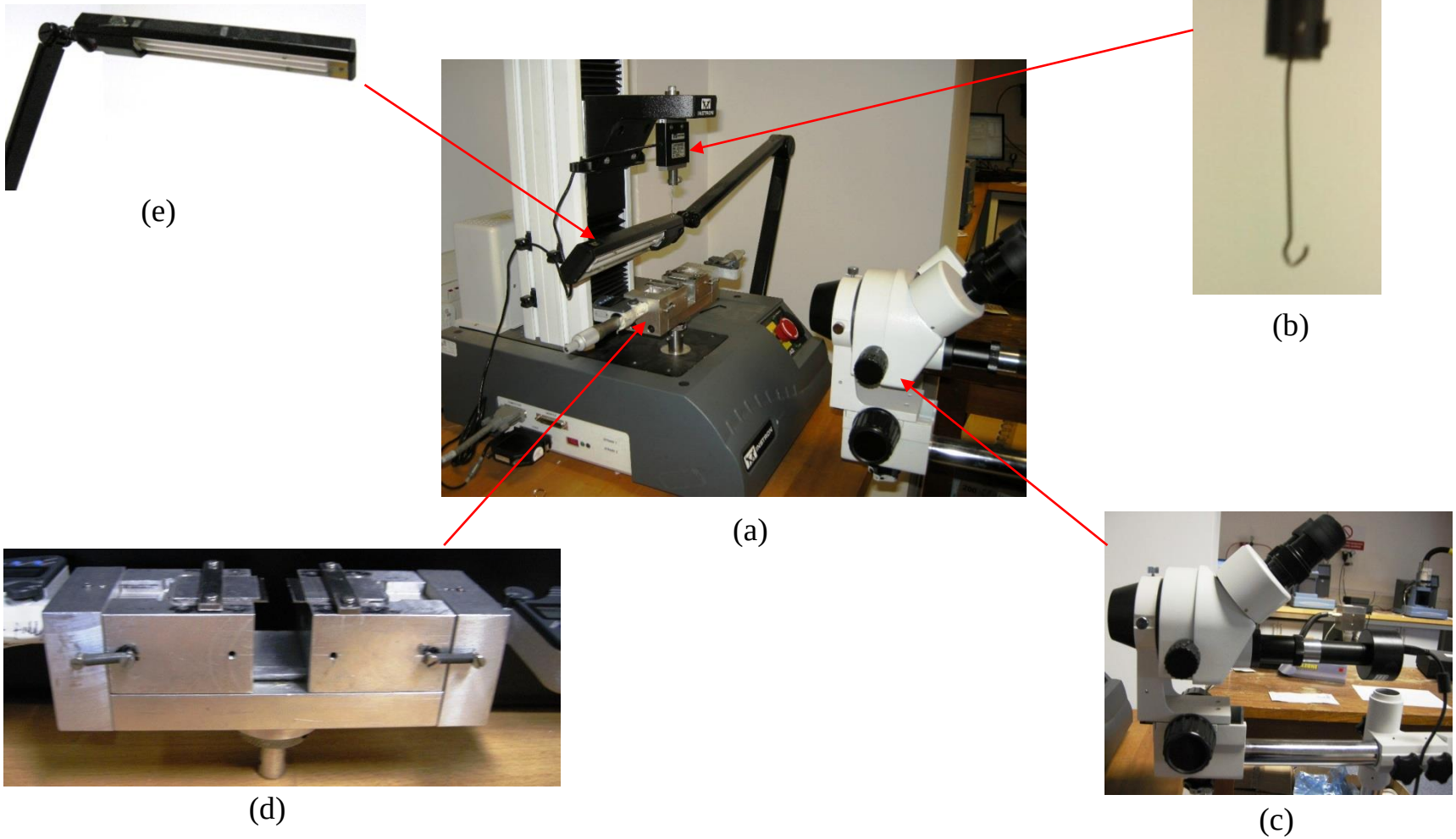

(e)

(b)

(a)

(d)

(c)

Figure 5.2: Test rig setup

The pull-out test rig used in the experimental programme was developed by the Strathclyde University Advanced Composite Research Group (Dr Liu Yang) [6] and is shown Figure 5.2. It allows either microbond or single fibre pull-out test to be carried out. The test rig comprises several components as listed below.

Instron 3342 Tensile Test machine (Figure 5.2a)

The Instron test machine sets the maximum load and extension rate for the pull-out test. The maximum load can either be 10 N or 100 N depending on the type of load cell used. The extension rate of the crosshead for the test ranges between 0.05 mm/min to 1000 mm/min.

Stereo microscope (Figure 5.2c) and Light (Figure 5.2e)

The stereo microscope with a magnification of 45X and light was used in the test rig to help in the pull-out test setup as the pull-out specimens are unclear to naked eye. The pulling out of the fibre was also observed during the test.

Pull-out/ Microbond jig (Figure 5.2d)

The pull-out/ microbond jig is attached to the bottom of the Instron machine and is essential to carry out the pull-out test [4, 6]. The jig is made up of two shearing blades and two micrometer heads which have a resolution of 1µm. The micrometer heads control the distance between the blades. The blades are used to constrain the film or droplet (depending on the type of test). The shearing blades play a central role as they are directly responsible for applying force to the matrix [4]

Full details of the pull-out test procedure are detailed in the section 5.2.5.

5.2.5 Single Fibre Pull-out Study

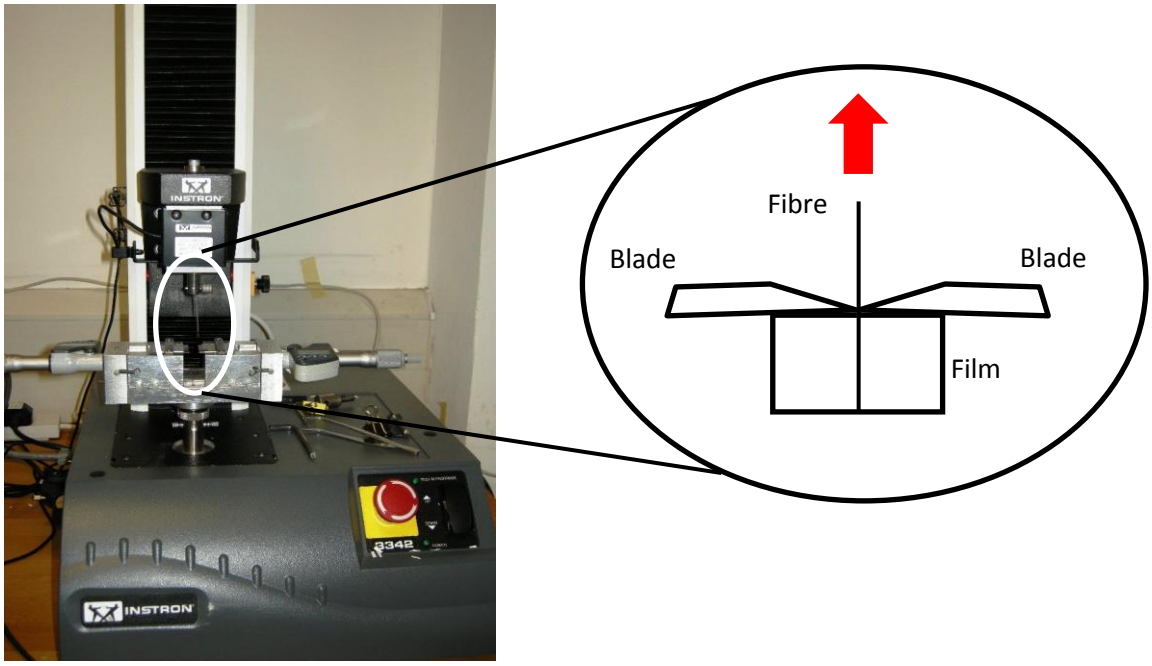

Figure 5.3: Pull-out test setup

The single fibre pull-out test was carried out at room temperature on the tensile test machine using the pull-out/ microbond jig, Figure 5.3. The hook attached to the load cell of 10N (Figure 5.2b) was used to fasten the pull-out sample to the Instron machine. The stereo microscope was attached with a camera that fed real time video to the computer and was used to help correctly position the sample and to witness pull-out of the fibre. The blades of the pull-out jig were then slowly brought together using the micrometer heads while monitoring their position with the aid of the microscope. The distance between the shearing blades just before testing equalled the diameter of the fibre. The extension rate of the crosshead on the Instron machine was set to 0.1mm/min and was kept constant for all fibre types. The commercial software programme Bluehill was used to control the tensile tester and produce a real time load – extension graph, an example of which is shown in Figure 5.4 for a typical Glass Fibre (GF) pull-out graph.

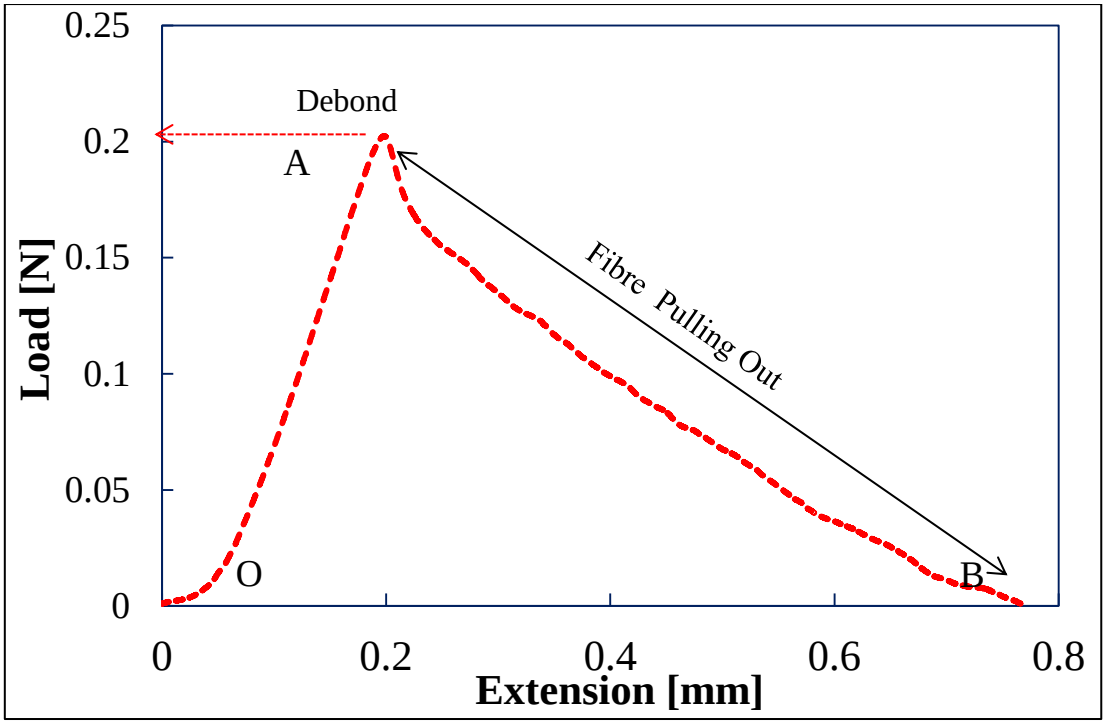

Figure 5.4: Typical pull-out graph of Glass fibre in Polypropylene

The load – displacement graph shown above describes various stages in the fibre pull-out process. At the start of the pull-out test the load increases as it is applied to the fibre until a maximum load is reached (O - A). At the maximum load the fibre fully debonds from the matrix. Immediately after debonding the load drops and then starts to decrease gradually due to the fibre being pulled out of the matrix and having to overcome frictional forces (A-B). Complete pull-out of the fibre from the matrix was either observed on a real time video supplied by the microscope or was taken when the load eventually reached zero. Interfacial strength (τ_{IFSS}) was calculated using equation 5.1[1, 4, 6]:

$$\tau_{IFSS} = \frac{F_{max}}{\pi D l_e} \tag{5.1}$$

where F_{max} is the maximum force taken from the load-displacement graph, D is the diameter of the fibre and (l_e) the embedded length. The embedded length of the fibre was obtained at

the end of the pull-out test by using the Letiza Ergolux microscope. Figure 5.5 shows the Polypropylene film and a channel of where the fibre had been embedded. The fibre embedded length was measured after the test because the fibre was unable to been seen when embedded in the film due to carbon black being present in the Polypropylene.

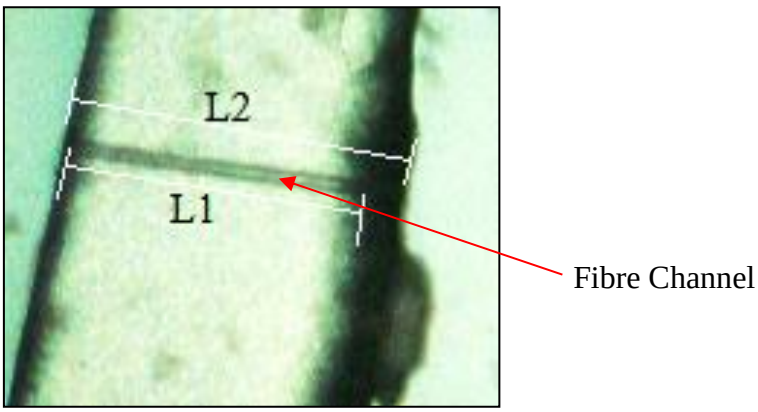

Figure 5.5: PP film after pull-out

Two lengths, L_1 and L_2 were taken to find the embedded fibre length because of the dark edges around the film made it hard to see the exact exit point of the fibre. L_1 is the minimum length the fibre could be embedded in matrix and L_2 is the overall length of the matrix. The average of these two lengths was therefore taken as the embedded fibre length (l_e).

5.3 Results and Discussion

5.3.1 Natural Fibre Study

Natural fibre sample preparation conditions differed from the original setup that was intended for Glass fibres due to the thermal sensitivity and diameter of the fibre. The diameter of natural fibres is greater than PET fibre therefore the thickness of the film to embed the fibres was investigated. The investigation was carried out on Sisal and the result is shown in Figure 5.6. It was observed that the film with the greater thickness appeared to slightly increase the

average of IFSS from being 3.9 MPa to 4.5 MPa. Therefore it was decided to manufacture thicker films for the natural fibre pull-out test. One plausible explanation is that the thicker film has more PP therefore the wetting of the fibre improves leading to better bonding.

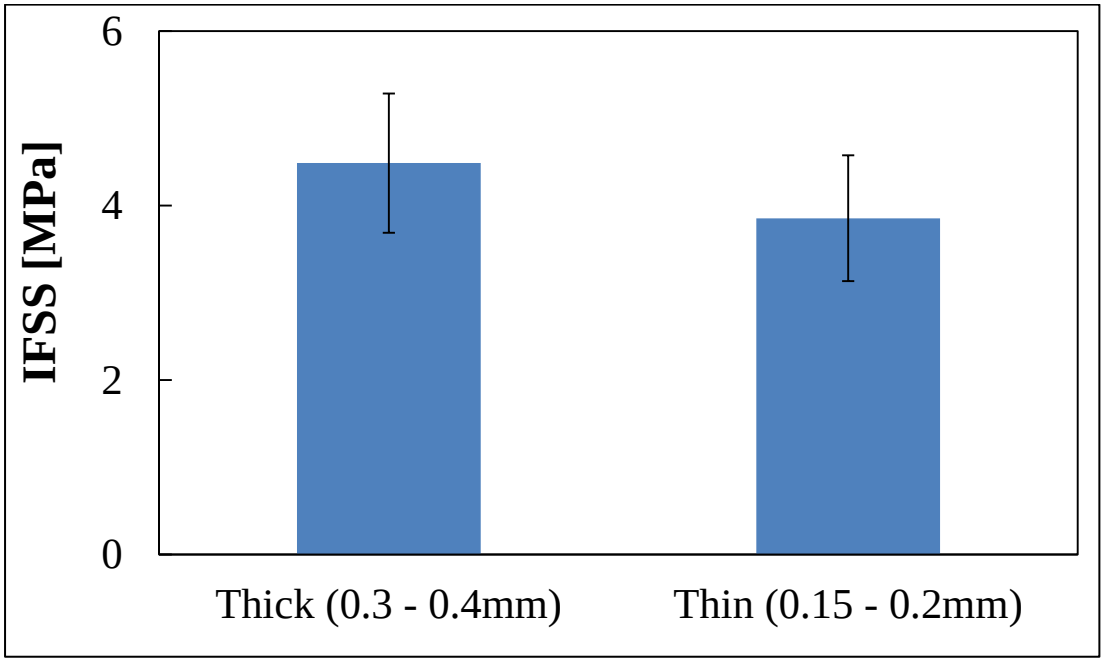

Figure 5.6: Natural fibre (Sisal) film thickness comparison

Along with the sample preparation being slightly different to Glass and PET fibre the effect of the method for estimating the interfacial embedded area on the calculation of IFSS was also investigated. Equation 5.1 uses the diameter of the fibre to calculate the interfacial strength but as reported by Park, Kenny and Adusumalli [9, 10, 11], natural fibres are not circular therefore using the diameter would most likely cause an inaccurate evaluation of IFSS. Consequently a study was carried out to compare the interfacial strength by firstly assuming the fibre was circular and then measuring the actual perimeter using image analysis software. Therefore for a non-circular fibre, Equation 5.1 changes from using the diameter to the perimeter, P, of the fibre to calculate the embedded area. The adapted formula is given in equation 5.2.

$$\tau_{IFSS} = \frac{F_{max}}{Pl_e} \quad (5.2)$$

The measuring of the natural fibre's perimeter was calculated after the pull-out test which meant a number of assumptions were made.

- The fibre pulling out of the matrix was clean and did not damage the fibre
- The fibre end was not harmed when debonding from the matrix
- The perimeter of the fibre was constant throughout the embedded length

The process to find the fibre's perimeter was similar to the process used in finding the fibre's cross sectional area; further details are noted in Chapter 3 Section 2.1.3. The comparison of the two equations for calculating the IFSS for Sisal and Flax is presented in the next two sections.

5.3.2 Sisal Study

Single fibre pull-out was carried out on Sisal fibre and Polypropylene with various percentages of Maleic Anhydride Polypropylene (MAPP) ranging from 0% to 5%. A minimum of fifteen samples for each percentage of MAPP were tested.

A typical pull-out graph of Sisal is illustrated in Figure 5.7. On first examination the shape of the graph is similar to the GF pull-out graph (Figure 5.4). However, a noticeable difference between GF and the Sisal pull-out graph is that load at which Sisal debonds from the matrix is nearly 10 times greater than the GF debond load which is due to the Sisal having a larger area then GF.

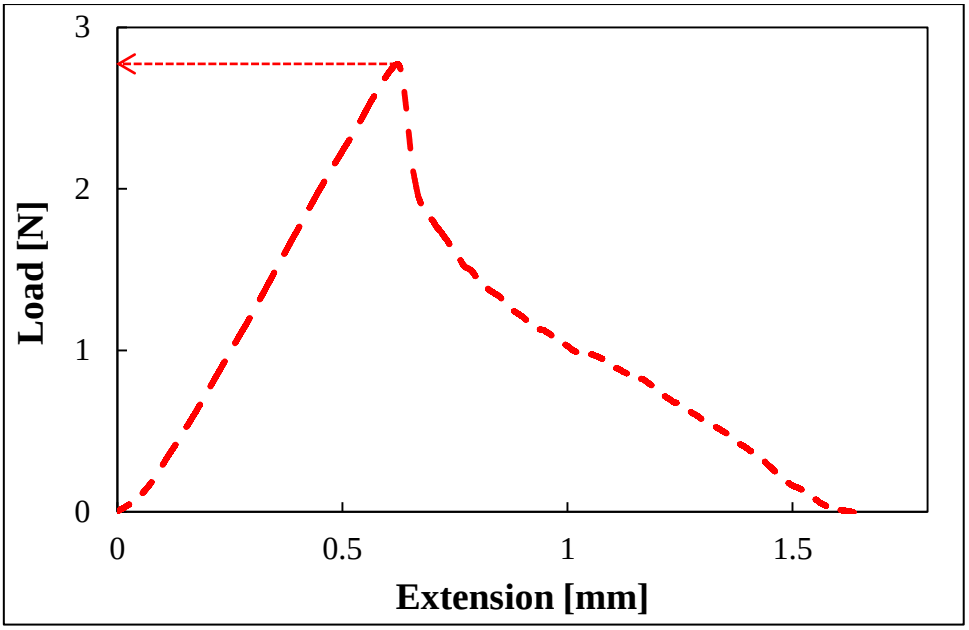

Figure 5.7: Typical Sisal pull-out graph

Initially the embedded area for Sisal was calculated assuming the fibre was circular and then after pull-out testing using the fibre's perimeter. The load against embedded area graph was plotted for both embedded areas calculated by using the diameter and the perimeter of the fibre and is shown in Figure 5.8 and 5.9.

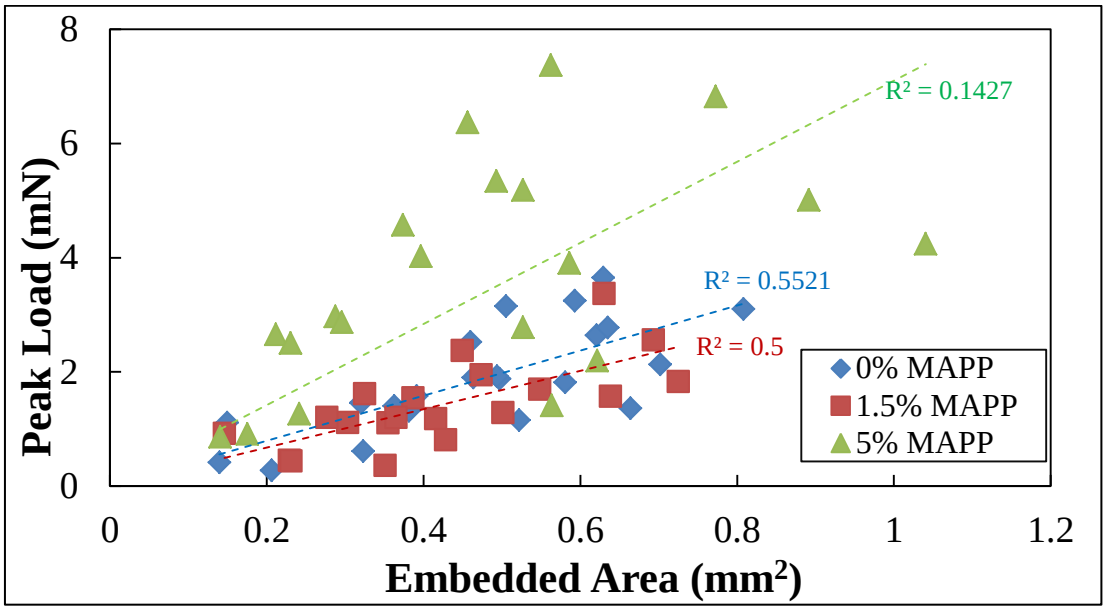

Figure 5.8: Peak load versus Sisal 'diameter' embedded area

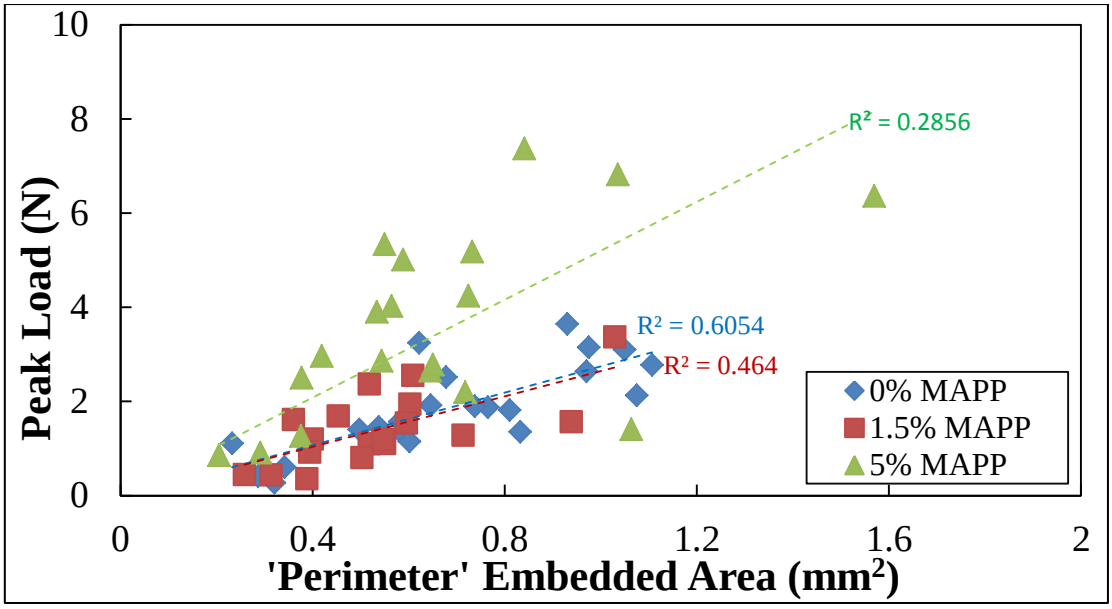

Figure 5.9: Peak load versus Sisal 'perimeter' embedded area

It can be observed that as the percentage of MAPP in the PP matrix increases, the IFSS increases. Figure 5.8 and 5.9 also shows a common trend for each percentage of MAPP, as the embedded area increases, the peak load is likely to increase which is expected from equation 5.1 and 5.2. Comparing the two graphs, it is observed that changing the way the embedded area is calculated changes the scatter of the graph. Using perimeter to calculate the embedded area decreases the spread of the results and this in turn would have an effect the results of the interfacial strength. A graph similar to the one plotted in Chapter 3 for comparing different area methods (Figure 3.27) was plotted of the circumference calculated using the diameter of the fibre against the measured perimeter of the fibre to find out why the embedded area increases using the perimeter of the fibre and the graph is shown in Figure 5.10. Figure 5.10 shows that the perimeter of fibre is larger than the circumference obtained by the assuming circularity of the fibre. This observation would explain why the embedded area calculated by the perimeter is larger than using the diameter of the fibre. The cross section of Sisal was therefore examined to see if there was a reason for the difference between the circumference and perimeter. Cross sections of two Sisal fibres are shown in

Figure 5.11. The cross section reveals that the Sisal fibres are not circular which was also proven in Chapter 3. It also shows that the diameter used to calculate the fibre's circumference underestimates the perimeter. Another noticeable point from the cross section is that the edges of the Sisal are rough whereas using the circumference as the perimeter assumes that the edges of the fibre are smooth. This difference could be an explaining factor along with the fibre non-circularity as to why the estimation of fibre perimeter using a diameter measurement combined with an assumption of a circular cross section gives an inaccurate measure of the perimeter.

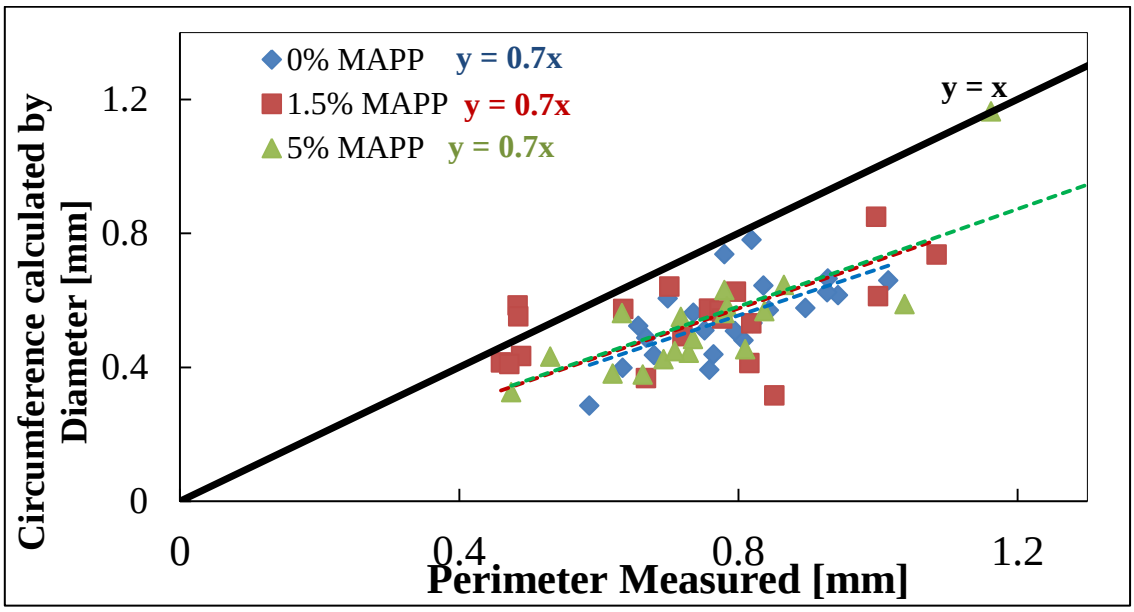

Figure 5.10: Circumference calculated by diameter versus perimeter measured

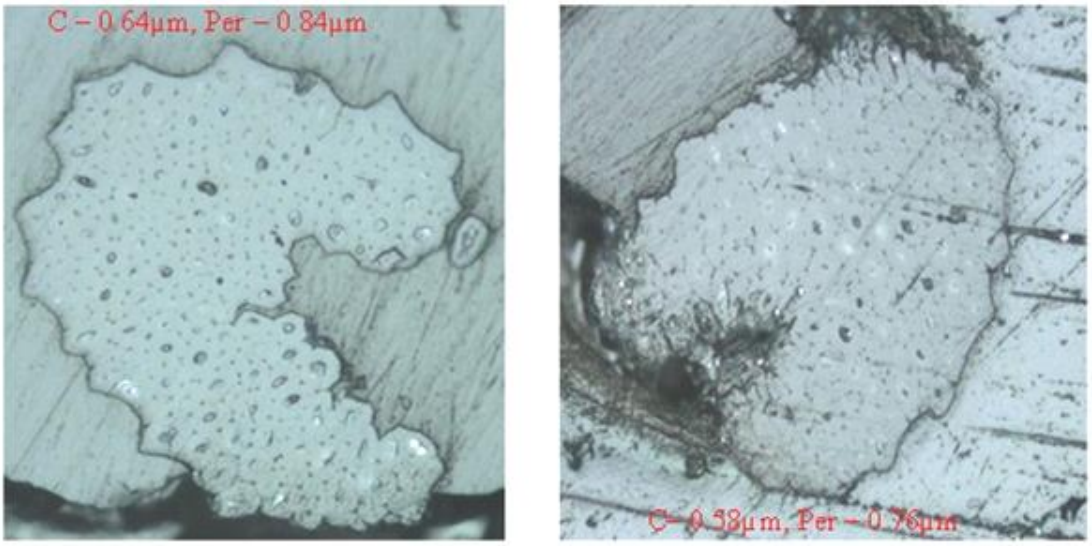

Figure 5.11: Sisal cross section

The interfacial shear strength was calculated for each percentage of MAPP using the diameter and the perimeter of the fibre. The average interfacial strength was then calculated and plotted against the percentage of MAPP to compare perimeter and diameter IFSS and can be observed in Figure 5.12.

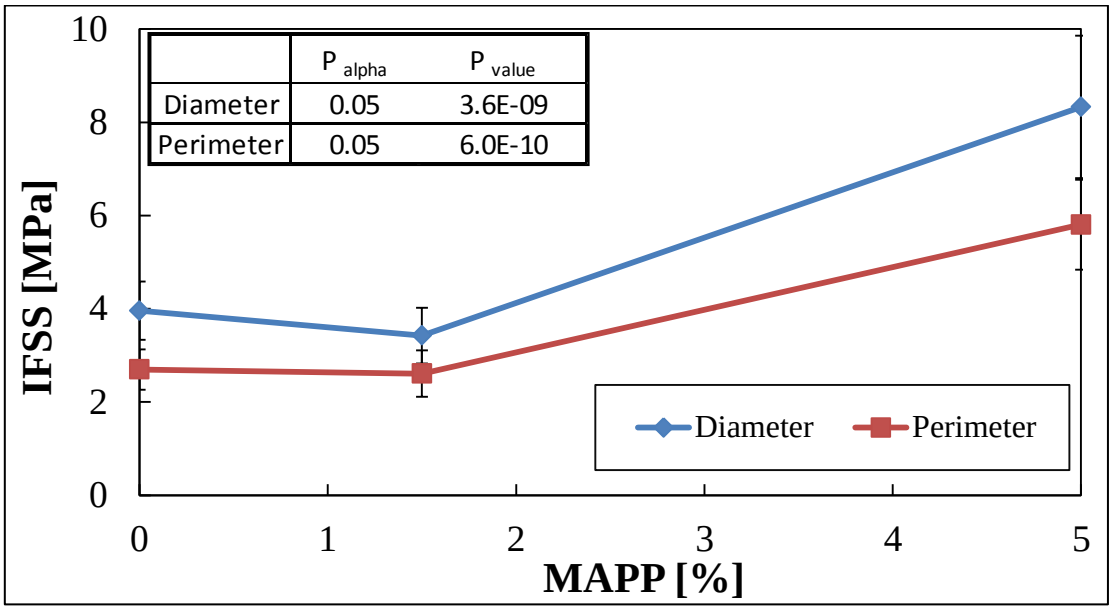

Figure 5.12: Sisal interfacial strength (IFSS) versus % MAPP

The IFSS decreases between 20 – 30% when using the perimeter instead of the diameter to calculate the embedded area. The difference in IFSS may be attributed by the difference in the embedded area. The circumference calculated by using the diameter of the fibre gives a smaller embedded area than the measured perimeter of the fibre. Therefore the diameter of the fibre would give a higher interfacial strength and can be observed in Figure 5.12. It can be concluded that by using the diameter to predict the interfacial strength for Sisal, this approach gives an overestimated result. This result has also been reported by Yan Li et al and Herrera Franco et al using Sisal fibre with a different matrix material [12, 13]. Figure 5.12 shows that there is no effect on interfacial strength when using 0% MAPP and 1.5% MAPP but the IFSS increases when using 5% MAPP.

5.3.3 Flax Study

A single fibre pull-out was also carried out on Flax and as with the Sisal tests different compatibiliser concentrations were investigated which were 0, 1.5 and 5% MAPP. A minimum of fifteen pull-out tests were carried out for each percentage of MAPP. A typical pull-out graph for Flax fibre has the same characteristics as Sisal and Glass fibre and can be seen in Figure 5.13. The load increases until a maximum is achieved at which point the fibre will start to be pulled out of the matrix. The load then starts to decrease gradually overcoming internal friction between the matrix and the fibre. Once again, comparing the Flax Load versus Extension graph to the GF graph it can be seen that the maximum load is nearly ten times larger than GF maximum load which is also noticed in the Sisal graph, Figure 5.7.

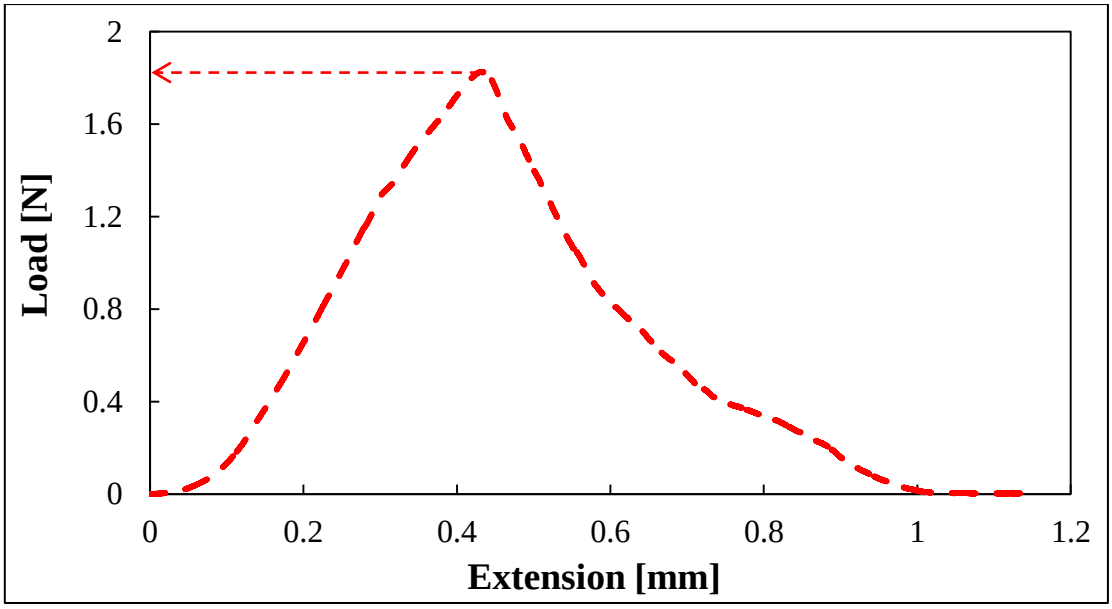

Figure 5.13: Typical pull-out graph of Flax fibre

The IFSS was calculated using the diameter and then subsequently using the perimeter of the fibre. The maximum force for individual pull-out specimens was plotted against the embedded area calculated by using the diameter and the perimeter of the fibre. The graphs are presented in Figure 5.14 and 5.15 respectively. Comparing the two graphs, it can be observed that there is no significant change in embedded area which is different to the Sisal fibre graphs (Figure 5.8 & Figure 5.9). A noticeable observation is that fibre perimeter decreases the spread of the results compared to the diameter results.

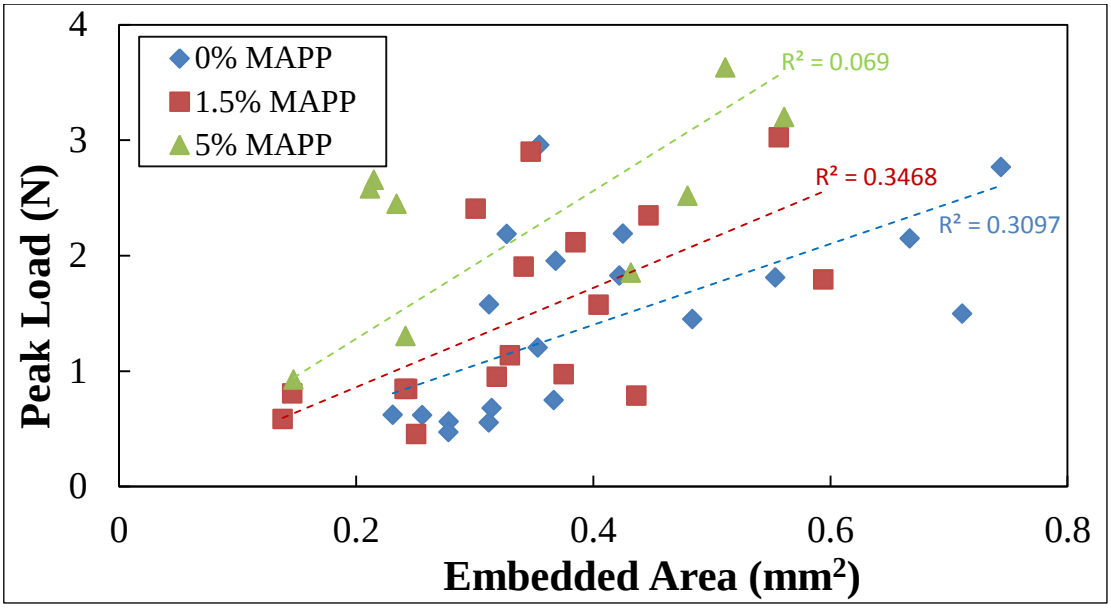

Figure 5.14: Peak load versus embedded area calculated with Flax diameter

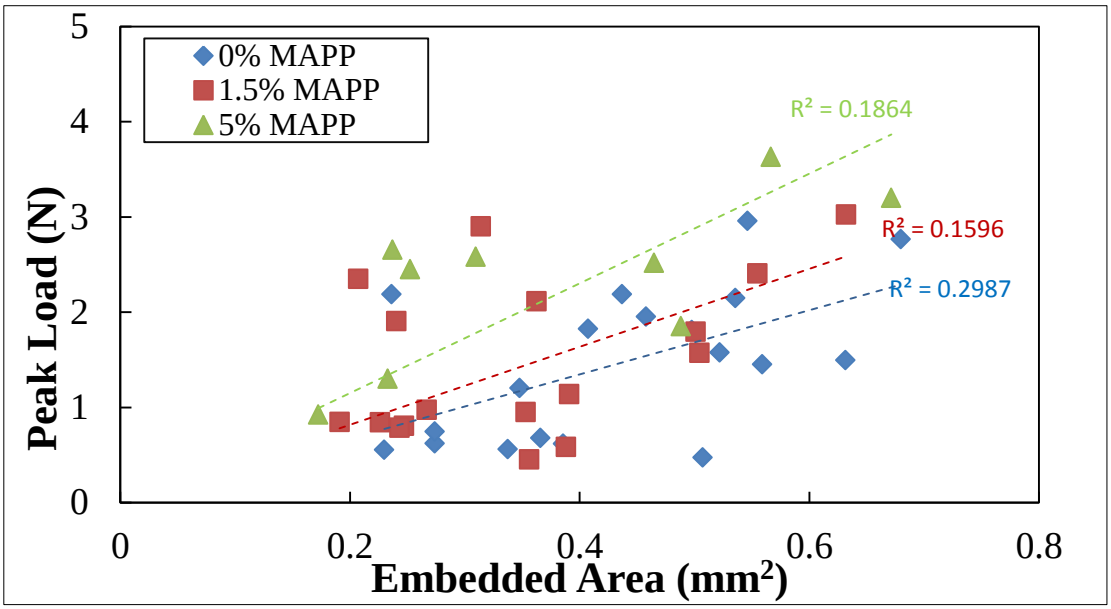

Figure 5.15: Peak load versus embedded area calculated with Flax perimeter

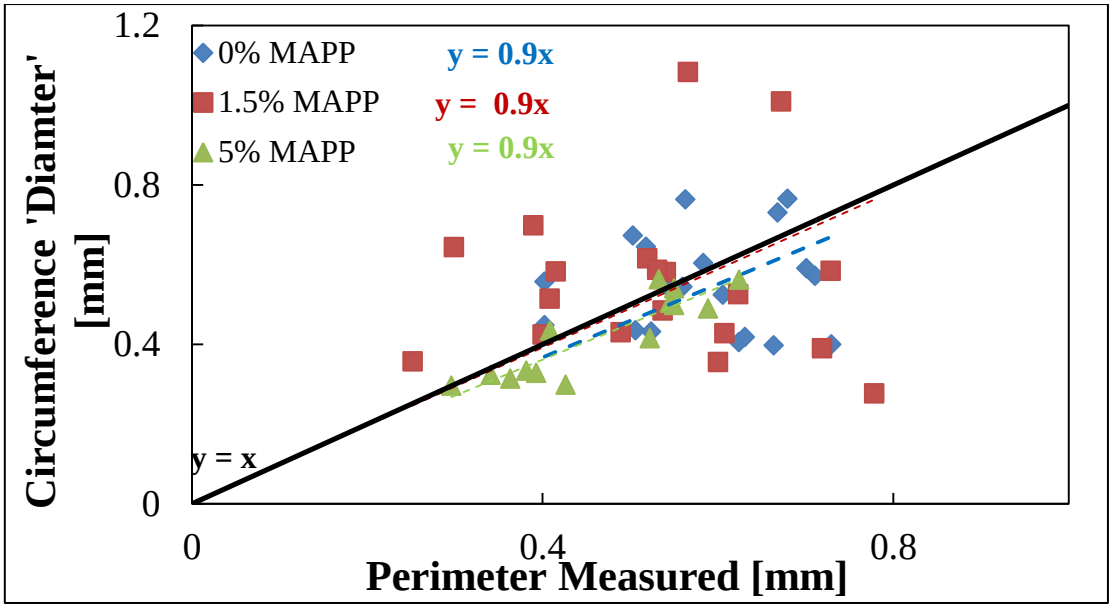

Figure 5.16: Circumference calculated by diameter versus perimeter measured

The embedded area results were investigated further by plotting the circumference of the fibre against the fibre's perimeter, Figure 5.16. Figure 5.16 show that circumference is approximately equal to the perimeter with a perimeter ratio of 0.9. The scatter shows the circumference both slightly under and over estimates the perimeter. An examination of the cross section of the fibre may explain the cause. The cross section of two Flax fibres is shown in Figure 5.17.

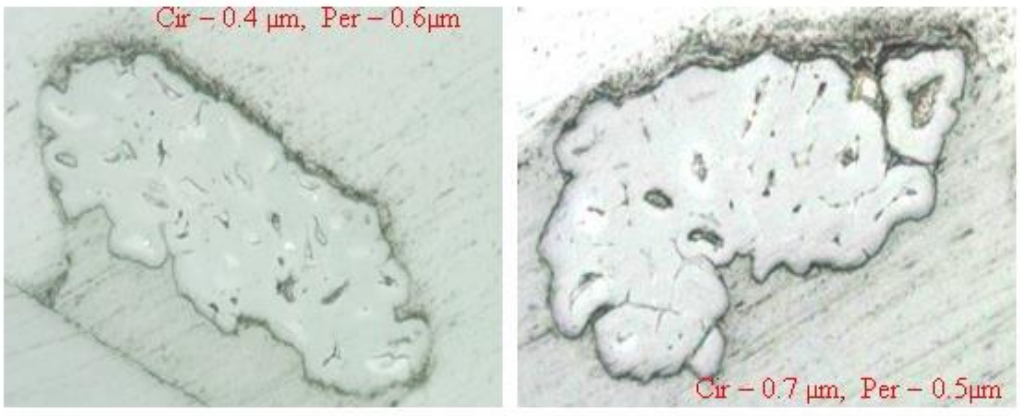

Figure 5.17: Cross section of Flax

The illustrated cross sections of Flax show that the fibre is not circular and that the diameter miscalculates the perimeter, this has also been observed by Thomason [13]. Thomason

showed that an ellipse is a much better shape than a circle to represent the cross section of natural fibres. Therefore Thomason's ellipse theory was applied to Flax to investigate if it could help justify, why using the diameter to calculate the perimeter is different to actual perimeter.

An ellipse centred on an origin can be expressed as the path of points X(t), Y(t) and is shown in Figure 5.18 below.

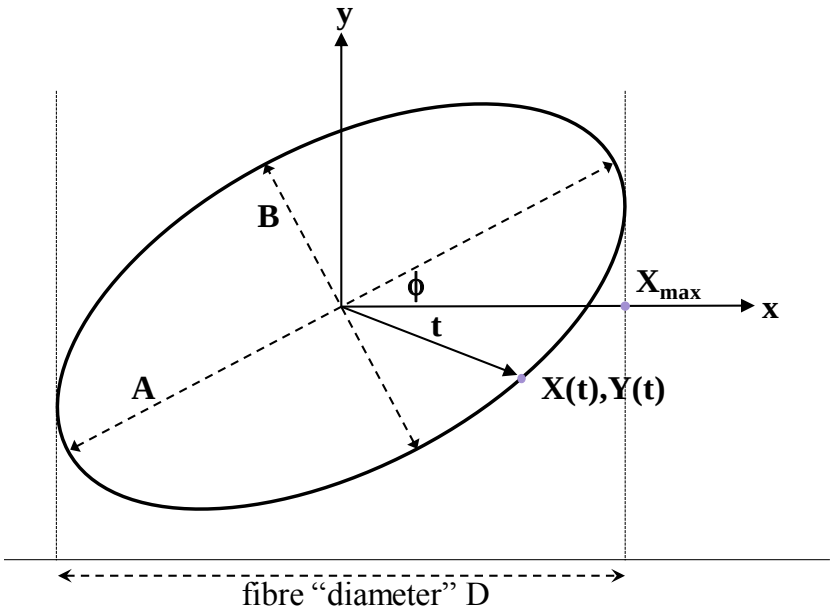

Figure 5.18: Ellipse centred on an origin

where,

$$X(t) = \tfrac{1}{2}A\cos(t)\cos(\phi) - \tfrac{1}{2}B\sin(t)\sin(\phi) \quad (5.3)$$

$$Y(t) = \tfrac{1}{2}A\cos(t)\sin(\phi) + \tfrac{1}{2}B\sin(t)\cos(\phi) \quad (5.4)$$

The parameter t varies from 0 to 180^{o}, A and B represents the ellipse's major and minor axes respectively. ϕ is the angle between the X axis and the major axis of the ellipse, A. The measured fibre diameter relates to the width of the ellipse in Figure 5.18 on the x axis which is equal to $2X_{max}$. X_{max} represents the maximum value of X for any angle of ϕ. The value for

Xmax at any angle of ϕ can be achieved by setting the differential of equation 5.3 to zero and solve for t_{max}. The average fibre diameter measured at several points along the length of the fibre can be ascertained over the range $0 < \phi < 90$ which is equivalent to X_{max} average value [13].

$$dX/dt = -½ASin(t)Cos(\phi) - ½BCos(t)Sin(\phi) = 0, \text{ hence } Tan(t_{max}) = -(B/A)Tan(\phi) \quad (5.4)$$

The perimeter of the ellipse can be estimated using equation 5.5, shown below. Where P corresponds to the perimeter of the ellipse.

$$P_{ellipse} = 2\pi\sqrt{0.5(A^2 + B^2)} \quad (5.5)$$

A perimeter ratio (circle/ ellipse) is plotted against the ellipse orientation and aspect ratio (A/B) of the ellipse and is shown in Figure 5.19. It can be observed that the orientation angle makes a significant contribution to the perimeter ratio as the angle increases the perimeter ratio decreases.

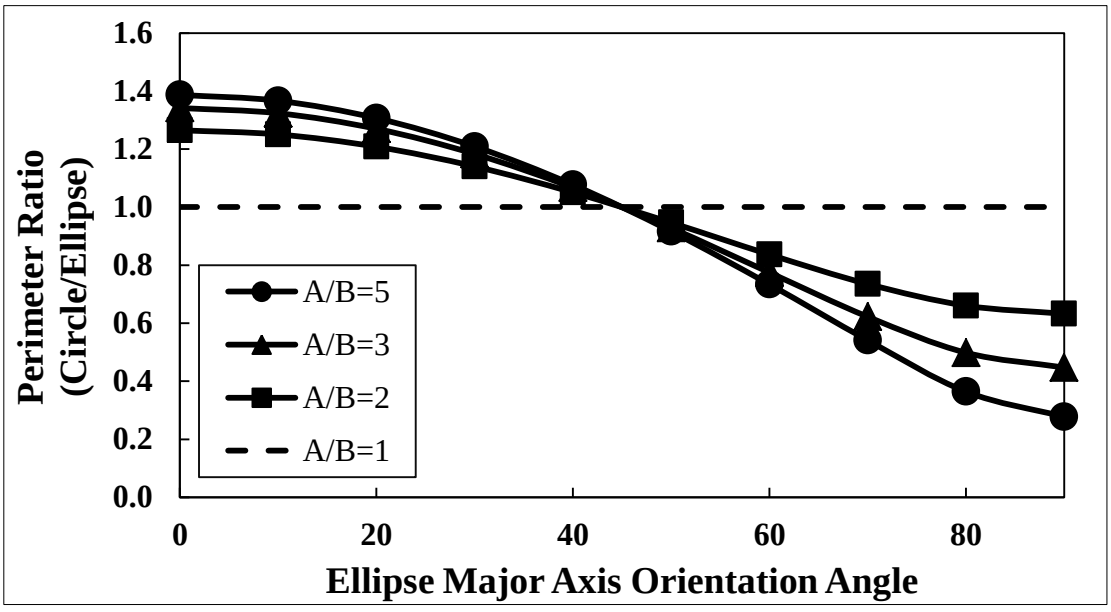

Figure 5.19: Perimeter ratio versus orientation and aspect ratio ellipse

Figure 5.19 also shows that as the aspect ratio of elliptical cross section does not significantly change the perimeter ratio. Therefore a graph of the average perimeter ratio is plotted against ellipse aspect ratio to investigate this further and is shown in Figure 5.20. It can be seen from Figure 5.20 that the elliptical aspect ratio decreases as the perimeter ratio decreases from 1 to 0.9. Comparing the perimeter ratio for Flax fibre obtained in Figure 5.16 to the results obtained in Figure 5.20 it can be said that ellipse is better representation of Flax cross section.

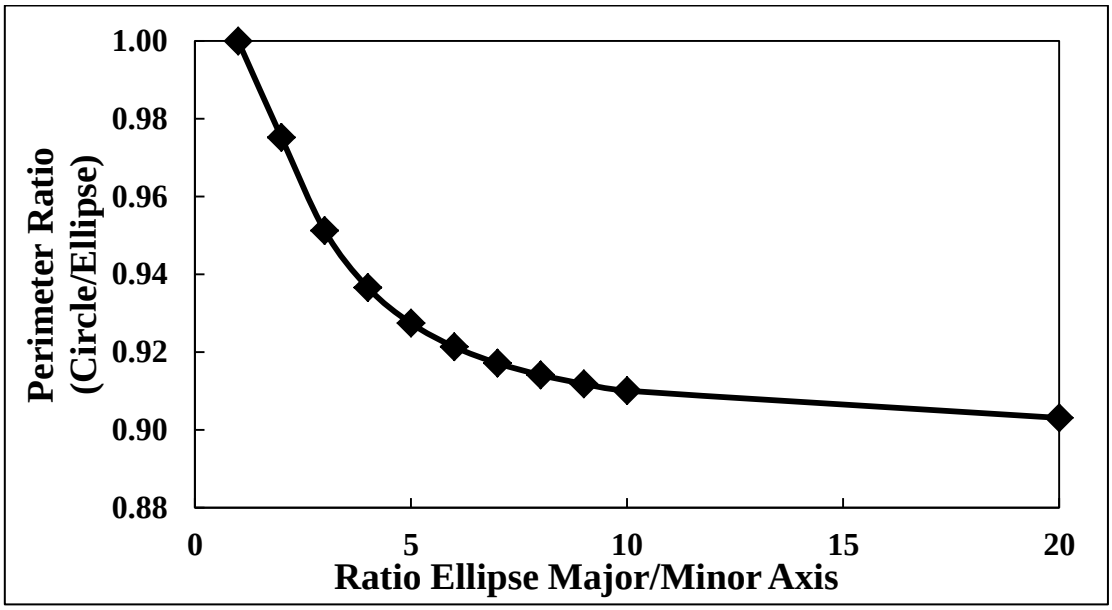

Figure 5.20: Average perimeter ratio versus aspect ratio of the ellipse

The results taken from Figure 5.14 and 5.15 were used to calculate and compare the interfacial strength for diameter and perimeter. The average IFSS for diameter and perimeter, with 95% confidence limits, were plotted for each percentage of MAPP used and is shown in Figure 5.21. Figure 5.21 shows that the IFSS values increase as the percentage of MAPP increases. The interfacial strength does not change substantially when using either the diameter or perimeter to determine the embedded area as the perimeter is equal to the circumference. The IFSS increases by 10% between the 0% and 1.5% MA for both perimeter and diameter whereas between 1.5% and 5% MAPP the IFSS result increases by 40%.

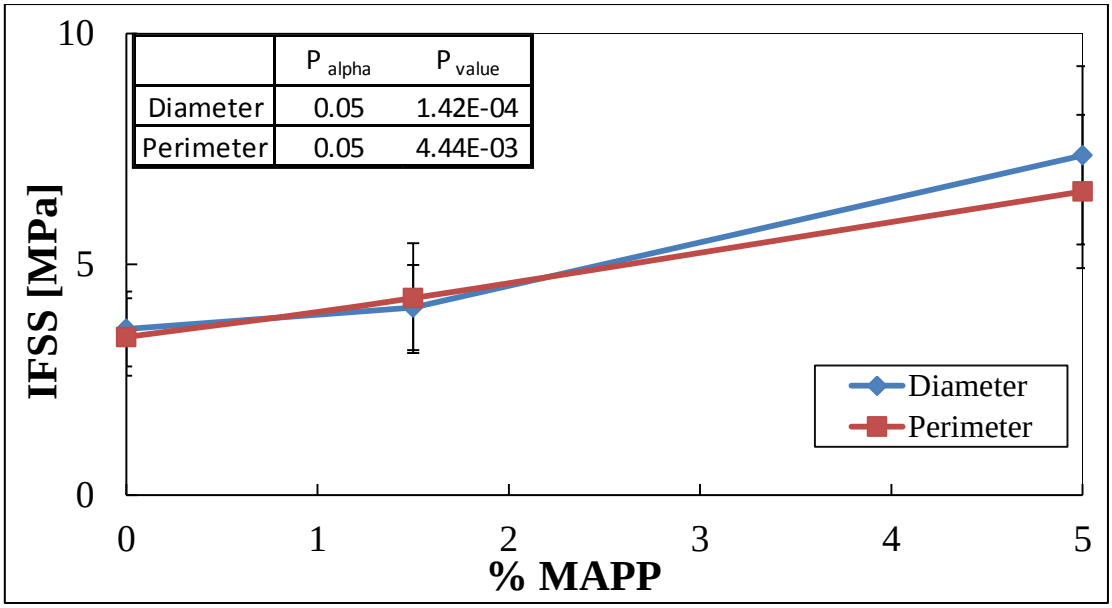

Figure 5.21: IFSS for diameter and perimeter versus percentage of MAPP

5.3.4 Polyethylene Terephthalate Fibre Study

Single fibre pull-out test were carried out on Polyethylene Terephthalate in Polypropylene with different percentage of MAPP ranging from 0 to 10%. Just like the natural fibre pull-out test, a minimum of fifteen samples were tested for each weight fraction of MAPP. Before pull-out was carried out the manufacturing temperature for creating PET-PP pull-out samples had to be investigated. The melting point of PET is 40^{o}C above the temperature of 220^{o}C and which the manufacturing temperature for GF pull-out samples from the original test. Therefore an investigation into how the sample preparation affects the interfacial strength between PET fibre and the PP film was carried out. The initial temperature was set at 190^{o}C, which was the temperature used to manufacture natural fibre pull-out samples. This temperature was high enough for the PP to melt and embed the fibre. The temperature was then increased in stages up to 220^{o}C and the average IFSS for each temperature was calculated and is presented in Figure 5.22. The results show that the average IFSS increased

slightly as the temperature increased. From these results it was decided to manufacture PET-PP pull-out samples at 220^{o}C to keep it consistent with the original manufacturing process.

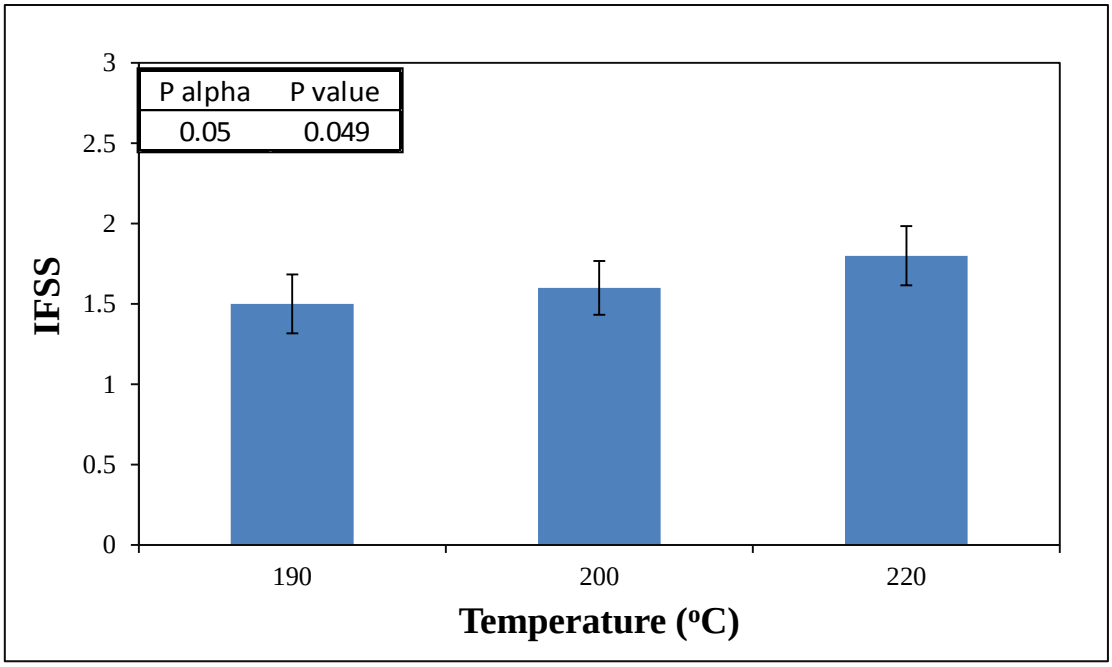

Figure 5.22: Interfacial shear strength against PET-PP manufacturing temperature

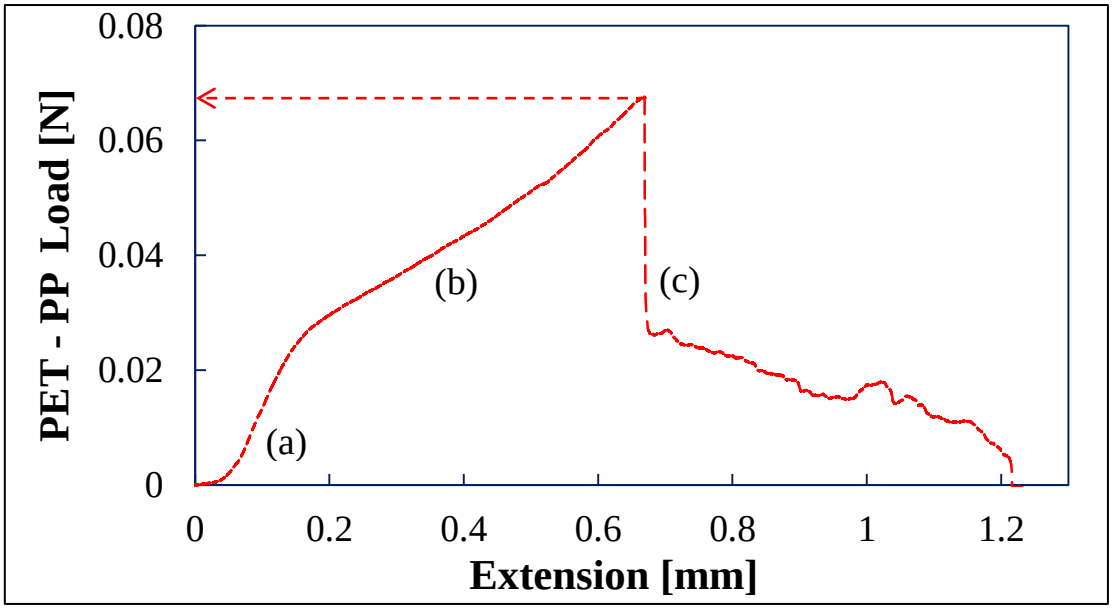

Figure 5.23: Typical PET-PP pull-out graph

A typical pull-out graph of PET-PP is seen in Figure 5.23. This graph is different to the GF and natural fibre graphs seen in Figure 5.4, 5.7 and 5.13. The PET-PP pull-out graph can be split in to three distinctive stages.

a. The force increases due to the fibre being stretched up to a certain load. At this load the graph's gradient changes creating a 'kink' in the pull-out plot. The cause of the 'kink' is discussed later in the chapter. (Figure 5.23a).
b. The force is still increasing after the 'kink' until a maximum force is achieved. At this force the fibre fully debonds from the matrix. (Figure 5.23b).
c. The force suddenly drops to a lower load immediately after debond. The force then decreases gradually as the fibre is being pulled out of the matrix overcoming frictional forces. (Figure 5.23c).

The average IFSS (with 95% confidence) versus percentage of MAPP is illustrated in Figure 5.24. Figure 5.24 shows that increasing the MAPP percentage from 0 to 1.5% has no significant effect on the IFSS. However, the IFSS of PET-PP increases by approximately 70% when increasing from 1.5 to 5% MAPP but does not change further from 5 to 10% MAPP. The maximum IFSS achieved for PET was 5.6 MPa at 5% MAPP. The results from Figure 5.24 show that the IFSS did not improve considerably with a small addition of MAPP but the IFSS increase greatly when the percentage of MAPP is increased to 5%. This observation was also seen in both natural fibres' pull-out graphs.

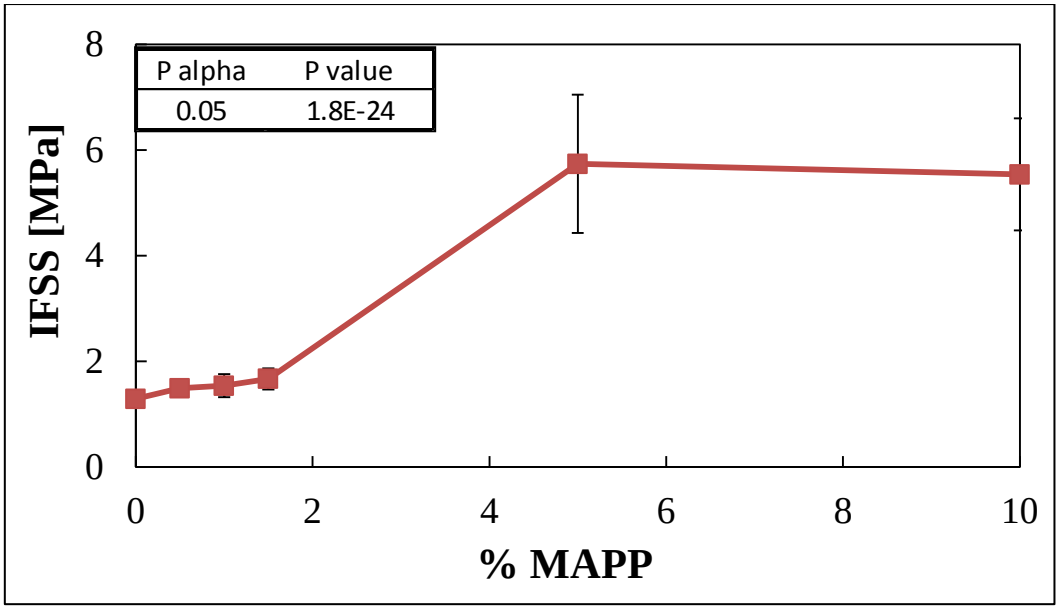

Figure 5.24: Average interfacial shear strength against the percentage of maleic anhydride (%MAPP)

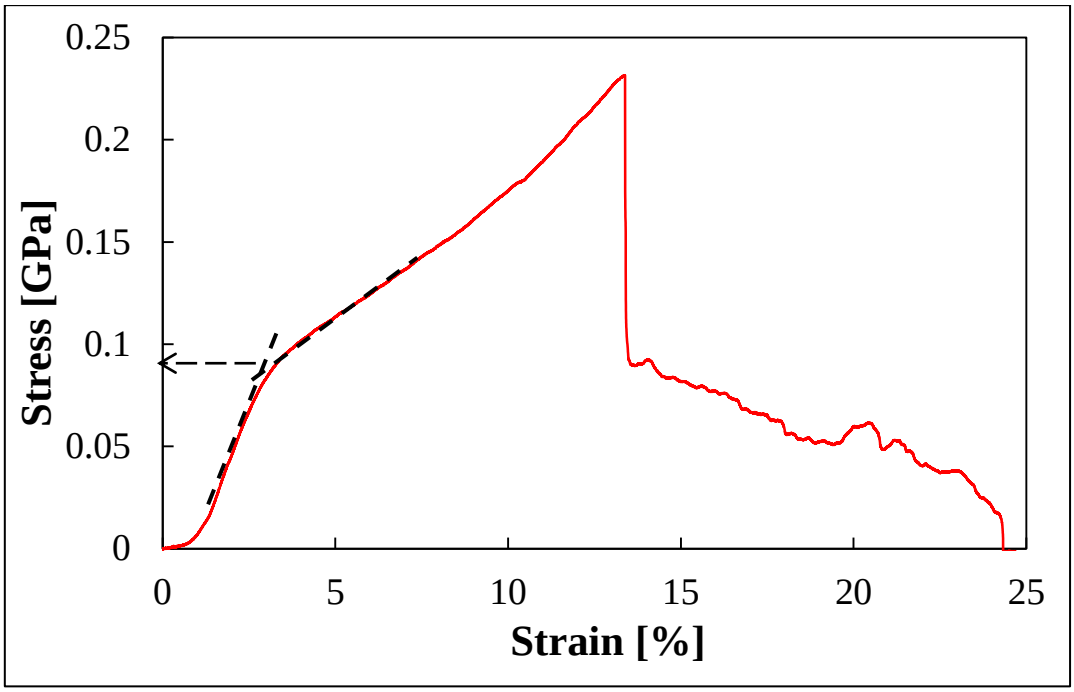

Figure 5.25: Stress versus strain PET-PP pull-out graph

The pull-out graph of PET-PP was investigated further due to an unexpected change in slope ('kink') in the initial stage of the test. Initially, the load at which the 'kink' occurred for the test was calculated. The 'kink' stress was determined by extending the gradient of the graph before and after the 'kink' and noting the stress at which the two lines intercept each other.

An example of calculating the 'kink' force is illustrated in the stress against strain graph in Figure 5.25. Table 5.3 shows the average stress point and modulus of the slope before and after the 'kink' with the 95% confidence limit for each percentage of MAPP pull-out samples. It can be observed from Table 5.3 that the change in slope happened at approximately the same stress level. The stress at which the 'kink' occurred appeared between 0.06 – 0.1 GPa and it can be seen clearly in Figure 5.26 that the stress point does not change depending on the percentage of MAPP. The data in Table 5.3 shows that the modulus before the 'kink' for all percentage of MAPP is greater than that calculated after the 'kink'. Table 5.3 also shows that the modulus before and after the 'kink' are approximately the same for all percentage of MAPP pull-out tests. From the Table 5.3 and Figure 5.26 it can be concluded that the same phenomenon is happening for each MAPP pull-out and this phenomenon is consequently probably not related to the fibre-matrix interface.

Table 5.3: Average kink stress, before and after kink modulus

MAPP (%)	**Stress** (GPa)	**95% Confidence**	**Average Modulus Before Kink** (GPa)	**95% Confidence**	**Average Modulus After Kink** (GPa)	**95% Confidence**
0	0.09	0.004	3.6	0.4	1.1	0.1
0.5	0.09	0.003	4.3	0.4	1.3	0.1
1	0.09	0.006	3.5	0.6	1.1	0.1
1.5	0.09	0.005	3.7	0.9	1.2	0.1
5	0.08	0.006	4.7	0.7	2.0	0.5
10	0.07	0.01	4.8	0.4	1.4	0.2

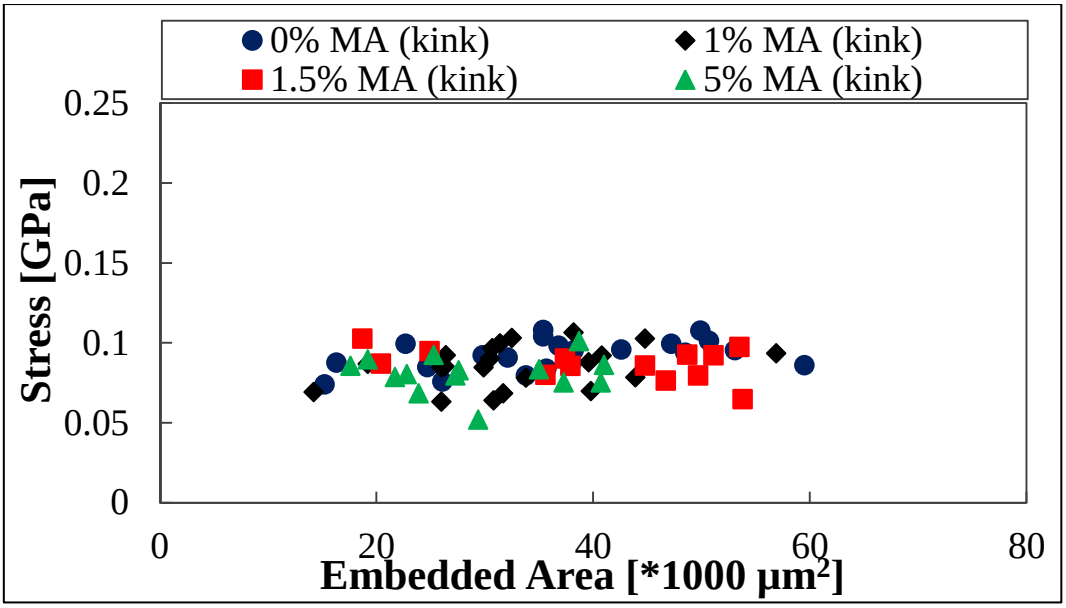

Figure 5.26: Kink stress against the embedded area

A 'kink' phenomenon has been identified in the force – displacement results if IFSS tests and reported by Mader and Wang [7, 14]. Mader et al noticed a 'kink' when undertaking pull-out with GF-PP and described this as the fibre initially debonding from the matrix [14]. This is one possible explanation for what is happening but the system differs in one key way as the fibre that is being used is a polymer which is more ductile than GF. Moreover the kink appears to be independent of the MAPP concentration which is known to strongly change the interfacial phenomena in these systems. Another reason that could cause the change in slope in the pull-out graph could be changes in the fibre. This reason was investigated further by carrying out tensile tests on PET fibre. Tensile tests were carried out on heat treated and non-heat treated PET fibre. Tensile test on heat treated fibre due to the free fibre in the pull-out test was heat treated in the sample manufacturing process. The heat treated fibres for tensile testing were given an identical thermal history as the pull-out specimens. Individual PET fibres were heated in the hot stage at 220^{o}C for four minutes and then removed to cool. The gauge lengths of the fibres were 5 mm, identical to the free fibre length for the pull-out specimens. A minimum of ten tensile tests were carried out for the heat treated and non-heat

treated fibres at the same extension rate as the pull-out test, 0.1mm/min. The stress - strain graphs of the two fibres were compared to the pull-out graph. To compare the pull-out and tensile graphs a mutual start point of 0.01N was set therefore the extension/ strain was reset to 0 and an end point of 6% strain was decided for comparability reasons. These points were decided upon as they represented the range in which the 'kink' occurred. Figure 5.27 compares the average stress against the strain of the pull-out, heat treated and non-heat treated fibre tensile test.

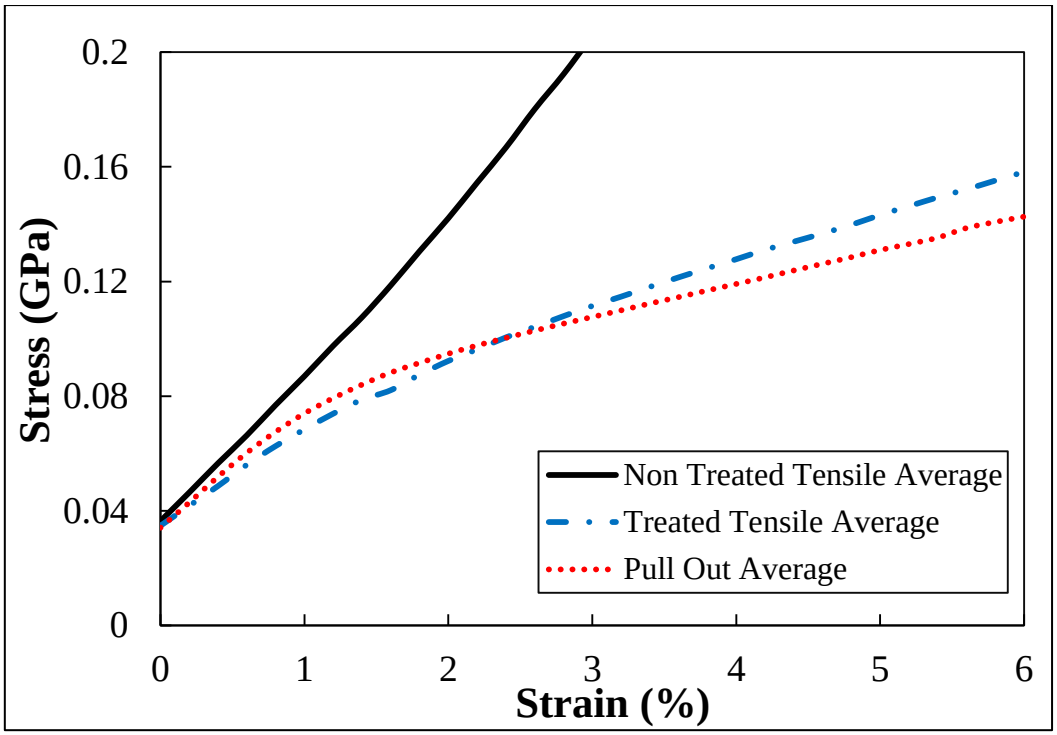

Figure 5.27: Average stress against strain for PET-PP pull-out, heat treated tensile & non treated tensile

Figure 5.27 shows that the stress strain curve of the heat treated fibre plotted overlays the pull-out graph. It therefore seems very likely that it is a fibre related phenomenon that is the causing the slope of the IFSS graph to change. Comparing the heat treated fibre and non-heat treated fibre stress strain curves it can be seen that heat treating the fibre changes the shape of the stress strain graph. This kink has also been identified by researchers such as Gupta et al and Cho et al [16–18]. Gupta carried out a series of experiments to investigate the effect of

heat setting on the PET fibres' mechanical and structural properties [15, 16, 18, 19]. In their studies they found that heat treating fibres with no mechanical constraint (free to relax) changed the fibre's structure considerably. The heat treatment on the 'free heated' fibre causes the amorphous and crystalline region of the fibre to be rearranged as described on page 83. In the initial stage of the tensile test the tie molecules take all of the force. Due to the reduction of tie molecules caused by heat treatment, the stress on the remaining tie molecules is high. This causes them to break at low load which leads to the fibre yielding. The stress is then applied to the molecules in the amorphous region where strain hardening may occur [15-17]. From previous research that has been carried out on heat treated PET fibre and together with the results from Figure 5.27 it can be determined that the cause of the 'kink' is due to the fibre being heat treated at 220^{o}C in the manufacturing of samples. The 'kink' can therefore be classified as the fibre's yield point.

5.3.5 Low Interfacial Shear Strength

The results of the IFSS for Sisal, Flax and PET shown Figure 5.12, 5.21 and 5.24 are relatively low compared to that of glass fibre. One reason for the low interfacial strength is due to residual radial compressive stress at the interface. The residual radial compressive stress is formed across the interface between the fibre and matrix due to the coefficient of thermal expansion between the fibre and matrix being different. The interfacial static friction associated with residual radial compressive stress may be the major contributor to the apparent interfacial shear stress in a system which has no or little chemical bonding. Therefore a reason for low IFSS could be attributed to the low residual radial compressive stress [21]. The radial residual stress is significantly influenced by the fibre's transverse properties. The residual radial compressive stress, σ_R, can be estimated using Raghava's model and the equation is shown below in equation 5.3 [22]:

$$\sigma_R = \frac{(\alpha_m - \alpha_f)(T_s - T_t)E_f E_m}{(1+v_f+2V_f)E_f + (1+v_m)V_m E_m} \qquad (5.3)$$

Where E_f and α_f is related to the transverse modulus and thermal expansion of the fibres. T_s and T_t are the matrix stress free temperature (125^{o}C for Polypropylene) and test temperature (25^{o}C). The values that were input in to equation 5.3 are shown in Table 5.4. The natural and PET fibre values were obtained from the work carried out in Chapter 4. Glass fibre and PP values were obtained from work carried out by Thomason [23]. Poisson's ratio for Glass fibre and PP were taken to be 0.22 and 0.33 for both longitudinal and transverse direction. The Poisson's ratio for PET and natural fibres are not defined. However it was found that the Poisson's ratio did not significantly alter the values of residual radial compressive stress. Glass fibre was used to compare the conventional reinforcement to the one being studied in this chapter. The residual radial compressive stress for PET, Flax, Sisal and Glass fibre against volume fraction is plotted and shown in Figure 5.28. Figure 5.28 shows that PET, Flax and Sisal have a much lower σ_R compared to glass fibre reinforcement. It is also observed from the graph that as the volume fraction increases the σ_R decreases. For a given polymer matrix, the relatively σ_R is mainly dependent on the fibre's properties for the transverse Modulus and CTE. A high transverse modulus and low transverse CTE for the fibre will give a high σ_R. PET fibre shows a higher σ_R than both natural fibres this could due to the transverse modulus being higher and the transverse CTE being lower, although in all cases these differences are small. It can be clearly seen from Table 5.4 and Figure 5.28 that anisotropic nature of the PET and both natural fibres contribute to the low σ_R therefore leading to a low value of IFSS. This relationship between low σ_R and anisotropic nature of the fibre has also been suggested by Thomason for Jute – Polypropylene composites [23].

Table 5.4: Properties of fibre and matrix

	PET	Flax	Sisal	Glass	PP
Longitudinal Modulus (GPa)	**7.5**	**56.9**	**15.5**	**72**	**1.5**
Transverse Modulus (GPa)	**1.9**	**1.26**	**1.33**	**72**	**1.5**
Longitudinal CTE (um/m^{o}C)	**22.1**	**-1.62**	**-45.3**	**5**	**120**
Transverse CTE (um/m^{o}C)	**70.3**	**72.5**	**76.3**	**5**	**120**

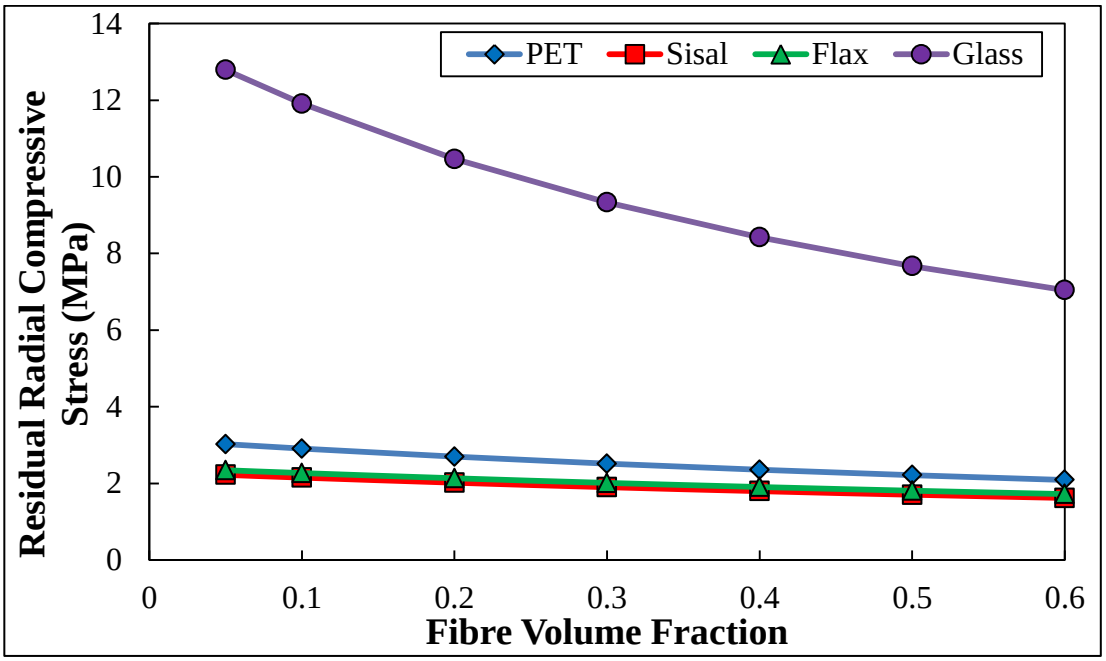

Figure 5.28: Fibre residual radial compressive stress versus volume fraction

5.4 Summary

Single fibre pull-out test were used to investigate the interfacial strength of three fibres which could be utilised as reinforcement for Polypropylene. The fibres that were investigated were Sisal, Flax and Polyethylene Terephthalate. The interfacial strength was investigated with various percentages of Maleic Anhydride in the Polypropylene matrix to find out if this influenced the IFSS.

The interfacial strength of Natural fibres, Sisal and Flax were calculated using the diameter and perimeter of the selected fibre. This was done to see if making the assumption that the fibre was circular could accurately predict the interfacial strength of the system (fibre and

matrix). It was discovered that Sisal IFSS change increased by 25% when assuming the fibre was circular whereas Flax IFSS did not change under identical conditions. Flax IFSS did not change significantly due to the fibre circumference being approximately the same as the perimeter. It was shown that increasing the percentage of MAPP increased the interfacial strength for both fibres. At 0% MAPP the IFSS for Sisal and Flax were 2.7 MPa and 3.4 MPa respectively. Subsequently it was found that using 5% MAPP increased the IFSS by 40% for both fibres. The IFSS in 5% MAPP for Sisal and Flax were 5.8 MPa and 6.6 MPa respectively.

The Polyethylene Terephthalate load versus extension graph was different to the natural and Glass fibre graphs. A 'kink' was witnessed when force was being applied to the fibre. The 'kink' occurred at approximately the same force for each measured percentage of MAPP. The kink was investigated further and it was found that the heat treatment of fibre during the pull-out sample manufacturing process was the cause of this phenomenon. It was found that increasing the percentage of MAPP increased the interfacial strength. The highest value of IFSS was achieved was 5.54 MPa at 5% MAPP.

The interfacial strength results for the PET, Flax and Sisal proved to be low compared to that of conventional fibre, Glass. A possible reason for the low IFSS could be due to the fibres anisotropic nature as the fibres have a low modulus and high CTE in transverse direction which produces a low residual radial compressive stress.

5.5 References

[1] G. Schoolenberg and J. L. Thomason, “An Investigation of glass fibre/Polypropylene interface strength and its effect on composite properties,” *Composites*, vol. 25, no. 3, pp. 197–203, 1994.

[2] M. R. Piggott, “The single-fibre pull out method: its advantages, interpretation and experimental realization,” *Composite Interfaces*, vol. 1, no. 3, pp. 211–223, 1993.

[3] L. Broutman, “Measurement of the fiber-polymer matrix interfacial strength,” *Interface in Composites*, pp. 27–41, 1969.

[4] L. Yang and J. L. Thomason, “Interface strength in Glass fibre–Polypropylene measured using the fibre pull-out and microbond methods,” *Composites Part A: Applied Science and Manufacturing*, vol. 41, no. 9, pp. 1077–1083, Sep. 2010.

[5] A. Arbelaiz, G. Cantero, B. Fernandez, and I. Mondragon, “Flax fiber surface modifications: Effects on fiber physical mechanical and Flax/Polypropylene interface properties,” *Polymer Composites*, vol. 26, no. 3, pp. 324–332, Jun. 2005.

[6] L. Yang and J. L. Thomason, “Development and application of micromechanical techniques for characterising interfacial shear strength in fibre-thermoplastic composites,” *Polymer Testing*, vol. 31, no. 7, pp. 895–903, Oct. 2012.

[7] J. P. Craven, R. Cripps, and C. Viney, “Evaluating the silk/epoxy interface by means of the Microbond Test,” *Composites Part A: Applied Science and Manufacturing*, vol. 31, no. 7, pp. 653–660, Jul. 2000.

[8] J.-M. Park, S. T. Quang, B.-S. Hwang, and K. L. DeVries, “Interfacial evaluation of modified Jute and Hemp fibers/Polypropylene (PP)-maleic anhydride Polypropylene copolymers (PP-MAPP) composites using micromechanical technique and nondestructive acoustic emission,” *Composites Science and Technology*, vol. 66, no. 15, pp. 2686–2699, Dec. 2006.

[9] M. A. López Manchado, M. Arroyo, J. Biagiotti, and J. M. Kenny, “Enhancement of mechanical properties and interfacial adhesion of PP/EPDM/Flax fiber composites using maleic anhydride as a compatibilizer,” *Journal of Applied Polymer Science*, vol. 90, no. 8, pp. 2170–2178, Nov. 2003.

[10] R.-B. Adusumalli, H. K. Weber, T. Roeder, H. Sixta, and W. Gindl, “Evaluation of experimental parameters in the microbond test with regard to Lyocell Fibers,” *Journal of Reinforced Plastics and Composites*, vol. 29, no. 15, pp. 2356–2367, Feb. 2010.

[11] Y. Li, C. Hu, and Y. Yu, “Interfacial studies of Sisal fiber reinforced high density Polyethylene (HDPE) composites,” *Composites Part A: Applied Science and Manufacturing*, vol. 39, no. 4, pp. 570–578, Apr. 2008.

[12] A. Valadez-Ggonzalez, J. M. Cervantes-uc, R. Olayo, and P. J. Herrera-Franco, "Effect of fiber surface treatment on the fiber – matrix bond strength of natural fiber reinforced composites," *Composites Part B: Engineering*, vol. 30, pp. 309–320, 1999.

[13] J. L. Thomason and J. Carruthers, "Natural fibre cross sectional area, its variability and effects on the deterrmination of fibre properties," *Journal of Biobased Materials and Bioenergy*, vol. 6, no. 4, pp. 424 – 439, 2013.

[14] E. Pisanova, S. Zhandarov, and E. Mader, "How can adhesion be determined from micromechanical tests ?," *Composites Part A: Applied Science and Manufacturing*, vol. 32, pp. 425–434, 2001.

[15] C. H. I. Wang and L. M. Hwang, "Transcrystallization of PTFE Fiber / PP Composites . II . Effect of transcrystallinity on the interfacial strength," *Journal of Polymer Science Part B: Polymer Physics*, vol. 34, pp. 1435 – 1442, 1996.

[16] V. B. Gupta and S. Kumar, "The effect of heat setting on the structure and mechanical properties of Poly (ethy1ene Terephthalate) Fiber . IV . Tensile properties other than modulus and their dependence on structure," *Polymer*, vol. 26, pp. 1897–1905, 1981.

[17] V. B. Gupta and S. Kumar, "The effect of heat setting on the structure and mechanical properties of Poly (ethy1ene Terephthalate) Fiber . 111 . Anelastic properties and their dependence on structure," *Polymer*, vol. 26, pp. 1885–1895, 1981.

[18] D. Hwan Cho, W.-R. Yu, J. H. Youk, and J. H. Yoo, "POLYMER Formation of micro-crystals in poly (ethylene terephthalate) fiber by a short heat treatment and their influence on the mechanical properties," *European Polymer Journal*, vol. 43, pp. 3562–3572, 2007.

[19] V. B. Gupta and S. Kumar, "The effect of heat setting on the structure and mechanical properties of Poly (ethy1ene Terephthalate) fiber . I . Structural changes," *Polymer*, vol. 26, pp. 1865–1876, 1981.

[20] V. B. Gupta and S. Kumar, "The effect of heat setting on the structure and mechanical properties of Poly (ethy1ene Terephthalate) fiber. 11 . The elastic modulus and its dependence on structure," *Polymer*, vol. 26, pp. 1877–1884, 1981.

[21] J. L. Thomason and L. Yang, "Temperature dependence of the interfacial shear strength in glass-fibre Polypropylene composites," *Composite Science and Technology*, vol. 71, no. 13, pp. 1600 – 1605, 2011.

[22] R. S. Raghava, "Thermal expansion of organic and inorganic matrix composites: A review of theoretical and experimental studies," *Polymer Composites*, vol. 9, no. 1, pp. 1–11, 1988

[23] J. L. Thomason, "Dependence of interfacial strength on the anisotropic fiber properties of jute reinforced composites," *Polymer Composites*, pp. 1525 – 1534, 2010.

Chapter 6

Effect of Fibre Weight Fraction in Composite Performance

6.1 Introductory Remarks

This chapter examines what, if any, effect the fibre weight fraction of a composite system has on the Polypropylene matrix and considers if the fibre weight fraction can be calculated successfully using the Differential Scanning Calorimetry (DSC) experimental technique. The effect of fibres on Polypropylene morphology was also investigated as it has been reported that certain fibres can act as a nucleation agent that can cause transcrystallsation which could change the mechanical properties of the composite by altering their interfacial characteristics.[1], [2], [3], [4]

6.2 Experimental Programme

The following section will provide full details of the three candidate materials under investigation, sample preparation procedure for the various experiments carried out in this study, apparatus used for the different tests and the various experimental procedures.

6.2.1 Materials

Materials that were used in this study were supplied by various companies. The three candidate materials that were being investigated were Polyethylene Terephthalate (PET), Sisal and Flax and details of each are shown in Table 6.1. Polypropylene (PP) was the matrix material for the different experiments carried out in this study. Table 6.2 provides information on the supplier and the different Melt Flow Index (MFI) of the PP. MFI is defined as a rate at which a mass of a thermoplastic material in grams can flow through a

capillary of specific size over a certain period of time which is usually ten minutes [5]. MFI has an inverse relationship to molecular weight of the polymer therefore low MFI, high polymer's molecular weight. It has been claimed that molecular weight affects the crystallisation/ transcrystallisation of the polymer [6, 7] therefore different MFI of PP was used in this study, Table 6.2.

Table 6.1: Fibre Type

Material	Type	Source
Polyethylene Terephthalate Fibre	Polymer Fibre, TEX 220	SABIC
Sisal	Natural Fibre	Wigglesworth (Brazil)
Flax	Natural Fibre	Wigglesworth (Germany)

Table 6.2: Polypropylene Type

Melt Flow Index (MFI, g/10min)	Material Code	Source
5.7	571P	SABIC
10.5	575P	SABIC
24	515A	SABIC
47	579S	SABIC
120	HGZ-1200	Marlex

6.2.2 Differential Scanning Calorimetry (DSC)

This section provides an overview of the sample preparation technique and the experimental procedure for examining the effect fibre weight fraction has on the Polyproplene (PP) matrix. It should be noted that only PP with a MFI of 47 was used in this investigation to keep consistency throughout this thesis as it same MFI used in Chapter 5. The experiments were carried out on a DSC (Figure 6.1) and each experiment took approximately two hours depending on the candidate material and test method, full details of which are provided below.

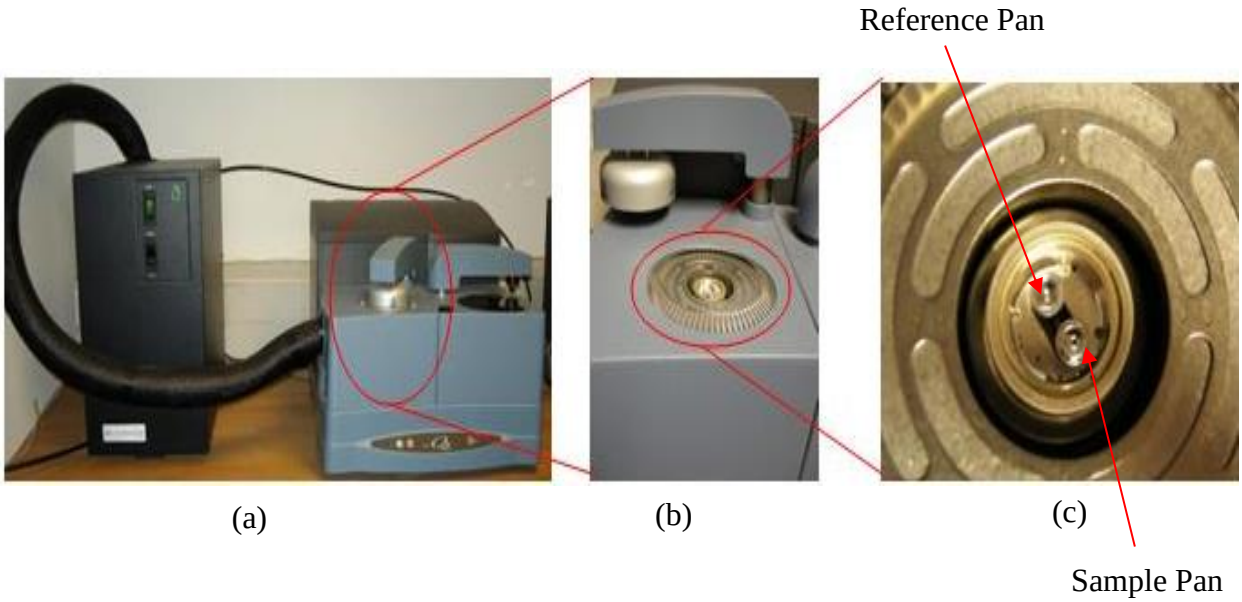

Figure 6.1: DSC Set up

6.2.2.1 Sample Preparation

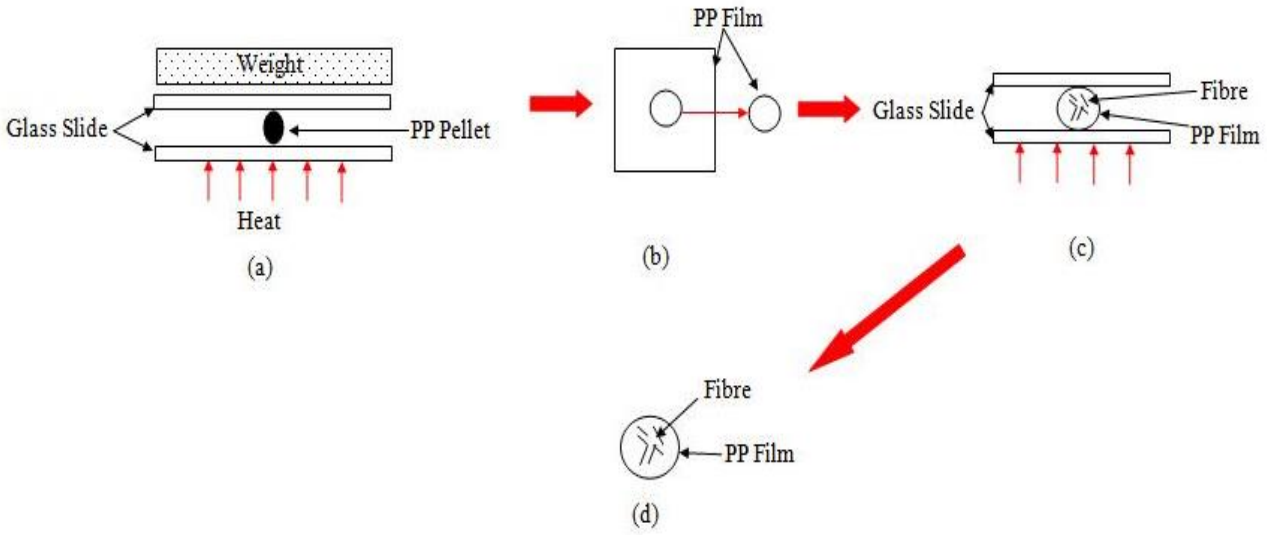

Figure 6.2: DSC mini composite manufacturing

The method used in manufacturing small composites for the DSC is shown above in Figure 6.2 and the procedure is discussed below. The sample preparation was maintained identical

and consistent so that a comparison of different weight fraction can be accurately be made. The procedure for manufacturing samples is described in three stages.

The first stage in the production of small composites a Polypropylene (PP) film was manufactured. To manufacture a PP film, a PP pellet was melted in between two glass slides on a hot plate at a temperature of 220^{o}C. A weight of approximately 2 kg was placed on top to create a thin film. This can be seen in Figure 6.2a. The glass slides with the PP melt is removed and left at room temperature to cool. Further details of manufacturing the PP film are specified in Chapter 5 Section 5.2.3. Once cooled, the PP film was carefully removed from the slides to avoid damage. The film is then ready for the next stage in the manufacturing process.

The second stage of the process was to create the various fibre weight fractions of the composite. This was done by initially using a hole punch to create a small PP circular film approximately 5 mm in diameter which was nearly the correct size for the DSC pan, Figure 6.2b. The circular film was then weighed to determine what percentages of fibres were in the composite after the manufacturing process, prior to any further processing. The PP film weighed approximately 1.7 ± 0.48 mg.

The third and final stage of the procedure was to manufacture the composite sample. This was done by reheating the circular PP film on a glass slide on the hot plate. The weighed fibres were then added to the molten film. Another glass slide is then was placed on top to sandwich the film and fibres, Figure 6.2c. The fibre and film were then left on the hot plate for thirty seconds to allow the fibres to be properly embedded into the film. Once the fibres were embedded into the film, the slides were then removed and left to cool to room temperature, Figure 6.2d. The composite were then reweighed to see if any fibres were lost in

the manufacturing process which would change the fibre weight fraction. The composite was now fully prepared and ready to be run in the DSC system.

A similar procedure was carried out on PP film without fibres (which, for the purpose of comparison will be described as pure PP in this thesis) and PET fibre not embedded in PP (designated as pure PET). The PP film was reheated after being weighed and the PET fibre was also put through the heating process. This was to replicate the heating process the fibres go through when embedding into the PP film in the composite manufacturing procedure. These two samples were manufactured to be used as a reference for the composite's results to be benchmarked against.

6.2.2.2 Differential Scanning Calorimetry Study

The DSC study was carried out in a TA Q2000 machine (Figure 6.1a) under nitrogen gas with composites comprised of PET, Sisal and Flax fibres at various weight content in Polypropylene matrix. Nitrogen gas was used as it was discovered that running the composites under air, the Polypropylene matrix degraded during the first cycle therefore repeat runs would not be possible on the sample and would lead to inaccurate results. Before the composite samples were tested, they were placed into a DSC pan. The type of pan used in this study was an aluminium 'hermetic' pan. The pan and lid were weighed first before a sample was placed into the pan. The weight of the pan and lid was noted and was in the region of 52.1 ± 0.3 mg. The composite was then placed into the pan and sealed shut using the TA DSC sample press. The sample in the sealed pan was then weighed. The weight of the sealed pan was subtracted from the empty pan and lid weight thus giving the composite mass. The composite weighed between 3 – 6 mg, depending on the fibre content. The weight of the sample is needed as the DSC uses the mass to track any changes when heating or cooling the sample. The sample pan is then placed into the front of the DSC chamber and this can be seen

in Figure 6.1c. A reference pan is also used and is loaded into the back of the DSC chamber. The reference pan is used to monitor any changes to the sample pan. If the sample pan changes and the reference pan does not alter then it is assumed that the composite is causing the change. The changes are then recorded by the DSC. A fuller exact description of the DSC process is given in Chapter 3 Section 3.2.4. The procedure used in this study varied depending on the type of fibre that was being analysed. The experimental approach for the different type of fibre is described in detail below, Table 6.3.

Table 6.3: DSC procedure for Various Fibre Types

<table>
<tr><th>PET Fibre Composite</th><th>Natural Fibre Composite</th></tr>
<tr><td>Equilibrate at -20^{o}C
Isothermal 2 minutes
Ramp 20^{o}C/min to 300^{o}C
Ramp 5^{o}C/min to 0^{o}C
Ramp 20^{o}C/min to 300^{o}C</td><td rowspan="2">Equilibrate at -20^{o}C
Isothermal 2 minutes
Ramp 20^{o}C/min to 200^{o}C
Ramp 5^{o}C/min to 0^{o}C
Ramp 20^{o}C/min to 200^{o}C</td></tr>
<tr><td>Equilibrate at -20^{o}C
Isothermal 2 minutes
Ramp 20^{o}C/min to 200^{o}C
Ramp 5^{o}C/min to 0^{o}C
Ramp 20^{o}C/min to 300^{o}C</td></tr>
</table>

Pure PP and pure PET fibre went through the same experimental testing routine as the composites. The results from pure PP and PET were used to calculate the ideal enthalpy (ΔH) for melt and crystallisation for various weight fractions. The ΔH values were then compared to the experimental results to see if the DSC can be used to calculate the composite's weight fraction and the results are presented in Section 6.3

6.2.2.3 Fibre Weight Fraction Calculation

Fibre weight fraction is essential to predict composite properties. Pure PP (PP_{100}) and pure PET (PET_{100}) enthalpy (ΔH) for melting and crystallisation from the DSC were used to calculate expected ΔH at various fibre weight fractions if PP and PET fibre has no effect on

each other such as PET not aiding crystallisation in PP. The equations used to calculate the various ΔH using PP and PET are shown below.

$$\Delta H_{PP\ @wf} = (1 - W_f)\Delta H_{PP\ 100} \quad (6.1)$$

$$\Delta H_{PET\ @wf} = W_f \Delta H_{PET\ 100} \quad (6.2)$$

where W_f is weight fraction percentage, $\Delta H_{PP\ 100}$ and $\Delta H_{PET\ 100}$ is the ΔH of pure PP and pure PET.

The weight fractions of the composites tested were also calculated by the ΔH's obtained by the DSC. This was done to see if DSC could be used to accurately predict the composite's weight fraction. The equations used to calculate the weight fraction of the composite are shown in equation 6.3.

$$W_f = 100 - \left(\frac{\Delta H_{PP\ Composite}}{\Delta H_{PP100}} * 100\right) \quad (6.3)$$

$$W_f = \left(\frac{\Delta H_{PET\ Composite}}{\Delta H_{PET100}} * 100\right) \quad (6.4)$$

where $\Delta H_{PP\ composite}$ is the PP ΔH of the composite obtained from the DSC and $\Delta H_{PET\ composite}$ is the PET ΔH of the composite also taken from the DSC trace .

The results obtained for ΔH for the different fibre content using the above equations were then related to the experimental results to see if the DSC can be used to calculate the fibre content in composites.

6.2.3 Crystallisation and Transcrystallisation

Details of the sample preparation procedure and experimental process of the investigation into the effect of fibres on Polypropylene morphology is given in this section. A variety of MFI of PP is used in this section to investigate the effect of molecular weight on the crystallisation and transcrystallisation of the polymer.

6.2.3.1 Sample Preparation

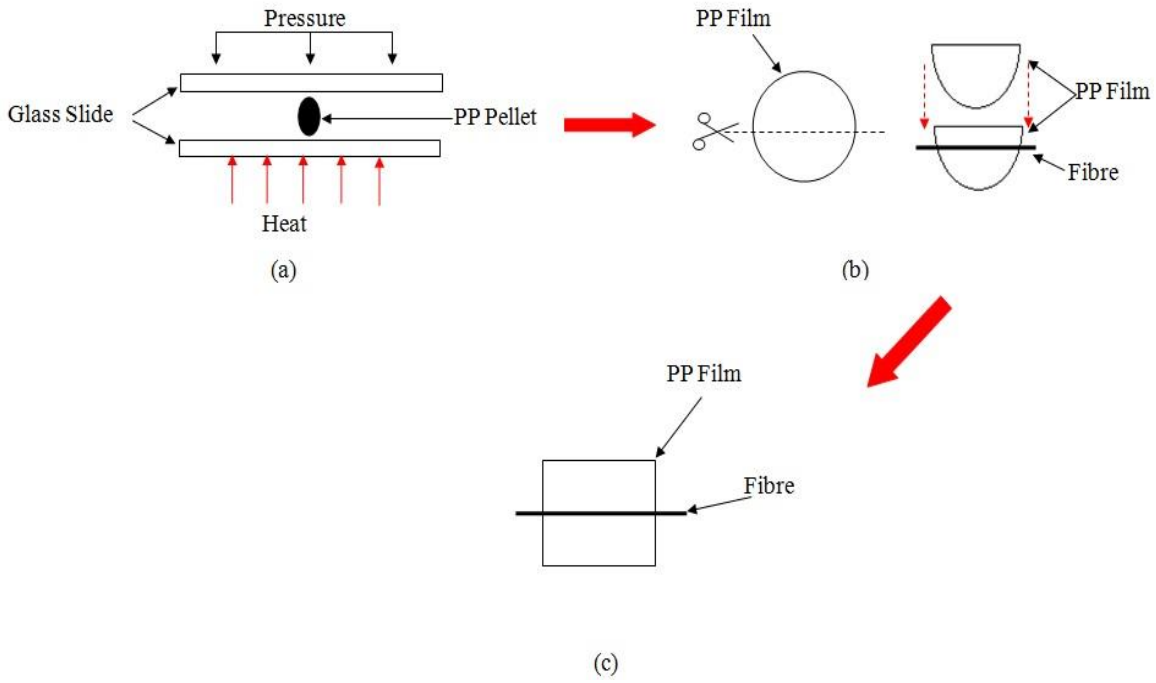

Figure 6.3: Crystallisation / Transcrystallisation set up

The sample manufacturing process for the crystallisation and transcrystallisation study was similar to the first stage of the production of the DSC samples. A PP film was created on the hot plate by sandwiching a PP pellet between two glass slides at a temperature of 220^{o}C. The glass slides were pressed together to manufacture a PP film as thin as possible, Figure 6.3a. The glass slides with the PP in the middle were then removed from the hot stage and left to cool to room temperature. PP film was carefully removed from the glass slide with tweezers

on to a contamination free surface. At this point the sample manufacturing for the crystallisation study was complete apart from cutting the film into a 20x20 mm square. The film for the transcrystallisation study was then cut into two using a scalpel and tweezers so as to avoid hand contact as this could contaminate the film which could then affect the investigation. One half of the PP film was placed onto a glass slide and a single fibre approximately 3 cm length was placed over the PP film. The other half of the PP film was then carefully placed on top of the fibre and film, making sure that the edges match up, Figure 6.3b. The glass slide and the sample of the PP film and fibre were then placed on the hot plate so that the fibre could be embedded into the film. A glass slide was then placed on top of the sample after one minute as this give sufficient time for the PP to melt and fibre to be embedded into the film. The glass slides were pushed together helping the fibre embed into the PP film and to create a thin film. A thin film is needed to help in the observation of transcrystallisation which occurs between the fibre and film. The glass slides and fibre – film sample were removed and left to cool to room temperature. Once the transcrystallisation and crystallisation sample had cooled down, the sample was cut in to a 20 x 20 mm square, Figure 6.3c. This was done so that a glass cover slip could be put over the sample to reduce degradation of PP in the next stage of the study.

6.2.3.2 Crystallisation and Transcrystallisation Study

The crystallisation and transcrystallisation study was carried out on a Mettler Toledo hot stage. The Mettler Toledo hot stage is divided in two parts, the Mettler Toledo FP90HT central processor and the Mettler Toledo FP82HT hot stage furnace, Figure 6.4. The hot stage has a temperature range between room temperature (25^{o}C) and 375^{o}C. The central processor controls the temperature of the hot stage furnace. The processor can be used to heat and cool the furnace at different temperature ramp rates

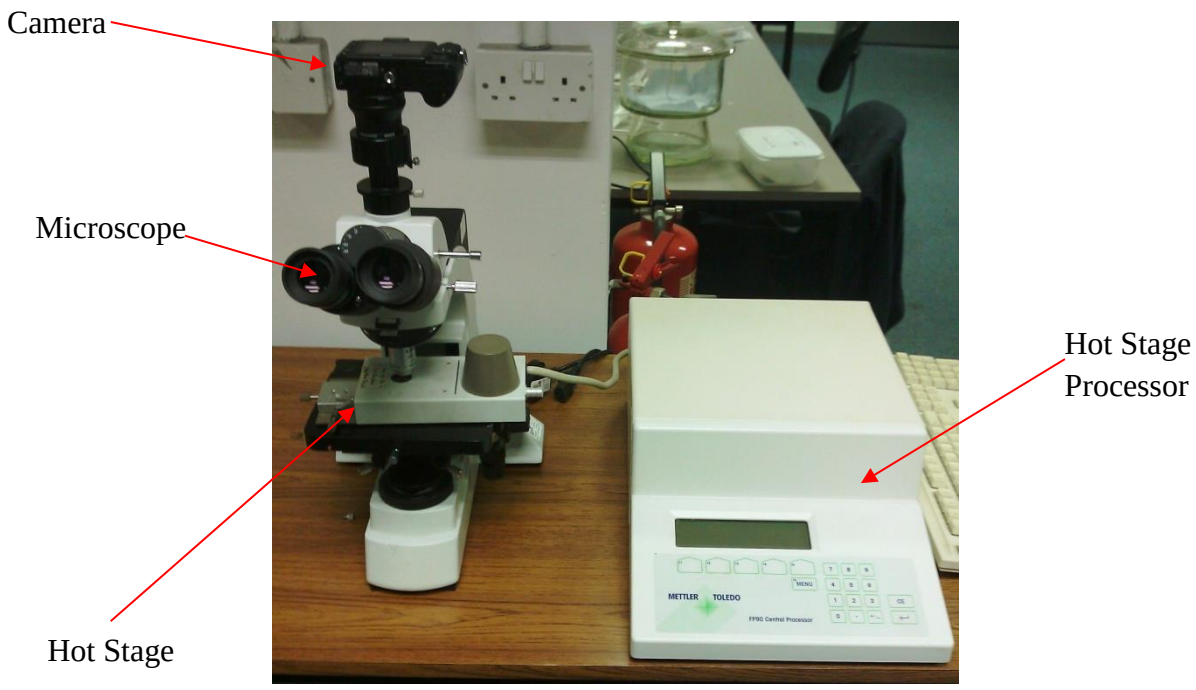

Figure 6.4: Crystallisation / transcrystallisation set up

The 20 x 20 cm PP film with / without the fibre was placed onto a glass slide and then a cover slip was placed on top. The slide with the specimen was placed into the hot stage at a temperature of 200^{o}C. The temperature remained at 200^{o}C for fifteen minutes to allow the removal of any thermal history that could have been created during the manufacture of the samples. The hot stage with the sample was then mounted on to the microscope and this can be seen in Figure 6.4. The type of microscope that was used was a L-Plan model with a 200x magnification. A Nikon COOLPIX P5100 digital camera was mounted on top of the microscope and this was used to record any changes that occur to the PP film through the experiment. The sample was cooled down to a crystallisation temperature at a controlled rate of 10^{o}C/minute. The crystallisation temperatures that were investigated were 130, 135 & 140^{o}C. After the temperature was ramped down to the desired crystallisation temperature and held for thirty minutes to allow for crystallisation /transcrystallisation to happen. Pictures

were taken throughout the thirty minutes to observe the growth and speed of the crystallisation of the film.

6.3 Results and Discussion

6.3.1 Differential Scanning Calorimetry

DSC was carried out on Pure PP with a melt flow index of 47 (MFI 47) and pure PET fibre before proceeding with the composite experiments. The melting and crystallisation ΔH obtained from the DSC runs were used to calculate ΔH for various weight fractions. The calculated weight fraction ΔH was used to compare with the composite results to see if the DSC could accurately calculate the fibre weight fraction. The DSC trace for pure PP and pure PET is shown below in Figure 6.5 and 6.6 respectively.

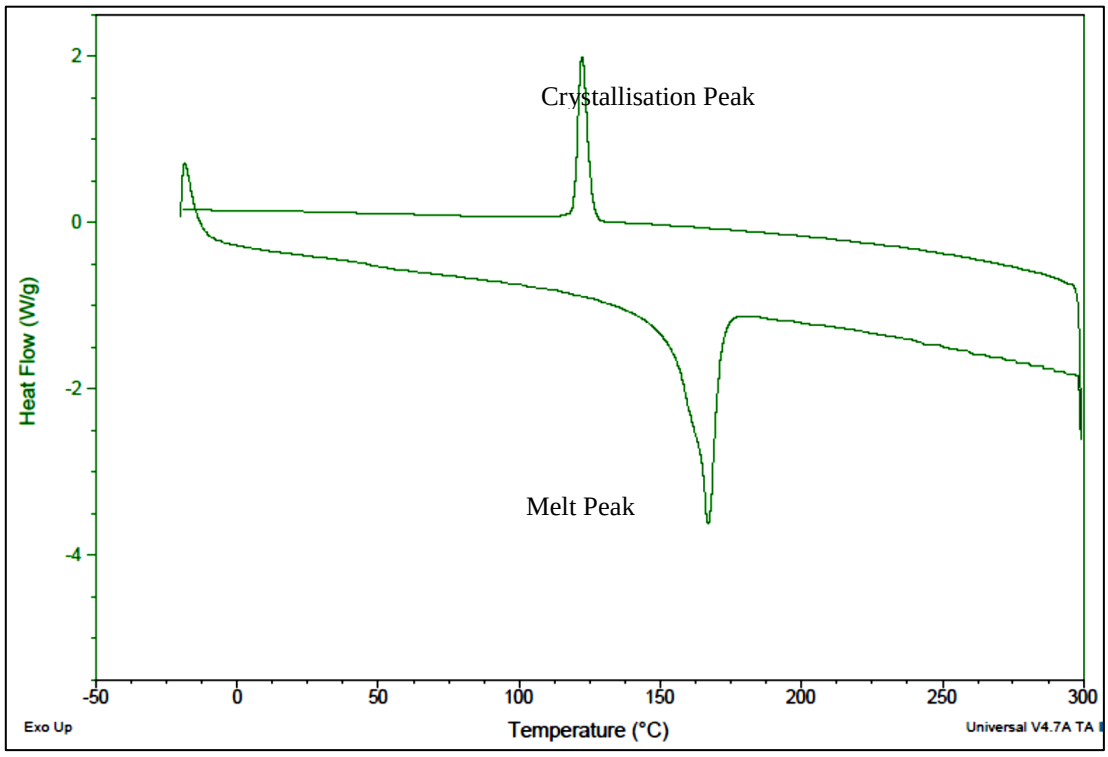

Figure 6.5: Pure PP DSC trace

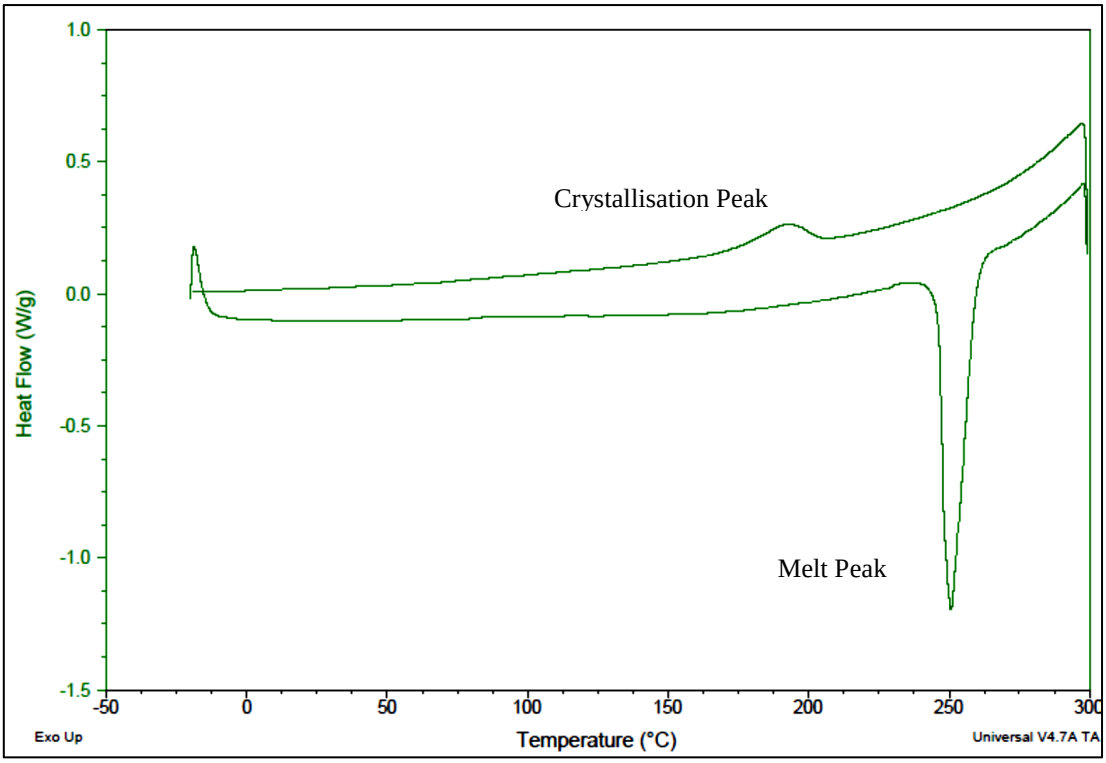

Figure 6.6: Pure PET DSC trace

Pure PP ΔH obtained from the first crystallisation and second melt were 103.8 and 107 J/g respectively. The ΔH value for pure PET fibre obtained from the first crystallisation and second melt were 38.17 and 42.22 J/g respectively. The first heat run was not used in the calculating the fibre weight fraction due to the uncontrolled thermal history of the sample preparation. These melting and crystallisation ΔH values were substituted in to equation 6.1 and 6.2 for PP and PET respectively to calculate different ΔH at various weight fractions. The results for PP and PET can be seen in Figure 6.7 and 6.8 respectively.

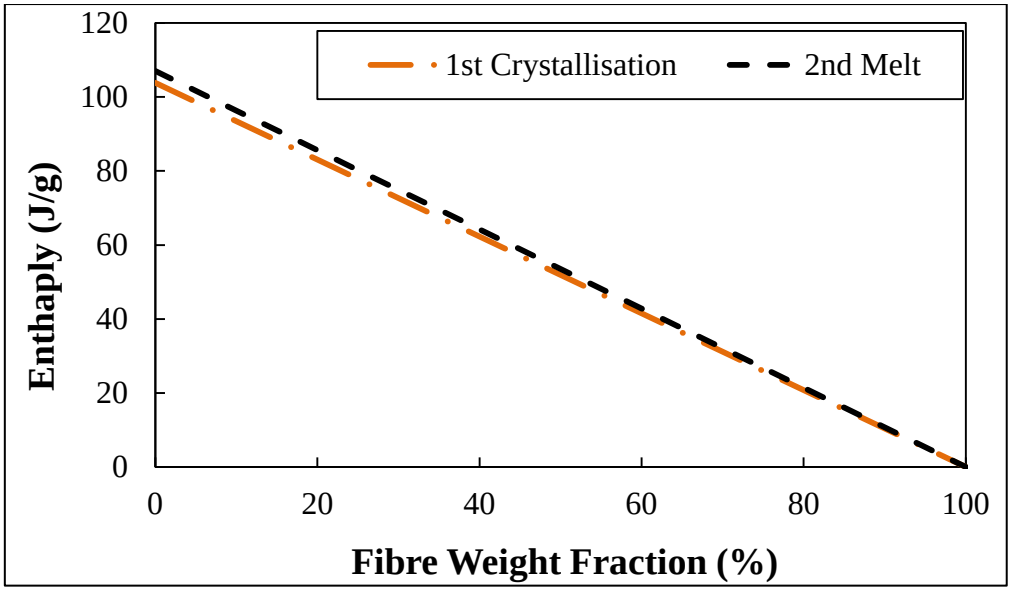

Figure 6.7: Pure PP calculated ΔH at various weight fractions

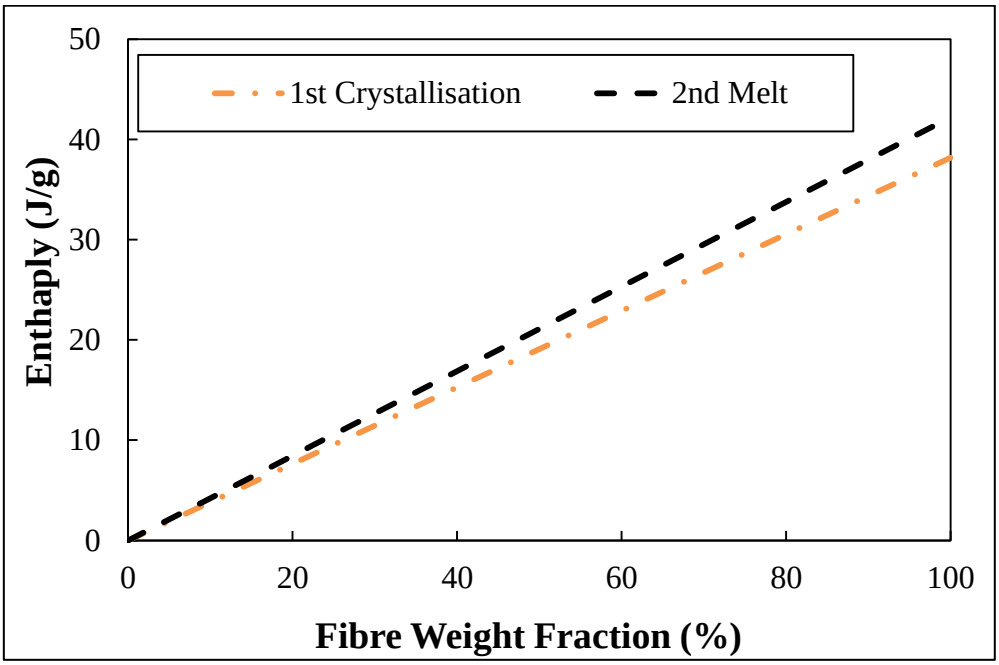

Figure 6.8: Pure PET calculated ΔH at various weight fractions

Figure 6.7 shows that the ΔH for melting and crystallisation of the PP should decrease as the fibre weight fraction increases, whereas the ΔH increases as the fibre weight content increases for the PET fibre. Figure 6.7 and 6.8 shows what the results should be if the PET fibre has no effect on PP and vice versa. The results are compared to the experimental results obtained by the composites in Sections 6.3.1.1 and 6.3.1.2.

6.3.1.1 Polyethylene Terephthalate

Before the results from the experiments carried out on the PET-PP composite are discussed, an explanation on how the fibre weight fraction is determined from the DSC trace is described below.

The PET-PP composites fibre weight fraction can be obtained from two different methods as the DSC trace for the composite will show two melting peaks. The first melting peak represents the PP matrix and the second melting peak characterises the PET fibre melt peak. The two melt peaks can then be used to compare against the ideal enthalpies calculated using equations 6.1 and 6.2 for the various fibre weight fractions. The results of the experimental enthalpies and fibre weight fraction are compared to the calculated enthalpies and fibre content to see if the DSC can be used to obtain the fibre weight fraction of the composites. A typical DSC trace that was created for PET-PP composite is shown in Figure 6.9.

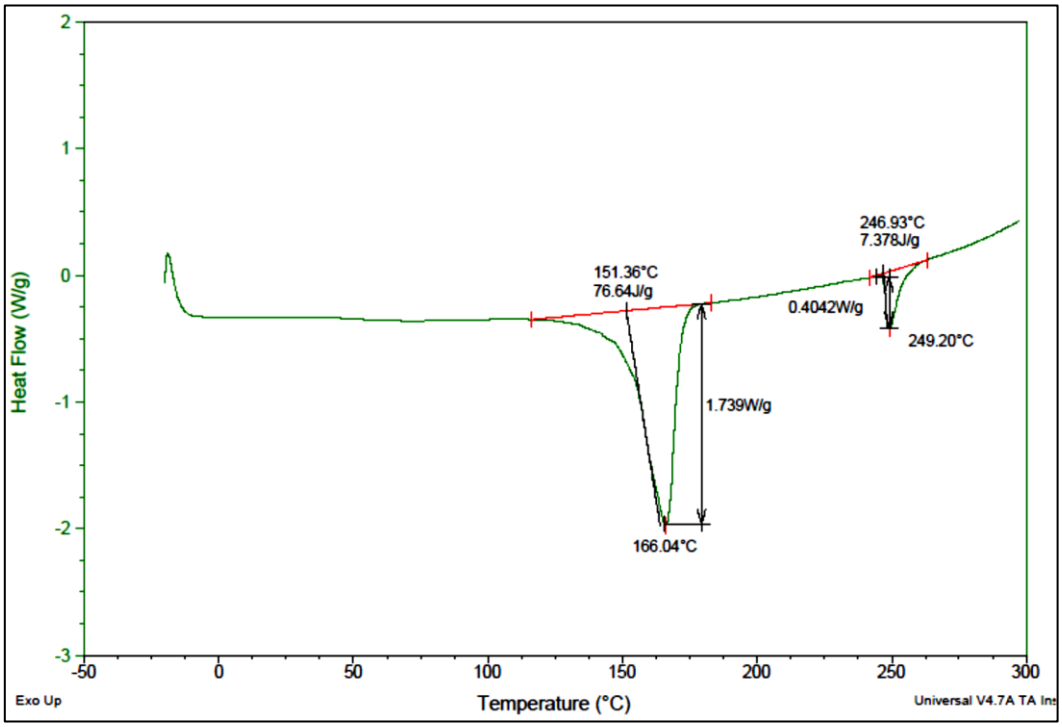

Figure 6.9: Example of PET-PP composite DSC trace

A DSC experiment was carried out on composites containing Polypropylene (MFI 47) and Polyethylene Terephthalate fibre. Two different DSC tests were carried out on these composites. The differences between the test procedures were on the first heating run. The first heating run for each test is described below.

1. The composite was heated up to 300^{o}C therefore melting the matrix and the fibre.

2. The composite was heated up to 200^{o}C hence only the matrix is melted.

Both runs were then cooled down at a rate of 5^{o}C/min to the same temperature of -20^{o}C and then ramped at 20^{o}C/min to 300^{o}C. A typical graph for the two run types can be seen in Figure 6.10. Figure 6.10 shows that for the first DSC run, the melt peak for both PP and PET is shown as the temperature is ramped high enough for both materials to melt, whereas only the PP melt peak in the first heating run is observed in the second DSC run which is to be expected as the temperature does not go high enough for the PET fibre to melt. In the second heating run of the second DSC test, the PP melt peak is shown but also the PET melt peak as the temperature is high enough for the PET fibre to melt, Figure 6.10.

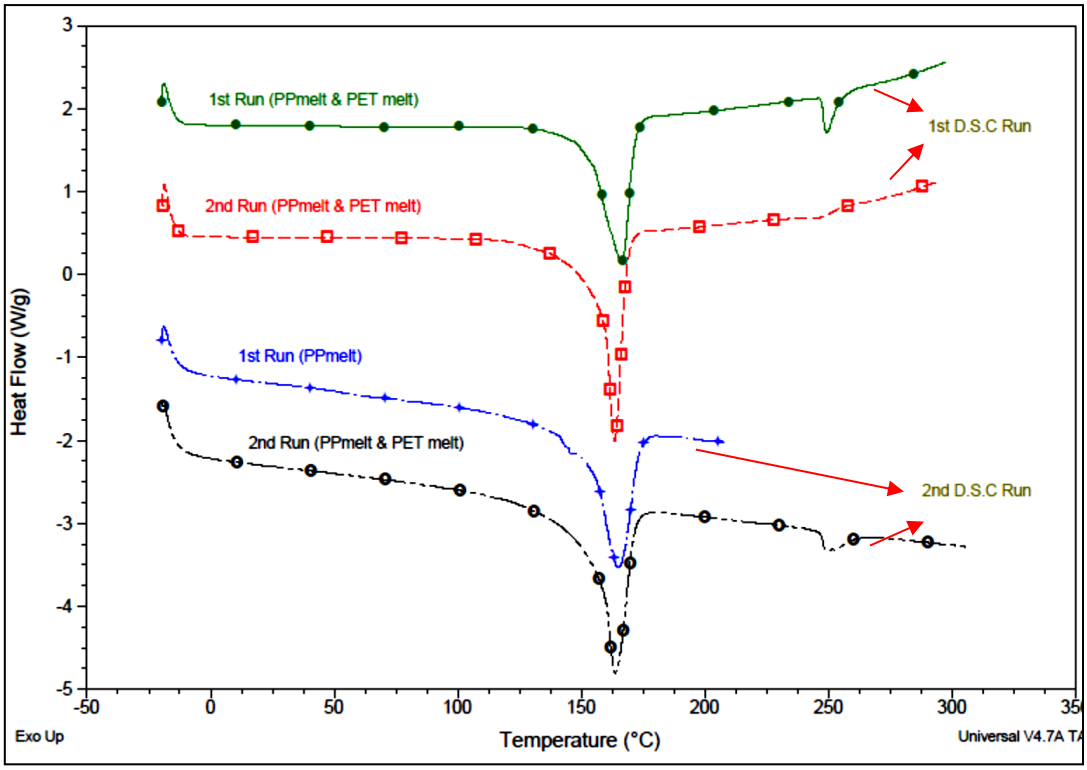

Figure 6.10: Example of the two different DSC run of PET fibre

The two different PET DSC experiments were carried out at various fibre weight fractions. The fibre weight fraction for each composite tested was calculated from the ΔH for melting and crystallisation by equation 6.3 for PP and PET. PET crystallisation enthalpy was not used in this study as it was only observed in fibre contents above 20%. Fibre weight content was calculated by substituting the ΔH of the composite and Pure PP into equation 5.3. Graphs were plotted showing the calculated fibre weight fraction by ΔH obtained from the DSC against the 'actual' weight fraction for the first and second DSC experiments are shown in Figures 6.11 and 6.12.

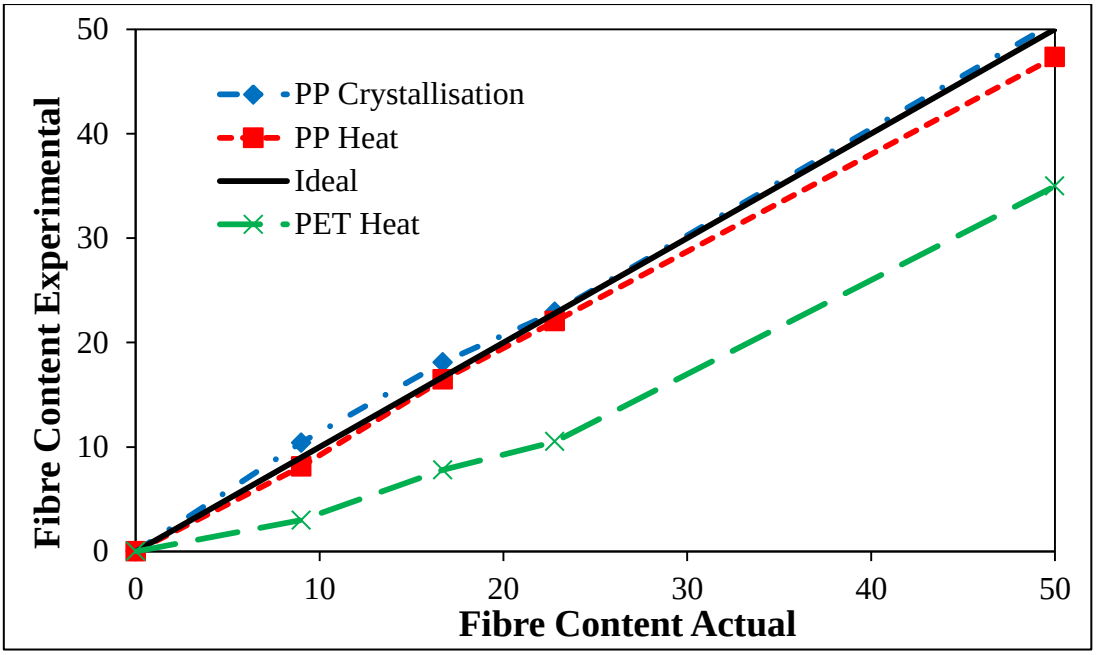

Figure 6.11: 1st DSC Run (PP and PET fibre melted on 1st heat run). Fibre content calculated from ΔH versus actual fibre content

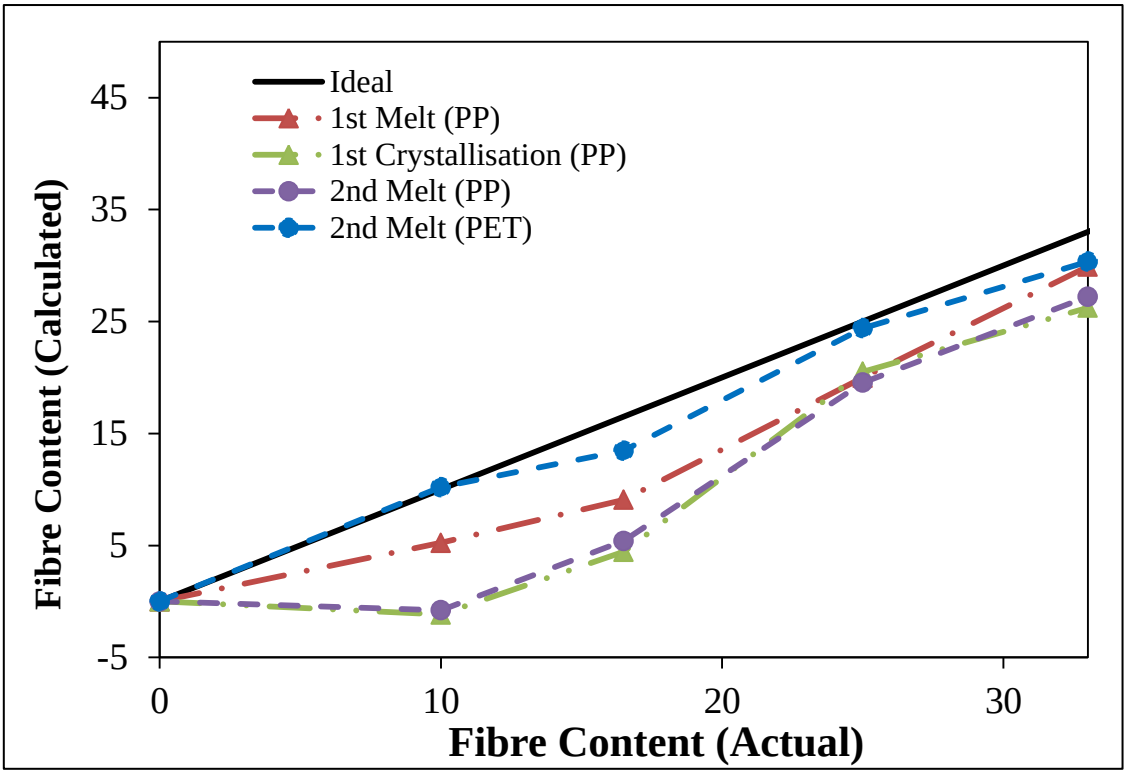

Figure 6.12: 2nd DSC run (Only PP melted on 1st heat run only). Fibre content calculated from ΔH versus actual fibre content.

Figure 6.11 shows the results for PP for both melt and crystallisation and the melt run for PET over a fibre weight fraction ranging from 0 - 50%. Only the PET melt run is shown in Figure 6.11, as the PET crystallisation was only seen in the fibre content greater than 30%. It can be observed from the graph (Figure 6.11), that the PP crystallisation and melt runs give reasonable results to calculate the fibre weight fraction by using the ΔH, whereas as it can be observed that the PET melt run underestimates the fibre content. PP crystallisation and PP second melt give similar fibre weight content, which is as expected as the ΔH are the same as the crystallisation of the PP and does not change between the crystallisation and melting cycles.

Figure 6.12 shows the results for PP for both melt and crystallisation runs and only the melt run for PET over a fibre content ranging from 0 – 33% was used to calculate the fibre content of the composite. It can be observed from the graph that the PET melt run approximately estimates the correct fibre content. The PP crystallisation and the melt run slightly underestimate the fibre weight fraction at 10 and 16.5%. A plausible explanation for the PP underestimations at 10 and 16.5% fibre content is that the PET fibre affects the PP matrix and therefore altering PP structure therefore affecting the melting enthaply of the PP. Hence comparing Figures 6.11 and 6.12 of the different DSC experiments for PET-PP composite it should be noted that to calculate the fibre weight fraction for PET- PP composite with PET fibre melting on the first run, the PP enthalpy should be used not the PET fibre enthalpy and for PET – PP composite with the PET fibre melting on the second run the PET fibre enthalpy should be used.

6.3.1.2 Natural Fibre (Sisal and Flax)

Just like the PET-PP composite, details of the how the Natural fibre (NF) – PP composite fibre content is determined from the DSC experiment is described before discussing the

results from the investigation. The NF-PP composites fibre weight fraction was calculated similar to the PET – PP composites except only the PP melt and crystallisation was used as no NF melting occurred. Equation 6.3 was used to calculate the fibre content from the experimental enthalpies and was then compared to the ideal results. The trace that would be created by the DSC for NF-PP composites is shown in Figure 6.13.

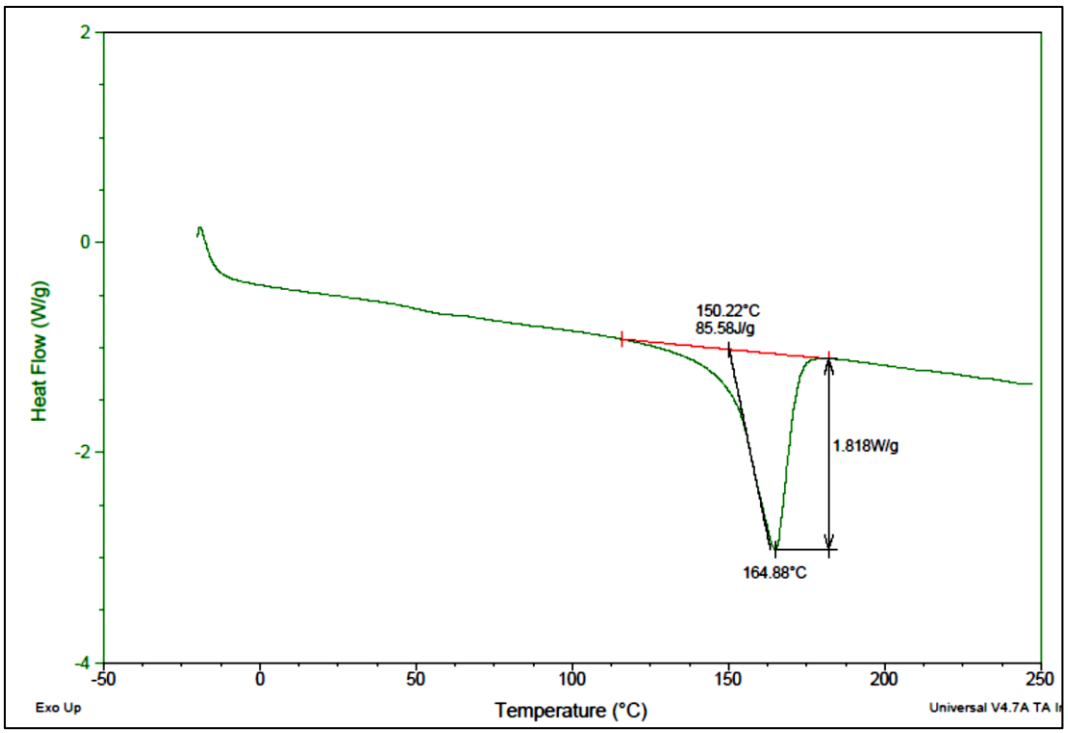

Figure 6.13: Example of NF-PP composite DSC trace

As with the PET fibre, composites containing Sisal and Flax fibres were manufactured over a range of fibre content (0 – 30%). Only one form of DSC experiment was carried out on these composites which only considered the PP melting and crystallisation ΔH. This was undertaken in this manner as natural fibres do not melt; they degrade above a temperature of 200^{o}C. As with PP –PET fibre composites, the ΔH of PP was used to calculate the weight fraction of each composite using equation 6.3. Graphs of the calculated weight fraction were plotted against the actual weight fraction of the composite for Flax and Sisal and are shown in Figure 6.14 and 6.15.

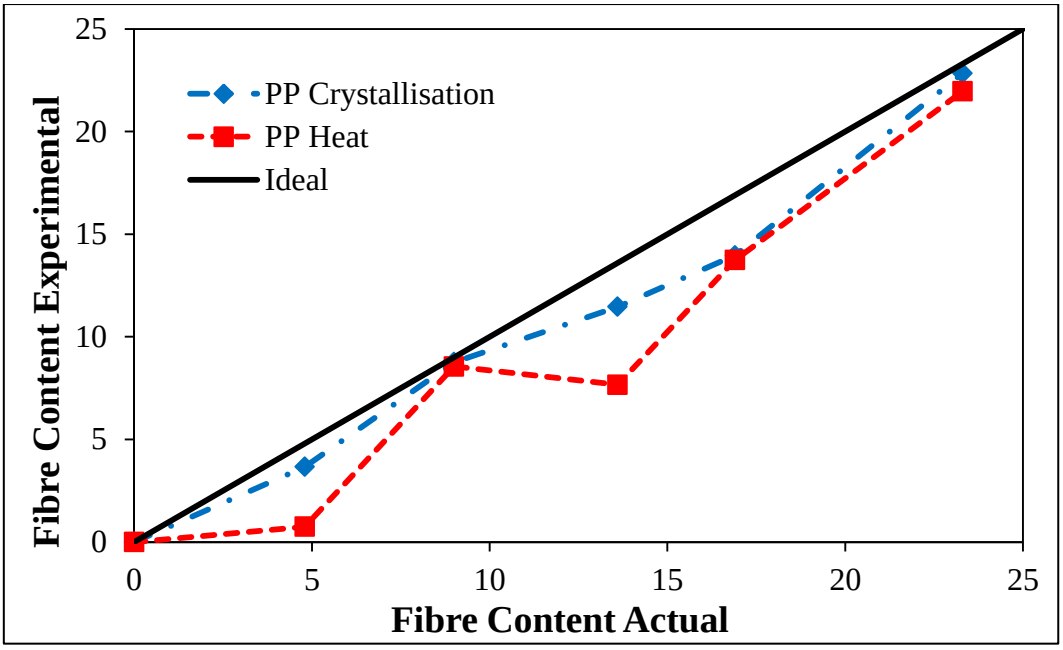

Figure 6.14: Flax Fibre Calculated Fibre Content versus Actual Fibre Content

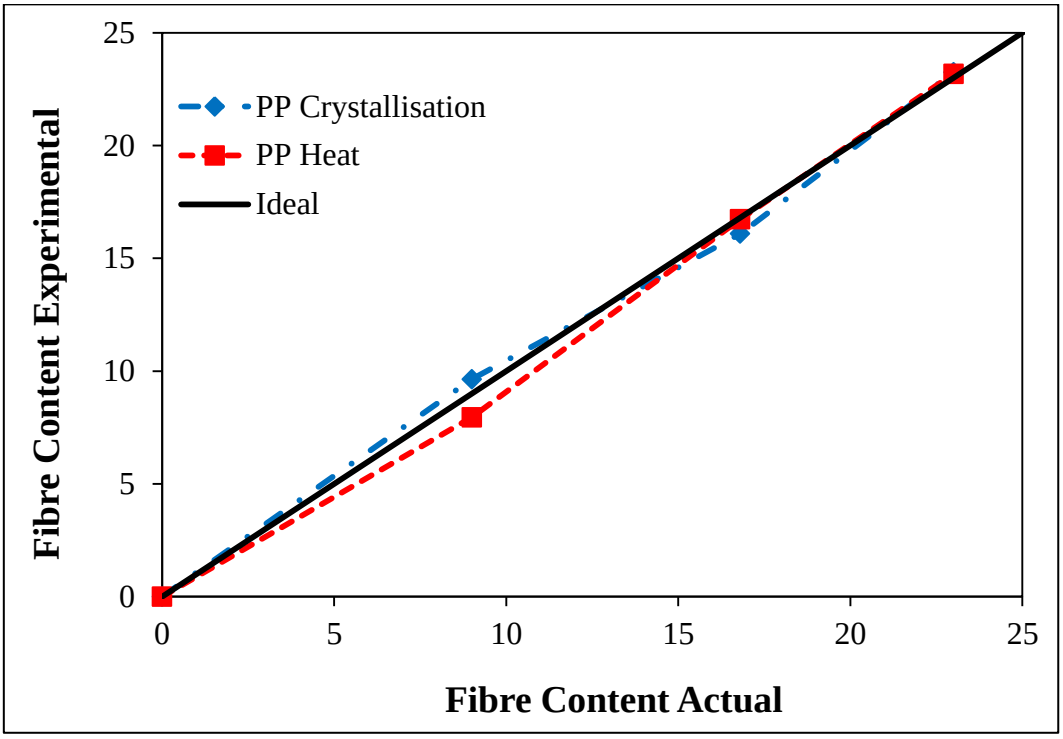

Figure 6.15: Sisal Fibre Calculated Fibre Content versus Actual Fibre Content

Figure 6.14 and 6.15 show the results of the calculated fibre content from the melting and crystallisation ΔH of PP for Flax and Sisal composites. The graphs show different trends, Flax fibre shows an underestimation of fibre content with accurate results at 10 and 23%

whereas the Sisal fibre both crystallisation and melt runs gives a good estimation of the fibre weight content. Comparing the results of both graphs shows the variation between different natural fibres. An explanation for Flax results having a low fibre content estimation could be down to the water in the Flax fibre not evaporating off during the sample manufacturing process but disappearing from the fibre during the experiment as dry fibres were not used.

The onset melting and crystallisation temperature were also studied, to find out if the fibres caused any effect to the PP which may have caused underestimation in fibre content in some of the composite calculations such as the fibres suppressing the melting and crystallisation of the PP. The onset melt and crystallisation temperature for PP were plotted against the fibre content and is shown in Figure 6.16 and 6.17.

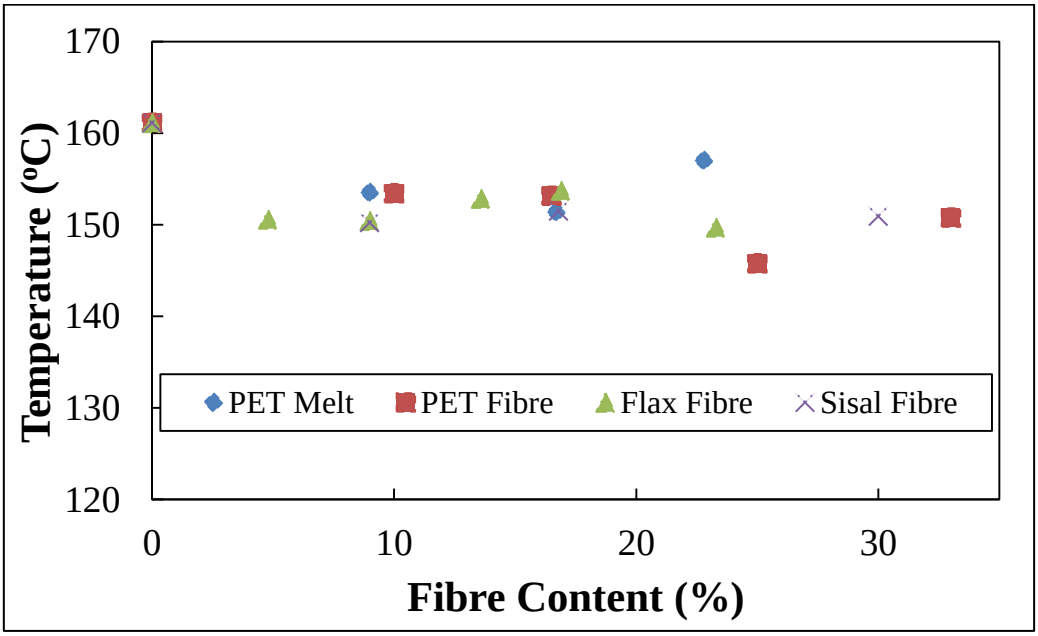

Figure 6.16: PP Onset Melt Temperature versus Fibre Content

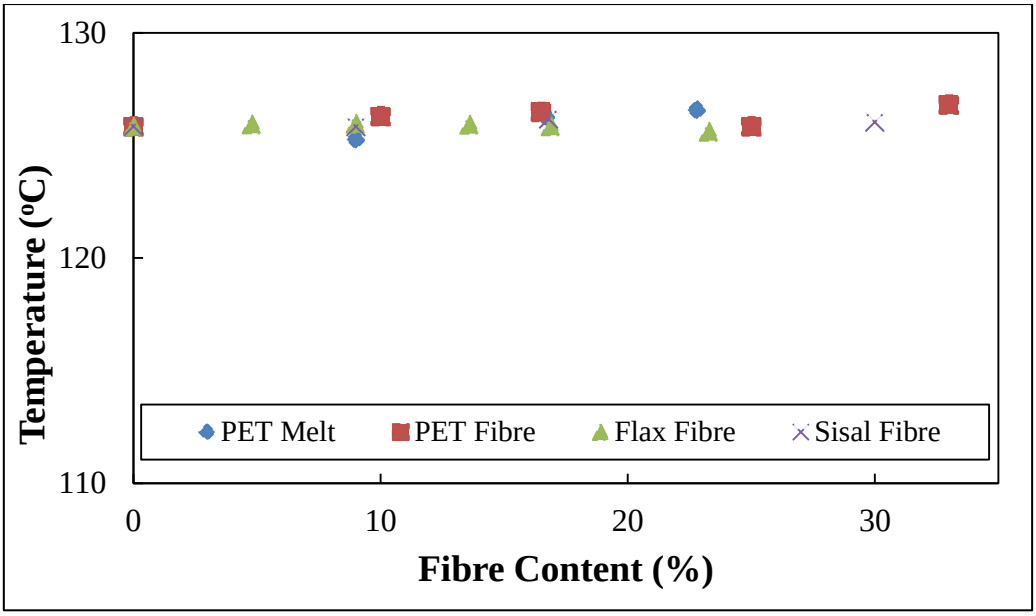

Figure 6.17: PP Onset Crystallisation Temperature versus Fibre Content

It is observed in Figure 6.16 that the onset melting temperature lowers with the addition of fibres. A possible reason for this is the wax found in natural fibres and the oil which is coated on the PET fibre after manufacturing lowers the onset of melting. The onset of crystallisation of PP does not significantly change with the addition of fibres. This is surprising as many researchers have reported that PET and Natural fibres act as a nucleating agent to PP but this is not observed from the DSC results. Therefore further research into the crystallisation/ transcrystallisation of PP with fibres was carried out.

6.3.2 Transcrystallisation and Crystallisation of PP

Transcrystallisation was carried out with PET, Sisal and Flax embedded in a film of PP with a MFI of 47. The fibre and film combination was cooled from 200^{o}C to a temperature of 135^{o}C at a rate of 10^{o}C/min and left for thirty minutes to observe any occurrence of transcrystallisation. The images taken after the thirty minutes at 200x magnification are shown in Figure 6.18.

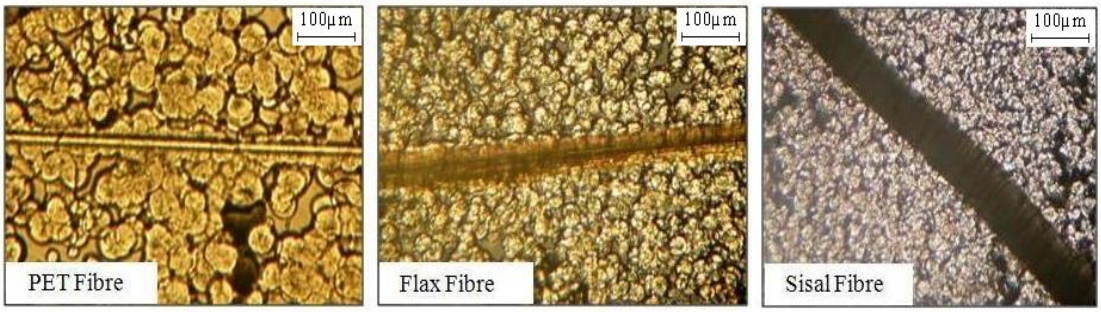

Figure 6.18: PP_{47} with PET, Flax and Sisal fibres at 130°C

Figure 6.18 shows that for all fibres transcrystallinity was not observed. The observation of no transcrystallinity occurring in PP_{47} explains why there was no change observed in the onset crystallisation temperature of PP from the DSC in Figure 6.17. It was therefore decided to investigate if the fibres or the PP were the cause of the problem and to why there was no trancrystallinity occurring. The fibres were then embedded into a PP film with a MFI of 10.5 and went through the same procedure as the PP_{47} film – fibre combination. The results from this study on $PP_{10.5}$ and fibres are shown in Figure 6.19.

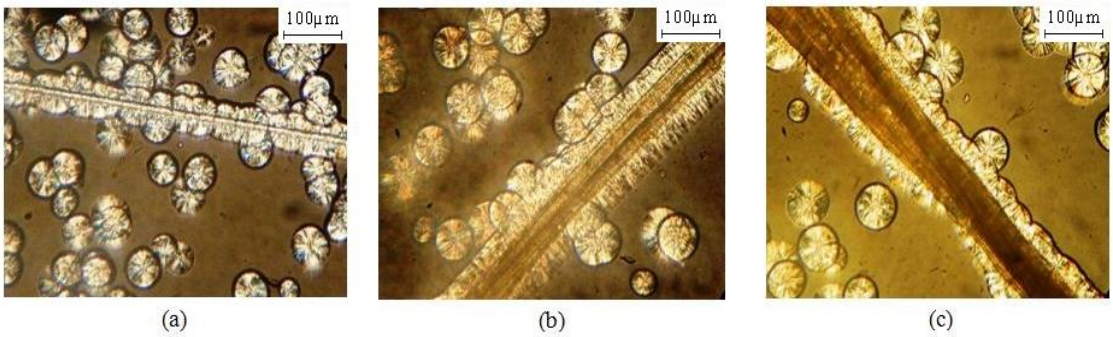

Figure 6.19:$PP_{10.5}$ with a) PET, b) Flax and c) Sisal

It can be seen from Figure 6.19 that fibres do act as nucleating agent creating crystal growth around the fibre. It can therefore be concluded that PP is the cause for the transcrystallinity not occurring at a melt flow index of 47. Thomason and Van Rooyen [8] also observed that the transcystallisation increases as the molecular weight of PP increases or MFI decreases. Therefore the crystallisation of PP at a range of MFI from 5.7 – 120 was investigated. This

investigation was undertaken to see if the MFI had an effect on the crystallisation of PP. The study looked at crystallisation on PP at different temperatures (130, 135 and 140^{o}C). As in the transcrystallisation study, the PP films were held at each temperature for thirty minutes to allow enough time for crystallisation. Photos were taken of the crystallisation process and the time it took for the PP to fully crystallise. The results of this study are shown in Figures 6.20 – 6.24 for MFI of 5.7, 10.2, 24, 47 and 120 at the various temperatures respectively.

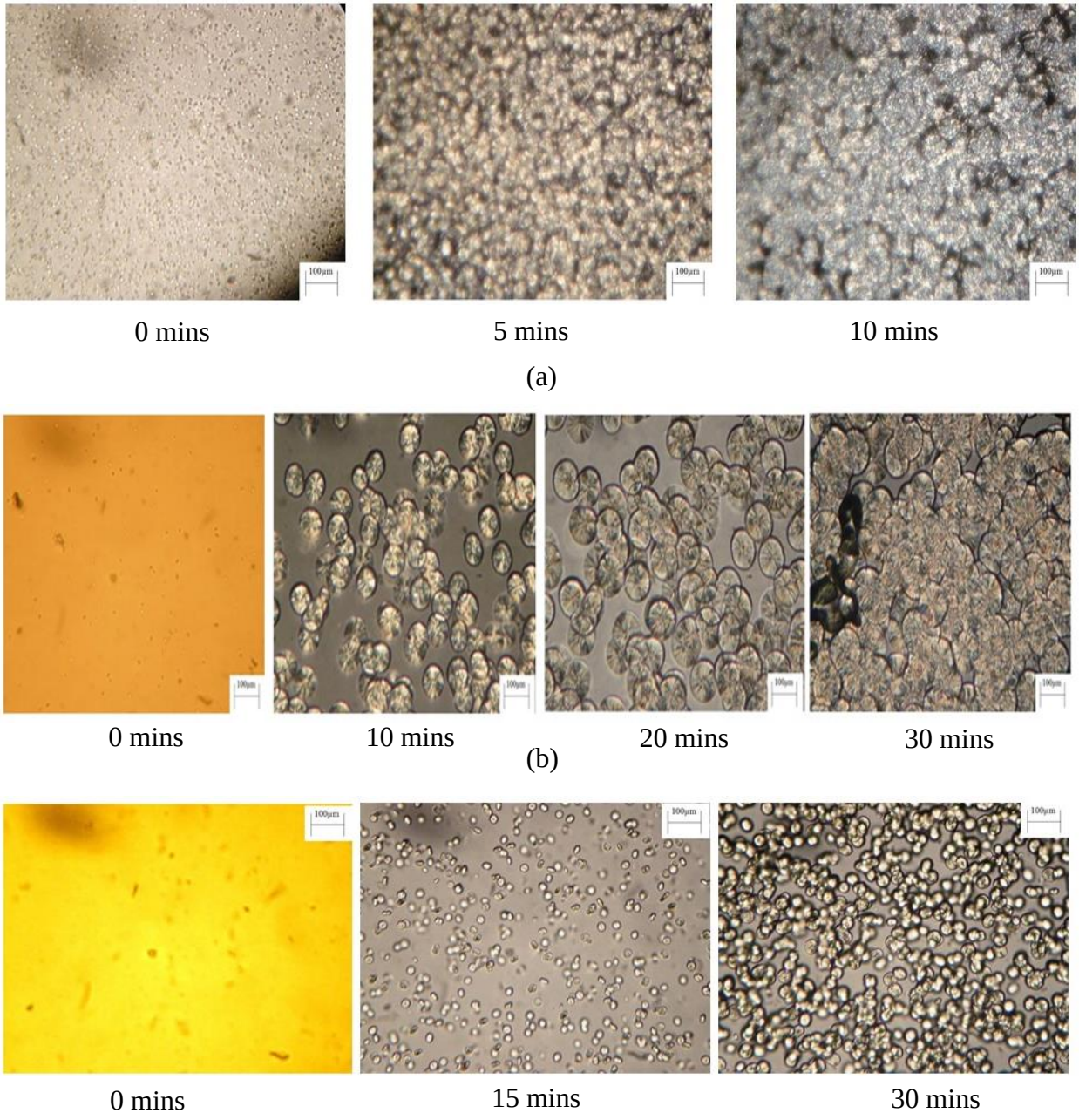

Figure 6.20: PP MFI 5.7 at a) 130^{o}C, b) 135^{o}C and c) 140^{o}C

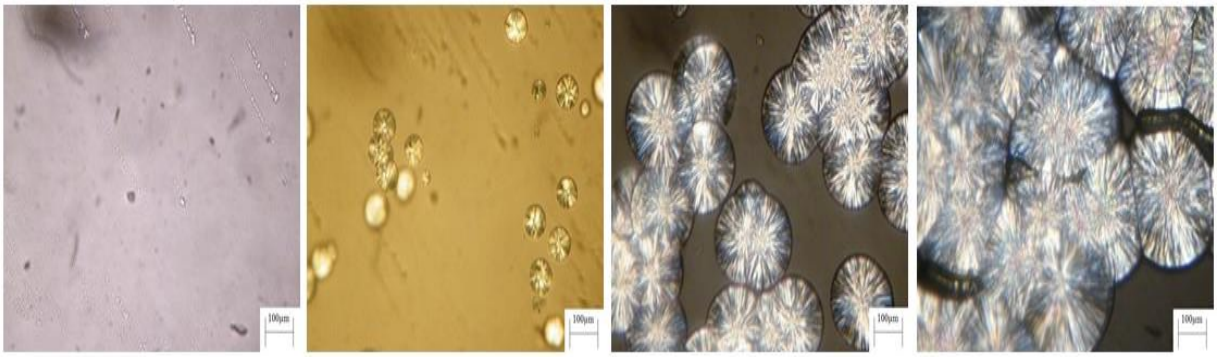

0 mins 5 mins 15 mins 30 mins

(a)

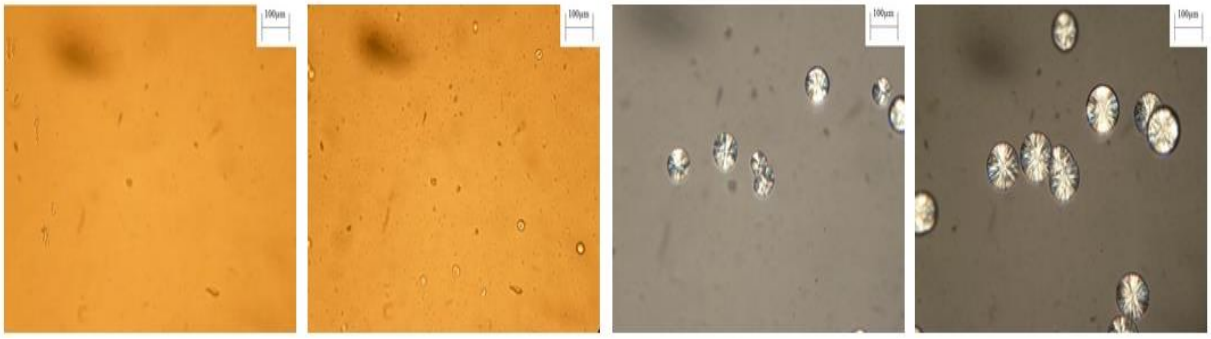

0 mins 5 mins 15 mins 30 mins

(b)

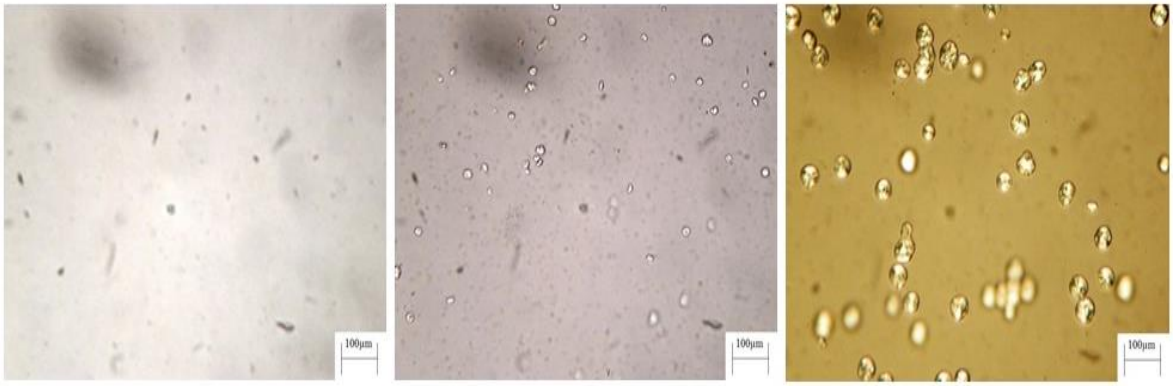

0 mins 15 mins 30 mins

(c)

Figure 6.21: PP MFI 10.5 at a) 130^{o}C, b) 135^{o}C and c) 140^{o}C

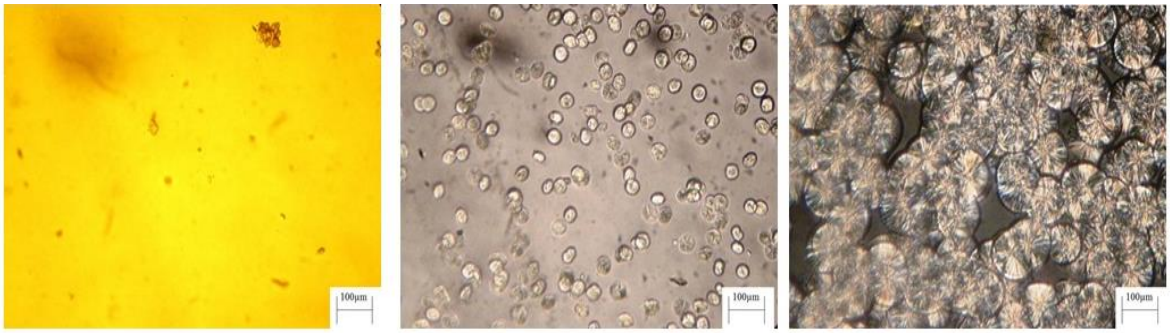

0 mins 5 mins 15 mins

(a)

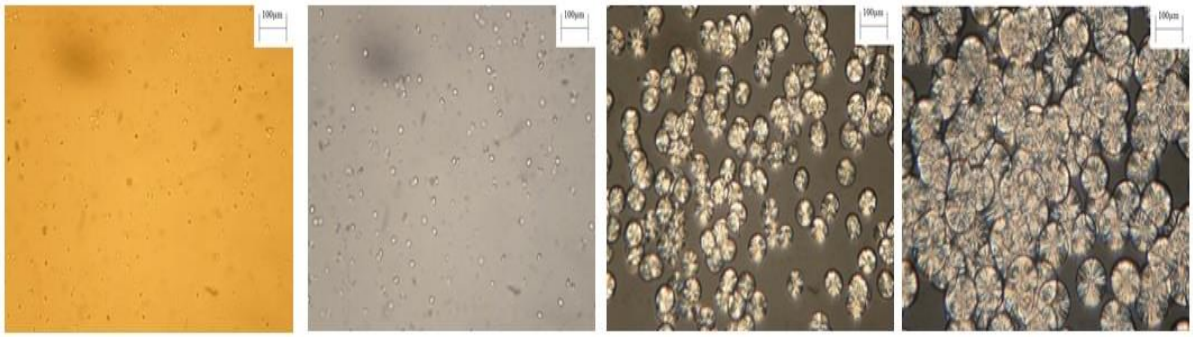

0 mins 5 mins 15 mins 30 mins

(b)

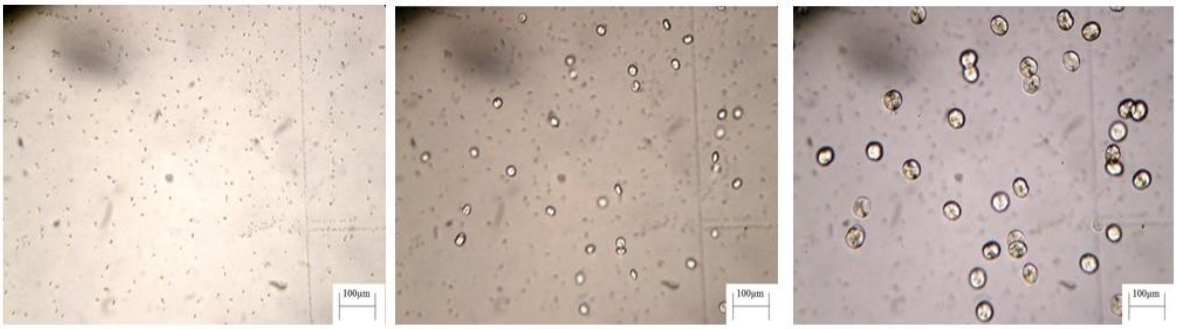

0 mins 15 mins 30 mins

(c)

Figure 6.22: PP MFI 24 at a) 130°C, b) 135°C and c) 140°C

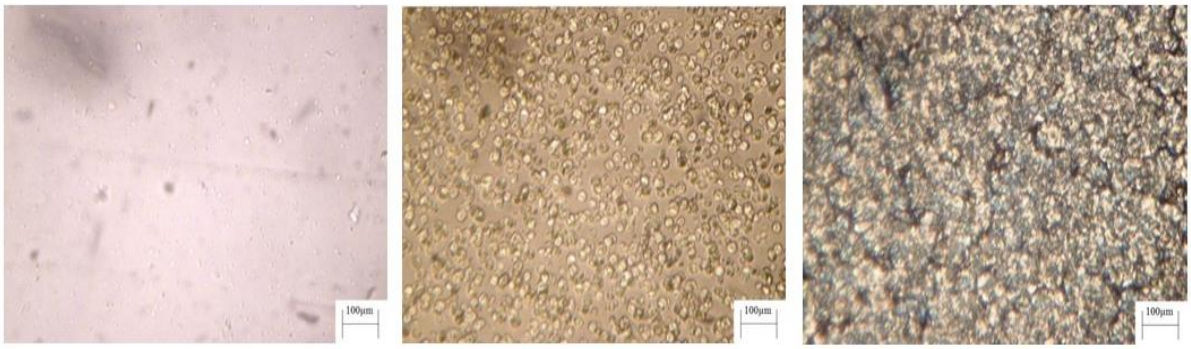

0 mins 2 mins 5 mins

(a)

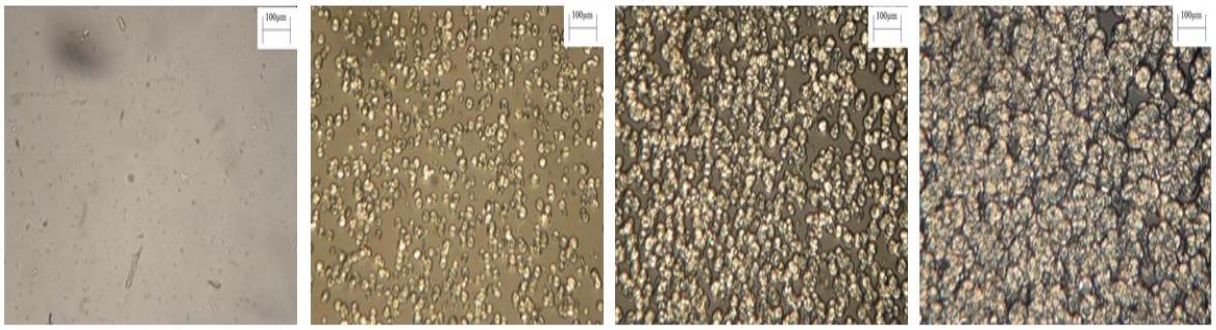

0 mins 5 mins 10 mins 15 mins

(b)

0 mins 15 mins 30 mins

(c)

Figure 6.23: PP MFI 47 at a) 130^{o}C, b) 135^{o}C and c) 140^{o}C

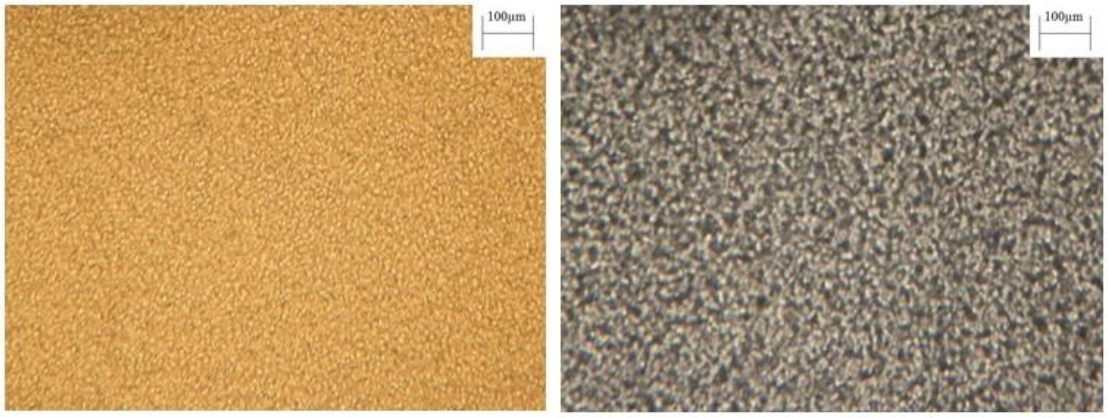

0 mins 5 mins

(a)

0 mins 5 mins 10 mins

(b)

Figure 6.24: PP MFI 120 at a) 135^{o}C and b) 140^{o}C

It can be seen from Figure 6.20 – 6.24 that the rate at which the PP crystallises is influenced by the temperature. As the crystallisation temperature increases the rate of crystal growth decreases which has reported by Quan and Thomason [7, 8]. This can also be clearly seen with $PP_{47,}$ Figure 6.23, as at 130^{o}C it took five minutes to fully crystallise whereas at 135^{o}C it took fifteen and at 140^{o}C it took the thirty minutes. Figure 6.20 - 6.22 shows the nucleation density of PP after thirty minutes for MFI 5.7, 10.5 and 24 decreases as the MFI increases, this observation was also seen by Folkes and Harwick [6]. However, results from this study also show above a MFI of 24 for PP the nucleation density increase as the MFI increases.

Figure 6.22 and 6.21 shows that the time for PP to fully crystallise for MFI of 24 and 47 took less than the study period of thirty minutes at a temperature of 130^{o}C. The MFI of 120 was only carried out at 135^{o}C and 140^{o}C as it took around five minutes to see full crystallisation at 135^{o}C. Therefore the crystallisation at 130^{o}C would be expected to be extremely quick. A reason for the nucleation density increasing at MFI of 47 and 120 is due to a nucleating agent being added to the PP. The nucleating agent suppresses the fibre's transcrystallinity which is why in the DSC results there was no change to the crystallisation onset or peak temperature. The addition of the nucleating agent to the PP was discovered after speaking to the manufacturer of the PP and it was only found out after all the experiments had been completed. Therefore it is suggested that work should be carried out in the future investigating PP composites with different MFI to see if a similar observation to PP_{47} occurs with other MFI of PP.

6.6 Summary

DSC was used to see if the fibre weight fraction can be calculated from the ΔH values associated with the PP or the PET. The composites were manufactured from PET, Flax and Sisal fibres with a Polypropylene matrix with a melt index of 47 and the fibre weight fraction was known before testing. The fibre weight fraction ranged between 0 – 50%. The crystallisation and melt ΔH of pure PP and pure PET were used to calculate the ΔH that would be expected from the composites at various weight fractions if the fibres did not affect the matrix and vice versa. The melt ΔH of the PET fibre were used as it was found that crystallinity was only observed after a weight fraction of 20%. Natural fibres did not show any ΔH therefore the PP ΔH values were used to calculate fibre weight fraction.

It was found that the PP ΔH for PET fibre melting on the first melt cycle and Sisal composite gave accurate estimation of the fibre weight fraction using the DSC but did not for Flax and

PET fibre melting on the second heat cycle. A reason for this underestimation could be due to the fibre suppressing the PP from fully melting which in turn affects the PP crystallisation. Another reason for the underestimation for Flax fibre is that not all the water evaporated off during the manufacturing process leading to the actual weight fraction being lower. It can be therefore said that the DSC can be used to calculate the fibre weight fraction of the composite depending on the composite fibre reinforcement type.

The onset melt and crystallisation temperatures were also studied. It was noticed that the onset melt temperature decreased when the fibres were added to the PP for all fibre types. The decrease in the onset temperature could be due to the oil that is coated on the PET fibre and wax that is found in the fibres which could stimulate the process of melting. The onset crystallisation temperature did not change with the addition of fibre which is surprising as it has been reported that natural fibres and PET fibre induce crystallisation in PP. However, this does tie in with the presence of the nucleating agent that is in PP_{47} which has a much greater effect on the crystallisation than the fibres.

Due to the observation of the fibres not inducing crystallisation in the PP with a MFI 47 (PP_{47}), it was decided to investigate further. It was found that transcrystallinity caused by the fibres did not occur in the matrix of PP_{47} but was observed in a PP matrix with a melt flow index of 10.5. Hence it was deduced that PP_{47} was the cause for transcrystallinity not occurring. Therefore the crystallisation of PP was investigated further over a variety of MFI and arrange of temperatures. It was observed that the increasing the crystallisation temperature reduced the speed of the crystal growth for all PP MFI. Another observation was that the nucleation density decreased as the MFI increased up till the melt flow index of 24 after which the nucleation density increased. The reason for the increase in nucleation density is due to a nucleating agent being added to the PP by the manufacturers. This nucleating agent therefore suppress the transcrystallinity that is caused by the fibres and the reason why

the DSC for PP crystallisation not varying. Therefore it could be said that DSC could be used for obtaining the volume fraction of PP composites as long as the PP has high nucleating density.

6.7 References

[1] N. Zafeiropoulos, C. Baillie, and F. Matthews, "A study of transcrystallinity and its effect on the interface in Flax fibre reinforced composite materials," *Composites Part A: Applied Science and Manufacturing*, vol. 32, no. 3–4, pp. 525–543, Mar. 2001.

[2] Y. X. Pang, D. Jia, H. J. Hu, D. J. Hourston, and M. Song, "Effects of compatiblizing agent on the morphology, interface and mechanical behaviour of Polypropylene/ polyethylene terephthalate blends," *Polymer*, pp. 357 – 365, 2000.

[3] M. A. López Manchado, M. Arroyo, J. Biagiotti, and J. M. Kenny, "Enhancement of mechanical properties and interfacial adhesion of PP/EPDM/Flax fiber composites using maleic anhydride as a compatibilizer," *Journal of Applied Polymer Science*, vol. 90, no. 8, pp. 2170–2178, Nov. 2003.

[4] C. H. I. Wang and L. M. Hwang, "Transcrystallization of PTFE Fiber / PP Composites. II . Effect of Transcrystallinity on the Interfacial Strength," *Journal of Polymer Science Part B: Polymer Physics*, vol. 34, pp. 1435 – 1442, 1996.

[5] "ASTM D1238-10 Standard Method for Melt Flow Rates of Thermoplastic by Extrusion Plastometer," *ASTM International*.

[6] M. J. Folkes and S. . Hardwick, "The molecular weight dependence of transcrystallinity in fibre reinforced thermoplastic," *Journal of Material Science Letters*, vol. 3, pp. 1071 – 1073, 1984.

[7] H. Quan, Z.-M. Li, M.-B. Yang, and R. Huang, "On transcrystallinity in semi-crystalline polymer composites," *Composites Science and Technology*, vol. 65, no. 7–8, pp. 999–1021, Jun. 2005.

[8] J. L. Thomason and A. A. Van Rooyen, "Transcrystallized interphase in thermoplastic composites Part II: Influence of interfacial stress, cooling rate, fibre properties and polymer molecular weight," *Journal of Materials Science*, vol. 27, no. 4, pp. 889–896, Feb. 1992.

[9] J. L. Thomason and A. A. Van Rooyen, "Transcrystallized interphase in thermoplastic composites Part I: Influence of fibre type and crystallization temperature," *Journal of Materials Science*, vol. 27, pp. 889–896, 1992.

Chapter 7

Conclusions and Future Work

7.1 Introductory Remarks

Composite performance is mainly influenced by the reinforcement fibre. The main objective of the work reported herein was to generate a deeper understanding of the fibre reinforcement characteristics and the effect these characteristics have on the overall composite. In this thesis the reinforcement fibres that were under consideration were PET, Sisal and Flax. To characterise these fibres and understand their influence on composite performance various experiments were designed and carried out. The findings obtained from the research carried out in this thesis are summarised in this chapter along with suggested work which may be carried out at some time in the future.

7.2 Key Findings

Throughout this work, many experiments were carried out to achieve the objectives that were set out in Chapter 1 Section 1.2. Several key findings were obtained from undertaking these experiments and are summarized below under the heading of the objectives.

7.2.1 Accurately determine the properties of the reinforcement fibres that are under consideration.

Fibre mechanical properties were determined by carrying out experiments using thermal analysis and tensile test equipment. The single fibre tensile test was carried out at room temperature over a range of gauge lengths to determine the strength and modulus of the PET, Sisal and Flax. The thermal analysis equipment that was used to observe the fibres thermal behaviour such as degradation was Differential Scanning Calorimetry (DSC) and Thermogravimetric Analysis (TGA). The key findings and observations to achieve the objective are detailed below.

- It was found that the Young's Modulus for PET fibre decreased after heat treatment but that heat treatment had no significant effect on the fibre strength.

- The modulus and strength of the natural fibres were determined by two different methods, firstly by using the fibre diameter and secondly, by employing the fibre cross sectional area (CSA) approach. Comparing the results from these two methods it was discovered that using the fibre diameter as the main basis underestimates the strength and modulus of the natural fibres. Therefore, to accurately determine the strength and modulus of the natural fibre the CSA of the fibre should be used.

- The results obtained for the Young's modulus for both Flax and Sisal are in good agreement with the literature values. Flax fibre Young's modulus measured using CSA was found to be 50.0 GPa. Sisal fibre Young's modulus measured for the CSA method was 20.7 GPa.
- It was found that both Sisal and Flax results for DSC and TGA had similar peaks. The first peak was proved to be caused by the water in the fibre evaporating off showing

the hydrophilic nature of natural fibres and the second peak was shown to be degradation of the fibres cellulose.

7.2.2 Investigate what the effect of the reinforcement fibres anisotropic nature has on the composite properties and determine the thermoelastic properties fibres.

Investigating the effect the fibre anisotropic nature has on composite properties and determining the fibre thermoelastic properties were achieved through using Thermomechanical Analysis (TMA) and Dynamic Mechanical Analysis (DMA) equipment and micromechanical modelling. Unidirectional composites were manufactured by vacuum infusion over a range of fibre orientation 0o - 90o. The TMA and DMA were employed to study the behaviour of the unidirectional fibre composites over a range of off – axis angles. The results obtained from the TMA and DMA were input into numerous mathematical and semi – empirical models to obtain the thermoelastic properties of the fibres. The observations and key findings for this objective are as followed.

- The DMA results show that as the off – axis angle increases, the composite modulus decreases for all the reinforcement fibres. The results obtained by the TMA show that the linear coefficient of thermal expansion increases as the off - axis angle increases. The results from the TMA and DMA convey the anisotropic nature of the fibres and the effect the fibres have on the composite behaviour.
- The longitudinal modulus calculated for all fibres using the semi – empirical models was found to be in good agreement with the results that was achieved through single fibre tensile testing at room temperature.
- It was found that the transverse modulus for PET, Flax and Sisal was established to be considerably lower than that obtained for that of the longitudinal direction. The

longitudinal modulus exceeds the transverse modulus by a factor of 3 for PET, 10 for Sisal and 40 for Flax across the temperature range.

- The linear coefficient of thermal expansion (LCTE) in longitudinal and transverse direction was calculated for the three reinforcement fibre (PET, Sisal and Flax). Comparing the longitudinal and transverse LCTE for all fibres, it was identified that the relationship between the transverse and longitudinal direction is similar. The fibres longitudinal LCTE is significantly lower than the fibres transverse LCTE.
- The thermoelastic properties obtained for PET, Sisal and Flax highlight the highly anisotropic nature of these fibres.
- The results obtained from investigating the thermoelastic behaviour shows that only using the longitudinal properties for anisotropic nature fibres in modelling composite properties will lead to an inadequate prediction of composite performance.

7.2.3 Investigate the interfacial shear strength between the fibres that are under consideration and the Polypropylene matrix.

Single fibre pull out was employed to investigate the interfacial shear strength between the fibres and Polypropylene matrix. The fibre pull out test was carried out on composite with a variety of percentages of Maleic Anhydride Polypropylene (MAPP) ranging from 0 – 10%. The investigation also looked into the anisotropic nature of the fibres and how it affects the interfacial strength. The interfacial shear strength (IFSS) of natural fibre was determined by using the fibre diameter and perimeter to see if the diameter under or overestimates the interfacial strength. The key observations and findings to accomplish the objective above are presented below:

- It was discovered by assuming circularity of natural fibre the IFSS was overestimated for the Sisal interfacial strength but had no significant effect on the interfacial strength

of Flax. The main reason for the difference in estimation of IFSS for Sisal is that the actual perimeter of the fibre is greater than the circumference, whereas for Flax the perimeter and circumference are approximately equal. Therefore it should be noted that when calculating natural fibre IFSS the perimeter of the fibre should be used and not assume circularity.

- The load- extension graph created by the PET fibre pull out test was found to be different to that observed by the natural fibre. A 'kink' was observed in the load – extension graph when the force was applied to the fibre and occurred at the same percentage of MAPP. The 'kink' phenomenon was establish by the heat treatment during the manufacturing process as the heat affected the structure of the PET fibre and the 'kink' is considered to be a fibre yield point.
- It was discovered that for all fibres the interfacial strength in a PP matrix increased in direct proportion to the MAPP percentage. The IFSS at 0% MAPP for PET, Flax and Sisal was 1.8 MPa, 3.4 MPa and 2.7 MPa respectively. The IFSS obtained at 5% MAPP for PET, Flax and Sisal was 5.5 MPa, 5.8 MPa and 6.6 MPa.
- It was noted that the interfacial strength for PET, Flax and Sisal in PP was considered relatively low compared to that of the conventional fibres (Glass fibre) in PP. A reason for this is due to the anisotropic nature of the fibres that contributes to a low residual radial compressive stress which leads to low interfacial shear strength. This key finding also contributes to the objective 7.2.2 as it looks at the effect of anisotropic nature of the fibre on the composite.

7.2.4 Investigate the use of experimental techniques to find if composite fibre weight fraction could be determined and the effect the fibres have on the morphology of the Polypropylene.

The DSC was used as the experimental technique to find out if the composite weight fraction of the composite could be obtained. The various enthalpies, ΔH, acquired for the different composites were used to see if the DSC could be used to obtain the composite fibre weight fraction. The composites were manufactured at various known fibre weight fractions ranging from 0 – 50% containing PET, Flax and Sisal in Polypropylene with a Melt Flow Index (MFI) 47. As well as using the DSC, the effect of fibres on Polypropylene morphology was also investigated to gain an understanding if the composite weight fraction could not be achieved through using the DSC. The Polypropylene morphology research was carried out through microscopy. The key findings for this objective are detailed below along with any main observations:

- It was discovered that the composite weight fraction for the PET and Sisal composites could be determined using the DSC, whereas it could not for the Flax composite. An explanation for this could be due to the water not evaporating off during the manufacturing process leading to an underestimation of fibre content. The Polypropylene matrix showed that fibres caused no effect on the crystallisation or melting temperature. A change in the crystallisation or melting temperature to the Polypropylene is to be expected if the fibres are to affect the morphology of the Polypropylene.
- Due to the DSC not being able to determine some of the composite weight fraction, microscopy was used to observe the effect of the fibres on the Polypropylene morphology. The results of this investigation showed that crystallisation of

Polypropylene with a MFI 47 were not affected by the fibres as no transcrystallisation was observed. This result supports the findings obtained from the DSC.

- It was found that the transcrystallisation of the Polypropylene occurred in lower Melt Flow Index of around 10.5. It was therefore concluded that Polypropylene with MFI of 47 was the cause for transcrystallinity not occurring.
- It should also be noted that crystallisation of PP was also investigated over a variety of MFI. It was discovered that the nucleation density decreased as the MFI increase up to the MFI of 24 after which the nucleation density increased. The reason for the increase in nucleation density is due to an addition of nucleating agent being added to the Polypropylene.
- The result above explains why there was no fibre effect on the PP47 observed by microscopy or DSC as the nucleating agent supresses the transcrystallinity that is caused by the fibres.

The key findings and observations shown above reveals how highly anisotropic the fibres under investigation are and how the fibres anisotropic nature can affect the composite performance. As well as the findings showing how the fibres properties affects the composite, the findings also show that to use the fibres under consideration as a reinforcement, the transverse properties of the fibres must be determined along with the longitudinal properties of the fibres as it will give a more accurate estimation of the composite properties.

7.3 Continuing Work

The work carried out in this thesis has also highlighted what research may be considered in the future. Some possible research themes are offered for consideration based on the findings of the work presented herein:

7.3.1 Composite Manufacturing and Testing

The work carried out in this thesis investigated the correct way into characterising the fibres under consideration and how the properties of these fibres could affect the composite performance. The initial progression on from the current work would be to manufacture composites with the fibres studied at various fibre volume fractions and undertaking a programme of mechanical testing for example, tensile, compression and impact tests. Carrying out this piece of work would clarify how the fibre anisotropic nature and interfacial shear strength affects the composite structural performance. Following on from the mechanical testing at room temperature, the next step could be to include investigating the composite sample response under different temperature and humidity conditions if the fibres are to be considered for use in, for example, the automotive industry. The findings in this thesis showed that the fibre properties decreased as the temperature increased therefore carrying out the testing at a variety of temperature conditions would show how the decrease in fibre properties affects composite performance. Testing under humidity conditions is also vital if these fibres are to be used in the automotive industry as literature has shown that natural fibres absorb water that affects their properties and how this would affect the composite.

7.3.2 Interfacial Shear Strength

The results presented in this thesis on interfacial shear strength between the fibres under consideration (PET, Flax and Sisal) and Polypropylene (PP) matrix has shown to be low compared to that of glass fibre. However the research showed that the interfacial shear strength improved by adding Maleic Anhydride Polypropylene (MAPP) to the PP matrix. Therefore, improving the bond between the fibres and PP should be investigated further. Literature [1, 2] has shown that the interfacial shear strength could be improved by adding

compatibiliser to the PP or treatment to the surface of the fibres with chemicals. Another piece of work that could be carried out is to investigate the interfacial shear strength across a range of temperatures and humidity conditions. Yang and Thomason have investigated the interfacial shear strength (IFSS) in Glass fibre (GF) Polypropylene composites over a temperature range -40^{o}C to 100^{o}C. The results from their research showed that the IFSS for GF-PP had significant dependence on the testing temperature [3]. Investigating the interfacial strength under the above circumstances would assist with the explanation of the composite performance when testing at these conditions and will tie in with the future work mentioned in Section 7.3.1.

7.3.3 Natural Fibre Characterisation

Throughout the course of the work presented in this thesis, the characterisation of natural fibres was one of the key areas. The findings presented herein showed that the actual cross sectional area (CSA) or perimeter of the fibre should be used to obtain the fibre's properties. The process used to obtain the fibre CSA in this research was quite destructive. Therefore to ascertain greater accuracy in the natural fibre's properties it is recommended that a non – destructive method should be developed to measure the CSA. One possible way to measure the CSA of non-circular fibres is to invest in a Dia-stron [4]. A Dia-stron is a tensile test machine that uses a laser to measure the CSA of the testing fibre, therefore the machine can be used to measure the CSA of irregular shaped fibres in a non-destructive way. Micromechanical models were also used to characterise natural fibres. These models assumed that the fibres are circular but as reported in this research natural fibres have an irregular CSA. Consequently, it is suggested that a micromechanical model needs to be developed to account for non – circular fibres to generate better estimation of fibre properties.

7.4 References

[1] I. Van de Weyenberg, J. Ivens, A. De Coster, B. Kino, E. Baetens, and I. Verpoest, "Influence of processing and chemical treatment of Flax fibres on their composites," *Compos. Sci. Technol.*, vol. 63, no. 9, pp. 1241–1246, Jul. 2003.

[2] X. Li, L. G. Tabil, and S. Panigrahi, "Chemical treatments of Natural fiber for use in Natural fiber-reinforced composites: A Review," *J. Polym. Environ.*, vol. 15, no. 1, pp. 25–33, Jan. 2007.

[3] J. L. Thomason and L. Yang, "Temperature dependence of the interfacial shear strength in glass-fibre Polypropylene composites," *Compos. Sci. Technol.*, vol. 71, no. 13, pp. 1600 – 1605, 2011.

[4] "Dia-stron." [Online]. Available: http://www.diastron.com/.